Modeling the effects of saline groundwater and irrigation water on root zone salinity and sodicity dynamics in agro-ecosystems

Syed Hamid Hussain Shah

Thesis committee

Promotor

Prof. dr. ir. S.E.A.T.M. van der Zee

Personal chair at the Soil Physics and Land Management Group
Wageningen University

Co-promotor

Dr. ir. R.W. Vervoort

Associate professor, Faculty of Agriculture, Food and Natural Resources,
The University of Sydney, Australia

Other members

Prof. dr. ir. R. Uijlenhoet, Wageningen University
Prof. dr. ir. J. Molenaar, Wageningen University
Dr. ir. H.P. Ritzema, Wageningen University
Dr. ir. L.C.P.M. Stuyt, Alterra, Wageningen UR

This research was conducted under the auspices of the Graduate School for Socio-Economic and Natural Sciences of the Environment (SENSE)

Modeling the effects of saline groundwater and irrigation water on root zone salinity and sodicity dynamics in agro-ecosystems

Syed Hamid Hussain Shah

Thesis

submitted in fulfilment of the requirements for the degree of doctor
at Wageningen University
by the authority of the Rector Magnificus
Prof. dr. M.J. Kropff,
in the presence of the
Thesis Committee appointed by the Academic Board
to be defended in public
on Tuesday 19 March, 2013
at 1:30 p.m. in the Aula.

Syed Hamid Hussain Shah

Modeling the effects of saline groundwater and irrigation water on root zone salinity and sodicity dynamics in agro-ecosystems

201 pages

PhD Thesis, Wageningen University, Wageningen, The Netherlands (2013)
With references, with summaries in Dutch and English

ISBN 978-94-6173-525-6

"O my Lord! Advance me in knowledge."

(QS 20 Taahaa: 114)

This book is dedicated to:

my dearest wife, Saba Hamid

and my lovely daughter, Syeda Areej Fatima

Table of Contents

CHAPTER 1

General Introduction

1. Introduction

1.1 Problem definition

Increased demands for water by municipal, industrial, agricultural and environmental consumers force conservation of high-quality water (*United Nations/World Water Assessment Programme, 2003*) and incorporation of recycled or other marginal quality water in enterprises such as agriculture where lower-quality water can be utilized (*Asano et al., 1996; Angelakis et al., 1999; Lazarova et al., 2001; Hamilton et al., 2007)*. A consequence of irrigation or capillary upflow from groundwater is that salts may concentrate in the root zone. Excess irrigation is required to periodically remove accumulated salts and maintains agro-ecosystems productivity. Where drainage is inadequate, the excess irrigation results in waterlogging that accelerates salinization. Consequences of such practices are evident world-wide. The Food and Agricultural Organization (2002) estimates the productivity of approximately 20-30 million irrigated hectares has been significantly decreased by salinity and that salinization results in the loss of an additional 0.25-0.5 million hectares each year globally. In 1990, 1.4 million hectares of irrigated California land were assessed as having a water table within 1.5m of the surface and 1.7 million hectares were determined to be saline or sodic (*Tanji, 1990*).

The work by Schoups et al. (2005) involving regional scale hydro-salinity modeling questions the sustainability of irrigated agriculture in the San Joaquin Valley, California because of inevitable salinization of soil and groundwater. Approximately 8.8 million hectares in Western Australia are threatened by rising water tables and may be lost to production by 2050 (*National Land and Water Resources Audit, 2001*). Despite installation of extensive drainage systems and groundwater management in recent years, some 25 percent (more than 5 million hectares) of the Indus River basin of Pakistan is still estimated to be affected by salinity, sodicity, and waterlogging (*Tanji and Kielen, 2002*). According to a report published by the FAO in 2000, the total global area of salt-affected soils including saline and sodic soils is 831 million hectares (*Martinez-Beltran and Manzur, 2005*), extending over all the continents including Africa, Asia, Australia, and the Americas. The challenge for water management is to maximize productivity under market and environmental constraints including protection of soil and water resources. Meeting the challenge will require a quantitative understanding of not only the

effects of water supply, but also the deleterious effects of salts and potentially toxic constituents (such as sodium) of marginal quality waters coming through irrigation or through capillary upflow from groundwater.

Deleterious effects of salinity on plant physiology result from reduced water availability due to decreased osmotic potential, specific ion toxicity, or investment in assimilates required to maintain plant activities under saline conditions (*Bernstein, 1975; Munns, 2002*), and by changes in soil solution matric and osmotic potential and soil hydraulic conductivity via feedback mechanisms (*Bernstein, 1975*). For example, a plant under saline conditions transpires less water than does a plant under less saline conditions (*Munns, 2002*). If both plants are supplied identical amounts of water by rainfall or through irrigation/groundwater, subsequent conditions of water contents, hydraulic conductivities and salt concentrations will differ (*Dudley and Shani, 2003*). Plant response to dry conditions cannot be explained simply by decreased matric potential but must also consider increased salinity (decreased osmotic potential) (*Shalhevet and Hsiao, 1986*).

In addition to salinity, soil sodicity (quantified by the Exchangeable Sodium Percentage) describes the proportion of the cation exchange capacity occupied by sodium ions. Sodicity problems are usually inherent with salinity having significant sodium content in irrigated clayey soil. High levels of sodium in irrigation water or groundwater typically result in an increase of soil sodium levels, which subsequently affect soil structural stability, infiltration rates, drainage rates, and crop growth potential.

The interrelation between sodicity and salinity levels in irrigation water or water coming through capillary flux from groundwater introduces a dual problem in terms of crop response, soil structure degradation, and irrigation management. An increase of water salinity has a positive consequence on the sodicity effect. Sodicity has less impact at higher electrolyte concentrations at any particular level (*McNeal, 1968*). On the other hand, low water salinity and high levels of sodicity can cause soil degradation and reduction in soil permeability (*McNeal, 1968*). Such degradation results in aeration and waterlogging problems which negatively affect the crop yield.

Sodicity-salinity effects on the physical and hydraulic properties of the soil are very complicated processes that can be influenced by many factors. The main factors that

control sodicity problems are soil type (*Felhendler et al., 1974; Quirk & Schofield, 1955*), clay type, and content (*Goldberg et al., 1991*), pH of the soil solution (*Suarez et al., 1984; Sumner 1993*), manner of application of irrigation water, initial water, salt, and cation contents (*Dehayr & Gordon 2005*), and organic matter. Therefore, the level/degree of soil structure degradation is unique for a given soil and its conditions as mentioned above (*Evangelou & McDonald, 1999*). In the following an introduction will be given to the methodology used and analysed in this thesis for soil salinity and sodicity development, their effects on reduction in saturated hydraulic conductivity, and optimal irrigation water management.

1.2 Modeling the effects of saline groundwater and irrigation water on root zone salinity and sodicity dynamics in agro-ecosystems

During the past four years, the interaction between groundwater and root zone have been taken into consideration by *Vervoort and Van der Zee* (2008; 2009), by *Ridolfi et al*. (2008), *Laio et al.* (2009), and *Tamea et al.* (2009). *Vervoort and Van der Zee* (2008; 2009) considered the water balance for a vegetated soil, but without accounting for the impact of drainage on ground water levels. This influence of drainage on groundwater levels was taken into consideration by *Ridolfi et al*. (2008), *Laio et al.* (2009), and *Tamea et al.* (2009) for unvegetated and vegetated soil. Whereas determining the influence of capillary upflow from the groundwater towards the root zone is of interest, in particular for semi-arid regions, the related hazards of salt accumulation in the root zone cannot be ignored. Water moving upward from the groundwater towards the root zone due to capillary forces is known to imply a salinization hazard (*Bresler et al., 1982; Howell, 1988*) and therefore shallow groundwater and water logging situations need to be avoided (*Berret-Lennard, 2003; Datta and Jong, 2002; Pichu, 2006*).

The Soil sodicity problem is more complicated than salinity in groundwater driven agro-ecosystems as it could result in the degradation of soil structure which makes the management options more complex (*Kaledhonkar et al., 2008*). Sodicity problems manifest at higher relative Na^+ concentration and lead to degradation of soil structure (*McNeal, 1968*). High levels of sodium in groundwater typically result in an increase of soil sodium levels, which affect soil structural stability, infiltration rates, drainage rates, and crop growth potential (*So and Alymore, 1993; Halliwell et al., 2001; McNeal, 1968*).

Therefore, the salinity model developed by *Shah et al*. (2011) has been extended for the sodicity modeling by using the Gapon equation used in salinity research.

Soil saturated hydraulic conductivity of the soil is the main characteristic that is responsible for the conveyance of water and salt during irrigation, during capillary upflow from groundwater, and plant water uptake (*Ezlit 2009*). Thus, it is crucial to determine the reduction in saturated hydraulic conductivity (*Ezlit, 2009*). At relatively high electrolyte concentrations, the swelling process is most likely to be responsible for reducing saturated hydraulic conductivity. At lower electrolyte concentrations the saturated hydraulic conductivity reduction is attributed mainly to the dispersion process (*McNeal, 1968, Ezlit, 2009*). The dispersion at low electrolyte concentration depends on the osmotic gradient generated between added water and soil solution within the micro-pores (i.e. diffuse double layer) within the clay crystalline structure (*Emerson & Bakker 1973*). Knowing the importance of salinity and sodicity and their effects on reduction in saturated hydraulic conductivity and consequently reduction in root zone fluxes have guided us towards the quantitative analysis of these hazards.

1.3 Objectives of the thesis

In order to quantify the soil salinity and sodicity development, we have modelled the simple mass balance approaches of water, salt, and cations. The cation exchange between soil solution and exchange complex is modelled by using the Gapon equation used in salinity research. The interrelation between salinity and sodicity is translated into reduction in saturated hydraulic conductivity by using the analytical expressions developed by *McNeal* (1968). The feedback effects of reduction in saturated hydraulic conductivity on the root zone fluxes, salinity, and sodicity are analysed for the range of climates, groundwater depths. In the second theme of thesis, we have used the analytical model developed by *Shani et al.* (2007) to optimize the irrigation water for the sequential farms along the river basin.

To overcome the problems and challenges as discussed above, the objectives of the study can therefore be divided into the following specific themes:

1. To develop a relatively simple model that emphasizes some dependencies only, to assess as transparent as possible, to what degree periodic salinity may cause soil sodicity under different climates, groundwater depths, and soil types.

2. To determine the analytical approximations of long term average fluxes, salt concentrations and soil sodicity (quantified by *ESP)* under different climates, root zone thicknesses, and groundwater depths.

3. To quantify the effect of reduction in saturated hydraulic conductivity on root zone fluxes under saline and sodic conditions for different groundwater depths under seasonal and non-seasonal rainfall.

4. To determine optimal water management strategies for water use chains using an explicit agro-physical model for yield reductions caused by salt stress.

Therefore, this thesis aims to investigate theoretically how the different input parameters such as rainfall/irrigation, capillary flux, groundwater salinity, and groundwater SAR (sodium adsorption ratio) affect soil saturated hydraulic conductivity. The presented analysis can be applied ranging from point scale to regional scale due to the relative simplicity.

1.4 Thesis outline

Besides this introduction (chapter 1), which sketches the outline of the work, this thesis contains six chapters with different aspects covering the main objectives and research themes mentioned in the previous paragraph. These chapters (2-6) are based on and structured as scientific papers published in or submitted to peer reviewed journals. **Chapter 2** presents the soil sodicity development as a result of periodical drought. We have developed a relatively simple model that emphasizes some dependencies only, to assess as transparent as possible, to what degree periodic salinity may cause soil sodicity. We showed how the different leaching fluxes lead to different level of equilibrium status of soil *ESP*, maximum and minimum salt concentration. The scope of **Chapter 3** is to assess, for a root zone in hydrological contact with groundwater, how salt accumulation is related to root zone water dynamics, with the emphasis on the variability of these dynamics caused by atmospheric forcing. The random fluctuations of root zone water saturation affect the fluctuations of salinity through the contributions of various fluxes into and out of the root zone. **Chapter 4** presents the modeling results of soil sodicity development due to capillary upflow from groundwater in a stochastic ecohydrological framework. The sodicity model developed in this chapter is based on the salinity model developed in Chapter 3. Based on the sodicity model, we have quantified the soil salinity

and sodicity development under different climates, groundwater depths, soil, and root zone thicknesses. In heavy clay soil, the long term calcium fraction in soil solution (f) becomes almost same as the groundwater calcium fraction (f_z). On the basis of these results, we can approximate long term fluxes (similar as *Laio et al., (2001)*), to derive analytically the long term salinity, and soil *ESP* under different climates, groundwater depths, and root zone thickness. In **Chapter 5,** an integrated model based on the salinity and sodicity model (chapter 3, 4) is presented. We have considered the feedback effects of saturated hydraulic conductivity due to salinity and sodicity on root zone fluxes, salinity, and sodicity. This model helps to find the conditions like weather seasonality, non-seasonality, groundwater depth, and degree of wetness of climate where feedback and no feedback effects are significant. In **Chapter 6**, we have developed a sequential model of irrigation that predicts crop yields and tracks the water flow and level of salinity along a river dependent on irrigation management decision. The model incorporates the agro-physical model of plant response to environmental conditions including feedbacks. For a system with limited water resources, we have compared the efficiency of outcomes when access rights to water are unregulated, water is not priced, and water loss occurs due to inefficient application with the outcomes of an optimally managed system. Finally **Chapter 7** summarizes the findings of this thesis and provides some recommendations for future research.

CHAPTER 2

Soil sodicity as a result of periodical drought

S. E. A. T. M. van der Zee, S. H. H. Shah, C. G. R. van Uffelen, P. A. C. Raats, N. dal Ferro

Department Soil Physics, Ecohydrology, and Groundwater Management, Environmental Sciences Group, Wageningen University, P. O. Box 47, 6700 AA Wageningen, Netherlands

Agricultural Water Management 97(2010) 41-49

2. Soil sodicity as a result of periodical drought

Abstract

Soil sodicity development is a process that depends nonlinearly on both salt concentration and composition of soil water. In particular in hot climates, soil water composition is subject to temporal variation due to dry-wet cycles. To investigate the effect of such cycles on soil salinity and sodicity, a simple root zone model is developed that accounts for annual salt accumulation and leaching periods. Cation exchange is simplified to considering only *Ca/Na* exchange, using the Gapon exchange equation. The resulting salt and *Ca/Na*-balances are solved for a series of dry/wet cycles with a standard numerical approach. Due to the nonlinearities in the Gapon equation, the fluctuations of soil salinity that may be induced, e.g. by fluctuating soil water content, affect sodicity development. Even for the case that salinity is in a periodic steady state, where salt concentrations do not increase on the long term, sodicity may still grow as a function of time from year to year. For the longer term, sodicity, as quantified by Exchangeable Sodium Percentage (*ESP*), approaches a maximum value that depends on drought and inflowing water quality, but not on soil cation exchange capacity. Analytical approaches for the salinity and sodicity developing under such fluctuating regimes appear to be in good agreement with numerical approximations and are very useful for checking numerical results and anticipating changes in practical situations.

Keywords: dry-wet cycles, root zone model, salinity, sodicity, water management, salt accumulation, leaching, ecohydrology.

2.1 Introduction

Soil sodicity refers to the relative accumulation of sodium (*Na*) in the soil solution and at the cation exchange complex and may induce severe structural degradation in those loamy and clayey soils that contain swelling minerals (*Bresler et al., 1982*). Whereas soil sodicity may occur in all climate zones (*Armstrong et al., 1996*), e.g. due to contact between soil and sea water, it is particularly a problem in arid and semi-arid regions. In those latter regions, good quality irrigation water may not be available, and poor quality groundwater may be in contact with the root zone through capillary upflow or used for irrigation purposes (*Richards et al., 1954; Szabolcs, 1989; So and Aylmore, 1993; Tedeschi and Dell'Aquila, 2005*). Moreover, due to shortage of good quality

irrigation water, particularly in areas with water scarcity (*Minhas et al., 2007; UNESCO, 2003*), also waste water is being re-used for irrigation. Particularly if this concerns domestic waste water, it may have high *Na*-concentrations resulting from the salt content of human food (*Tedeschi and Menenti, 2002*).

Soil sodicity is usually quantified by the Exchangeable Sodium Percentage (*ESP*), which is the proportion of the cation exchange capacity occupied by sodium ions. If *ESP* becomes too large (e.g. over 15%), the hazard of organic and inorganic colloid dispersion upon introducing good quality water (such as rainwater) becomes large. Swelling, compression of larger pores, and a severe and often irreversible reduction of hydraulic conductivity can be the result (*So and Aylmore, 1993; Halliwell et al., 2001*). Since the development of soil sodicity is gradual, and often irreversible within limits imposed by reasonable time scales and costs, it is essential to anticipate its onset. Unfortunately, relatively simple conceptual tools such as the leaching requirement for salinity control (*Richards et al., 1954; Howell, 1988; Corwin et al., 2007*) are not available for sodicity control.

Cation exchange as described by the Gapon equation, which is favored in soil salinity research, is nonlinear with regard to the total salt concentration as well as regarding the salt composition (*Bolt, 1982; Kaledhonkar et al., 2001*). In view of this nonlinearity, and the observed periodical salinity due to periodic drought (*Minhas et al. 2007; Tedeschi and Dell'Aquila, 2005*), it is worthwhile to explore how such nonlinearities affect the hazard of sodicity development. The aim of our paper is to develop a relatively simple model that emphasizes some dependencies only, to assess as transparent as possible, to what degree periodic salinity may cause soil sodicity.

2.2 Model development

The proposed model considers a homogeneous root zone, similar to the ecohydrological models considered by *Vervoort and van der Zee* (*2008, 2009*). The water balance of this root zone is simplified to cycles that consist of a period in which leaching of water is zero, followed by a period where leaching occurs. Only two cations are explicitly modeled, i.e., *Na* and *Ca*, where we make the common assumption that often present *K* behaves similar to *Na* and that *Mg* behaves similar to *Ca*. The type of anion is left out of consideration, which implies that chemical precipitation is ignored. Changes in

salt concentration and distribution of *Ca* and *Na* are due to variations in time of incoming water (such as capillary rise/upflow, rainfall, irrigation), of drainage (leaching) and of evapotranspiration. Thus, we have schematized the water and salt balance as in Figure 2.1.

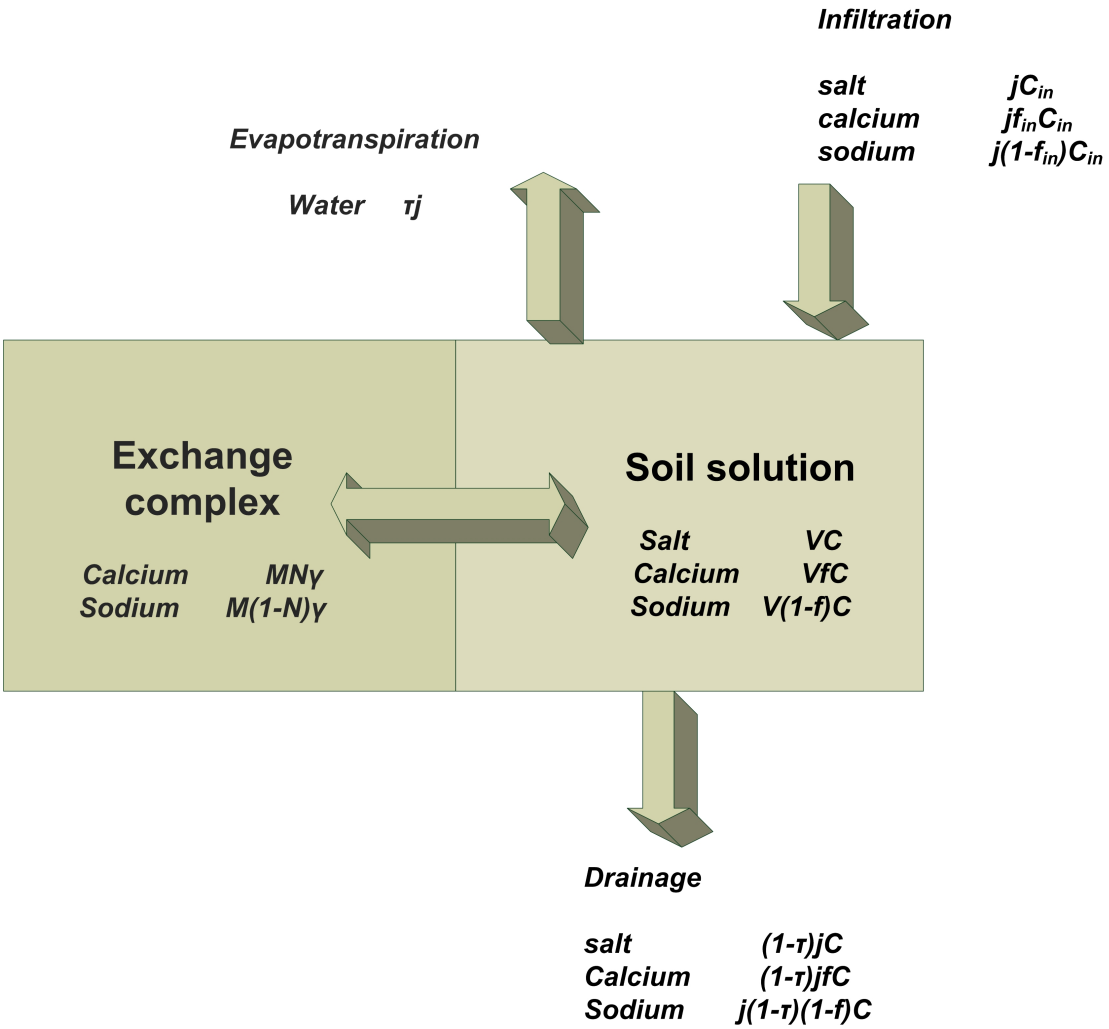

Figure 2.1: Illustration of root zone model comprising of cation exchange complex, soil solution, inputs/losses at soil surface, and losses at root zone base. Symbols defined in text and in list of symbols.

For simplicity, we consider only two periods or seasons, of equal duration. To assume different durations, or more than two periods with more realistic boundary conditions would complicate the analysis, without changing its essence, hence our simple schematization.

Infiltrating water enters the root zone at rate j (l/m^2/y) with a designated salt concentration C_{in} (mol$_c$/l) with concentrations equal to $f_{in}C_{in}$ mol$_c$/l of Ca^{2+} and (1-f_{in}) C_{in}

mol_c/l of Na^+. A part of the water evapotranspires at rate τj, i.e., τ represents the fraction of infiltrating water that evaporates from the root zone. We assume that neither sodium nor calcium leave the soil with the water that evapotranspirates. Water drains from the root zone at a rate equal to $(1-\tau)j$.

The amount of water in the root zone is denoted by V. The total amount of salt in the soil solution equals VC, comprising calcium equal to VfC and sodium $V(1-f)C$. The salt concentration and composition in the drainage water are assumed to be identical to those in the soil solution.

At the exchange complex, calcium equals $MN\gamma$, where M is the dry mass of the soil (kg_{soil}/m^2), N is the fraction of calcium in the complex, $(1-N)$ represents the Na^+ fraction and γ (mol_c/kg_{soil}) the soil cation exchange capacity (or CEC), which is a measure of the capacity of a soil to hold the major cations: calcium, magnesium, sodium and potassium. Inflow of water that contains salts causes changes of the salt concentration C, and the concentrations of calcium and sodium, fC and $(1-f)C$, respectively, in the solution. For simplicity, we assume the applicability of the Local Equilibrium Assumption (LEA) between solution and exchange complex composition.

For the accumulation period, we assume no drainage and $\tau = 1$, whereas for the leaching period we have leaching without evapotranspiration, hence $\tau = 0$, and for all times the amount of root zone water V is assumed constant. Water quality parameters in principle differ for these two periods.

For the root zone, we first need the salt balance which equates the change of total salt content in the root zone (calcium, sodium) $V\Delta C$ with the mass of salt entering the soil $jC_{in}\Delta t$ minus the mass of salt leaving the root zone $(1-\tau)jC\Delta t$, i.e.

$$\frac{dC}{dt} = \frac{jC_{in} - (1-\tau)jC}{V}. \qquad \textbf{(2.1)}$$

Note that the total salt balance is not affected by cation exchange, provided that all concentrations are expressed on an equivalent basis. Also, in equation (2.1), the ratio V/j can be interpreted as the turnover time of water in the system. The cycle starts with the accumulation period, for which we assume that no leaching occurs by setting $\tau = 1$, hence

$$\frac{dC}{dt} = \frac{jC_{in}}{V}. \qquad \textbf{(2.2)}$$

Integration of (2.2) with respect to time gives, for a concentration equal to C_0 at the beginning of the present cycle:

$$C(t) = C_o + \frac{jC_{in}t}{V}, \qquad \textbf{(2.3)}$$

i.e. a linear increase of the concentration C with time t.

In the leaching period, $\tau = 0$, hence

$$\frac{dC}{dt} = \frac{j(C_{in} - C)}{V} = \frac{jC_{in}}{V} - \frac{jC}{V}. \qquad \textbf{(2.4)}$$

Integration of (2.4) with respect to time gives an exponential decrease of the concentration C with time t:

$$C(t) = \frac{b}{a} + (C_o - \frac{b}{a})\exp(-at) \qquad \textbf{(2.5)}$$

with $b = \frac{jC_{in}}{V}$ and a is the inverse turnover time and equal to $\frac{j}{V}$.

With (2.3) and (2.5), successive cycles of accumulation and leaching periods can be evaluated if for each cycle C_0 is updated, or, alternatively, (2.1) can be numerically integrated for the same purpose.

In addition to the water and salt balances, we need to model the cation composition of the solution and exchange phases. To do so, we can express our model in terms of either *Ca* or *Na*. Choosing the first option, we have for the total calcium content in the soil

$$T = fCV + NM\gamma. \qquad \textbf{(2.6)}$$

The change of calcium content ΔT is the difference between the masses of calcium entering the root zone ($jf_{in}C_{in}\Delta t$) and leaving the soil system $j(1-\tau)fC\Delta t$. Therefore,

$$VC\frac{df}{dt} + Vf\frac{dC}{dt} + M\gamma\frac{dN}{dt} = jf_{in}C_{in} - j(1-\tau)fC. \qquad \textbf{(2.7)}$$

We can rewrite dN/dt in terms of df/dt and dC/dt, after choosing an appropriate exchange equation for the functional dependence $N(f,C)$, where N is the fraction of calcium in the exchange complex. We choose the Gapon equation and we assume the Gapon constant K_G =0.5 $(\text{mol/l})^{-1/2}$ (*Bolt and Bruggenwert, 1976*), which is an equilibrium constant that links adsorbed and soil solution phase between monovalent and divalent cation ratio.

$$\frac{(1-N)}{N} = K_G \frac{(1-f)C}{(fC/2)^{1/2}} \qquad \textbf{(2.8)}$$

The Gapon equation implies a larger affinity of the exchange complex for divalent than for monovalent cations, and this affinity is a decreasing function of the total concentration of the solution *C*. The Gapon constant is assumed to be same in the range of 0<ESP<100. It is important to note that the approximate constancy of the 'Gapon constant' is limited to fractional amounts of sodium 1-N< 0.5 (c.f. Figure 1 and text below it in Bolt, 1967; see also Bolt, 1982, p. 45, where the 1969 edition of Richards et al. (1954) is cited as a basis for restricting the range of applicability to 1-N<0.4). Solving equation (2.8) for *N* gives:

$$N = \frac{1}{1 + K_G (2C)^{1/2} (\frac{1}{(f)^{1/2}} - (f)^{1/2})} \quad , \qquad \textbf{(2.9)}$$

and differentiating (2.9) with respect to time, we obtain

$$\frac{dN}{dt} = N^2 (\frac{K_G (f)^{1/2}}{(2C)^{1/2}} - \frac{K_G}{(2fC)^{1/2}}) \frac{dC}{dt} + N^2 (\frac{K_G (C)^{1/2}}{(2f)^{1/2}} + \frac{K_G (C)^{1/2}}{(2f^3)^{1/2}}) \frac{df}{dt} . \qquad \textbf{(2.10)}$$

Combining equations (2.7) and (2.10) yields

. **(2.11)**

$$\frac{df}{dt} = \frac{[jf_{in}C_{in} - j(1-\tau)fC + [\frac{M\gamma N(1-N)}{2C} - Vf]\frac{dC}{dt}]}{[VC + M\gamma N^2 K_G (C/2)^{1/2} (\frac{1}{(f)^{1/2}} + \frac{1}{f(f)^{1/2}})]}$$

This expression is numerically integrated where *f*, *C*, and *M* are time dependent, leading to updated values for *f*, and *N*. Total calcium, in mol_c/kg_{soil}, is obtained from equation (2.6) and division by *M*, dry mass of the soil (kg_{soil}/m^2). Here the subscript c in mol_c refers to the fact that concentrations are expressed on an equivalent (or mole charge) basis.

The numerical integration of both equations (2.1) and (2.11) is done with the classical Runge-Kutta 4th order method in the R environment, particularly with the "odesolve" package (*Press et al., 1992*). We consider the accumulation and the leaching periods, which differ, for the reference situation (first line in Table 2.1) as

1. Incoming salt concentration values in the accumulation and leaching periods are different. In the accumulation period, we assume poor quality water (20 $mmol_c/l$), while in the leaching period, we assume it to be of good quality (2 $mmol_c/l$).
2. Calcium and sodium fractions are different as in the accumulation period the calcium fraction *f* is 0.05 and consequently sodium fraction (1-*f*) equals 0.95, and in the leaching period we have fractions of 0.25 and 0.75, respectively.

Table 2.1: Input data for calculations of salinity and sodicity in different figures

Figure				initial values		Accumulation period					Leaching period				
	V (l/m^2)	M (kg/m^2)	γ (mol_c/kg)	C (mol_c/L)	f	j $(l/m^2/y)$	C_{in} (mol_c/L)	f_{in}	t (y)	τ	j $(l/m^2/y)$	C_{in} (mol_c/L)	f_{in}	t (y)	τ
2.2,2.3,2.4	90	390	0.25	0.0098	0.98	300	0.02	0.05	0.5	1	300	0.002	0.25	0.5	0
2.6,2.8,2.9	90	390	0.03	0.0098	0.98	300	0.02	0.05	0.5	1	300	0.002	0.25	0.5	0
Low CEC			0.03												
High CEC			0.1												
2.5,2.7	90	390		0.0098	0.98	300	0.02	0.05	0.5	1	300	0.002	0.25	0.5	0
Low values	30		0.15			300		0.2			300		0.33		
High values	90		0.45			900		0.6			900		1		

2.3. Results and discussion

Figure 2.2 shows the development of total salts, calcium and sodium as the result of a period of 6 months irrigation with poor quality water ($C_{in,a}$ = 20 $mmol_c/l$ or 0.02 mol_c/l, SAR = 27 $(mmol/l)^{1/2}$), followed by a leaching period with good water quality for irrigation. In the leaching period, irrigation water quality is

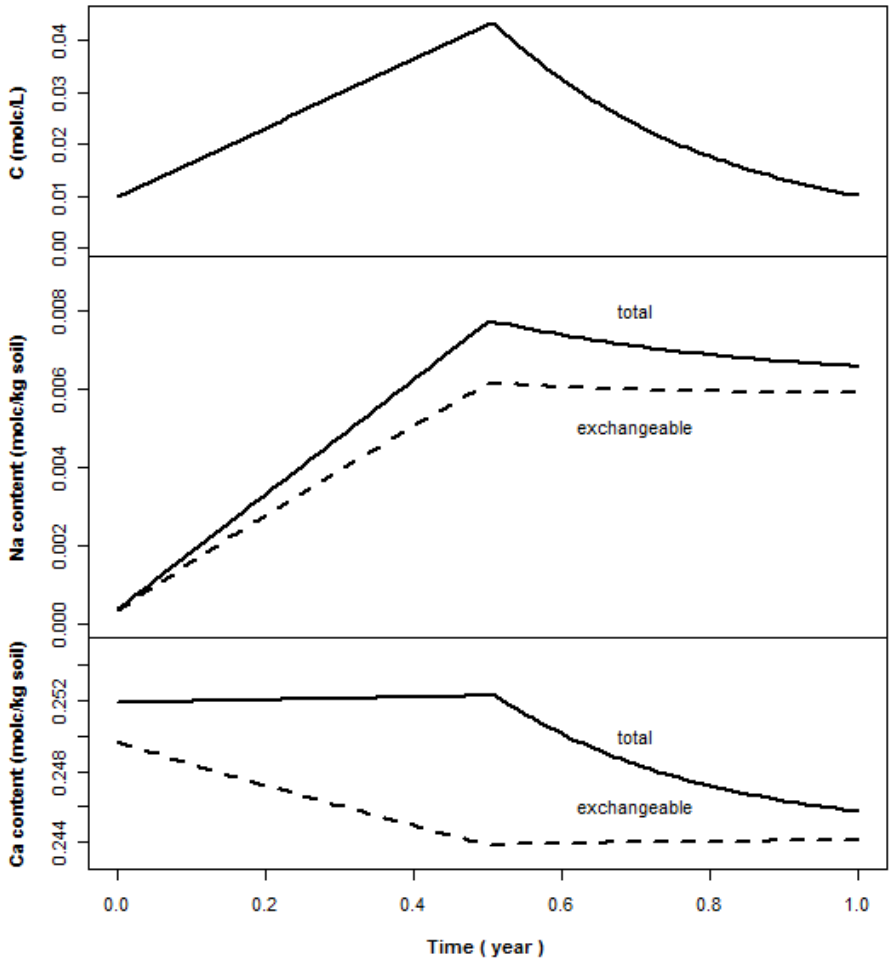

Figure 2.2: Salt concentration *C*, sodium contents and calcium contents during an accumulation period followed by a leaching period, both of half a year. Parameters of Reference case Table 1.

characterized by low electrical conductivity (EC_w = 0.2 mS/cm or $C_{in,l}$=0.002 mol_c/l) and lower SAR (equal to 3 $(mmol/l)^{1/2}$) than in the first part of the year. SAR is the sodium concentration divided by the square root of the divalent ion concentrations divided by 2

and EC is a measure of the conduction of electricity through water or soil water extract. As Figure 2.2 reveals, the salt concentration increases during the accumulation period because saline water enters the root zone, whereas leaching does not occur and all water that enters the soil is used for evapotranspiration ($\tau = 1$). We have made the common assumption that water that is evapotranspirated does not contain salts, i.e. that the salts present in the water remain in the soil. After half a year, the leaching period begins. We have chosen our parameterization for the case shown in Figure 2.2, such that soil salinity at the end of an entire cycle of one year is the same as that at the beginning of that year. In other words, as far as the total salinity is concerned, a periodic steady state is assumed to prevail from the outset. For successive cycles, the accumulation periods are described by equations (2.2) and (2.3) and the leaching periods by equations (2.4) and (2.5). Soil salinity increases linearly during the accumulation periods and decreases exponentially during the leaching periods, corresponding, respectively, to equations (2.3) and (2.5). If either an entire accumulation-leaching cycle is considered or a sequence of accumulation-leaching cycles, the initial concentration C_o and the input concentration C_{in} are different in equation (2.3) and (2.5), i.e. they are time dependent.

Whereas the salt concentration in the root zone has not increased at the end of each year, this is different for the *ESP* of the soil. Figure 2.2 shows that the sodium content, both in the soil solution as well as in the exchange complex, increases strongly during the accumulation period, due to the higher salinity of the incoming water, as well as due to the high sodium fraction of the irrigation water ($1\text{-}f = 0.95$). The adsorption of *Na* leads to desorption of *Ca* and this exchanged *Ca* must be present in the soil solution as no leaching occurs in this period. As total *Ca* does not change much, a significant redistribution occurs: part of *Ca* in soil redistributes from solid to solution phase. The driving force of this redistribution is the dominance of *Na* in the irrigation water and the decreased preference of the exchange complex for *Ca* at elevated salinity (*Bolt and Bruggenwert, 1976; Appelo and Postma, 2005*). During the leaching phase, when good quality irrigation water is used, partly for flushing the root zone, exchangeable *Ca* is almost constant, but total *Ca* decreases. This shows that part of the *Ca* desorbed during the accumulation phase is leached in the subsequent leaching phase. In other words, the results of Figure 2.2 imply that the nonlinearity of exchange causes *Ca* to be exchanged

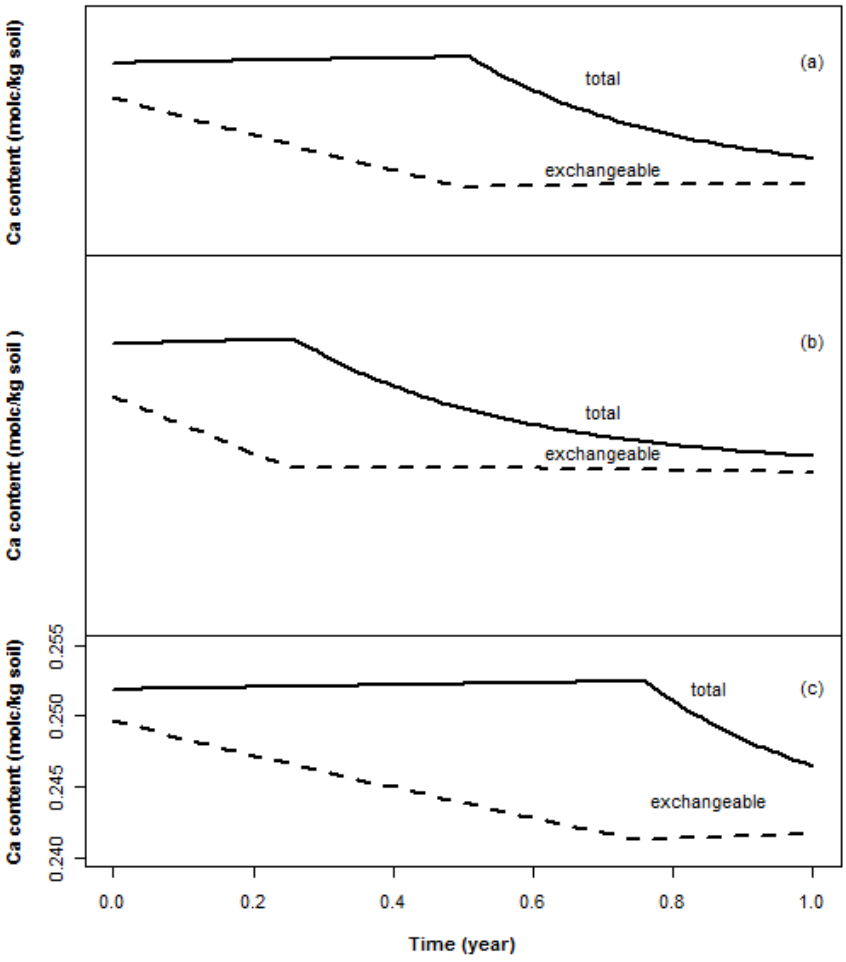

Figure 2.3: Quantity of total calcium (solid lines) and calcium in exchange complex (dashed lines) for three different durations of the periods of accumulation and leaching. Fig. 2.3a gives reference case of 0.5 year, Figure 2.3b and 2.3c give accumulation periods of 0.25 and 0.75 year. Other parameters correspond to Figure 2.2.

by *Na* during periods with elevated salinity, by which *Ca* is prone to removal during the leaching period. The combination of nonlinearity of the Gapon equation and the fluctuating salinity (*C*) leads to a preferential leaching of *Ca* and an increasing *ESP* even if salinity as such does not change from year to year.

For illustration, in Figure 2.3 we show that the duration of accumulation and leaching periods does not affect the essence of preferential leaching of *Ca*. Increasing the duration of the accumulation period (Figure 2.3b-c) leads to a proportional increase of the amounts of *Na* and *Ca* added during this period. It does not, however, lead to proportional increase of the leached *Ca*, due to the nonlinearity of exchange.

Figure 2.4 illustrates the behavior of calcium between soil solution and exchange complex. Calcium is desorbed during accumulation, as ionic strength increases and sodium adsorbs. This is due to the decreasing preference of the solid phase for divalent cations when ionic strength increases. The calcium that is thus released by the complex is prone to leaching in the following leaching period where better quality water enters the soil and removes ions through leaching. For the shown first cycle, we observe that no desorption occurs during the leaching period. Instead, a slight re-adsorption of calcium occurs as the total salt concentration *C* decreases temporarily.

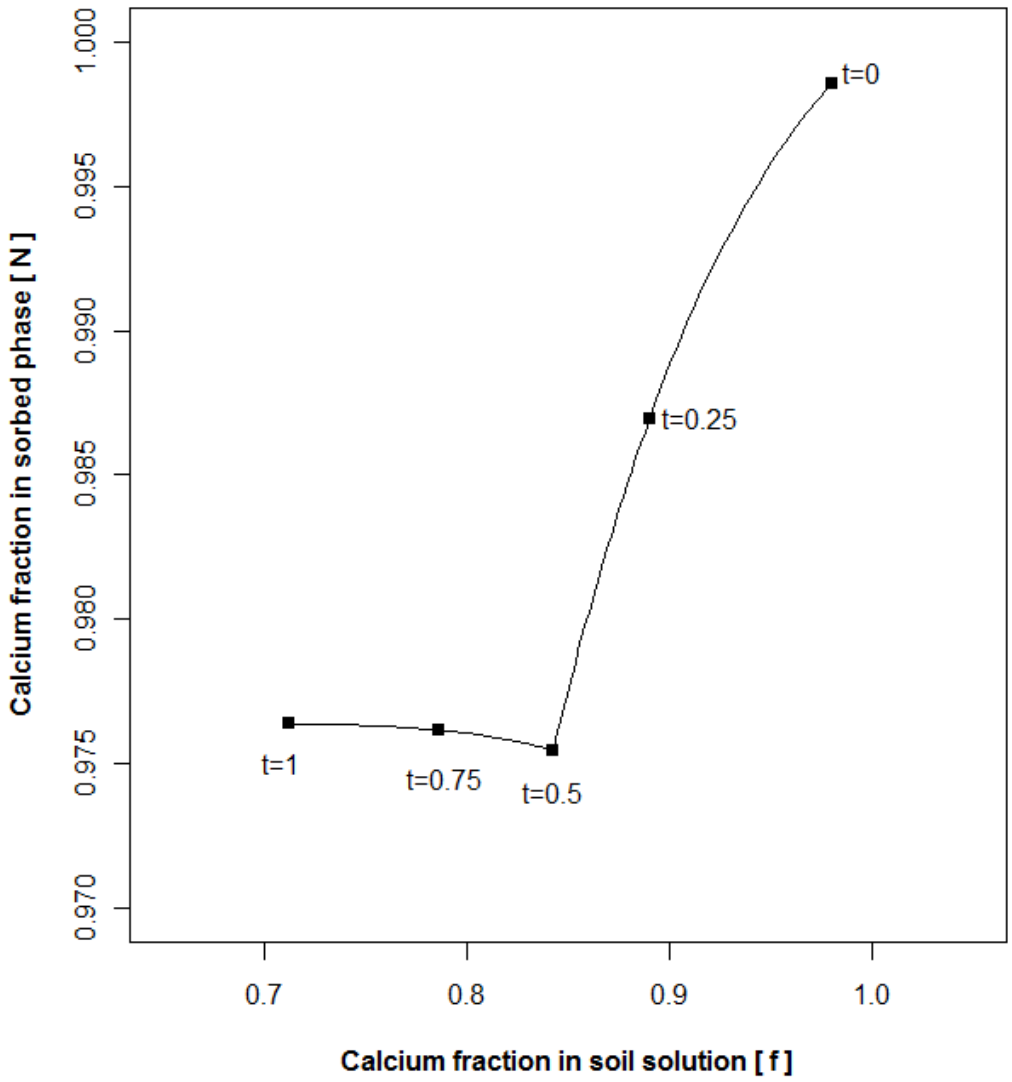

Figure 2.4: Phase (*f*,*N*) diagram showing adsorbed calcium fraction (*N*) as a function of dissolved fraction (*f*) during the first cycle of accumulation and leaching period.

In Figure 2.5 we show the change of total concentration and of *ESP* for fifty years, where each year has an accumulation and leaching period of half a year according to the reference situation of Table 2.1). We considered two different values of *CEC*. The *CEC* was chosen to agree to two different soil textures, i.e., a low value (*CEC* = 3 $mmol_c/100g_{soil}$) and a higher one (*CEC* = 10 $mmol_c/100g_{soil}$). Both *CEC*-values have been chosen relatively small to obtain a periodic steady-state for *ESP* within a short period of time. The general behavior is composed of two features. The first feature is the alternation between accumulation and leaching, resulting in the sawtooth pattern of Figure 2.5. We observe an increasing salinity and sodicity during each accumulation period, followed by the leaching of relatively saline/sodic water during each leaching period. The second feature is the longer (more than annual) term trend, where the salinity (*C*) is at periodic steady state whereas the sodicity (*ESP*) changes over a series of years.

In Figure 2.5, we have chosen the conditions such that the periodic total salinity $C(t)$ does not show an increasing trend. Instead, salinity increases in the accumulation (drought) period, to reduce again in the leaching period towards the initial value. This situation could be referred to as the one where water management with regard to salinity control is adequate: salinization in the dry season is compensated exactly by leaching during the wet season. For this situation, the salinity shows a sawtooth sequence in time, that does not reveal a trend for longer times (more than one year). In the real world the adjustment of salinity following a change in water management may take longer than one year, particularly if the new leaching fraction is low. Such situations are considered later (see especially Figure 2.8). However, for ESP this is not the case. Due to the nonlinear (square root) behavior with respect to total salinity (*C*) of the Gapon equation and the interannual *C*-variability, the sodicity shows an increasing trend for the first years towards a new final periodic pattern at an elevated *ESP*-level. As Figure 2.5 reveals, the approach towards the new dynamic equilibrium is slower if *CEC* is larger. This again is understandable, as with larger *CEC*, the quantity of *Ca* that needs to leach, and therefore the amount of *Na* that needs to be added in irrigation or groundwater to attain a designated *ESP*, becomes larger. For designated (constant) water quality, the volume and therefore the time to reach a new steady state increase with increasing *CEC*. The mathematical expressions that describe the time dependence of total concentration and of

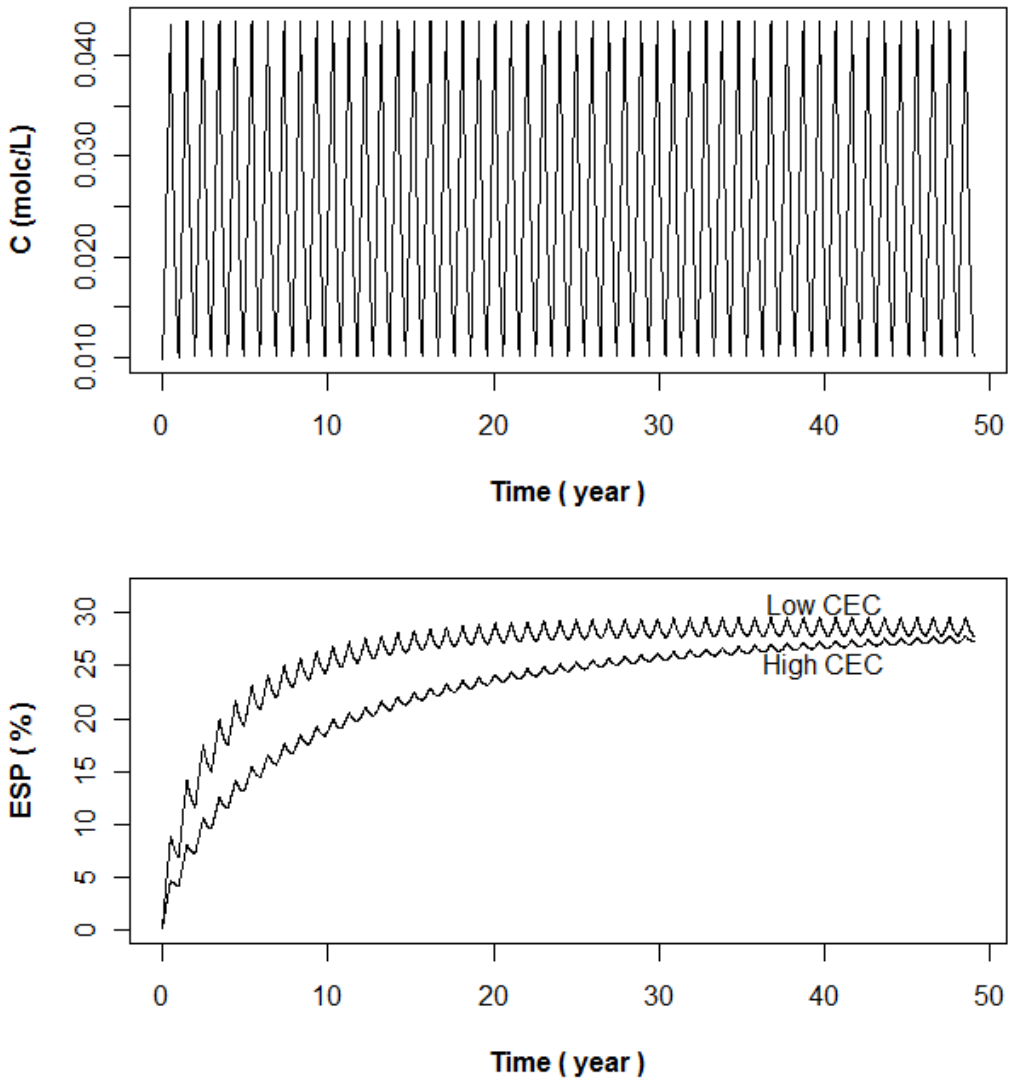

Figure 2.5: Soil salinity (*C*) and sodicity (*ESP*) of two different rootzone systems that differ only regarding *CEC*. Low CEC = *3* $mmol_c/100g_{soil}$ and high *CEC* = $10mmol_c/100g_{soil}$.

ESP give more detailed information on how the approach towards a dynamic equilibrium depends on system parameters. As Figure 2.5 reveals, the final situation regarding both *C* and the average *ESP* does not depend on the *CEC,* except that, as expected, the fluctuation of the *ESP* is smaller if the *CEC* is larger, also in the ultimate periodic steady state situation. Again, this is understandable, as on the longer term, both *C* and *ESP* depend on the quality of water entering the root zone (and temporal drought) rather than on soil properties, in complete agreement with the 'water quality controlled' (as opposed to 'complex dominated') situation mentioned by *Bolt and Bruggenwert* (1976, p71-72). The *ESP*-fluctuations depend on the periodic changes in incoming water quality and the

buffering capacity (CEC).

In Figure 2.6, we show a 3D representation in *f-N-t* space of the temporal changes of the composition of the soil solution and the exchange complex. After initial, large and almost proportional changes in solution and sorption phase chemistry, follows a very regular almost time independent pattern of intra-annual changes. Figure 2.6 also shows the development of the calcium fraction in the accumulation and leaching periods during 50 years. It is clear that in the exchange complex, chemical changes require a larger time to equilibrate, due to the large retardation factors involved. Thus, the Ca^{2+} ratio in the exchange complex N is more buffered than the Ca^{2+} ratio in soil solution as shown by the larger fluctuations between monovalent and divalent cations in the soil solution compared to the exchange complex.

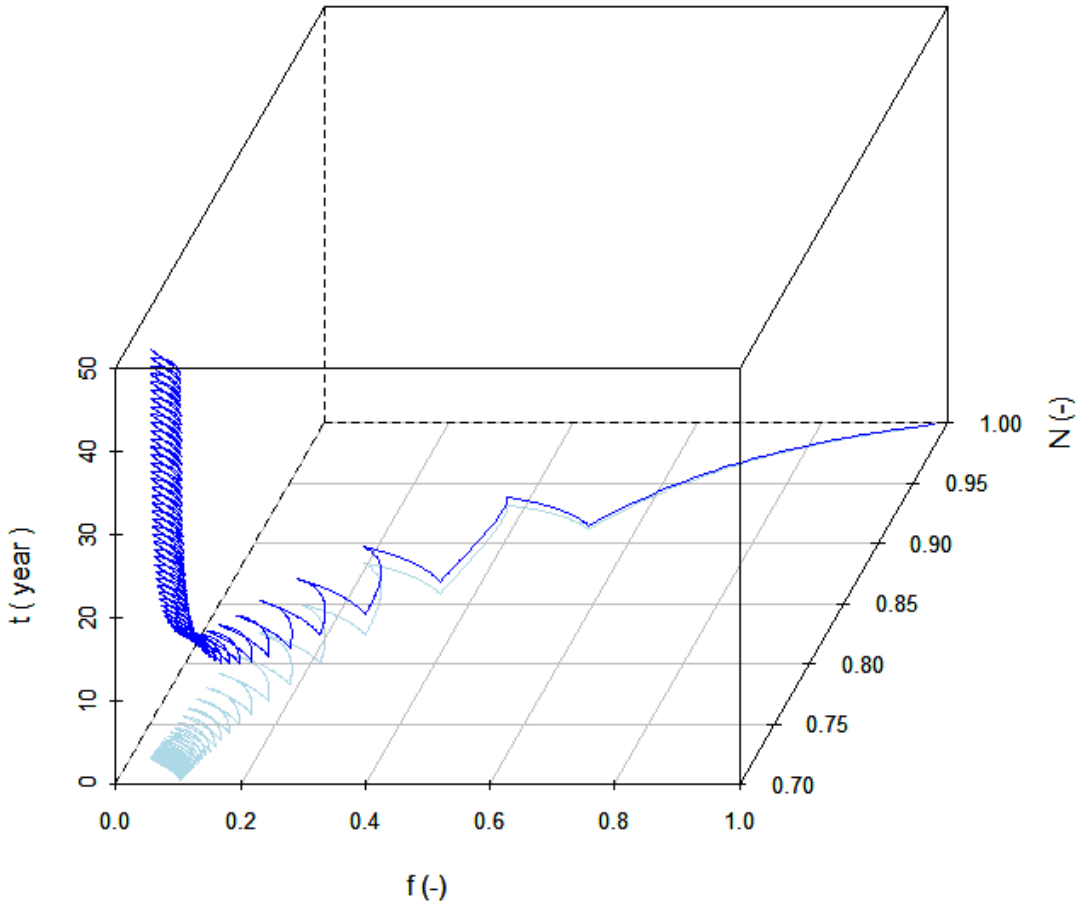

Figure 2.6: 3D graphic representation. The fraction (*N*) of calcium in the exchange complex is related with its fraction (*f*) in soil solution during a time period (*t*) of 50 years. The bottom line shows the projection of the vertical curve on the f-N plane. *CEC* = 3 $mmol_c/100g_{soil}$.

The results of Figure 2.5 that present the periodic steady state where minimum concentrations after each leaching period are always the same and small, indicate the importance of the concentration fluctuations: the higher concentrations as well as Ca-fractions in the incoming water both dictate the developing *ESP* and *ESP* may not return to its initial conditions even if concentration does. For that reason, we compare in Figure 2.7 situations (F) with fluctuating salinity (C), and situations without such fluctuations. We assume that for the non-fluctuating case (NF) the input concentration C_{in} and input salt fraction f_{in} are chosen such that the total salt and Ca masses added to the root zone are the same for fluctuating (F) and non-fluctuating cases (NF). For the non-fluctuating case, we assumed that 50% of water evaporates and 50% leaches, hence $\tau = 0.5$. We observe in Figure 2.7 that the differences between fluctuating and non-fluctuating cases are quite significant. The case F has larger maximum concentrations than the case NF. *ESP* increases most for the non-fluctuating situations, where consistently very poor quality water is entering soil, which leads to a much worse (regarding ultimate *ESP*-values) final situation. Given the high ESP values for t> 10 years, the assumed constancy of the 'Gapon exchange constant' is no longer valid (c.f. Figure 1 and text below it in *Bolt,* 1967; see also *Bolt,* 1982, p. 45, where the 1969 edition of *Richards et al.* (1954) is cited as basis for restricting the range of applicability to 1-N<0.4). The changes for case F are relatively fast, but stabilize at more moderate, yet problematic, values. In view of the same inputs of salt and calcium for both cases F and NF, and the larger maximum concentrations for case F compared with case NF, we conclude that the fluctuations of both C and f lead to a faster approach of the deteriorated periodic steady state for the *ESP*, but at a smaller average *ESP* level. For irrigation water management, it seems that a correct prognosis of the potential development of salinity as well as sodicity needs to take into account fluctuations in boundary conditions too.

2.3.1 Long term maximum and minimum salt concentrations

If water, salt, and sodium inputs vary greatly through the seasons, it is of profound interest for water and irrigation managers, to be able to quickly make a prognosis of the salinity and sodicity that may be the result and to do so with sufficient accuracy. For practical assessments, it is attractive if complicated numerical approximations can be avoided, in view of the specialist knowledge that is needed, but also because of

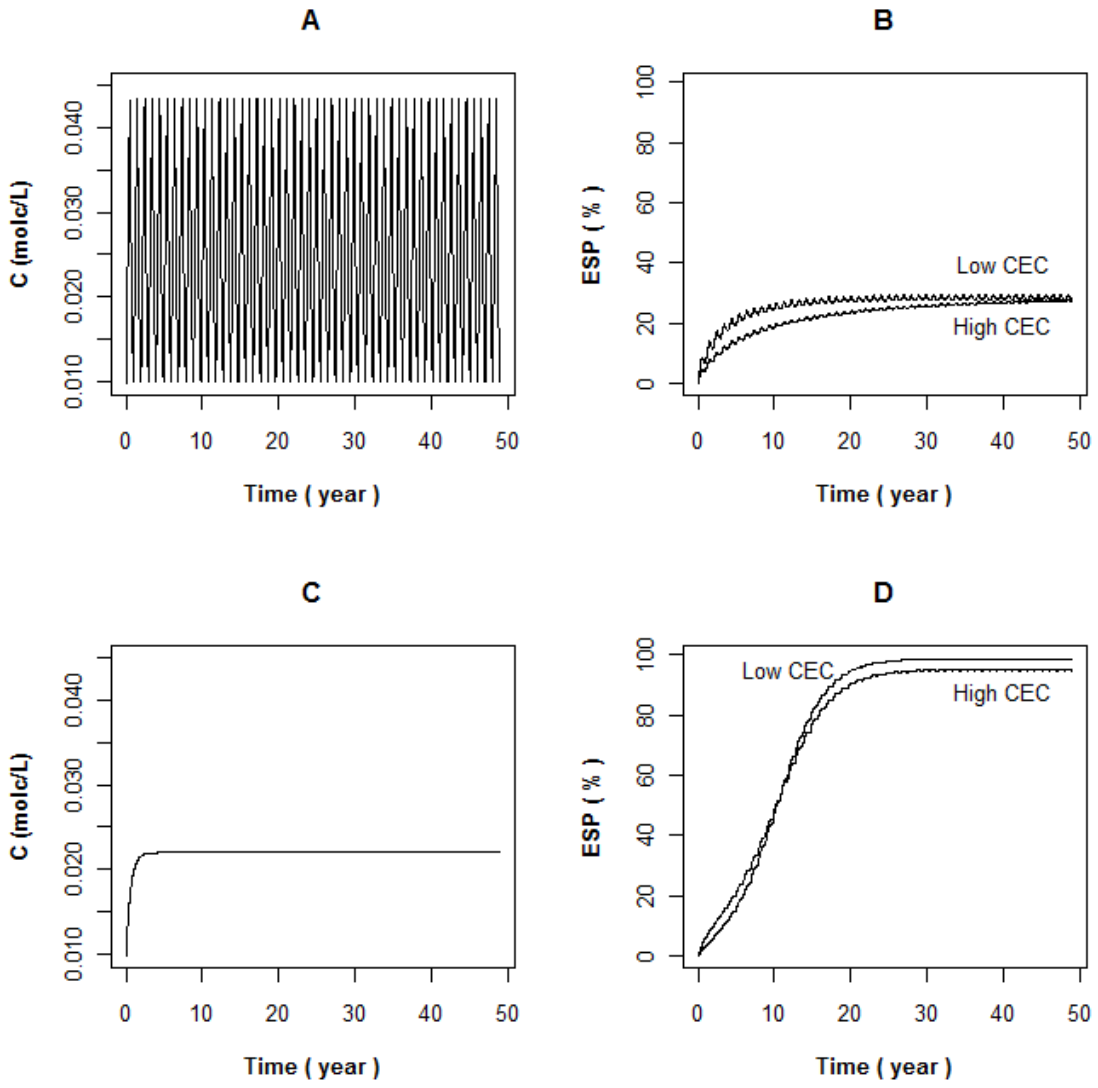

Figure 2.7: Comparison (*C*,*ESP*) of the cases with and without salinity fluctuations. The reference case (A,B) is compared with non-fluctuating situation where incoming water has an averaged quality (C) (average concentration of accumulation and leaching period of Table 2.1).

alternative approaches may be more transparent and therefore convincing and educational.

Of main interest for our purpose are the maximum and minimum concentrations that develop, in view of their effects on sodicity. In the following, we calculate the maximum and minimum concentrations, C_{max} (end of accumulation period) and C_{min} (end of leaching period), of the *C(t)* sawtooth pattern. Let C_a be the concentration at the end of the accumulation period and the beginning of the new leaching period and C_l the concentration at the end of the previous leaching period and at the beginning of the

accumulation period. From equation (2.2) it follows that the concentration at the end of accumulation period is given by:

$$C_a = C_l + \frac{j_a t_a C_{in,a}}{V}. \qquad \textbf{(2.12)}$$

From equation (2.4), we obtain the concentration C^*_l, at the end of the next leaching period:

$$C = C_{in,l} - [C_{in,l} - C_l - \frac{j_a t_a C_{in,a}}{V}]\exp(-\frac{j_l t_l}{V}) \cong C^*_{l.}. \qquad \textbf{(2.13)}$$

Only in the case of a periodic steady state (defined as the absence of a gradual change in the concentration levels at time scales exceeding a few years), will the concentrations at the end of successive leaching periods be the same, as the mass accumulated each cycle equals the mass leached during the next leaching period. For that situation, we can eliminate the concentration at the end of the leaching periods (as C_l^* becomes equal to C_l) by combining (2.12) and (2.13), to obtain after some rewriting an expression for the maximum concentration (at the end of each accumulation period):

$$C_a^m = \frac{j_a t_a C_{in,a}}{V}\left[1 - \exp\left(-\frac{j_l t_l}{V}\right)\right]^{-1} + C_{in,l}. \qquad \textbf{(2.14)}$$

The corresponding minimum concentrations in the periodic steady state are obtained by combining (2.14) and (2.12). The numerical simulations (obtained by integrating eq. (2.1)), the numerically integrated analytical result (eqs. (2.12) and (2.13)) and the maximum and minimum values in the periodic steady state (eqs. (2.14) and (2.12) valid for $t \rightarrow \infty$) appeared in good agreement [not shown] and motivated us to pursue a completely analytical result for the maximum and minimum concentrations at all times.
First, if we define:

$$\Delta t \equiv t_a + t_l; \quad t_a = t_l; \quad G \equiv \frac{j_a C_{in,a} \Delta t}{2V} + \frac{j_l C_{in,l} \Delta t}{2V},$$

and assume that all mass of the solute ($G.V$) is applied instantaneously at the beginning of each cycle of duration Δt, which implies that the leaching period covers this entire duration Δt. It is easy to derive for that case, that the concentration as a function of time is given by

$$C(t) = G.\sum_{i=1}^{n} \exp\left[-\frac{j_l}{V}\left(t - (i-1).\Delta t\right)\right], \qquad \textbf{(2.15)}$$

Observe that in this equation, we applied all mass instantaneously, and j_l was taken as in the definition of G and Table 2.1. Since in Table 2.1, the water fluxes j were equal for accumulation and leaching periods, respectively, this is the same as assuming that all incoming water is attributed to the leaching period whereas the incoming salt mass is given instantaneously (no water). Other options for 'averaging' fluxes were not explored in this paper. In (2.15), we recognize that a mass that has entered the root zone several cycles (i=1…n) ago is still contributing a little to the concentration building up towards a periodic steady state, as this mass has not yet leached completely. In (2.15), n=1 in the time interval $0<t<\Delta t$, n=2 for the time interval $\Delta t < t < 2\Delta t$ …n=n for the time interval $(n-1)\Delta t < t < n\Delta t$. Each term in the sum represents the contribution to $C(t)$ by one of the discrete solute applications at time intervals Δt, the term for i=1 representing the most recent application and the term for i=n representing the first application. From (2.15) follows that the successive relative maximum concentrations for the case of instantaneous inputs are given by

$$C_{\max} = G.\sum_{i=1}^{i=n} \exp\left(-\frac{j_l}{V}(i-1)\Delta t \right), \qquad \textbf{(2.16)}$$

where n=1 for the first relative maximum, which is equal to G, n=2 for the second relative maximum, …n=n for the nth relative maximum. This series of relative maxima is equivalent to the standard geometric series (*Beltman et al., 1996*)

$$\sum_{i=1}^{i=n} k\alpha^{i-1} = k\frac{1-\alpha^{n}}{1-\alpha}. \qquad \textbf{(2.17)}$$

Hence the nth relative maximum concentration is given by:

$$C_{\max} = G.\left[\frac{1-\left(\exp\left(-\frac{j_l}{V}\Delta t \right)\right)^{n}}{1-\exp\left(-\frac{j_l}{V}\Delta t \right)} \right]. \qquad \textbf{(2.18)}$$

The minimum concentration at the end of the nth leaching period is given by $(n+1)$th maximum minus G:

$$C_{\min}(n) = C_{\max}(n+1) - G. \qquad \textbf{(2.19)}$$

In order to check the validity of the above expressions, we have plotted the geometric series solution results (eqs. (2.18)-(2.19)) denoted by C_{max}, C_{min}, as well as $C(t)$ obtained by numerically integrating eq. (2.1) for different combinations of water fluxes j_a and j_l during, respectively, the accumulation and leaching periods. Figure 2.8 shows the maximum and minimum concentrations as well as the fully numerical results (obtained by integrating equation (2.1) for appropriate boundary conditions numerically), if the leaching period flux decreases from 300 l/m^2/year towards 15 l/m^2/year, and the concentration that builds up during 50 years increases considerably. Furthermore, the time needed to attain a periodic steady state increases also. The agreement between the numerical and analytical results is good and such good agreements were also obtained for a number of other situations, where we varied e.g. the volume of water (90 l/m^2) in the root zone. Increasing V leads to increasing dilution of salt entering the root zone with irrigation water and causes a smaller salt concentration in the root zone (see definition of G) and a longer time before the periodic steady state sets in. These effects can be anticipated on the basis of eq. (2.18), and similarly, the impact of changing j_a, and the incoming concentrations can be predicted.

The last panel (F) of Figure 2.8 shows how the *ESP* changes as a function of time, for the five cases of panels A-E. We can make the following observations: (1) *ESP* requires a longer time to attain the periodic steady state than C, (2) increasing concentrations $C(t)$ lead to larger *ESP*-values, and (3) larger concentrations $C(t)$ do not lead to proportionally larger final *ESP*-values.

Since the development of $C(t)$ can be well predicted, it is worthwhile to assess how well the $ESP(t)$-values can be predicted. For this purpose, we calculated both the concentration C and the *ESP* as a function of time, for the reference case values of j_a, j_l, V, C_{ina}, $C_{in,l}$ and f_a as well as for the cases where these parameters were 0.3 times and 2 times as large, respectively. As is apparent from the governing equations, changing the accumulation period flux j_a or changing its concentration $C_{in,a}$ is giving the same result and therefore a duplication. With the analytically determined maximum and minimum concentrations for t=50 years, using equations (2.18) and (2.19), and the Gapon equation, we determined $ESP(C_{max})$ and $ESP(C_{min})$, and their arithmetic average: analytically determined *ESP* (ESP_A).

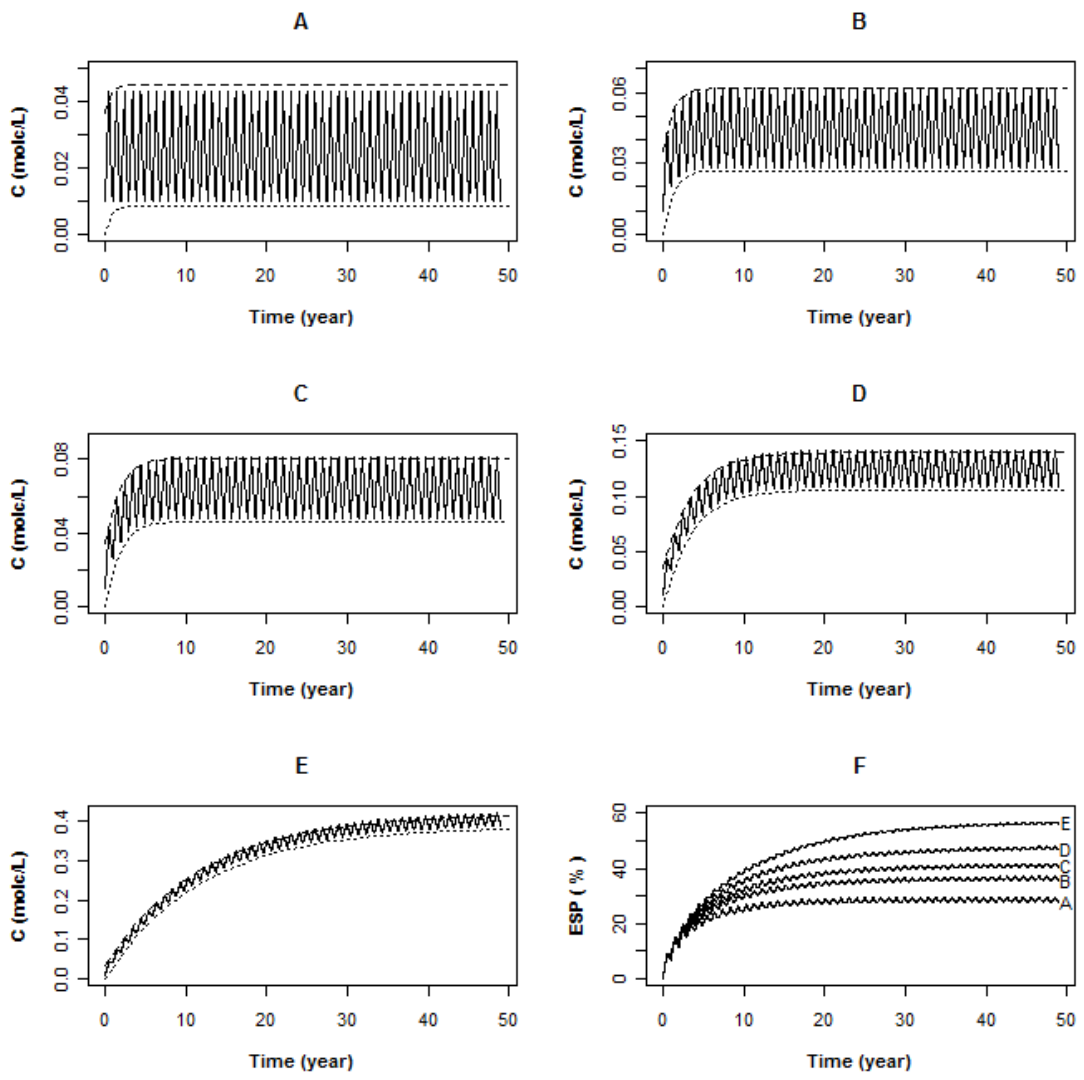

Figure 2.8: Salt concentration obtained numerically (*C*: solid line), maximum salt concentration (*Cmax*; upper dashed line, eq.(18)) and minimum salt concentration (*Cmin*; lower dashed line, eq.(19)) for the reference case (Table 1) where j_l is varied from 300 (panel A), 150 (B), 100 (C), 50 (D), and 15 l/m^2/year (E). Panel F shows *ESP* as a function of time, for the five cases of panel. A-E. The lowest curve in panel F corresponds to panel A, second lowest curve corresponds to panel B, and similarly other remaining curves correspond to panel C, D, and E respectively.

In view of the slight temporal variations, we determined numerical *ESP*(ESP_N) simply as being equal to the maximum numerically obtained *ESP*-value. The agreement between ESP_A and ESP_N is shown in Figure 2.9 and appears to be good enough to allow this fully analytical procedure as a reasonable prediction for *ESP*-values that develop under fluctuating salt levels. Obviously, to assess the sodicity status of a soil it is not sufficient to determine the composition of the soil solution, but in addition the composition of the exchange complex should be determined.

In this paper, we have not taken into consideration that the cations may also form chemical precipitates and minerals with anions. Such reactions would be expected predominantly for the divalent cations calcium and magnesium, with anions such as carbonates, bicarbonates, and sulfates. We ignored chemical precipitation as well as dissolution of solid salts and minerals, to keep the analysis as simple as possible. If precipitation were accounted for, that would in general lead to additional removal of *Ca* and *Mg* from the soil solution, as their salts and minerals (involving carbonates, bicarbonates, sulphates) are less soluble than those of *Na* and *K*. Since precipitation is usually a faster process than dissolution, dissolution during the inflow of water with better quality during the leaching process is unlikely to cause all precipitated *Ca* and *Mg* to enter the soil solution again. Hence, it is plausible that taking precipitation and dissolution into account would amplify the increasing *ESP* during salinity fluctuations.

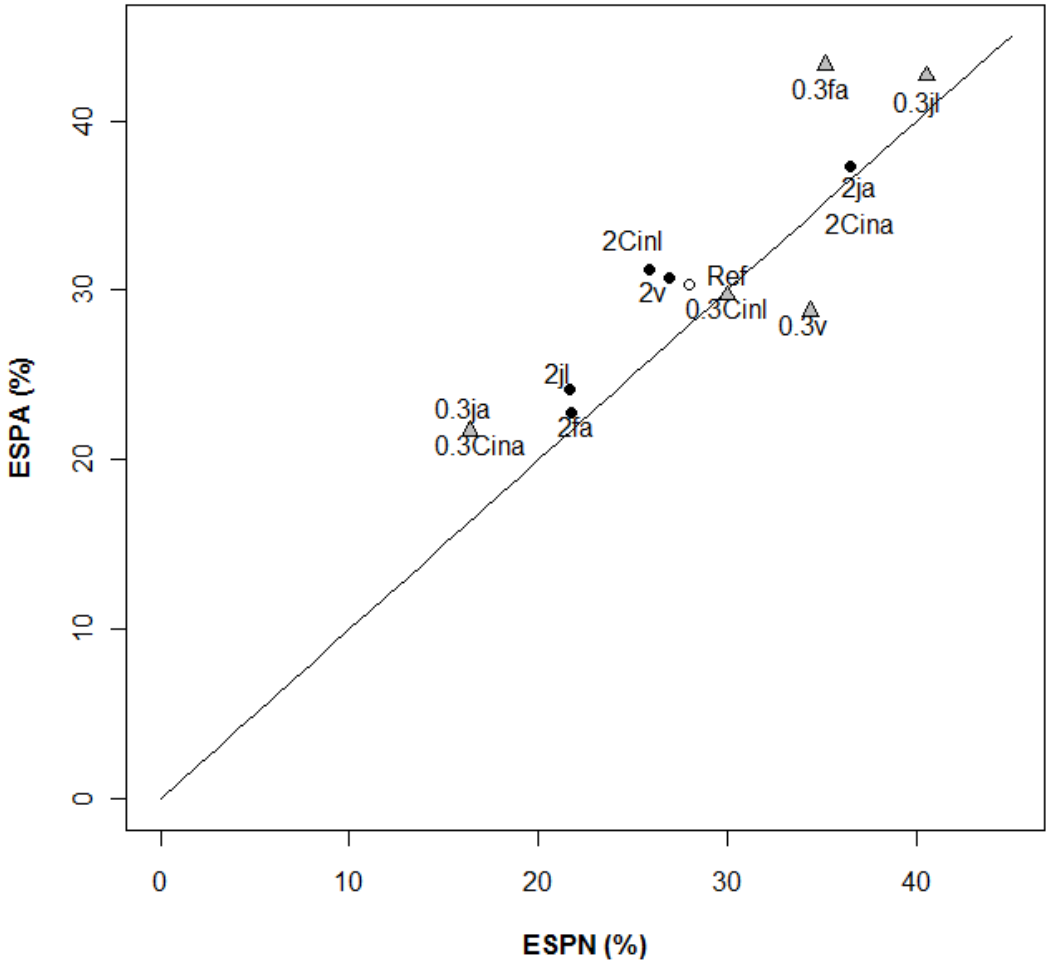

Figure 2.9: Comparison of analytically determined ESP_A and numerically determined ESP_N where six parameters are varied compared with their reference case values.

2.4. Conclusions

In this paper, we considered the change in sodicity for a soil, that is subject to temporal variations of soil salinity, e.g. due to periodic drought. Since model transparency improves our understanding of cause-effect relationships, we favored a model with small or modest complexity. A root zone model, similar to the approach advocated in ecohydrology (*Rodriguez-Iturbe and Porporato, 2004, Vervoort and van der Zee, 2008, 2009*) appeared suitable for that purpose.

We have shown that fluctuations in salt concentration in the soil solution can lead to sodicity (i.e., an increase in *ESP* to possibly hazardous levels) even in the absence of a gradual increase of salt concentration at time scales larger than one year. The motor of such increasing sodicity can be the variation of salinity and sodium concentration in incoming water as a function of time, even when at the end of the year, the salt concentration C has returned to its initial (and low) value. Even if soil and water salinity are controlled by wise water management, for sodicity this may not be the case: soil chemical aspects of soil water management may be more demanding than salinity management in a more strict sense, i.e., aimed at controlling salt concentrations. The extent to which irrigation managers allow soil to dry out between water applications becomes a factor to take into consideration in water management.

Whereas our work is limited to conceptual and modeling work, our results are supported by current strategies for conjuctive use of good quality canal and poor quality ground water (*Kaledhonkar et al., 2001*) and experimental evidence (*Minhas et al., 2007*). Both our model and the mentioned experiments show that an increase of *ESP* is possible due to cyclical variations in salinity. Confirmation also comes from field experiments of *Tedeschi and Dell'Aquila* (*2005*) that show an increase of soil salinity and sodicity during a seven year cycle. Experimental evidence was presented by *Miller and Pawluk* (*1993*) that fluctuations of the salt concentration can be accompanied by an increase of sodium.

For the root zone model, it appeared feasible to develop very simple analytical approximations for the concentration levels that correspond with the periodic variations. To obtain a rapid impression of the salinity levels that may develop, and thus, to get a

feeling for sodicity changes, the analytical approximations can be very useful and assist in practical, soil chemically based water management.

However, for an accurate assessment, some of the made limitations may need further consideration. For instance, the assumption of a constant Gapon constant has been mentioned to limit the actual validity range of *f*-values. Ignored was also the effect of salt concentration, *C*, and the composition of the exchange complex, *N*, on the soil hydraulic functions. As reviewed by *Bresler et al.* (*1982, pp 38-52*), in particular the alternation of large and small concentrations can have profound effects on the hydraulic functions as soon as Na occupies more than a few percents of the cation exchange complex. This feedback renders systems as considered in this paper even more complicated and worthwhile of investigation.

Acknowledgements

The first author acknowledges support of the International Research Training Network NUPUS, funded by the German Research Foundation (DFG; GRK 1398) and Netherlands Organization for Scientific Research (NWO; DN 81-754) and the Wageningen University IPOP programme ”Kust en Zee”. The second author acknowledges funding by the Higher Education Commission (HEC), Government of Pakistan.

We thank AWM Editor J.D. Oster for his pertinent comments, particularly regarding the range of constancy of the 'Gapon exchange constant' and the effect of sodicity on soil physical properties.

CHAPTER 3

Stochastic modeling of salt accumulation in the root zone due to capillary flux from brackish groundwater

S. H. H. Shah[1], R. W. Vervoort[2], S. Suweis[3], A.J. Guswa[5], A. Rinaldo[3,4], S. E. A. T. M. van der Zee[1]

[1]Soil Physics, Ecohydrology and Groundwater Management, Environmental Sciences Group, Wageningen University, P.O.B. 47, 6700 AA, Wageningen, Netherlands

[2]Hydrology Research Laboratory, Faculty of Agriculture, Food and Natural Resources, The University of Sydney, Australia

[3]Laboratory of Ecohydrology, ECHO/IEE/ENAC/EPFL, École Polytechnique Fédérale, Lausanne, Switzerland.

[4]Dipartimento IMAGE, Universita di Padova, Padua, Italy

[5] Picker Engineering Program, Smith College, 100 Green Street , Northampton, MA 01060, USA

Water Resources Research 47 (2011) W09506

3. Stochastic modeling of salt accumulation in the root zone due to capillary flux from brackish groundwater

Abstract

Groundwater can be a source of both water and salts in semi-arid areas, and therefore capillary pressure induced upward water flow may cause root zone salinization. To identify which conditions result in hazardous salt concentrations in the root zone, we combined the mass balance equations for salt and water, further assuming a Poisson-distributed daily rainfall and brackish groundwater quality. For the water fluxes (leaching, capillary upflow, and evapotranspiration), we account for osmotic effects of the dissolved salt mass using Van't Hoff's law. Root zone salinity depends on salt transport via capillary flux and on evapotranspiration, which concentrates salt in the root zone. Both a wet climate and shallow groundwater lead to wetter root zone conditions, which in combination with periodic rainfall enhances salt removal by leaching. For wet climates, root zone salinity (concentrations) increases as groundwater is more shallow (larger groundwater influence). For dry climates, salinity increases as groundwater is deeper due to a drier root zone and less leaching. For intermediate climates, opposing effects can push the salt balance in either way. Root zone salinity increases almost linearly with groundwater salinity. With a simple analytical approximation, maximum concentrations can be related with the mean capillary flow rate, leaching rate, water saturation and groundwater salinity, for different soils, climates and groundwater depths.

3.1 Introduction

Recently, a system analysis framework has been developed for the stochastic modeling of the soil water balance, in particular for rain-fed semi-arid ecosystems. This framework initially did not consider feedback of the groundwater with the root zone soil water dynamics. However, it is apparent that groundwater can be an important and even dominant factor with regard to vegetation development and patterning (*i.e. Lamontagne et al., 2005; Mensforth et al., 1994; Scott et al., 2006; Thorburn and Walker, 1994; Walker et al., 1993*).

During the past two years, interactions between groundwater and the root zone have been taken into consideration by *Vervoort and Van der Zee* (2008; 2009), by *Ridolfi et al*. (2008), *Laio et al.* (2009), and *Tamea et al.* (2009). *Vervoort and Van der Zee* (2008; 2009) considered the water balance for a vegetated soil, but without accounting for the impact of drainage on ground water levels. This influence of drainage on groundwater levels was taken into consideration by *Ridolfi et al*. (2008), *Laio et al.* (2009), and *Tamea et al.* (2009) for unvegetated and vegetated soil.

Whereas determining the influence of capillary upflow from the groundwater towards the root zone is of interest, in particular for semi-arid regions, the related hazards of salt accumulation in the root zone cannot be ignored. Water moving upward from the groundwater towards the root zone due to capillary forces is known to imply a salinization hazard (*Bresler et al., 1982; Howell, 1988*) and therefore shallow groundwater and water logging situations need to be avoided (*Berret-Lennard, 2003; Data and Jong, 2002; Pichu, 2006*). This understanding as such is not new. For instance, in Hungary, the depth of the groundwater level is a major factor in assessing the risk of root zone salinity and sodicity (*Szabolcs, 1989; Toth, 2008; Toth and Szendrei, 2006; Van Beek et al., 2010; Varrallyay, 1989*). The awareness that salts need to be leached to avoid soil salinity, is expressed in the concept of leaching fraction as given in the famous Handbook 60 (*Richard et al., 1954*). This concept has continued to be investigated throughout the past decades (*Corwin et al., 2007; Rhoades, 1974; Rhoades et al., 1973*). Besides the leaching fraction, both analytical and numerical modeling approaches for soil salinization have been elaborated, which are complementary in that they emphasize different aspects of the transport phenomena. For instance, *Raats (1975)* considered depth-time trajectories of water particles analytically, considering root water uptake (*RWU)* and the effect of *RWU* on salt concentrations. In this analysis, he calculated the depth-time trajectories of elements of water, steady and transient salinity profiles, and responses of salinity sensors at various depths following a step increase and a step decrease of the leaching fraction. An analysis with similarities to *Raats*, for linearly adsorbing solutes, was presented by *Schoups and Hopmans* (2002) for different scenarios.

In addition to such analytical, or analytically inspired numerical modeling, fully numerical models have been developed such as UNSATCHEM (*Simunek et al., 1996)*,

SWAP (*Kroes et al., 2008*), and HYDRUS (*Simunek et al., 1998; Simunek et al., 1999; Somma et al., 1998*). With these tools, it is possible to assess in detail how water flow, solute (salt) transport, and root water uptake affect each other. Although they are computationally more demanding than analytical models, computational power rapidly increases and this makes this constraint less important.

The scope of this paper is to assess, for a root zone in hydrological contact with groundwater, how salt accumulation is related to root-zone water dynamics, with the emphasis on the variability of these dynamics caused by atmospheric forcing. We are interested in the impact of climate drivers such as rainfall intensity, precipitation frequency, and evaporative demand, along with the influence of capillary upflow from the water table. In this work, we presume that the primary source of salt is from groundwater rather than irrigation water, as in the case of *Suweis et al.* (2010).

To keep the emphasis on precipitation timing and intensity, we follow the framework presented in *Rodriguez-Iturbe and Porporato* (2004) and consider the root zone as a single layer without resolving the dynamics of infiltration. *Guswa et al.* (2002; 2004) examined conditions where such a simplification is appropriate; they found that when vegetation has the ability to compensate for heterogeneous distributions of soil moisture, either through hydraulic redistribution, or compensatory uptake, the single layer and spatially explicit models gave similar results. Such compensation ability has been demonstrated for plants in many different ecosystems (*Caldwell et al., 1998; Dawson, 1993; Domec et al., 2010; Green et al., 1997; Katul and Siqueira, 2010; Nadezhdina et al., 2010; Oliveira et al., 2005*).

To understand the development of salinity of the root zone, we consider a conceptual model of a homogeneous root zone with thickness Z_r (cm), porosity ϕ and groundwater Z (cm) below the soil surface: Figure 3.1. The root zone water balance is studied in the probabilistic framework of *Vervoort and Van der Zee* (2008) in view of the random character of rainfall. The random fluctuations of root zone water saturation affect the fluctuations of salinity through the contribution of the various fluxes into and out of the root zone, and this balance is the primary scope of this article.

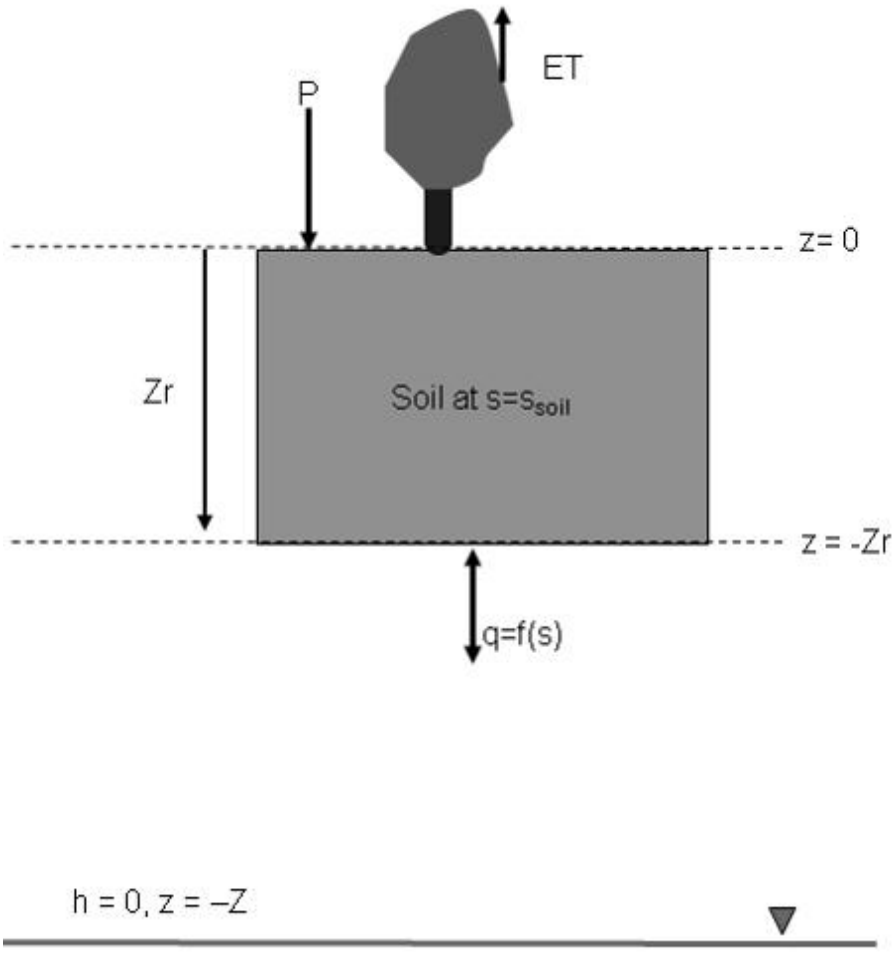

Figure 3.1. Conceptual model for groundwater uptake by vegetation in a semi-arid system.

3.2 Methods

3.2.1 Background theory

Our point of departure is the ecohydrological model including capillary upflow described by *Vervoort and van der Zee* (2008). Evaporation and rainfall occur at the soil surface and affect mainly the water storage in the root zone. No hysteresis occurs and the soil water profile below the root zone has a steady state. We assume that the groundwater level is constant, which means that the fluctuations in the groundwater level occur at a much larger time scale than the fluctuations in climate drivers (i.e., years versus days and weeks). We further assume that the soil is initially free from salts and that all salt originates from the groundwater, in what commonly is called primary salinization (*Szabolcs, 1989; Varrallyay, 1989*).

We have water flow due to rainfall/irrigation (*P*), leaching (*L*), capillary upflow (*U*), and evapotranspiration (*ET*). This leads to the water balance equation

$$\phi Z_r \frac{ds}{dt} = P - ET(s) + U(s) - L(s) \qquad \textbf{(3.1)}$$

Where s is the soil saturation ($0 < s < 1$), and we distinguished all inflow and outflow water fluxes, instead of just a loss function, as they may carry different salt loads.

Rainfall is modeled as a marked Poisson process with a mean storm arrival rate λ (event/day) and each storm carries a random amount of rainfall (*Rodriguez-Iturbe et al.*, 1999). Following *Laio et al.* (2001), the climate is subsequently defined by the parameters λ′ and γ which arise from the Poisson distributed daily rainfall. The parameter λ′ is equal to $\lambda e^{-\Delta/\alpha}$, where Δ is the interception depth (cm), α is the mean storm depth (cm/event). The parameter γ is equal to $\frac{\phi Z_r}{\alpha}$ or, equivalently, 1/γ is the root zone weighted mean storm depth.

The effective normalized water loss function of the root zone (i.e. $\rho = (ET(s)+L(s)-U(s))/(\phi Z_r)$), that also takes into account the effect of the interaction with the groundwater is (*Vervoort and Van der Zee*, 2008):

$$\rho = \begin{cases} (\eta - m_2)\left(\dfrac{s - s_{cr}}{s^* - s_{cr}}\right) & s_{cr} < s \le s^* \\ \eta - m_1\left[1 - e^{\beta(s - s_{\lim})}\right] & s^* < s \le s_{\lim} \\ \eta + m\left[e^{\beta(s - s_{\lim})} - 1\right] & s_{\lim} < s \le 1 \end{cases}$$

$$m_2 = \frac{K_s G}{\phi Z_r}$$

$$m_1 = \frac{m_2}{\left[1 - e^{\beta(s^* - s_{\lim})}\right]} \qquad \textbf{(3.2)}$$

$$m = \frac{K_s}{\phi Z_r\left[e^{\beta(1 - s_{\lim})} - 1\right]}$$

$$\eta = \frac{E_{\max}}{\phi Z_r}$$

where the dimensionless parameter G is a function that describes the relationship of the capillary flux with the groundwater depth, the bubbling pressure (h_b) and the hydraulic shape parameters α_e and b and has the following functional form (*Eagleson*, 2002):

$$G = \alpha_e \left(\frac{h_b}{Z - Z_r} \right)^{2+3/b} \quad \textbf{(3.3)}$$

The parameters m_2 and m_1 are constants, where m_2 represents the maximum capillary flux for a given groundwater depth and hydraulic properties (encapsulated in G), while m_1 is equal to m_2 normalized for the reduction in capillary flux with increased saturation.
We use β as a soil hydraulic shape parameter, which is related to b, the slope of the water retention curve.

The first important boundary is s_{lim} , which defines the point where, coming from the saturation end, the soil storage moves from leaching (L) to capillary upflow (U), i.e. the point where $L = U = 0$. In other words, at any point wetter than s_{lim}, $U = 0$ and at any point drier than s_{lim}, $L = 0$. If we move from s_{lim} towards drier conditions, we will reach an important boundary s_{cr}, which depends on the water table depth. This point is the soil saturation for which $U = ET$ and thus the resultant loss from soil storage is 0. The soil will never dry out below this level of soil saturation because at this point (and below), the potential capillary flux is either equal to or greater than the actual evaporation losses and thus all evaporation demand can be supplied by the capillary flux. Further, s^* is the soil saturation level at which the transpiration becomes limited by available soil moisture, s_w is soil saturation at wilting point, which is used for calculating s_{cr}. Finally, E_{max} is the maximum evapotranspiration (*Rodriguez-Iturbe and Porporato*, 2004) and η is the root zone depth normalized version of E_{max}.
Because the loss function (3.2) is fundamental for this work, we show it in Figure 3.2 for different groundwater depths from soil surface (Z in cm) and one combination of 'other' parameters such as soil type, climate and vegetation. Note that this loss function represents net loss of water from the root zone since it incorporates the effect of capillary upflow, which is a gain to the root zone.

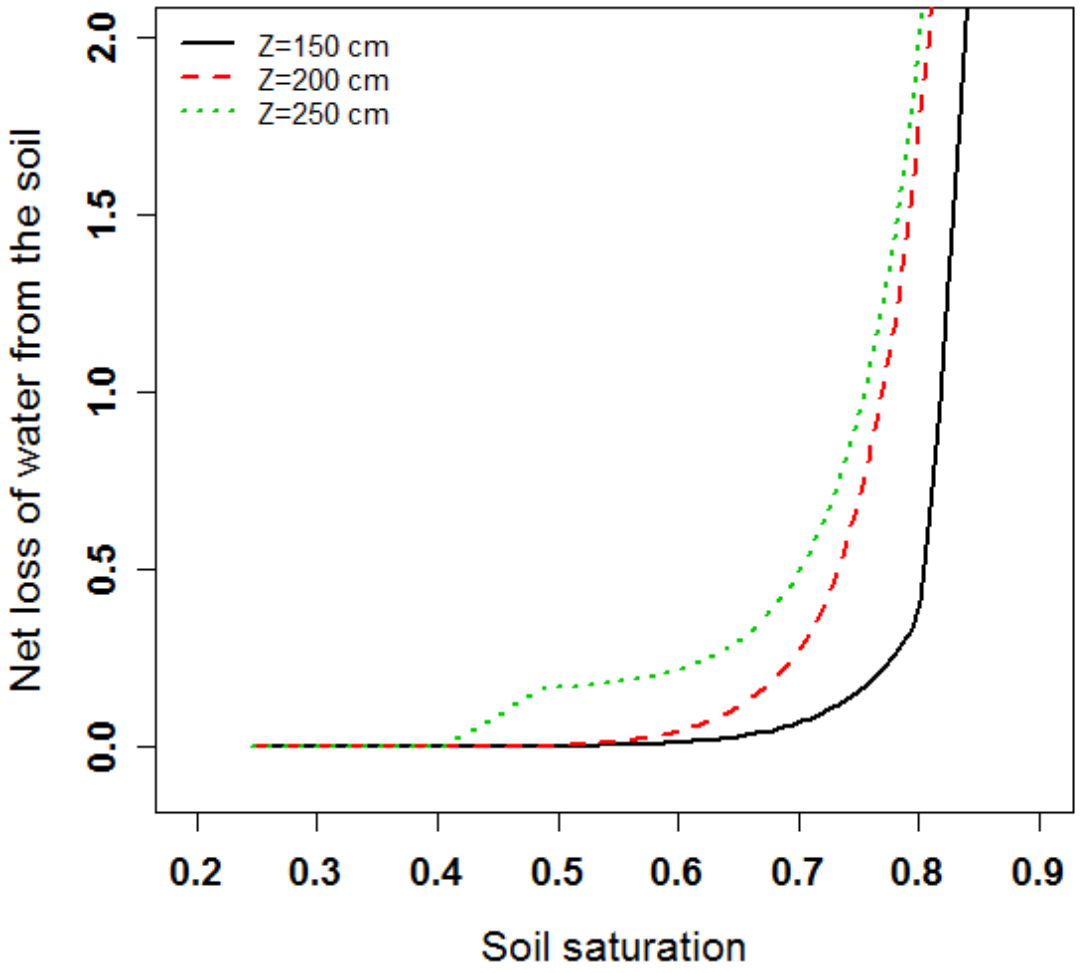

Figure 3.2. Graphical representation of equation 3.2 (net loss of water as a function of soil saturation) for sandy clay loam soil (*SCL*, Table3.1) under three different groundwater depths (*Z* = 150 cm, *Z* = 200 cm, *Z* = 250 cm). E_{max} = 0.37 cm/day and vegetation is trees (Table 3.2).

In contrast to the more traditional Eagleson approximation (*Eagleson*, 1978, which we applied in *Vervoort and van der Zee,* 2009), drainage and capillary upflow never occur simultaneously in this function, more specifically, it contains a switching behavior for which the switching point (s_{lim}) is dependent on the groundwater depth. In order to separately calculate the capillary upflow (U), we have used equation 4 (*Vervoort and Van der Zee*, 2008) and the leaching flux has been calculated by using the lower limit of soil saturation (excluding the η parameter) of equation 3.2. The maximum evapotranspiration (E_{max}) has been calculated by using the *Teuling and Troch* (2005) equation. We checked that sum of separate loss function and combined calculation of the fluxes combined in (3.2) indeed gave the same result.

$$q_{total}(s) = \begin{cases} -m_2 & s_{cr} < s \le s^* \\ -m_1\left[1 - e^{\beta(s - s_{\lim})}\right] & s^* < s \le s_{\lim} \end{cases}$$

$$m_2 = \frac{K_s G}{\phi Z r} \qquad \textbf{(3.4)}$$

$$m_1 = \frac{m_2}{\left[1 - e^{\beta(s^* - s_{\lim})}\right]}$$

Also in Figure 3.2, the impact of *ET* can be seen when the ground water level is deep and cannot be observed for shallow water tables. For shallow water levels, the effect of *ET* is not visible, because capillary upflow is in balance with *ET* losses. Basically the impact of capillary upflow is that at some value of *s* the total loss (*ET* – *U*) from the root zone actually equals zero. The soil will never dry out below this level of soil saturation because at this critical saturation (s_{cr}) and below, the potential capillary flux is either equal to or larger than the actual evaporation losses and thus all evaporation demands can be supplied by the capillary flux. In reality, below s_{cr} the potential capillary upflow will be reduced until capillary upflow matches the actual *ET*. This also implies that s_{cr} is the minimum soil saturation level that the soil will reach a particular groundwater level, *ET* demand curve, and soil type and therefore these factors depend on s_{cr}. For shallow groundwater tables, s_{cr} is equal to s^* and for deep groundwater tables, s_{cr} is equal to s_w. As a result the ET signal is more clearly visible for deep groundwater tables in Figure 3.2.

The model as formulated in eq. (3.1) and (3.2) can be solved analytically to give the soil saturation probability density function (*Vervoort and Van der Zee*, 2008), but all other salt related variables and the separate fluxes (i.e., *U*, *L*, *ET*) must be calculated numerically. In this study, we will concentrate on the situation where the capillary fluxes supply sufficient moisture so $s_{cr} \ge s_w$ and $m_2 > \frac{E_w}{\phi Z_r}$, where E_w is the residual soil evaporation. Strictly speaking, equation (3.2) only applies in the case that $m_1 < \eta$, which means $s_{cr} < s^*$, or where the capillary fluxes are too small to maintain evapotranspiration at maximum capacity (*Vervoort and Van der Zee*, 2008).

A different situation arises for very shallow water tables, where $m_1 > \eta$. In this case $s_{cr} > s^*$ and equation (3.2) simplifies to two piecewise linear sections (see eq. (11) of *Vervoort and van der Zee*, 2008), which means the capillary fluxes allow

evapotranspiration to always be at its maximum capacity and soil water saturation never drops below s^*.

3.2.2 Salt Transport Equation

Whereas in general, each of the water fluxes implies salt transport, some of these dominate salt accumulation. Except for special cases such as coastal regions that experience salt spray (*Suweis et al.*, 2010), the salt flux involved with atmospheric deposition and rainfall may be often ignored. Irrigation with water containing salts means salt fluxes at the soil surface are important (*Bresler*, 1981; *Runyan and D'Odorico*, 2010), where the use of waste water for irrigation is a special case (*Jalali et al.*, 2008). Still, in this paper, we disregard both poor quality irrigation water and salt deposition via rainfall. Plants may uptake salts and dicotyledonous halophytic plants and crops may even require some NaCl for optimal growth (*Rozema and Flowers*, 2008). However, the mass fluxes involved in salt uptake and removal from the field in harvested products are generally quite limited (*Shani et al.*, 2007). For the present case, we therefore only consider the salt mass fluxes due to capillary flux from groundwater, which in this study has a constant concentration C_Z (for our reference case equal to 0.02 mol_c/L) and is unaffected by the processes in the root zone, and the leaching towards groundwater of salts that have accumulated in the root zone. We obtain the following balance equation for the salt mass M:

$$\frac{dM}{dt} = \phi Z_r \frac{dsC}{dt} = U(s)C_Z - L(s)C \qquad \textbf{(3.5)}$$

where C is the salt concentration in the root zone in mol_c/L, C_z is the salt concentration of the groundwater at depth Z in mol_c/L, M is the salt mass in mol_c/m^2 , and s is the soil saturation. As (3.5) shows, we disregard chemical interactions such as sorption and precipitation or dissolution (*Shani et al.*, 2007; *Van der Zee et al.*, 2009). Since we focus on easily soluble salts such as NaCl that dominate seawater and are often the most important salts for ground water (*Appelo and Postma*, 2005), the omission of chemical interactions is appropriate. We recognize that even for sodium, this is an approximation (*Bolt*, 1982; *Kaledhonkar et al.*, 2001; *Van der Zee et al.*, 2009). The coupled equations (3.1) and (3.5) are solved numerically to provide root zone saturation, salt mass and concentration, and the contribution of various water and salt fluxes.

The matric potential ($h(s)$) of the root zone controls the water fluxes. In the analysis of *Vervoort and Van der Zee* (2008), however, the main variable is the soil water saturation, s, which is uniquely related to the matric potential. In the present case, besides the matric potential that predominantly reflects capillary forces, the osmotic potential is also important, given the presence of salts. Therefore, we need to combine the matric and osmotic potentials, and following the concept of chemical potential, determine a 'virtual' saturation, s_v, using $s(h)$, which then controls evapotranspiration, capillary and leaching fluxes. Assuming validity of Van't Hoff's law, we used a salinity correction based on additive properties of matric and osmotic potentials (*Bras and Seo*, 1987; *De Jong van Lier et al.*, 2008) even though this convention can be disputed. The osmotic potential follows the Van't Hoff's Law. Once the ionic components of the salt solution in the root zone is known, π (C) is a linear function of the salt concentration C, which can be written as

$$\pi(C) = kC \tag{3.6}$$

where π is osmotic potential (MPa), C is the salt concentration expressed as mol_c/L, and k is a coefficient that includes the effect of temperature, electrolyte properties, and unit conversion factor, which is equal to 3.6 $MPa.L/mol_c$. The osmotic potential can subsequently be combined with the *Brooks and Corey* (1966) equation which describes the matric potential relationship with soil saturation:

$$h(s) = h(1)\left(\frac{s}{s_s}\right)^{-b} \tag{3.7}$$

Where $h(1)$ is the saturated soil matrix potential (MPa), b is a parameter related to conductivity and tortuosity (pore size distribution index and related to the earlier mentioned parameter β), and s_s is soil saturation (s_s =1). We can combine (3.6) and (3.7) and rearrange to obtain the virtual saturation s_v (*Bras and Seo*, 1987).

$$s_v = s_s h(1)^{1/b}\left(h(1)\left(\frac{s}{s_s}\right)^{-b} + kC\right)^{-1/b} \tag{3.8}$$

The resulting virtual soil saturation is the soil saturation available to plants taking into account both matric and osmotic effects.

3.2.3 Calculations

Numerical simulations were based on a similar parameterization as *Vervoort and Van der Zee* (2008) (Table 3.1 & 3.2) and therefore allows for comparison with their results (which were focused towards analytical pdfs of the root zone water saturation).

Table 3.1. Soil properties used in the simulations. Soil hydraulic data are based on standard Australian soils in "Neurotheta" (*Minasny and McBratney*, 2002).

Soil type	ϕ (porosity)	K_s (cm/day)	b	$\overline{\Psi}_s$ (MPa)	Ψ_{s,s_h} (MPa)	s_{fc}
Heavy Clay (HC)	0.45	2.82	16.2	-1.4E-3	-10	0.88
Medium Clay (MC)	0.44	6.04	13.5	-1.7E-3	-10	0.87
Light Medium Clay (LMC)	0.42	3.51	13.5	-1.5E-3	-10	0.86
Sandy Clay Loam (SCL)	0.37	52.08	6.41	-1.2E-3	-10	0.73
Loamy Sand (LS)	0.37	175.3	4.52	-0.7E-3	-10	0.57

Different Australian soils were considered where the porosity ϕ was set equal to θ_s as estimated with the van Genuchten pedotransfer functions in Neurotheta (*Minasny and McBratney*, 2002).

Table 3.2. Vegetation properties used in the simulations following *Porporato et al.* (2001).

	Trees
Zr **(cm)**	100
Δ **(cm)**	0.2
$E_{\max}$ **(cm/day)**	0.5
E_w **(cm/day)**	0.01
$\psi_{s,s*}$ **(MPa)**	-0.12
$\psi_{s,sw}$ **(MPa)**	-2.5
Leaf area index (ξ)	2.5*

* from (*Whitehead and Beadle*, 2004)

Some representative climate parameters were calculated from long term rainfall data for several locations in Australia (*Vervoort and Van der Zee*, 2008) and this defined the range of possible values for α and λ used in this article. The climate is characterized by $\alpha\lambda/E_{max}$ which gives dimensionless values; 0.89, 1.35, and 1.89 for dry, semi-arid and wet climate respectively. These dimensionless values are calculated on the basis of input values of α and λ used in the rainfall model. Maximum evaporation (E_{max}) was calculated using the *Teuling and Troch* (2005) equation and values are listed in Table 3.3.

Table 3.3. Climate properties used in simulations and these properties were calculated using the methods described by *Rodriguez-Iturbe et al.* (1984).

Climate	α (cm/event)	λ (event/day)	Modelled rainfall input (cm/day)	E_{max} (cm/day)
Dry	1.1	0.3	0.33	0.37
Semi-arid	1.25	0.4	0.5	0.37
Wet	1.4	0.5	0.7	0.37

In the model, we assume that only part of the real rainfall may enter the root zone. Note that real rainfall is not exactly the same as rainfall input (input values of $\alpha\lambda$), because rainfall model generates relatively less rainfall than the rainfall input taking into account interception. The really modelled rainfall is also called achieved rainfall or actual input. If the amount of rainfall is greater than the current storage capacity, which is related with 1 - s, then the excess rainfall is lost due to runoff and remaining rainfall enters the system

for soil saturation calculations (following the original model by *Laio et al.* (2001)). Surface runoff due to a limited infiltration capacity could also be considered (*Appels et al.*, 2011), but will not affect the main message of our paper especially for larger root zone thicknesses. Model calculations were done for a simulated time of 100 years, as this was needed to reach a steady state salt concentration. In view of the boundary conditions that change with time, this refers to a steady state in the trend of erratically fluctuating state variables, such as saturation, salt mass, concentration, and various fluxes. In our analysis, the first simulated year was ignored as a warm up period, and results were therefore obtained for a 99 year period and mean were stabilized during this period as shown in Table 3.4. For the period after the initial conditions had decayed, long term (pseudo-steady state) statistics were calculated. Typically, statistics and pdfs required computed times larger than 20 years. We determined these properties for the period ranging from about year 30 to year 100, but for comparison with the analytical solution for saturation in Figure 3.3, about a threefold larger period was considered to more accurately determine the pdfs. All the values under each climate are calculated for 1 realization of rainfall function as different realizations only cause small variations in the numerical outcomes.

Table 3.4. Long term average values of salt concentration, soil saturation, salt mass, capillary flux, leaching flux, evapotranspiration(soil saturation), change in soil saturation storage and runoff for six groundwater depths and three climates. The actual input represents the precipitation generated by the Poisson model using the standard α and λ parameters (Table 3.3) taking into account interception (*Laio et al.* 2001). The numerical error column represents the water balance closure error in the model for the 99 year simulations presented here.

GW Depth (cm)	Salt Conc. (C) (mol_c/L)	Relative Sat. (s)	Salt mass (mol_c/m^2)	Capillary Flux (cm/day)	Leaching flux (cm/day)	ET(s) (cm/day)	dS (cm/day) ($\times 10^{-5}$)	Runoff (cm/day) ($\times 10^{-5}$)	Actual input (cm/day)	Numerical error (cm/day) ($\times 10^{-5}$)
150	0.054	0.771	15.220	-0.137	0.058	0.298	-3.040	8.180	0.219	-0.11
200	0.056	0.697	14.423	-0.117	0.048	0.288	-3.270	0.000	0.219	-0.135
250	0.062	0.643	14.681	-0.083	0.033	0.269	1.450	0.000	0.219	-0.018
300	0.066	0.592	14.342	-0.055	0.022	0.252	8.510	0.000	0.219	-0.086
350	0.065	0.552	13.157	-0.037	0.015	0.240	8.370	0.000	0.219	-0.109
400	0.061	0.524	11.675	-0.026	0.012	0.233	6.490	0.000	0.219	-0.124
150	0.034	0.772	9.741	-0.134	0.090	0.354	-1.250	31.900	0.310	-0.516
200	0.035	0.700	9.050	-0.112	0.076	0.347	-1.090	5.200	0.310	-0.524
250	0.037	0.647	8.701	-0.078	0.054	0.334	-0.786	1.830	0.310	-0.497
300	0.036	0.600	7.871	-0.050	0.038	0.322	0.671	0.910	0.310	-0.536
350	0.033	0.567	6.761	-0.033	0.029	0.314	-0.396	0.174	0.310	-0.554
400	0.028	0.543	5.677	-0.023	0.023	0.309	-1.800	0.000	0.310	-0.553
150	0.015	0.780	4.437	-0.107	0.161	0.371	-1.370	53.500	0.426	2.15
200	0.015	0.711	3.843	-0.084	0.138	0.371	-1.340	2.010	0.426	2.12
250	0.013	0.666	3.216	-0.055	0.109	0.371	-4.530	0.000	0.426	1.95
300	0.010	0.631	2.426	-0.033	0.089	0.369	-8.150	0.000	0.426	1.8
350	0.008	0.608	1.710	-0.020	0.080	0.365	-10.500	0.000	0.426	1.76
400	0.005	0.595	1.184	-0.013	0.076	0.363	-11.900	0.000	0.426	1.74

3.3 Results

3.3.1 Comparison of analytical and numerical pdfs of soil saturation

For the water balance, only one factor differs compared with the situation considered by *Vervoort and Van der Zee* (2008), which is the effect of the osmotic potential. In Figure 3.3, we show the pdfs of root zone water saturation for the cases with and without accounting for osmotic effects for three groundwater depths (Z = 150 cm, Z = 250 cm, Z = 350 cm) under dry climate ($\alpha\lambda/E_{max}$ = 0.89) and wet climate ($\alpha\lambda/E_{max}$ = 1.89). The actually achieved rainfall was 0.219 cm/day and 0.426 cm/day respectively (Table 3.4). First, we compare the numerically determined pdfs for different climates and ground water levels, Z, with the analytical results without osmotic effect of *Vervoort and Van der Zee* (2008). This comparison was not done in that paper, and in fact we found little evidence of the accuracy of such analytical solutions in the literature cited in that paper. For the comparison, we used the numerically achieved values of α and λ. The general agreement between numerical and analytical pdfs is quite good. The numerical pdfs (for all climates) slightly underestimate the analytical pdfs of soil saturation especially for deeper groundwater levels, where they shift somewhat to the dry end compared to the analytical solutions. The first main reason for this difference is the bias caused by small sample on which the pdfs of the numerical results are based. This bias decreases as the sampling period increases and the moments stabilize. The second reason is that the actually achieved rainfall taking into account interception from the rainfall model is relatively less than the input rainfall and this error increases as the climates switches from dry to wet climate. The numerical results of Figure 3.3 are based 100 K day simulations, but still demonstrate some difference between the analytical and numerical results which are due to under prediction of rainfall from rainfall model.

Figure 3.3 also reveals that the osmotic effect moves saturations to higher values. This is logical, as the salt effects decrease evapotranspiration losses as well as leaching losses, whereas it increases capillary influxes (hygroscopic effect). limited, particularly for deeper groundwater. Still, as leaching prevents saturation to move much past s_{lim} (see Figure 3.3), the pdfs become a bit more peaked.

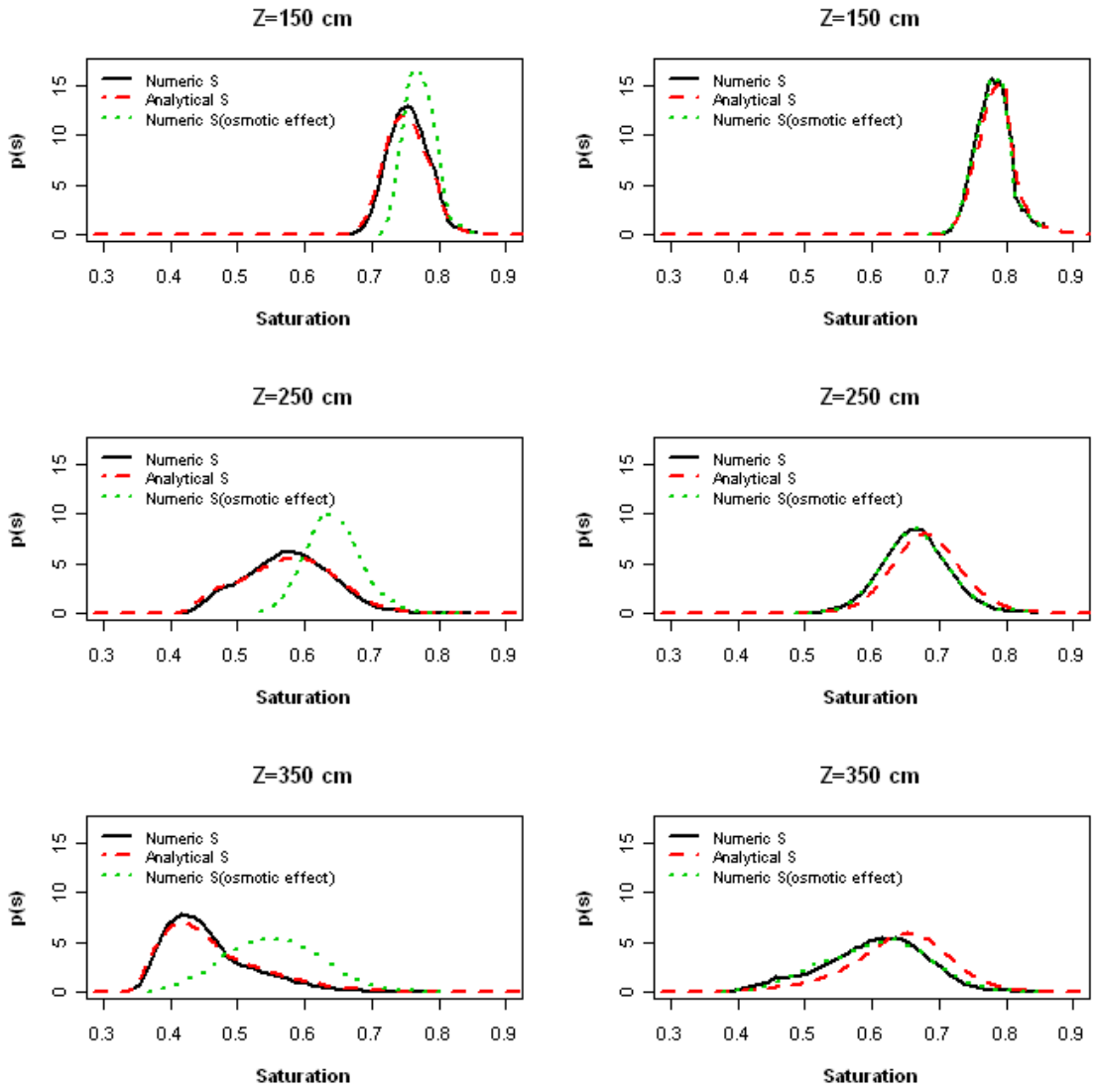

Figure 3.3. Pdfs of numerical saturation without osmotic effects, analytical saturation and the numerical saturation with osmotic effects for a dry climate ($\alpha\lambda/E_{max}$ = 0.89, left side) and wet climate ($\alpha\lambda/E_{max}$ = 1.89 cm/day, right side) under three groundwater depths (Z = 150 cm, Z = 250 cm, Z = 350 cm). The vegetation is trees (Table 3.2), and the soil is a sandy clay loam (*SCL*, Table 3.1).

3.3.2 Salt mass and the related pdf

For a sandy clay loam soil type (*SCL*) and a root zone thickness (Z_r) of 100 cm, the evolution of the salt mass and the related pdfs are shown in Figure 3.4. The temporal development of salt mass is shown for three climates (dry ($\alpha\lambda/E_{max}$ = 0.89), semi-arid ($\alpha\lambda/E_{max}$ = 1.35), and wet climate ($\alpha\lambda/E_{max}$ = 1.89)) and three groundwater depths (Z= 150 cm, Z= 200 cm, Z=250 cm). The primary results of numerical calculations are the patterns of salt mass as a function of time, but it is easier to observe the differences between different groundwater levels and climate from the pdfs of salt mass. These are

shown for six groundwater depths (Z= 150-400 cm in 50 cm increments). The dynamics of the salt mass lead to three major observations: (i) a wetter climate leads to a smaller salt mass in the root zone, (ii) the salt mass is larger for a shallow groundwater level than for a deeper groundwater level, (iii) in relative terms, the variability between groundwater depths is greater for the wet climate; however, in absolute terms the opposite is true: the means differ by 5 mol_c/m^2 in the dry case, but only 3 mol_c/m^2 for the wet case.

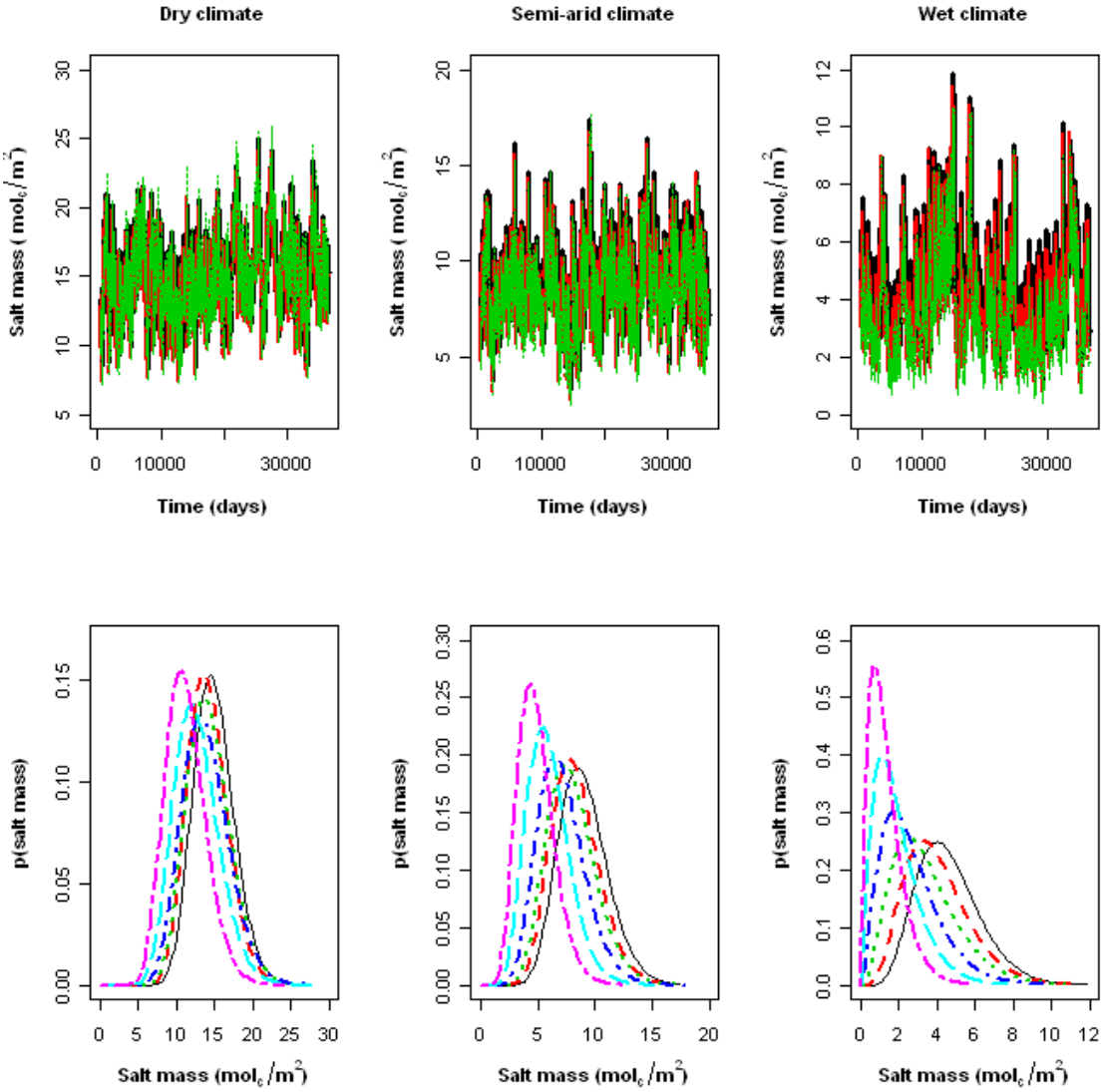

Figure 3.4. Development of the salt mass during 99 years for 3 different groundwater depths (Z = 150 cm (black color), Z = 200 cm (red color), Z = 250 cm (green color)) below soil surface. The pdfs of salt mass are shown for six groundwater depths (Z = 150 cm (black color), Z = 200 cm (red color), Z = 250 cm (green color), Z = 300 cm (blue color), Z = 350 cm (turquoise color), Z = 400 cm (pink color)). Both salt mass and related pdfs are plotted for three different climates (dry climate ($\alpha\lambda/E_{max}$ = 0.89), semi-arid climate ($\alpha\lambda/E_{max}$ = 1.35), wet climate ($\alpha\lambda/E_{max}$ = 1.89)). The vegetation is trees (Table 3.2), and the soil is a sandy clay loam (*SCL*, Table 3.1).

3.3.3 Salt concentration and the related pdf

For the same combinations as in section 3.2 (and Figure 3.4), the results are shown in Figure 3.5 as the salt concentration and the related pdf. The behavior of salt concentration leads to three major observations: (i) for a wet climate, the salt concentration is smaller than for the other climates, (ii) largest concentrations are found for a dry climate, with a maximum for groundwater levels of about 3 m below the soil surface (i.e., 2 m below the 100 cm thick root zone), and (iii) for a wet climate, the salt concentration has a maximum at shallower groundwater level, whereas for the other climates, the largest concentrations are found for intermediary groundwater depths. This pattern is consistent with the patterns for the salt mass. That the salt concentration is not necessarily dependent on the groundwater depth in a monotonous way is indicative of counteracting effects of rainfall and capillary upflow.

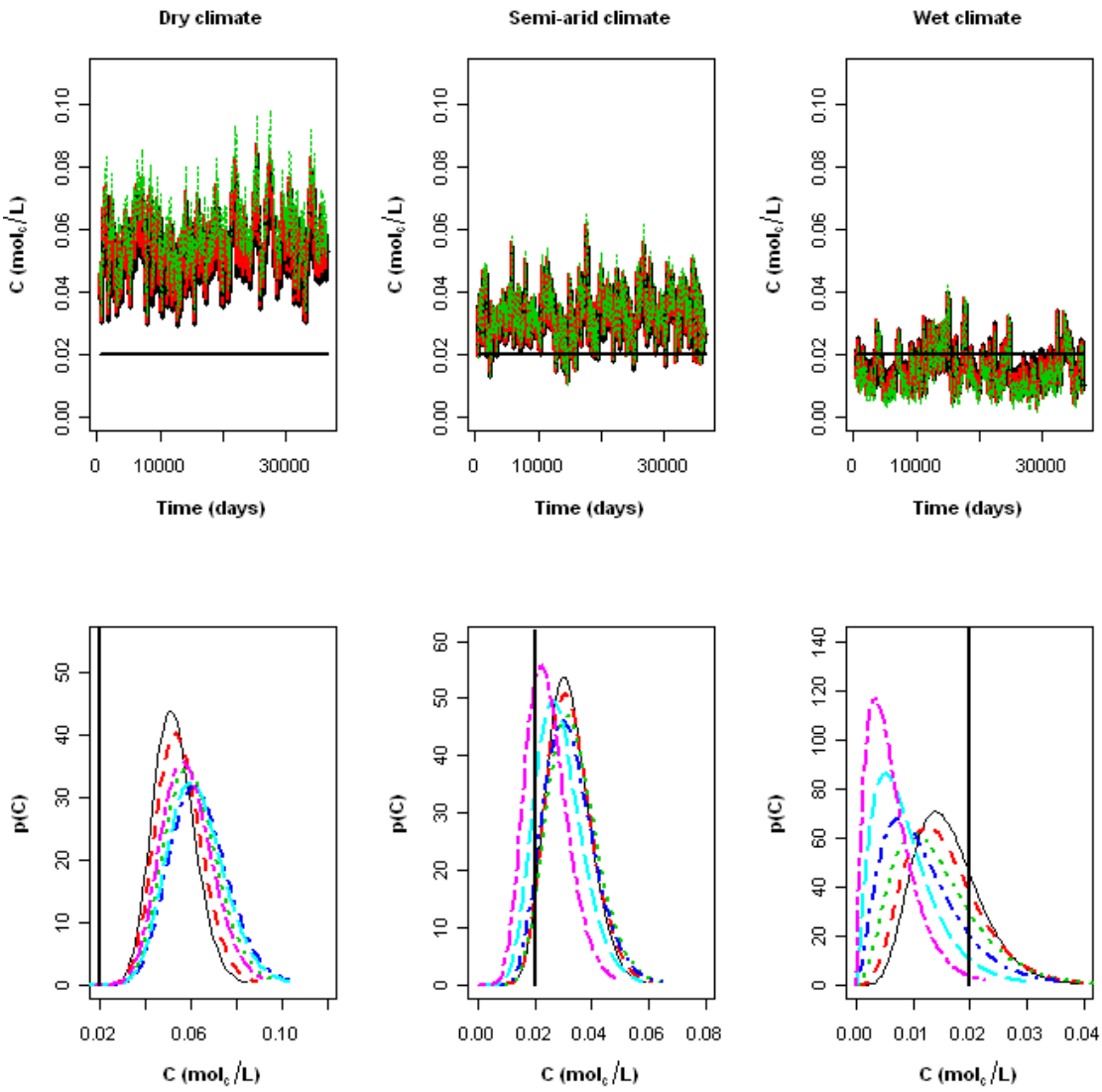

Figure 3.5. Development of the salt concentration during 99 years for 3 different groundwater depths (*Z* = 150 cm (black color), *Z* = 200 cm (red color), *Z* = 250 cm (green color)) below soil surface. The pdfs of salt concentration are shown for six different groundwater depths (*Z* = 150 cm (black color), *Z* = 200 cm (red color), *Z* = 250 cm (green color), *Z* = 300 cm (blue color), *Z* = 350 cm (turquoise color), *Z* = 400 cm (pink color)). The horizontal and vertical solid back line shows the groundwater salt concentration (C_z = 0.02 mol$_c$/L). The vegetation is trees (Table 3.2), and the soil is a sandy clay loam (*SCL*, Table 3.1). Other conditions as in Figure 3.4.

3.3.4 Effect of varying soil type

Besides different climates and groundwater levels, parameters such as soil type, root zone depth, and groundwater salinity affect the concentration in the root zone. For this reason, we considered different soil types listed in Table 3.1, where we observe that these soils differ in several hydraulic parameters, but mainly in the hydraulic conductivity. The long term average root zone concentration was calculated and is

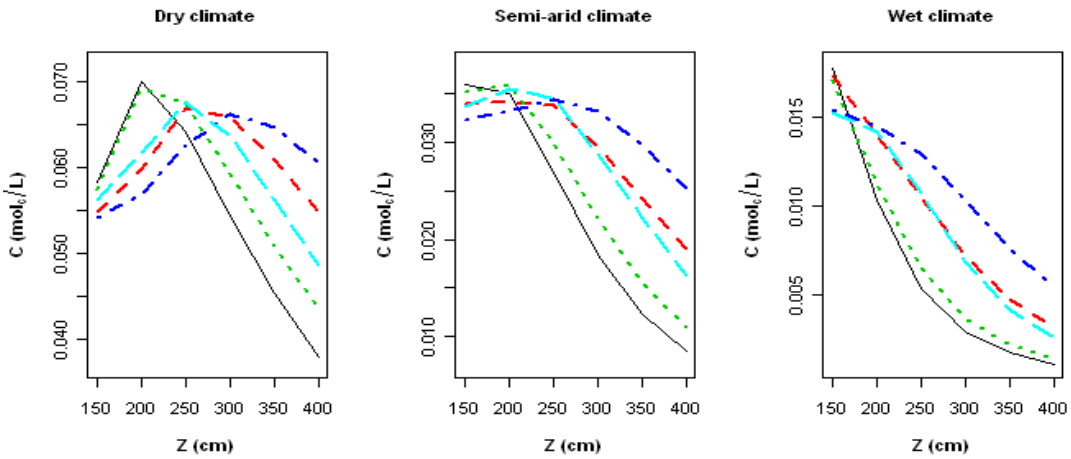

Figure 3.6. Long term average salt concentration as a function of six different groundwater depths (Z = 150 cm, Z = 200 cm, Z = 250 cm, Z = 300 cm, Z = 350 cm, Z = 400 cm) under different soil types (heavy clay (*HC*, black color), medium clay(*MC*, red color), light medium clay(*LMC*, green color), sandy clay loam(*SCL*, blue color), and loamy sandy soil(*LS*, turquoise color), Table 3.1). Other conditions as in Figure 3.4.

presented as a function of the hydraulic conductivity of the five soils in Figure 3.6. For all three climates and larger Z, the average root zone concentration increases as the hydraulic conductivity increases, with one exception (loamy sand (*LS*), which has the largest hydraulic conductivity). However, as the climate becomes drier, a reversal is seen for shallow ground water: the average root zone concentration increases as hydraulic conductivity decreases. In interpreting this figure, it is necessary to appreciate that the above observations are all based on long term average concentrations. Particularly for the leaching process under dry conditions, short term high intensity showers may control leaching, rather than the average, and be dominant in how the concentration level develops.

3.3.5 Effect of root zone thickness and groundwater salinity

Besides the differences between soil type, groundwater level and climate (evapotranspiration demand and rainfall), vegetation is a further important aspect to salt accumulation. A range of properties of vegetation can be important, e.g. those of Table 3.2. To focus on the system behavior, we varied the root zone thickness, Z_r, and the ground water salinity (i.e. the impact of osmotic stress). To separate the effect of root zone thickness from ground water depth, we varied Z_r for different distances of capillary upflow: Z-Z_r, (*Vervoort and Van der Zee*, 2008; 2009). In Figure 3.7, we show the results of varying root zone thickness for a wet and for a dry climate.

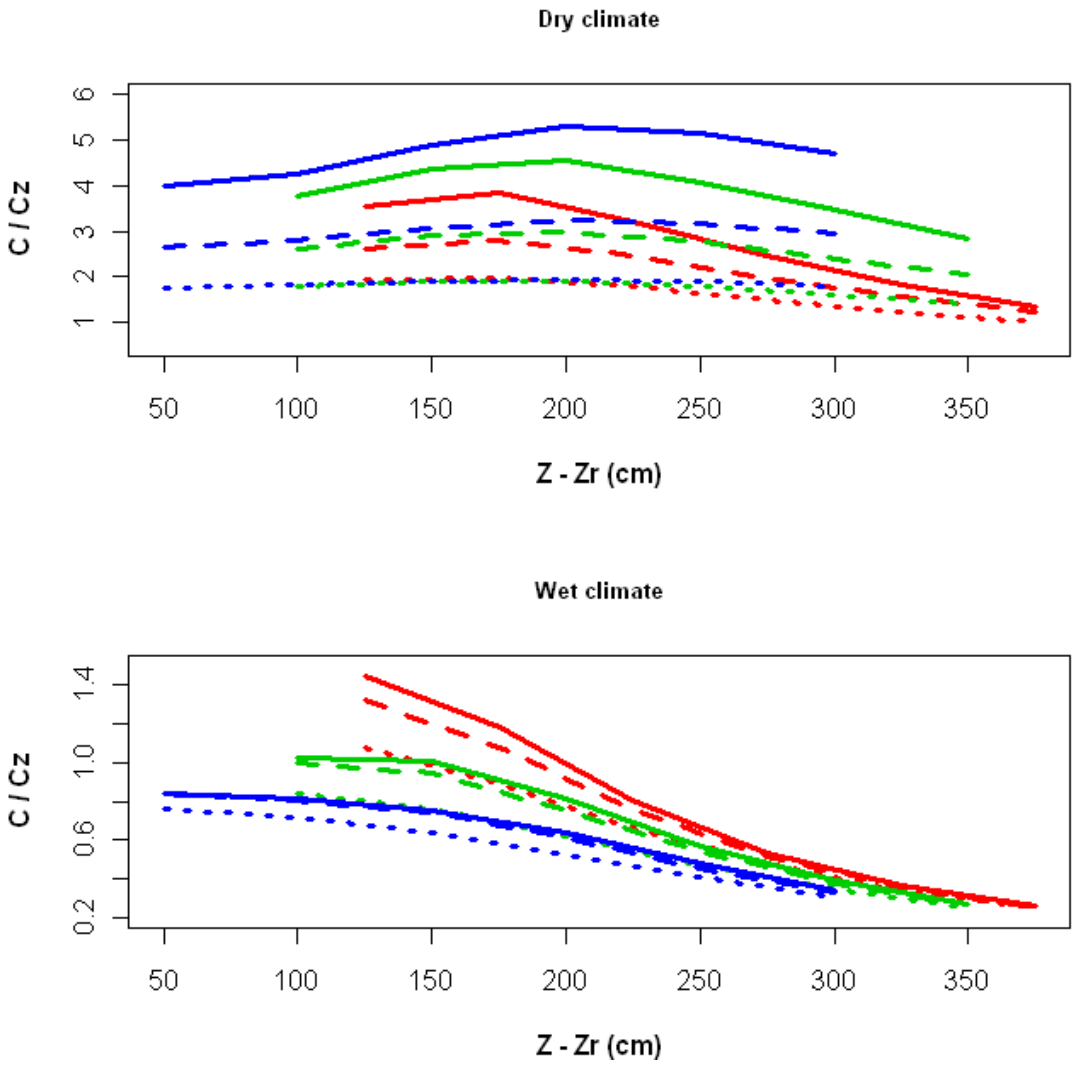

Figure 3.7. The long term average salt concentration as a function of ($Z - Zr$) for different root zone thickness (red colour (Z_r = 25 cm), green colour (Z_r = 50 cm), blue colour (Z_r = 100 cm)) under different groundwater salinities (C_z = 0.01 mol_c/L (solid line), C_z = 0.02 mol_c/L(dashed line), C_z = 0.04 mol_c/L(dotted line)) and two climates (dry climate ($\alpha\lambda/ E_{max}$ = 0.89), wet climate ($\alpha\lambda/ E_{max}$ = 1.89)). The vegetation is trees (Table 3.2), and the soil is a sandy clay loam (*SCL*, Table 3.1).

The concentration of salt in the ground water C_Z was varied, following: C_Z = 0.02 mol_c/L (reference), 0.01 mol_c/L and 0.04 mol_c/L for a dry and a wet climate.

For the wet climate, the average salt concentration in the root zone decreases monotonically with increasing $Z–Z_r$ (distance of ground water to below root zone), which has been observed already in Figure 3.5. As the latter figure already indicates, such a monotonic decrease does not occur for the dry climate, as is indeed apparent from Figure 3.7.

Considering that for Figure 3.7 the root zone thickness decreases by a factor of four, whereas the involved relative concentration change increases by a factor of 1.5 for the wet climate, this indicates that root zone thickness has a modest effect. For the dry climate, the relationship between C/C_Z and distance between root zone and ground water is non-monotonic and the impact of root zone thickness is larger than for the wet climate. Larger salinities are found as root zone thickness increases (as opposed with the wet climate) and in particular, the impact of salinity of ground water is much larger than for the wet climate.

3.3.6 Mapping the root zone salinity as a function of climate parameters

Practically, it is of interest to recognize which combination of factors lead to adverse salinity levels in the root zone. Therefore, we map the combinations of two climate parameters (α,λ) that result in a particular salinity in Figure 3.8. For a range of rainfall parameters (α = 1.1 – 1.4 cm/event, λ = 0.3 – 0.5 event/day), the *SCL* soil, root zone thickness (Zr = 100 cm), and a groundwater level equal to Z = 300 cm, we calculated the resulting (99 year average root zone) salt concentrations of Figure 3.8a. This range of rainfall parameters covers the three values of $\alpha\lambda$ (climate parameters) that were so far considered in this paper (with $\alpha\lambda$ ranging from 0.33 cm/day to $\alpha\lambda$ = 0.70 cm/day, Table 3).

Since the critical groundwater depth (Z) (where salt concentration is maximum) is 300 cm for sandy clay loam soil (Z = 300 cm, $\alpha\lambda$ (actual input) = 0.219 cm/day in Table 3.4), we have selected this groundwater depth in order to visualize the effect of small and large frequent events on the range of root zone salt accumulation. The range of numerically obtained salt concentrations in the root zone as shown in Figure 3.8a exceeds the critical value (0.04 molc/L) where production of sensitive plants decreases. For these conditions, concentrations increase as the climate becomes drier, which is in agreement with Figure 3.4. In addition, rainfall frequency affects the salinity that will develop. As rainfall occurs less frequently, salinity increases to greater levels.

At a first glance, frequency seems to have a lesser effect on salinity than other parameters like rainfall quantity, root zone thickness, and groundwater depth. Therefore, the results of Figure 3.8b are also sensitive to other parameterizations. For instance, we conducted calculations that are parameterized for a wheat crop, with Z_r = 65 cm and a

matric potential where transpiration becomes limited that is representative for wheat ($\psi_{s,s*}$ = -0.09 MPa (*Kroes et al., 2008*)), a ground water level of Z = 200 cm, and a range of α (1 – 1.2 cm/event) and λ (0.1 – 0.2 event/day) parameters.

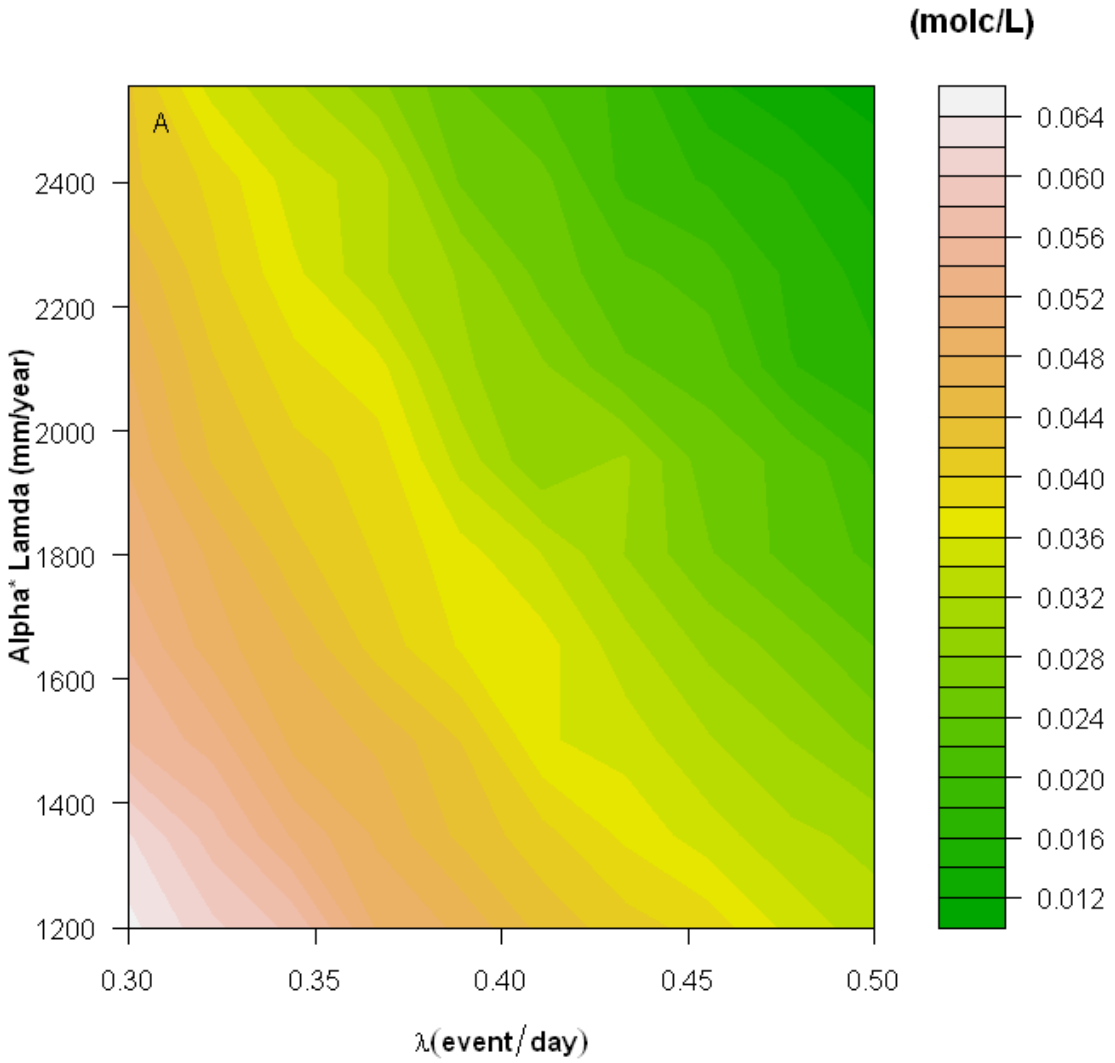

The results shown in Figure 3.8b indicate that the average salt concentrations are greater than for Figure 3.8a and also comparable with the critical levels derived from Handbook 60 (*Richards et al.*, 1954). In addition, the contour lines of average salt concentration are almost vertically oriented in Figure 3.8a and Figure 3.8b. As the climate becomes strongly drier, the salt concentration increases and subsequently contour lines become almost horizontally oriented (not shown). In these severe conditions, average salt concentration exceeds the critical value (0.08 mol_c/L) where only tolerant plants can show good primary production.

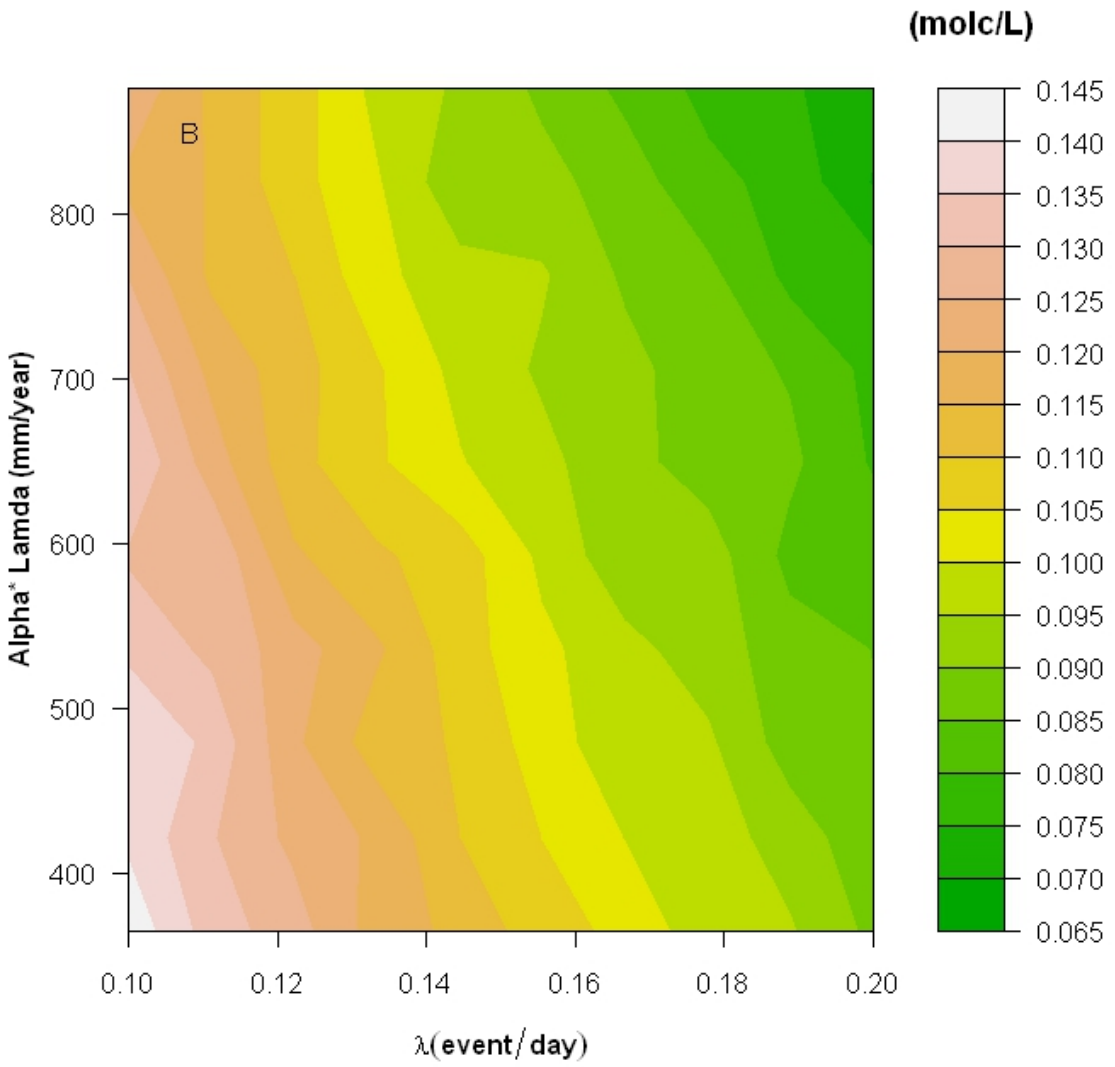

Figure 3.8. A. Contour lines of average salt concentration (mol_c/L) as a function of rainfall ($\alpha\lambda$ in mm/year) and rainfall frequency (λ = 0.3-0.5 events/day). The groundwater depth (Z) is 300 cm, and vegetation is trees (Table 2). B. Contour lines of average salt concentration (mol_c/L) as a function of rainfall ($\alpha\lambda$ in mm/year), and rainfall frequency (λ = 0.1-0.2 events/day). The groundwater depth (Z) is 200 cm, Z_r = 65 cm.). The vegetation is a wheat crop (except for the root zone depth and $\psi_{s,s*}$ = -0.09 MPa, all parameters from Table 3.2). The soil is a sandy clay loam (*SCL*, Table 3.1).

3.3.7 Analytical approximation

The erratic patterns of concentration as a function of time are caused by the Poisson rainfall and can be conceived as resulting from an input of salt mass due to capillary flow from groundwater and the leaching due to rainfall. Assuming constant salt inputs (Y) in terms of concentration units (i.e., input of mass of salt divided by root zone water volume), occurring instantaneously with a recursion time of Δt and followed by

periods of leaching, with a leaching flow rate equal to j_l, a root zone water volume equal to V, and n the number of years, the maximum concentrations of the developing saw tooth pattern can be approximated by (*Van der Zee et al.*, 2010).

$$C_{\max} = Y\left[\frac{1-\left(\exp\left(-\frac{j_l}{V}\Delta t\right)\right)^n}{1-\exp\left(-\frac{j_l}{V}\Delta t\right)}\right] \qquad \textbf{(3.9)}$$

The minimum salt concentration is calculated by subtracting the salt input (Y) from the C_{max} value

$$C_{\min}(n) = C_{\max}(n+1) - Y \qquad \textbf{(3.10)}$$

To check whether this simple approach captures the dynamics of the random patterns presented earlier, we use the annual averages of the numerically determined drainage rates and capillary flux to approximate the water flux, j_l (cm/year) and capillary flux (cm/year), and, with the long term averaged water saturation and the root zone porosity (ϕ), we estimate the root zone water volume as $V = \phi Z_r <s>$. The recursion time is set equal to one year and the applied salt mass (in concentration equivalents) is equal to Y (mol_c/L) = $(<U>C_Z) / (\phi Z_r <s>)$, where the mean capillary flux and water saturation were again taken from the numerical calculations. In all cases, we used averages for simulation times exceeding 10000 days. Using equation (3.9), and equation (3.10), we calculated the maximum concentrations and the minimum concentrations for the erratic patterns of salt concentration (Figure 3.9). Whereas for the dry climate the agreement is not good, particularly for deeper groundwater levels [not shown], for the semi-arid (Figure 3.9) and wet climate [not shown], the agreement is reasonable to good for the time period exceeding 10000 days and the average of minimum and maximum concentration gives a good impression of the long term mean C value.

In equation (3.9), the term to the power n decays rapidly. Therefore, we can simplify this equation further by ignoring this decaying term, to obtain

$$C_{\max} = Y\left[1-\exp\left(-\frac{j_l}{V}\Delta t\right)\right]^{-1} = Y.X \qquad (3.11)$$

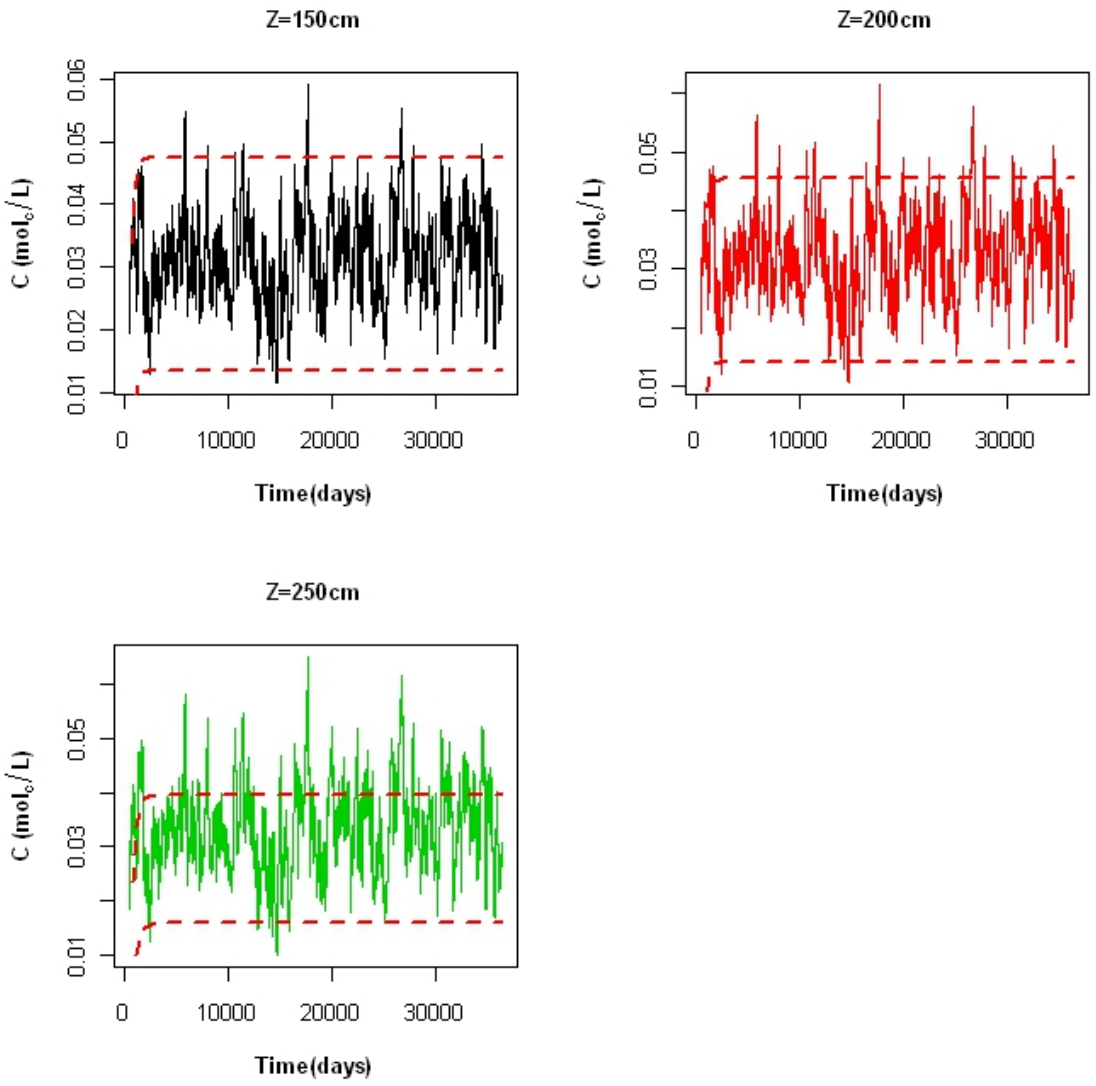

Figure 3.9. Comparison of long term concentrations with analytical approximation (C_{max} and C_{min}) for semi-arid climate ($\alpha\lambda/E_{max}$) = 1.35). The vegetation is trees (Table 3.2), and the soil is sandy clay loam (*SCL*, Table 3.1).

We can approximate C_{max} with the 84% percentile C-value in the numerical concentration pdfs, and

$$Y.X = \frac{\langle U \rangle C_Z}{\phi Z_r \langle s \rangle} X, \quad X = \left[1 - \exp\left(-\frac{j_l}{V} \Delta t \right) \right]^{-1}, \quad \frac{j_l}{V} = \frac{\langle L \rangle}{\phi Z_r \langle s \rangle}.$$

For five soil types, different groundwater depths and climates, we calculated $Y.X$ and plotted the approximated maximum concentration as a function of this product in Figure 3.10. Considering the coarse approximation, the agreement is quite good. As the climate

becomes wetter, soil saturation, evapotranspiration and leaching increase, but the capillary upflow decreases.

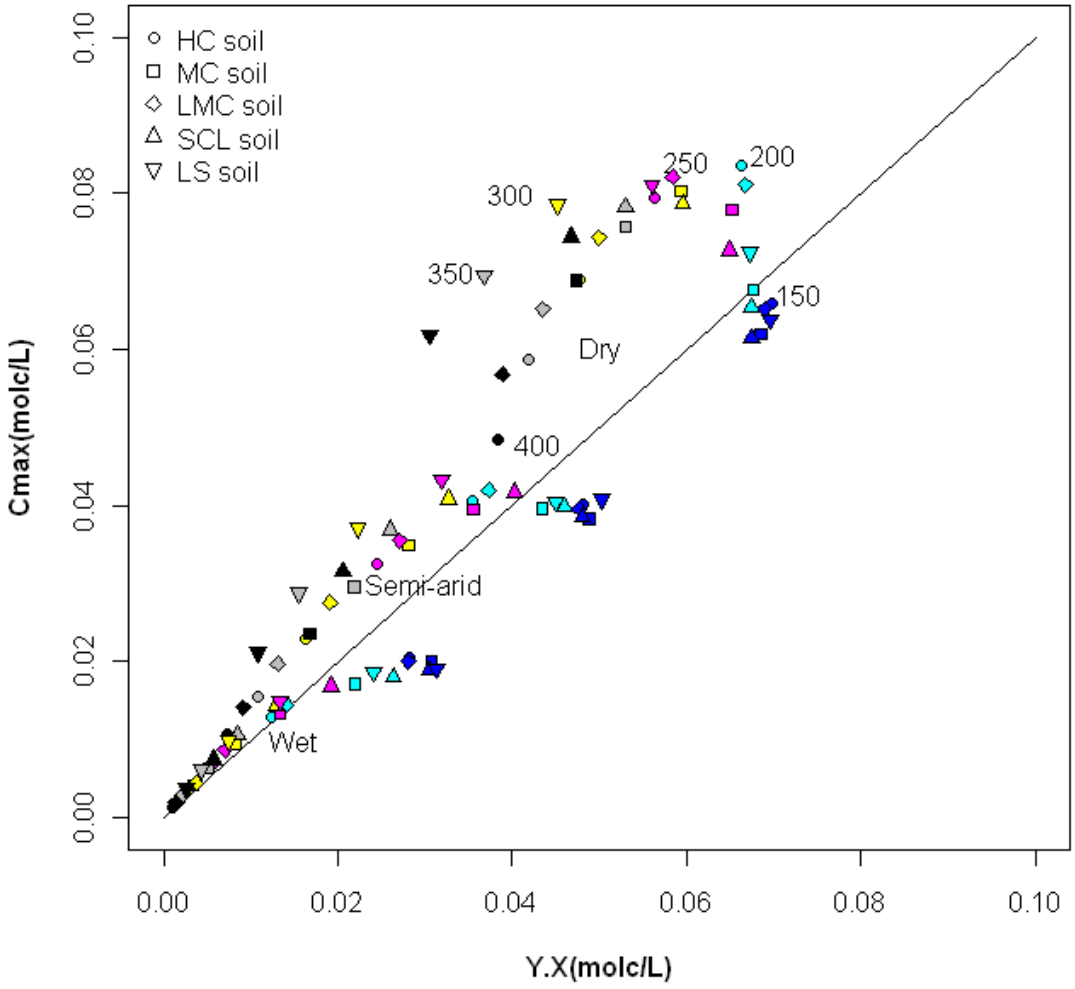

Figure 3.10. Comparison of C_{max} (the 84% percentile C-value in pdf) and $Y.X$ (equation 11) for six different groundwater depths, five different soil types (Heavy clay soil, Medium clay soil, Light medium clay soil, Sandy clay loam soil, Loamy sand soil, Table 3.1) under three different climates (dry climate ($\alpha\lambda/E_{max}$) = 0.89, semi-arid climate ($\alpha\lambda/E_{max}$) = 1.35, and wet climate ($\alpha\lambda/E_{max}$) = 1.89). The vegetation is trees (Table 3.2).

Since salt transport is caused by the capillary flux, less salt enters the root zone for a wetter climate and this leads to smaller values of C_{max}. Therefore, the C_{max} values for a wet climate are small and in the lower left corner of Figure 3.10, and for a dry climate relatively large. An even coarser approximation is gained by directly comparing the capillary flux U with the leaching flux L. Despite that these fluxes vary as a function of time, on average, if U is larger than L it is probable that the concentration in the root zone becomes larger than in the groundwater, whereas if U<L, it is likely that salts enter the

root zone, but are flushed effectively. Hence, in the latter case, concentrations in the root zone remain below C_z (not shown).

3.4 Discussion

In Figure 3.3, the pdf of water saturation of the root zone is shown for dry and wet climates. Of interest is that for the wet climate, the pdf including osmotic effects is not much different from those where these effects are ignored. Quite different is the case for the dry climate, where osmotic effects have a major impact on the wetness of soil. Not shown is the pdf for the semi-arid climate, but there, osmotic effects are still minor and only slightly larger than for the wet climate. Considering (Figure 3.5) that long-term average root zone salinities change from wet to dry, from about 0.01, to 0.03, to 0.06 mol_c/L, respectively, it is clear that osmotic effects for the present parameterization may affect the water and salt balances only if concentrations exceed approximately 0.04 mol_c/L.

The salt concentration and salt mass trajectories through time are quite erratic and where a long term trend is absent or insignificant, the short term fluctuations easily cover 50% of the concentration range and even more for the range of salt mass, for each of the climates considered.

To appreciate the effects of two dominant factors, i.e. climate and groundwater depth (Z), the probability density functions of salt mass and salt concentration enable a better comparison than the trajectories. For salt mass, the trends are quite simple: salt mass increases as the climate becomes drier, and as the depth to groundwater decreases. Both tendencies can be readily understood by considering that as climate becomes drier, root zone water used for evapotranspiration is replenished by brackish water capillary upflow from groundwater, whereas leaching of salt decreases. As groundwater becomes shallower, capillary upflow increases and salt concentration in the root zone decreases due to the dilution effect and this dilution effect decreases with the increase of groundwater depth. Therefore, salt concentration is maximum at intermediary groundwater levels. Furthermore, as the climate switch from wet to dry, the shift of the pdf of salt mass to the right becomes gradually smaller. Relatively speaking, the shift is largest for the wet climate, which is due to rainfall surplus (Table 4: P-ET-R, R=runoff).

However for the considered cases the absolute shift of the pdf is relatively constant for all climates (about 4 – 5 mol_c/m^2).

For concentration, which is the result of combining the pdfs of salt mass and water storage in the root zone, the shift of the pdf cannot be related with climate and groundwater level quite so easily. The reason is that for the dry and semi-arid climates, the pdf shifts more to larger concentrations for the groundwater depths of 300 and 250 cm, i.e., the distance between groundwater and root zone has a non-monotonous impact on the long term average root zone concentration.

This more complex behavior than for salt mass must be due to counteracting processes, and two logical candidates are (i) leaching and (ii) dilution. Leaching removes salts that have accumulated in the root zone, and the condition necessary for this to happen is a sufficiently large amount of rainfall, that exceeds the available (unused) water storage capacity. Hence, wet conditions due to antecedent rainfall or close proximity of groundwater favors leaching under modest rainfall quantities. A thin root zone also favors leaching, as it implies a small water storage capacity of this zone.

For the wet climate, the frequent rainfall leads to a pdf of water saturation at the wet end, which is quite symmetrical for all groundwater depths (only shown for three groundwater depths in Figure 3.3). This leads to pdfs of salt mass and concentration, respectively, that are not much different in shape and that show the same sequence: a shift to the higher values as groundwater is shallower and root zone conditions are wetter. For the dry climate, the water saturation pdf (including osmotic effects!) has shifted to smaller saturations for all groundwater depths, and as groundwater levels are deeper, the pdf of saturation is centered around smaller *s*-values, with a few excursions to larger *s*-values. The salt mass pdf's for the dry climate and shallow groundwater levels almost collapse, but the water stored in the root zone decreases rapidly as groundwater levels drop, which causes larger concentrations. For levels of 350-400 cm, the water saturation does not change appreciably anymore compared with 250-300 cm, yet salt mass does, and this is reflected by the pdf of the concentration that has shifted to largest values for the intermediate 250-300 cm groundwater levels. The semi-arid climate also shows this non-monotone behavior of the pdf of salt concentration, though less distinct as the dry climate.

For the wet climate, ground water with a salinity of 0.02 mol_c/L enters the root zone and is diluted by mixing with infiltrating rain water. Despite fluctuations over the years, salt inputs from below are on the longer term balanced by salts that are leached in a volume of water that is larger than capillary upflowing water, and a concentration that is less than that of ground water. Whereas for the wet climate, leaching can explain the salt accumulation, for the dry climate, little water leaching occurs as there is a rainfall deficit on average. The numerical results indicate that on average the capillary upflow rate for the dry climate is larger than the leaching rate, yet on the long term, salt fluxes balance. For a groundwater salt concentration of 0.02 mol_c/L (reference case) and average root zone salinities that are approximately three times as large as C_z, the capillary upflowing water dilutes the root zone water, particularly if capillary upflow is relatively large, for shallow groundwater levels (Figure 3.7). This dilution is appreciable and counteracted by removal of root zone water during dry spells. Incidental showers on a root zone with highly concentrated water after dry spells lead to a rapid loss of salts amounting to 25-50% of the stock before the shower (Figure 3.4). Hence, the non-monotone behavior of C as a function of Z is due to smaller concentrations in the root zone, C, by dilution with less saline ground water if capillary upflow, U, is large (shallow ground water), or due to small values of U (at deep groundwater) and leaching of saline root zone water. At groundwater depths where the dilution effect by upflowing groundwater becomes negligible, the largest concentrations are found as this volume becomes less significant (around Z= 250 – 300 cm) compared with root zone stored water but still comparable to the leached water volumes.

Looking at the long term average concentrations in the root zone for different soil types, in Figure 3.6, a sequence is found for deeper ground water levels that shows larger concentrations if the saturated hydraulic conductivity increases. The differences in the retention curves appear to be of secondary importance as can be seen from the *LMC* and *MC* soils that have virtually the same water retention curve, but are shifted with regard to each other in Figure 3.6. Furthermore, the sequence is the same for deeper ground water levels, for all three climates. It is apparent that the soils with a larger saturated hydraulic conductivity (the main parameter in which these soils differ) show largest concentrations, (the loss function of all soil types also confirms that net loss of water increases with the

increase of hydraulic conductivity and subsequently causes larger concentrations) both for conditions where the root zone is more concentrated ($C/C_Z>1$) and for conditions where concentrations are diluted compared with ground water salinities (mainly wet climates). This suggests that the hydraulic conductivity is limiting with regard to upflow of brackish water, and the more limiting it is, the smaller root zone concentrations become.

For shallow ground water depths with wet conditions, and for very large hydraulic conductivity (i.e., the *LS* soils), the hydraulic conductivity is not limiting. Here the salt accumulation becomes indifferent with respect to the soil type, or the reverse happens: larger hydraulic conductivities lead to smaller concentrations as less runoff and more infiltration occurs that dilutes root zone water, and leaching is more efficient.

As was mentioned before, the thickness of the root zone affects the leaching potential, as it is linearly related with the water volume as well as the salt mass that can be stored by the root zone. Due to this relationship, root zone thickness, Z_r, also influences surface runoff, which depends on the water storage volume that is still available to infiltrating water. We conducted simulations where we considered two alternatives: (i) runoff occurs as in all other calculations (default), or (ii) runoff is added to leaching. It appeared that runoff does not result in a significant effect. For thin root zones, where the water storage capacity is smallest and runoff should be most significant, changes were only up to 20% of the long term averaged concentration in the root zone. For thicker root zones (50 or 100 cm), effects were negligible. Hence, runoff is discarded in the present analysis as a factor that might affect the salt accumulation. The insignificant effect of runoff on the root zone salt concentration can be explained by the low frequency intensive showers that effectively decrease the root zone salt concentration. Adding runoff to the leaching flux (as a check on its impact) hardly increases salt leaching, as the root zone has already been rinsed.

Also of importance is the impact of osmotic effects on the calculations. For the wet climate (Figure 3.7), it was ascertained that runoff explained about 50% of the, relatively small, C/C_Z-difference between the root zone thickness of 25 cm or larger (50, 100cm). The remainder, which is only significant for ground water salinities changing from 0.02 to 0.04, are due to osmotic effects. Hence, it is clear that osmotic effects start

to play a role at a concentration of about 0.04 mol_c/L, as was mentioned earlier. For the dry climate, where salinity levels are larger, it is clear that besides the root zone thickness effect, also the osmotic effects are important (Figure 3.7): it shifts the concentration levels up to larger values, yet to smaller relative values (C/C_Z). This latter effect is due to osmotic effects on different water fluxes leading to larger root zone wetness, hence larger dilution (Figure 3.3).

Although runoff does not appear to affect the results much, the reservoir size (Z_r) is important as fluctuations in fluxes become more attenuated when the reservoir increases. For the wet climate, it is plausible that 'extreme events' are drought periods, and for the dry climate, extreme events would be wet, leaching periods. The impact of Z_r are consistent with that picture: in wet climates, thicker root zones attenuate drought effects and decrease the salinizing impact of large U and small L (evapotranspiration being quite constant). In dry climates, thicker root zones attenuate the capability of rain showers to rinse salts, leading to more saline conditions.

We compared Figure (3.8) with the related analysis by *Suweis et al.* (2010). Their Figure 3.2 (*Suweis et al.*, 2010) showed the long term average salt accumulation (in terms of salt concentrations) as a function of annual rainfall and rainfall frequency. As they ignored groundwater influences on the root zone water saturation and salinity, salt concentration levels depends only on the leaching potential of rainfall events. For their case, small showers may rewet the root zone, but have little salt leaching potential whereas large showers have a large leaching potential. In their analysis salt enters the root zone through precipitation only. In our work, the rain is considered free of salt and capillary flow from groundwater brings both water and salts to the root zone. Hence, if groundwater is sufficiently shallow to wet the root zone, most rain showers will cause leaching, and the leaching efficiency will improve if precipitation is distributed over more events. With larger and less frequent events, the system is less efficient at removing salts. Large events supply more water than is needed to flush the root zone and the lower frequency of these events leads to a net increase in the salt concentrations. This implies that with increased climate variability (decrease in λ and increase in α) the influence of runoff becomes greater ([*Entekhabi et al.*, 1992; *Kim*, 2005; *Milly*, 2001).

Figure 3.9 shows that with a relatively simple approach, the dynamics (in terms of a mean concentration and a band width around this average) can be reasonably approximated. Hence, if a rough indication is all that is needed, the demanding numerical computations may not be necessary. The limitation of this analytical approach is obvious: input was needed that can only be obtained by those demanding numerical computations, that one might want to avoid. This limitation may not be as prohibiting as it seems. If crops are concerned, the yield, which is easily measured, is well correlated with relative transpiration ([*Rodriguez-Iturbe and Porporato*, 2004; *Shani et al.*, 2007). This transpiration plus evaporation (controlled by irradiation, air humidity, LAI and soil water saturation) should, on the long term, be derived from rainfall and capillary flux, where the first one can be measured relatively simply, evaporation can be reasonably well predicted, and the latter can therefore be calculated. Furthermore, the soil water status can be easily monitored.

The pdfs of M and C react differently on Z and climate, and both are the result of opposing effects: wetness due to a wet climate or due to the proximity of groundwater favors leaching, the proximity of groundwater level also favors salt import by the root zone layer and the water balance determines whether the capillary upflowing water, U, will concentrate or dilute the root zone with regard to salt concentration. For the long term average fluxes, salt concentrations and mass converge to a mean value with irregular variations around this mean. However, salt inputs and outputs will balance, hence

$$UC_Z = LC \leftrightarrow \frac{C}{C_Z} = \frac{U}{L}$$

and therefore the values of these fluxes determine whether root zone concentrations will become larger or smaller than those in the groundwater. Many factors affect these fluxes, such as climate, groundwater depth and soil type, and in view of opposing effects, salt accumulation in the root zone is a complex issue for sustainable planning of crop, soil, and groundwater specially in semi-arid regions (*Corwin et al.*, 2007). In agreement with Handbook No. 60 of the USDA (*Richards et al.*, 1954), concentrations of 2, 4, and 8 mS/cm in terms of electrical conductivity (or 0.02, 0.04, and 0.08 mol_c/L in terms of concentration or 1×10^5, 2×10^5, and 4×10^5 Pascal in terms of osmotic pressure) are indicative of salt stress. These concentrations refer to salinity ranges in the saturated

extract (see Handbook No. 60) for no adverse effects ($C < 0.02$), adverse effects for sensitive ($0.02 < C < 0.04$) and many plant species ($0.04 < C < 0.08$), and severe adverse effects where only tolerant plants show a good primary production ($C > 0.08$). The soil saturation in our analysis varies as a function of time, and moreover, the relationship between water content in the field and in the saturated extract depends on several soil properties, besides soil saturation. For an impression, we indicate the gravimetric water content of the saturated paste extract (75% by weight of dry soil) and field capacity (25% by weight of dry soil; see also Table 9.1, in their chapter 9) as given by (*Bolt and Bruggenwert*, 1976). Apart from osmotic effects, root zone salinity cannot be considered to be a simple function of other factors, such as groundwater depth, root zone thickness, climate and soil. However, if a rough indication suffices, a simple analysis may give a sufficiently accurate prediction.

Though root zone fluxes vary as a function of time, on average, if capillary upflow is larger than leaching flux it is probable that the salt concentration in the root zone becomes larger than the concentration in the groundwater. If capillary upflow is less than the leaching flux, salts entering the root zone may be flushed out effectively, and the concentration in the root zone remains below groundwater salt concentration. We conclude that if we know the groundwater depth, groundwater salinity, climate, and soil type, we can do a quick assessment whether capillary upflow would be greater or less than the leaching flux and the resulting root zone salt concentration. Runoff may affect the overall water and salt balances. For a shallow root zone, the impact of runoff is larger than for a large root zone. For the presently considered cases, runoff was insignificant for the salt balance.

3.5 Conclusions

Capillary groundwater fluxes influence the soil moisture balance in a limited range of groundwater levels, as was discussed by *Vervoort and Van der Zee* (2008). In their analysis, the impact of salt on the water balance was not considered. If groundwater is brackish or saline, the upward capillary fluxes carry along salt that may accumulate in the root zone. These salts may lead to a reduced transpiration due to the moisture stress

caused by osmotic effects. In this paper, we consider the salt dynamics in the root zone, and take osmotic effects on the water fluxes into account.

The upward transport of salts from groundwater into the root zone is larger if the upward water flow rate is larger, but since it may also induce the root zone to become wetter on average and more prone to solute leaching events, the salt concentration that develops depends in a complex way on capillary upward flow. The long term salt concentration is not a monotonically increasing or decreasing function of the various system parameters such as hydraulic conductivity, groundwater depth, or climate parameters. Dependencies can be different, as was shown by comparison of effects with those found by *Suweis et al.* (2010), where salt inputs derived only from atmospheric deposition.

Salt accumulation in the root zone is characterized by very erratic patterns of concentration and salt mass as a function of time, caused by the Poisson distributed of daily rainfall. If we allow these patterns to stabilize, it is possible to determine the pdfs of important variables. If the stochasticity of weather is replaced by the average root zone water fluxes, a simple analytical approximation is feasible.

Acknowledgements

Part of this research was done with funding by the Higher Education Commission of the Government of Pakistan for S.H.H.S., the Wageningen University IPOP program “Kust en Zee” and the Knowledge for Climate Research Program, Netherlands. We appreciate the funding by WIMEK (Wageningen Institute of Environmental and Climate Research) for the sabbatical visit of R.W.V. in Wageningen, and support of EPFL-ENAC for the sabbatical visit of SvdZ to EPFL, Lausanne, Switzerland. AR and SS also acknowledge ERC Advanced Grant RINEC-227612 and by SFN grant 200021_124930/1.

CHAPTER 4

Modeling of soil sodicity development due to capillary upflow from groundwater: an ecohydrological approach

S. H. H. Shah[1], S. E. A. T. M. van der Zee[1], A. Leijnse[1], R. W. Vervoort[2]

[1]Soil Physics, Ecohydrology and Groundwater Management, Environmental Sciences Group, Wageningen University, P.O.B. 47, 6700 AA, Wageningen, Netherlands

[2]Hydrology and Geo-information Sciences Research Laboratory, Faculty of Agriculture, Food and Natural Resources, The University of Sydney, Australia

To be submitted

4. Modeling of soil sodicity development due to capillary upflow from groundwater: an ecohydrological approach

Abstract

Soil salinity and sodicity development in groundwater driven agro-ecosystems play a major role in soil structure degradation. To identify which conditions lead to soil sodicity, we have modeled the coupled water, salt, and cation balances. The root zone salinity *C* and sodicity *ESP* gradually change to their long term average values. These long term average values are independent of the cation exchange capacity *CEC*. The rate of change depends inversely on the size of the root zone reservoir, i.e., on root zone thickness for *C*, and additionally on *CEC*, for *ESP*. Soil type can have a large effect on both the rate of approach of the long term steady state salinity and sodicity, and on the long term levels, as it affects the incoming and out-going water and chemical fluxes. Considering two possible sources of salts, i.e., groundwater and irrigation water (here represented by rainfall), the long term salt concentration *C* of the root zone corresponds well with a flux weighted average of infiltrating and upflowing salt mass divided by the average water drainage. In full analogy, the long term *ESP* can be approximated very well for different groundwater depths and climates. A more refined analytical approximation, based on the analytical solution of the water balance of *Vervoort and Van der Zee* (2008), leads to a quite good approximation of long term salinity and sodicity, for different soils, groundwater depths, and climates.

4.1 Introduction

Global food production will need to increase with 38% by 2025 and 57% by 2050 (*Wild, 2003*) if food supply to the growing world population is to be maintained at current levels. Most of the suitable land has been cultivated and expansion into new areas to increase food production is rarely possible or desirable. The aim, therefore, should be to increase yield per unit of land rather than the area cultivated. A final limiting factor is the fact that an estimated 15% of the total land area of the world has been degraded by soil erosion and physical and chemical degradation, including soil salinization (*Wild, 2003*).

According to a report published by the FAO in 2000, the total global area of salt-affected soils including saline and sodic soils is 831 million hectares (*Martinez-Beltran and Manzur, 2005*), extending over all the continents including Africa, Asia, Australia, and the Americas.

The main sources of soil salinity and sodicity development are groundwater and irrigation. In discharge areas of the landscape, water and dissolved salts exit from groundwater to the soil surface. The driving force for upward movement of water and salts are hydraulic gradients including evaporation from the soil and plant transpiration. Salt accumulation is high when the water table is less than a threshold depth (*Shah et al., 2011; So and Aylmore, 1993; Szabolcs, 1989*). However, this threshold depth may vary depending on soil hydraulic properties and climatic conditions.

Salts introduced by irrigation water can also be stored within the root zone because of insufficient leaching. Poor quality irrigation water, low hydraulic conductivity of soil layers, as found in heavy clay soils and sodic soils, and high evaporative conditions accelerate irrigation-induced salinity. Use of highly saline effluent water and improper drainage and soil management increase the risk of salinity and sodicity in irrigated soils.

Salt-affected soils deteriorate as a result of changes in the proportions of certain cations and anions present in the soil solution and on the exchange sites. These changes lead to osmotic and ion-specific effects as well as to imbalances in plant nutrition, which may range from deficiencies in several nutrients to high levels of sodium (Na). Such changes have a direct impact on the activities of plant roots and soil microbes, and ultimately on crop growth and yield (*Fortmeier and Schubert, 1995; Grattan and Grieve, 1999; Mengel and Kirkby, 2001; Naidu and Rengasamy, 1993*).

Sodic soils are an important category of salt-affected soils that exhibit unique structural problems as a result of certain physical processes (slaking, swelling, and dispersion of clay) and specific conditions (surface crusting and hard setting) (*Halliwell et al., 2001; Qadir and Schubert, 2002; Shainberg and Letey, 1984; So and Alymore, 1993; Sumner, 1993*). These problems can affect water and air movement, plant available water holding capacity, root penetration, seedling emergence, runoff and erosion, as well as tillage and sowing operations (*Oster and Jayawardane, 1998*). Sodic and saline-sodic soils account for about 60 per cent of the world's salt-affected area (*Tanji, 1990*).

Although no hard data exists, it is generally recognized that a large proportion of these soils occur on land belonging to smallholder farmers, who rely on that land to satisfy their food and feed needs (*Qadir et al., 2006*).

Soil sodicity is usually quantified by the Exchangeable Sodium Percentage (*ESP*), which is the proportion of the cation exchange capacity occupied by sodium ions. If *ESP* becomes too large (e.g. over 15%), the hazard of organic and inorganic colloid dispersion upon introducing good quality water (such as rainwater) becomes large. Since the development of soil sodicity is gradual, and often irreversible within limits imposed by reasonable time scales, it is essential to anticipate its onset. Unfortunately, relatively simple conceptual tools such as the leaching requirement for salinity control (*Corwin et al., 2007; Howell, 1988; Richards et al., 1954*) are not available for sodicity control especially in groundwater driven agro-ecosystems.

Cation exchange as described by the Gapon equation, which is favored in soil salinity research, is nonlinear with regard to the total salt concentration as well as regarding the salt composition (*Bolt, 1982; Bresler 1982; Kaledhonkar et al., 2001; Simunek et al., 1996; Van der Zee et al., 2010*). In view of this nonlinearity, and the observed periodical salinity (*Minhas et al. 2007; Tedeschi and Dell'Aquila, 2005*), it is worthwhile to explore how such nonlinearities affect sodicity development in groundwater driven agro-ecosystems. To study these systems, an ecohydrological sodicity model is developed that builds on an earlier model of soil water dynamics (*Vervoort and van der Zee 2008*) and on the salinity extension by *Shah et al.* (2011). In general, simple water balance, salt balance and cation balance approaches are efficient in terms of simulation time and number of input parameters to diagnose the fate of soil and vegetation under different soil type, climate, groundwater depths, soil *CEC*, and root zone thickness.

The main aims of our current paper are (i) to quantify and understand how soil salinity and sodicity develop under different soil type, soil *CEC*, root zone thickness (Z_r), climate, and groundwater depths (Z), (ii) to determine the long term and short term behavior of soil ESP for different groundwater depths, climates, and soil saturated hydraulic conductivity, (iii) to determine the analytical approximations of long term

average fluxes, salt concentrations and soil ESP under different climates, root zone thicknesses, and groundwater depths.

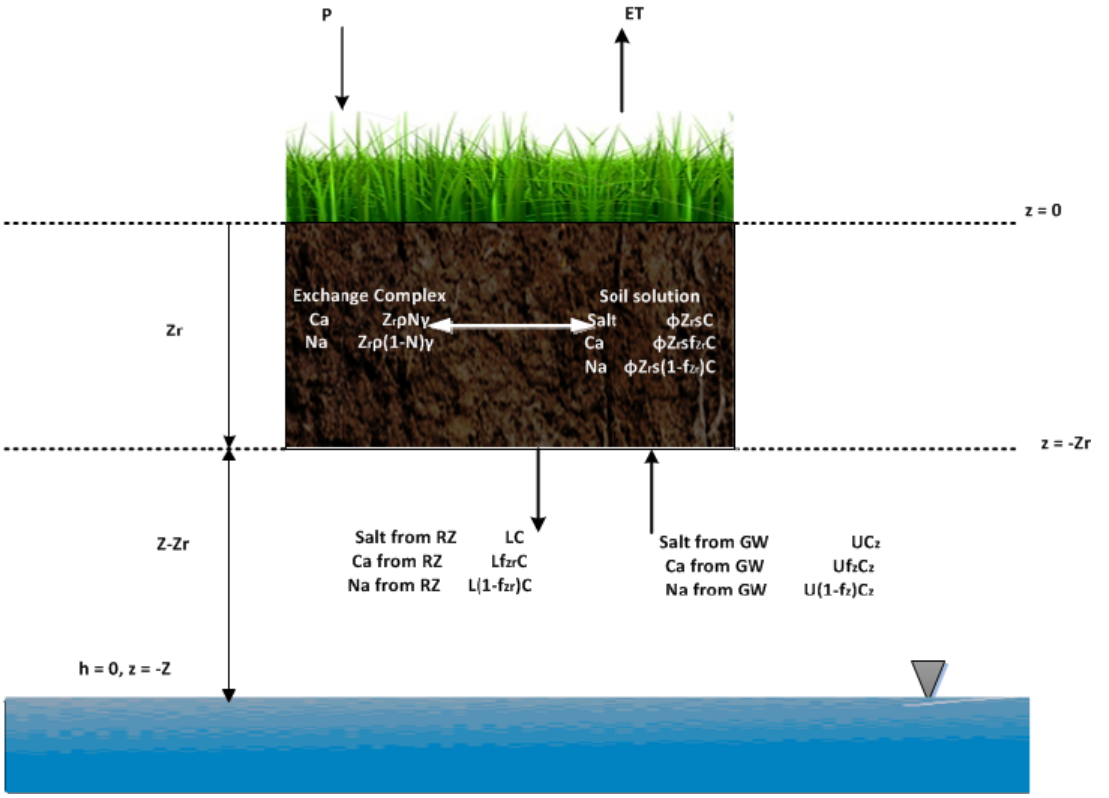

Figure 4.1. The conceptual model for saline groundwater uptake by vegetation in a semi-arid system. The symbols RZ, GW, C_z, and f_z, refer to root zone, groundwater, groundwater salt concentration, and groundwater calcium fraction respectively.

4.2 Methods

4.2.1 Background theory

The salinity model developed by *Shah et al.* (2011) has been extended for the present modeling. In Figure 1, the conceptual model of our system is shown. We consider a root zone with thickness Z_r and groundwater at a depth equal to Z. For soil sodicity calculations, the main assumptions are the same as used by *Shah et al.* (2011): (i) Soil evaporation, capillary upflow, drainage, and rainfall mainly affect the root zone water storage; (ii) Hysteresis is ignored and the profile of soil water below the root zone with regard to water saturation and fluxes is in steady state; (iii) The groundwater level at depth Z below the soil surface is constant, because fluctuations in groundwater level take relatively more time to occur compared to the fluctuations of climate drivers (solar

radiation, greenhouse gas effect); (iv) The soil is initially free of salts and not sodic. This is an attractive reference, as it enables both the assessment of the rate of changes and the long term salinity and *ESP*. Soil salinity and sodicity develop due to capillary upflowing water from the groundwater into the root zone, which conventionally in this discipline is called primary salinization and sodication (*Shah et al., 2011*; *Szabolcs, 1989; Varrallyay, 1989*).

The water balance equation (*Shah et al., 2011*) comprising rainfall/irrigation (*P*), leaching (*L*), capillary upflow (*U*), and evapotranspiration (*ET*) can be defined as:

$$\phi Z_r \frac{ds}{dt} = P - ET(s) + U(s) - L(s) \qquad \textbf{(4.1)}$$

Where ϕ is soil porosity, s is soil relative saturation, and Z_r is the root zone thickness.

Rainfall (*P*) is modeled at a daily time scale following a marked Poisson model following earlier work (*Shah et al., 2011, Laio et al., 2001; Rodriguez-Iturbe and Porporato, 2004*), using parameters α (the mean storm depth, cm/day) and λ (the mean time between storm events /day).

4.2.2 Root zone salt balance

We have used the salt balance as used by *Shah et al.* (2011). The salt concentration affects the evapotranspiration due to matric and osmotic effect; therefore we have combined the Van't Hoff's law and water retention function (*Brooks and Corey, 1966*) to calculate the virtual saturation (*Bras and Seo*, 1987; *Shah et al., 2011*). The resulting virtual soil saturation is the soil saturation that reflects the availability that plants sense, and depend on both matric and osmotic effects. Other fluxes were kept independent of the osmotic potential. Primary reason is that whereas the chemical potential may affect the driving force, the hydraulic conductivity function is determined by the matric potential, but not by the osmotic potential. We believe that accounting for the osmotic potential in the various other fluxes (than evapotranspiration) would bias the analysis, whereas our parsimonious approach does not easily allow separating osmotic impacts on gradient and on constitutive relationships.

We obtain the following balance equation for the salt mass *M* (*Shah et al.,* 2011):

$$\frac{dM}{dt} = \phi Z_r \frac{dsC}{dt} = U(s)C_Z - L(s)C \qquad \textbf{(4.2)}$$

Where C is the salt concentration in the root zone in mol_c/L, C_z is the salt concentration of the groundwater at depth Z in mol_c/L, M is the salt mass in mol_c/m^2.

4.2.3 Root zone cation balance

In addition to the water and salt balances covered by *Shah et al.* (2011), we have to model the cation composition of the solution and exchange phase for sodicity. The total mass of calcium in the root zone is the sum of calcium mass in the soil solution ($\phi Z_r f_{Zr} Cs$) and calcium mass in the exchange complex ($Z_r \rho \gamma N$).

$$T_{Ca} = \phi Z_r f_{Zr} Cs + Z_r \rho \gamma N \tag{4.3}$$

Where T_{Ca} is the total calcium mass in the root zone in mol_c/m^2, f_{Zr} is the calcium fraction in the soil solution, s is the relative water saturation, ρ is the dry bulk density of soil in kg_{soil}/m^3, γ is the soil cation exchange capacity in mol_c/kg_{soil}, and N is the calcium fraction in the exchange complex. Soil cation exchange capacity (γ) is the maximum quantity of total cations that a soil is capable of holding for exchange with the soil solution. Exchangeable sodium percentage (*ESP*) is the amount of adsorbed sodium (1-N) on the soil exchange complex expressed in percent of the cation exchange capacity (γ).

The change of calcium content ΔT_{Ca} is the difference between the masses of calcium entering the root zone ($Uf_Z C_z \Delta t$) and leaving the soil system ($Lf_{Zr} C \Delta t$). Therefore

$$\frac{dT_{Ca}}{dt} = \phi Zr Cs \frac{df_{Zr}}{dt} + \phi Z r f_{Zr} s \frac{dC}{dt} + \phi Z r f_{Zr} C \frac{ds}{dt} + Z_r \rho \gamma \frac{dN}{dt} = U f_Z C_Z - L f_{Zr} C \tag{4.4}$$

We can only rewrite dN/dt in terms of df/dt and dC/dt, after choosing an appropriate exchange equation for the functional dependence $N(f_{Zr}, C)$. We choose the Gapon equation, because it is quite common in salinity related research, despite its empirical nature. We assume a Gapon constant $K_G = 0.5$ $(mol/L)^{-1/2}$ (*Bolt and Bruggenwert, 1976*), in the Gapon equation given by

$$\frac{1-N}{N} = K_G \sqrt{C} \, \frac{1-f_{Zr}}{\sqrt{f_{Zr}/2}} \tag{4.5}$$

in a dimensionless form. Equation (4.5) implies a larger affinity of sorption of divalent cations compared to monovalent cations, and this affinity decreases as the total concentration of salt (C) increases.

Rewriting equation 4.5 for N gives:

$$N = \frac{1}{1 + K_G\sqrt{2C}\left(\frac{1}{\sqrt{f_{Zr}}} - \sqrt{f_{Zr}}\right)} \tag{4.6}$$

Differentiating equation 4.6 with respect to time, we obtain

$$\frac{dN}{dt} = N^2\left(\frac{K_G\sqrt{f_{Zr}}}{\sqrt{2C}} - \frac{K_G}{\sqrt{2f_{Zr}C}}\right)\frac{dC}{dt} + N^2\left(\frac{K_G\sqrt{C}}{\sqrt{2f_{Zr}}} + \frac{K_G\sqrt{C}}{\sqrt{2f_{Zr}^{\ 3}}}\right)\frac{df_{Zr}}{dt} \tag{4.7}$$

We obtain an explicit form of df_{Zr}/dt by using equation (4.4) and (4.7)

$$\frac{df_{Zr}}{dt} = \frac{Uf_zC_z - Lf_{Zr}C - \phi Z_r f_{Zr}C\frac{ds}{dt} + \left(\frac{Z_r\rho\gamma N(1-N)}{2C} - \phi Z_r f_{Zr}s\right)\frac{dC}{dt}}{\phi Z_r Cs + Z_r\rho\gamma N^2 K_G\sqrt{C/2}\left(\frac{1}{\sqrt{f_{Zr}}} + \frac{1}{f_{Zr}\sqrt{f_{Zr}}}\right)} \tag{4.8}$$

The calcium fraction (f_{Zr}) calculated from equation 8 is used in equation 6 to calculate the calcium fraction in exchange complex (N), which gives indirectly the sodium fraction in the exchange complex (1-N) and finally the soil *ESP* ((1-N)*100).

$$ESP = 100\left[1 - \frac{1}{1 + K_G\sqrt{2C}\left(\frac{1}{\sqrt{f_{Zr}}} - \sqrt{f_{Zr}}\right)}\right] \tag{4.9}$$

The equations (4.1), (4.2) and (4.8) are solved together numerically to provide root zone saturation, salt mass and salt concentration (C), soil sodicity (quantified by *ESP*), and the contribution of various water fluxes.

4.2.4 Numerical calculations

We consider two soil types (which we call a heavy clay and sandy clay loam), that differ only in K_s (5 cm/day and 50 cm/day respectively). Other soil hydraulic parameters values were ϕ (soil porosity) = 0.42, b (pore size distribution index) = 13.5 (*Shah et al., 2011*), and are assumed to be the same for both soil types. The vegetation parameters values for a grass Zr = 40 cm, E_w (soil evaporation at wilting point) = 0.013 cm/day, $\psi_{s,s*}$ (matric potential at which stomatal closure begins) = -0.09 MPa, and $\psi_{s,sw}$ (matric potential at which stomatal closure is complete) = -4.5 MPa were based on *Fernandez-*

Illescas et al., (2001). Maximum evapotranspiration (E_{max} = 0.32 cm/day) is calculated by using equation 3 in *Teuling and Troch* (2005) and a leaf area index for grass (ξ = 2.5) from *Asner et al.* (2003). Similar to earlier work (*Shah et al., 2011; Vervoort and Van der Zee, 2008*), representative climate parameters were calculated from long term rainfall data for several locations in Australia to obtain possible values for α and λ used in this article (Table 4.1).

Table 4.1. Climate properties used in numerical simulations and these properties were calculated from observed data using the methods described by *Rodriguez-Iturbe et al.* (1984).

Climate	α (cm/event)	λ (event/day)	Modelled rainfall input (cm/day)
Dry	1.1	0.3	0.33
Semi-arid	1.25	0.4	0.5
Wet	1.4	0.5	0.7

Initial soil and groundwater physical and chemical parameters for the reference case were assumed for the calcium fraction in the soil solution (f_{Zr}=0.98), groundwater (f_z=0.05) (*Van der Zee et al., 2010*), initial root zone salt concentration (C=0.00098 mol_c/L), groundwater/irrigation water salt concentration (C_z=0.02 mol_c/L) (*Srinivasamoorthy et al., 2008; Sadashivaiah et al., 2008; Shah et al., 2011*), dry bulk density of soil (ρ=1560 kg_{soil}/m^3) (*Richards et al., 1954*), soil cation exchange capacity (γ =0.20 mol_c/kg_{soil}) (*Ezlit, 2009; Sustainable soils and Management, 2005*), initial *ESP* of root zone (*ESP*=0.045 %) and groundwater/irrigation water (ESP_Z=29.82 %). Equation

(4.8) is simulated to lead to the calcium fraction in soil solution (f_{Zr}), from which we obtained the calcium fraction in the exchange complex (N) (equation 4.6) and soil sodicity (quantified by *ESP*).

4.3 Results and Discussion

4.3.1 Temporal changes of salt concentration and soil *ESP* for sandy clay loam soil and heavy clay soil

As the soil *CEC* increases, the amount of sodium in the soil solution required to exchange with calcium in the exchange complex increases. To identify the times where soil *ESP* reaches steady state, we have simulated the process for different groundwater depths, a range of climates and root zone thicknesses. Steady state is defined as the state where soil *ESP* is in dynamic equilibrium with respect to temporal exchange of cations between soil solution and exchange complex. We use the term dynamic equilibrium for saturation, rootzone salt concentration, and *ESP* when these vary dynamically in time around a constant mean value. The equilibrium is reached because the loss of Na from the root zone equals the supply of Na to the root zone averaged over a longer period.

Figure 4.2A demonstrates how the soil *ESP* and salt concentration vary dynamically in response to rainfall for a 25 cm root zone thickness for sandy clay loam soil and heavy clay soil. Although soil *ESP* for different values of *CEC* reaches a dynamic equilibrium, the magnitude of soil *ESP* (for a given groundwater depth, root zone thickness, and climate) decreases slightly with increasing soil *CEC* (Figure 4.2A). The rate of change towards the new dynamic equilibrium is slower if *CEC* is larger, as the quantity of calcium (*Ca*) that needs to exchange with sodium (Na) in the root zone increases with increasing *CEC*. Hence, the amount of sodium (*Na*) that needs to be transported from the irrigation/groundwater to reach a specific *ESP* becomes greater. As the long term *ESP* is independent of *CEC*, according to the Gapon equation, the values of *ESP* depend only on *CEC* (and root zone thickness) if that limiting state has not yet been attained. The final *ESP* of sandy clay loam soil (SCL) for different *CEC* shows relatively smaller dependence of *ESP* on *CEC* compared to heavy clay soil (HC). The reason is that the magnitude of fluxes (capillary and leaching) in sandy clay loam soil is relatively greater than the heavy clay soil. These greater magnitude fluxes in sandy clay loam soil cause the final soil ESP to deviate 2%-4% from ultimate value, whereas the final *ESP* for

heavy clay soil under different *CEC* shows independence (Figure 4.2A). As the temporal variations of salt concentration are in dynamic equilibrium, therefore, the corresponding pdfs of salt concentration for both soil types show the steady state pdfs. Also the corresponding pdfs of soil ESP for sandy clay loam soil approach the dynamic equilibrium relatively faster than heavy clays due to greater magnitude of fluxes (Figure 4.2B).

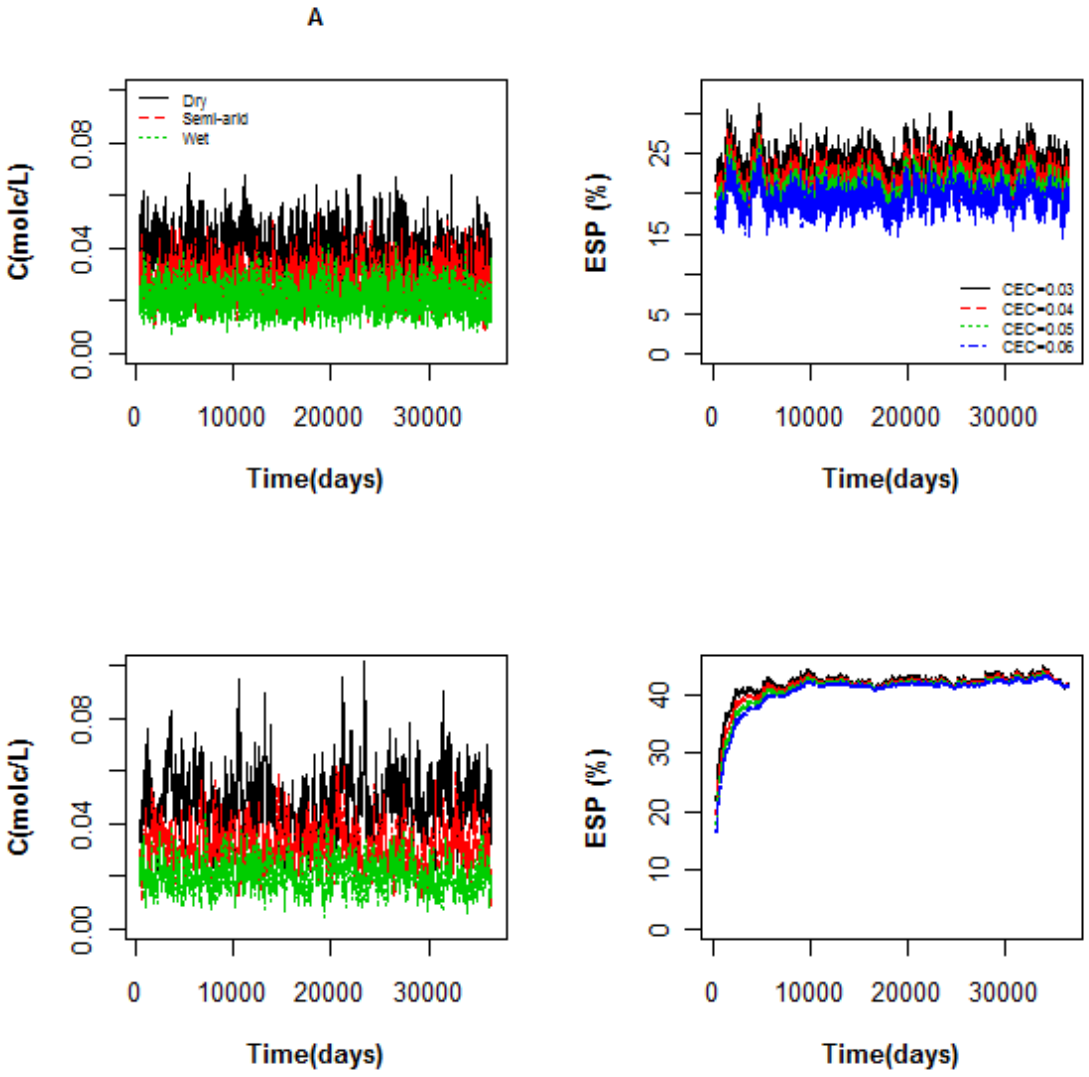

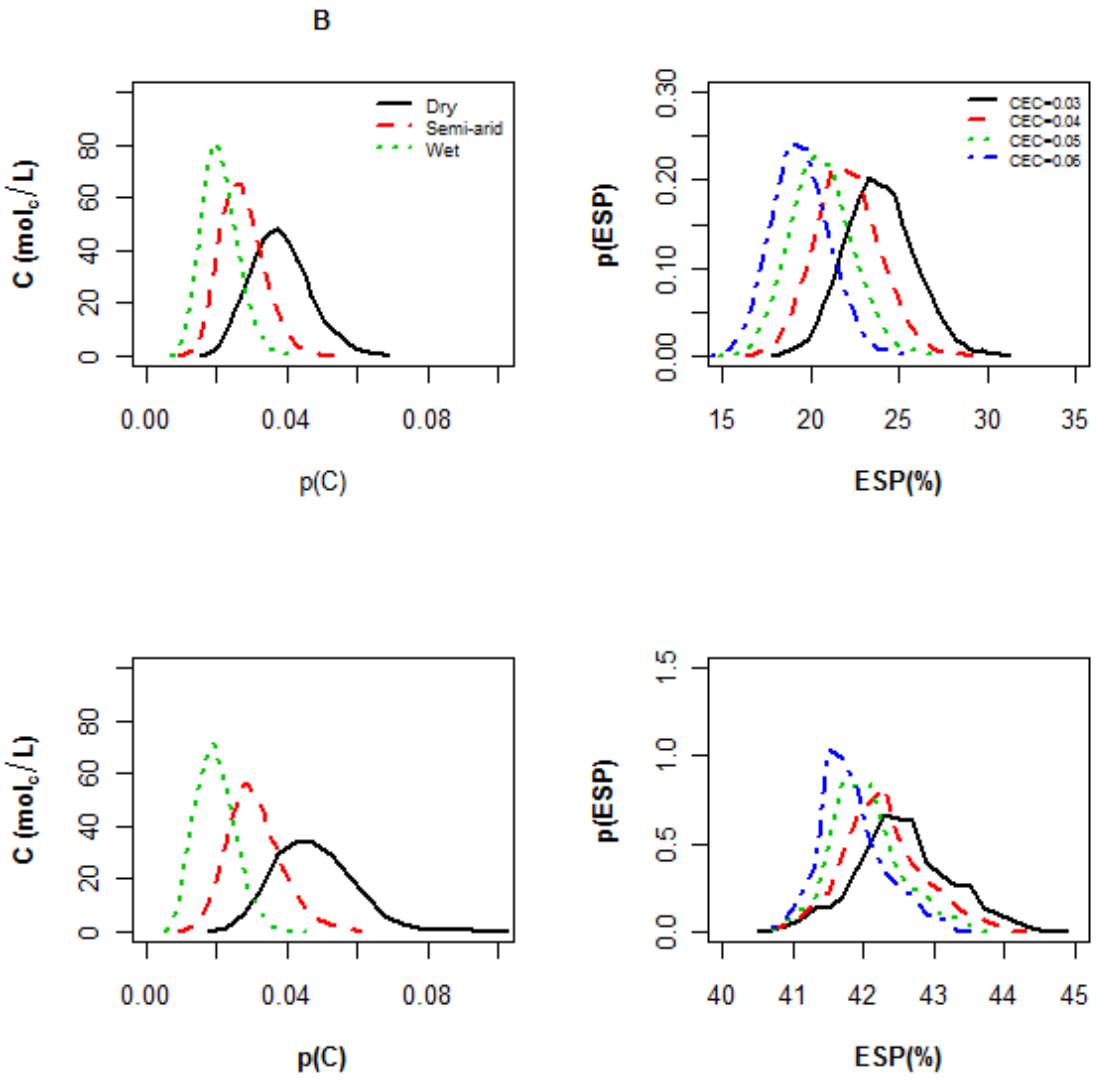

Figure 4.2. A. Temporal variations of salt concentration for sandy clay loam soil (top left panel) and heavy clay soil (bottom left panel) under three climates (dry, semi-arid, wet). Temporal variations of soil *ESP* under different soil *CEC* (0.03 mol_c/kg_{soil}, 0.04 mol_c/kg_{soil}, 0.05 mol_c/kg_{soil}, 0.06 mol_c/kg_{soil}), dry climate, groundwater depth (Z) = 125 cm, and two soil types (top right panel: sandy clay loam, and bottom right panel: heavy clay). B. The probability density functions (pdfs) of salt concentration for last 99 years for both soil types (top left and bottom left panels) and soil ESP for last 99 years in case of sandy clay loam soil (top right panel), in case of heavy clay soil for last 73 years (bottom right panel) correspond to above Figure 4.2A. The root zone thickness (Z_r) is 25 cm, and vegetation is grass. Other conditions are the same as mentioned in numerical calculation section 2.4.

The heavy clay soil used in the simulation has a smaller saturated hydraulic conductivity (K_s) and subsequently smaller fluxes than the Sandy Clay Loam. The development of salt concentration deals with only the soil solution phase in the root zone, whereas the development of soil *ESP* depends on both the soil solution phase and exchange complex of the root zone. In other words, the salt mass coming from the

groundwater balances the salt mass leaching from the root zone due to frequent movement of capillary and leaching flux, which bring salt concentration into dynamic equilibrium faster than soil *ESP*. In contrast, the development of soil *ESP* is relatively complex due to the non-linearity in Gapon equation. As a result, the soil *ESP* takes a longer time to reach dynamic equilibrium compared to the salt concentration (Figure 4.3A).

Similar to the sandy clay loam, the magnitude of soil *ESP* for heavy clay soil decreases if the climate switches from the dry climate to wet climate. Overall, it means that the smaller saturated hydraulic conductivity of the heavy clay soil appears to be the influential parameter in addition to climate type, groundwater depth, root zone thickness determining whether soil *ESP* levels rise above the critical level of 15 (*Richard et al., 1954*). Also soil *ESP* is relatively more sensitive to soil saturated hydraulic conductivity compared to groundwater depth regarding the variability and crossing the threshold level of soil *ESP*. Also the corresponding pdfs of salt concentration show that salt concentration approaches the dynamic equilibrium relatively faster than the soil ESP due to the same reason as explained in above paragraph (Figure 4.3B).

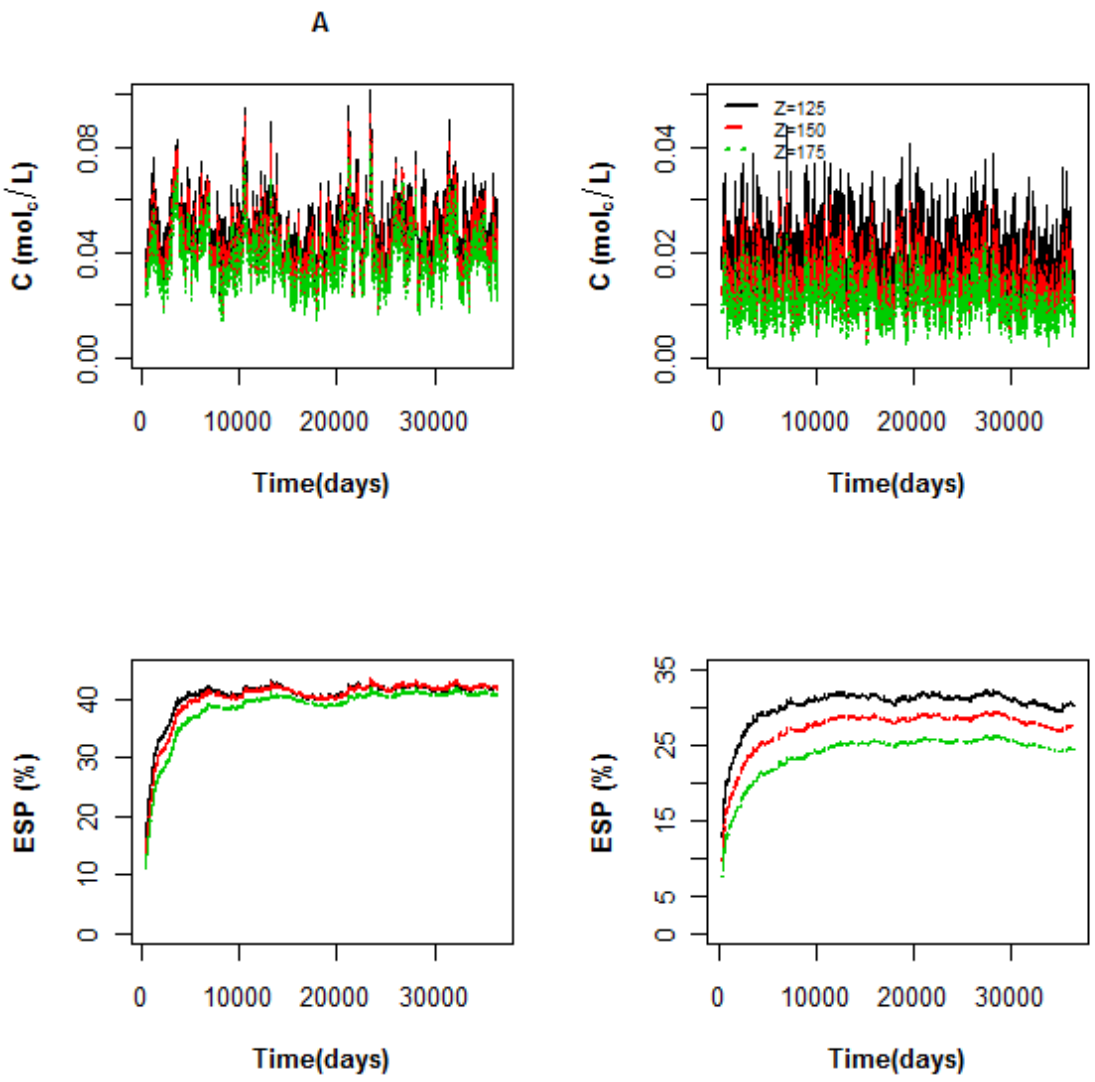
A
C (mol$_c$/L)
0.00
0.04
0.08
0
10000
20000
30000
Time(days)
C (mol$_c$/L)
0.00
0.02
0.04
Z=125
Z=150
Z=175
0
10000
20000
30000
Time(days)
ESP (%)
0
10
20
30
40
0
10000
20000
30000
Time(days)
ESP (%)
0
5
15
25
35
0
10000
20000
30000
Time(days)

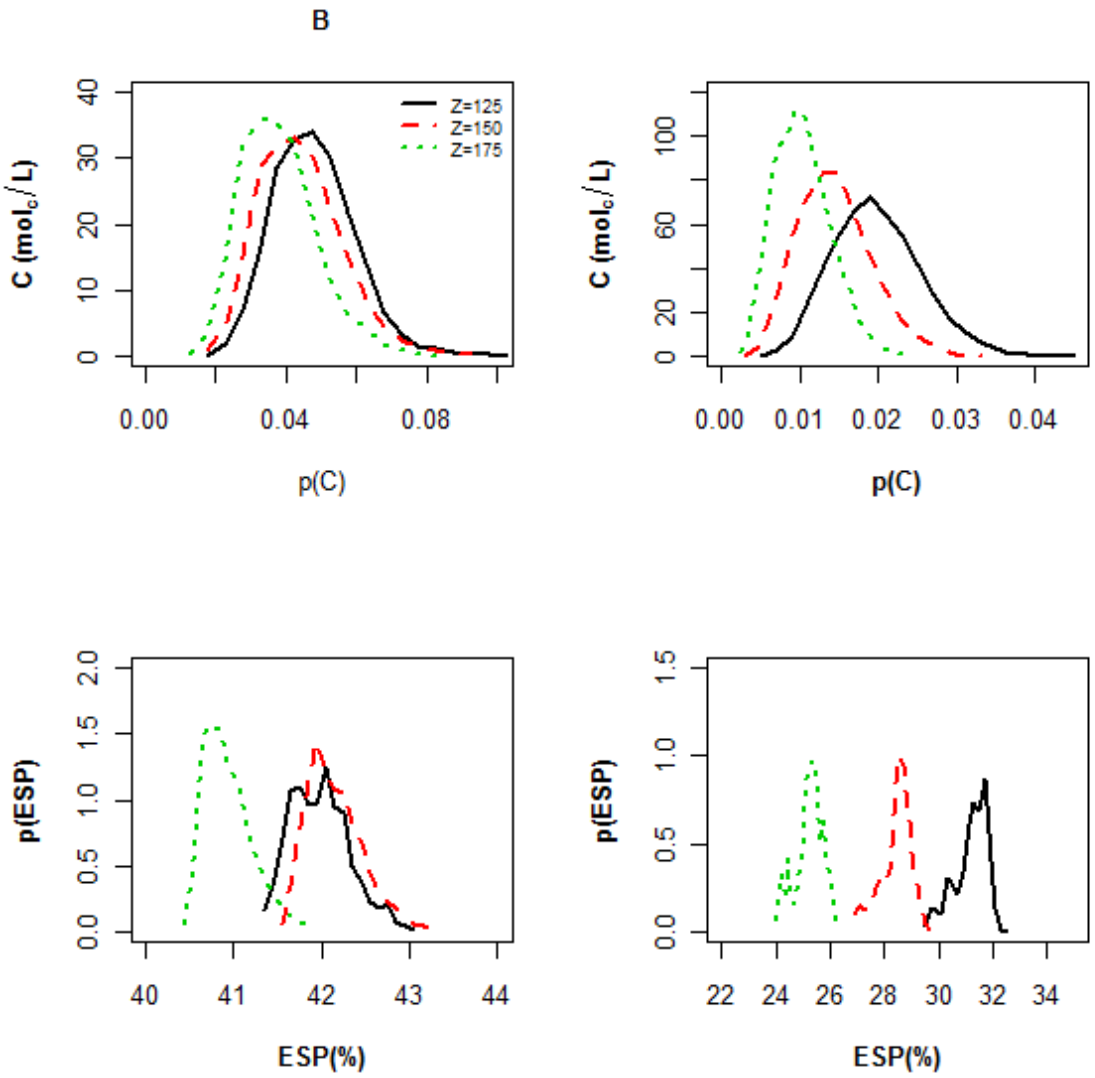

Figure 4.3. A. Temporal variations of salt concentration (*C*) and soil ESP (for 2nd row; *CEC* = 0.05 mol$_c$/kg$_{soil}$) under three different groundwater depths (*Z* = 125 cm, *Z* = 150 cm, *Z*= 175 cm) and two climates (left side: dry, right side: wet; Table 1). B. The pdfs of salt concentration for last 90 years (top left and right panels) and soil ESP for last 20 years (bottom left and right panels) correspond to above Figure 4.3A. The soil is heavy clay, root zone thickness (Z_r) is 25 cm, and vegetation is grass. Other conditions are the same as mentioned in numerical calculation section 2.4.

Furthermore, the fluctuations of soil *ESP* for heavy clay soil are greater, but the soil ESP decreases during the last 15 years in wet climate. The reason is that we have generated the soil *ESP* for only one rainfall realization. We have also simulated the process for different rainfall realizations for each groundwater depth, and can observe that soil *ESP* during the last 15 years might also increase (Figure 4.4). If the realization has less rainfall, the soil ESP increases due to the dominant effect of salt mass arising from the capillary flux from the groundwater. If the realization has more rainfall, the

groundwater effects decrease which causes a decrease in the salt concentration and subsequently soil *ESP*. It means that this is purely the effect of the rainfall realizations.

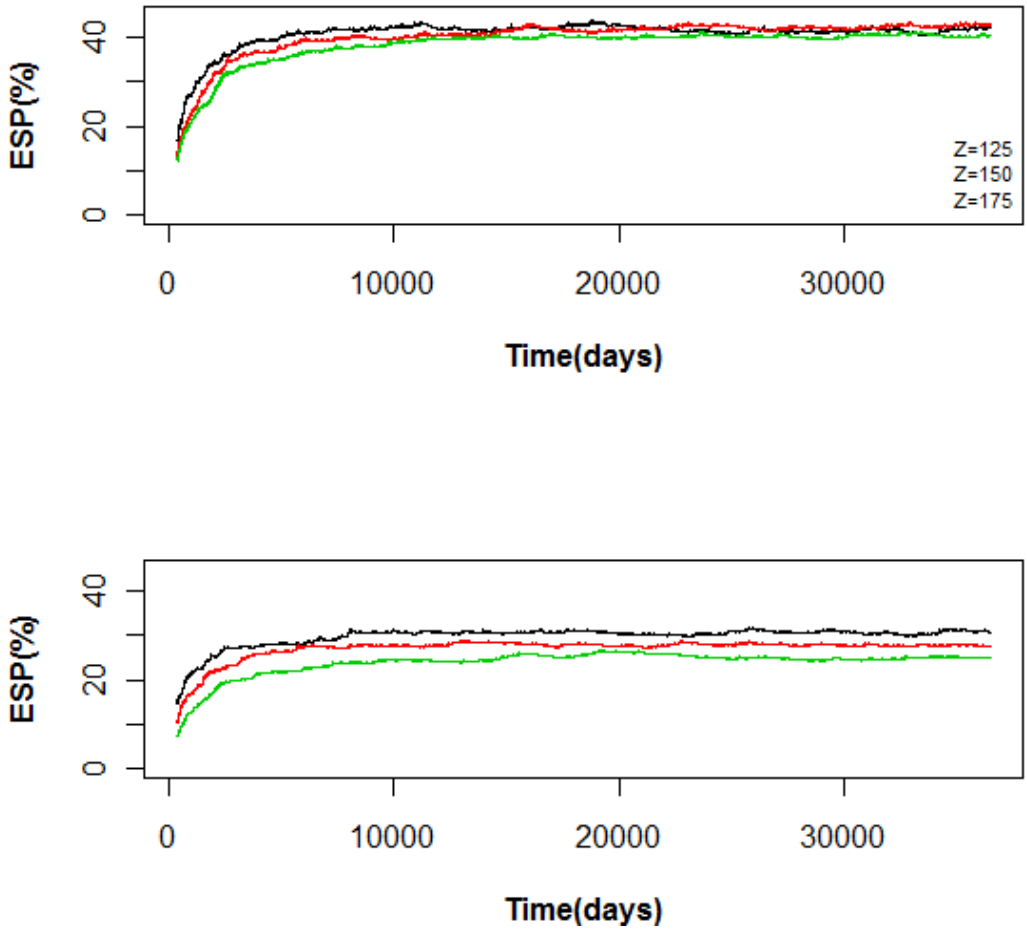

Figure 4.4 Temporal variations of soil ESP (*CEC* = 0.05 mol_c/kg_{soil}) under three different groundwater depths (*Z* = 125 cm, *Z* = 150 cm, *Z*= 175 cm) and two climates (top panel: dry, bottom panel: wet; Table 1). The soil ESP under each groundwater depth is generated with a different rainfall realization. Other conditions are the same as in Figure 4.3.

4.3.2 Long term behavior of soil *ESP*

In our approach of considering a simple root zone reservoir, the main state parameters (saturation *s*, total concentration *C*, and *ESP*) change rapidly from their initial condition at short time, to approach a long term constant average value. For a linear reservoir, an exponential function describes such a change. In view of the rapid approach to its asymptotic behavior of saturation, the assumption of a linear reservoir is appropriate for the total concentration, hence we may write:

$$C(t) = C_{t=\infty}[1 - \exp(-K_C t)] \qquad \textbf{(4.10)}$$

For the *ESP*, we may also assume such an expression for the changes as a function of

time, although the relationship between total concentration and *ESP* is nonlinear (Equation 4.5). Thus,

$$ESP(t) = ESP_{t=\infty}[1 - \exp(-K_{ESP}t)] \quad \textbf{(4.11)}$$

Here $C_{t=\infty}$ and $ESP_{t=\infty}$, represent *C* and *ESP* at infinite times and K_C and K_{ESP}, the inverse characteristic times (1/year), which are the fitting parameters. The two characteristic times depend on the 'buffering' capacity of the rootzone reservoir to changes. Hence, these times depend on the rootzone thickness, but in the case of *ESP*, also on *CEC*. To assess the relationship between soil *ESP* and climate, and saturated hydraulic conductivity, we fitted a simple linear (excluding exponential term) function to the larger times' soil *ESP* signal for the sandy clay loam soil and heavy clay soil with a root zone thickness of 25 cm. To characterize the rate of approaching the long term limiting behavior, for the heavy clay soil, we fitted equations (4.10) and (4.11) for different root zone thickness over the whole range of data. Particularly for larger root zone thicknesses (*Zr*= 50 cm, *Zr*= 100cm), soil *ESP* needs more time to approach a dynamic equilibrium. Figure 4.5 shows the long term average *ESP* as a function of climate under three groundwater depths (*Z* = 125 cm, *Z* = 150 cm, and *Z* = 175 cm). The period selected for calculating average and variance of residuals ranges from 50 years to 100 years, to avoid the initial change towards the dynamic steady state. The fitting quality of the linear model on the last part of the soil *ESP* is determined by using the statistical measure root mean square error (RMSE), which ranged between 0.7 and 0.9.

In a dry climate, the magnitude of soil *ESP* is greater due to the dominant effect of capillary flux compared to leaching flux causing greater exchange rate of cations (Na/Ca) between soil solution and exchange complex. Therefore, the overall variance of soil $ESP_{t=\infty}$ for dry climate is greater compared to semi-arid ($\alpha\lambda$ = 0.5 cm/day) and the wet climate ($\alpha\lambda$ = 0.7 cm/day). In addition, the variance of soil $ESP_{t=\infty}$ for wet climate is relatively greater than semi-arid climate, which just indicates the uncertainty due to considering a single realization. Similarly, the magnitude of soil *ESP* decreases with increasing soil saturated hydraulic conductivity. The overall variability of soil $ESP_{t=\infty}$ further varies as a function of soil saturated hydraulic conductivity (Figure 4.6). For soils having a smaller saturated hydraulic conductivity, the magnitude of fluxes from the groundwater and leaving the root zone are smaller than for a soil having a greater

saturated hydraulic conductivity. Therefore, variance in a sandy clay loam soil is greater than in heavy clay soil (Figure 4.6). Furthermore, the variance soil $ESP_{t=\infty}$ for medium clay (Ks = 25 cm/day) is relatively smaller than heavy clay soil (Ks = 5 cm/day), which again indicates the uncertainty due to considering a single realization.

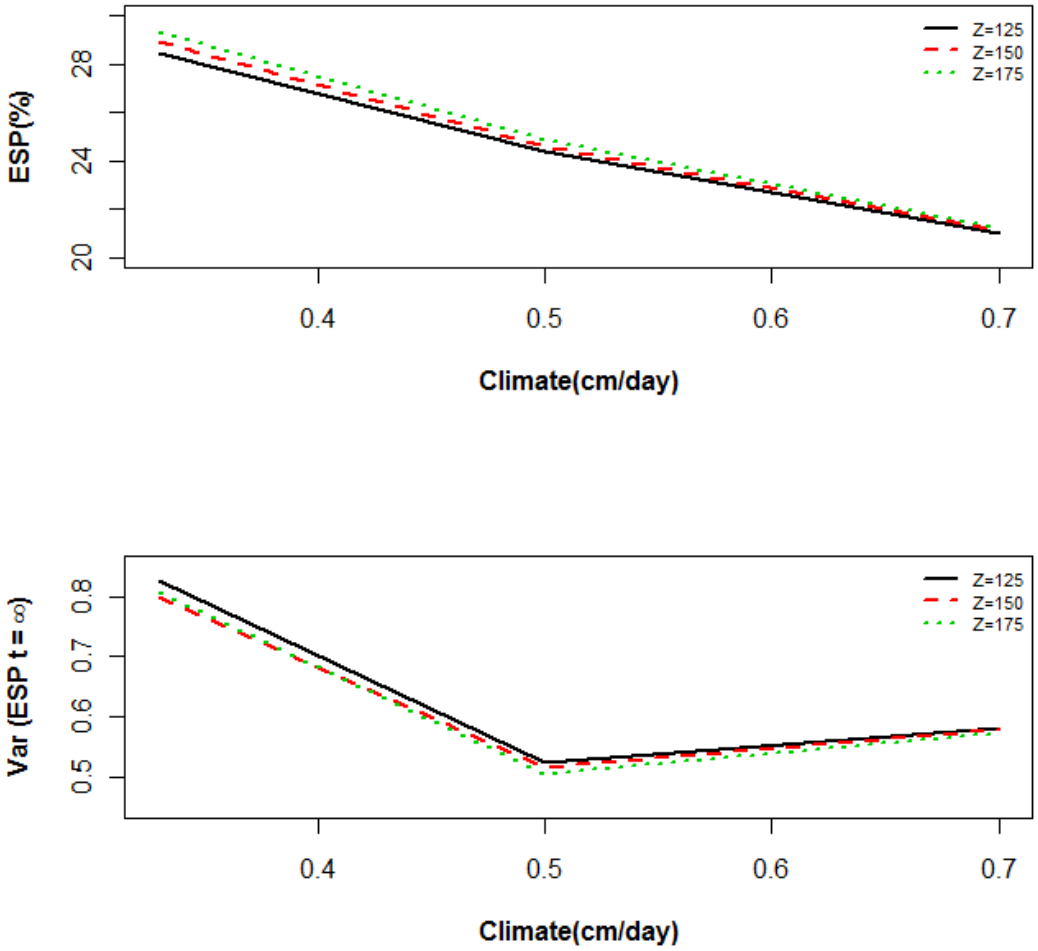

Figure 4.5. Long term (last 50 years) average, and variance of soil $ESP_{t=\infty}$ as a function of climate ($\alpha\lambda$ in cm/day) for three groundwater depths (Z=125 cm, Z=150 cm, Z=175 cm). The soil is sandy clay loam, root zone thickness (Z_r) is 25 cm, and vegetation is grass. Other conditions are the same as mentioned in numerical calculation section 4.2.4.

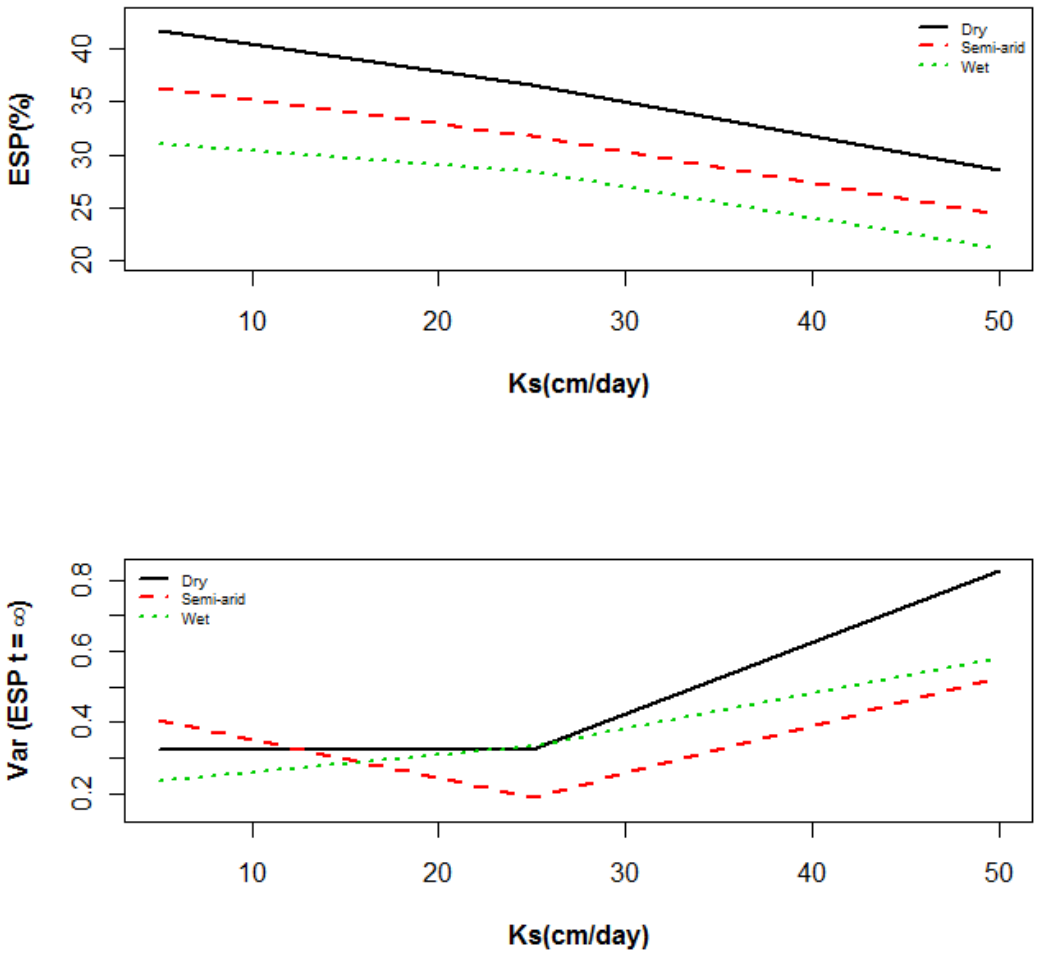

Figure 4.6. Long term (last 50 years) average, and variance of soil $ESP_{t=\infty}$ as a function of soil saturated hydraulic conductivity (K_s in cm/day) under one groundwater depth (Z=125 cm). Root zone thickness (Z_r) is 25 cm, and vegetation is grass. Other conditions are the same as mentioned in numerical calculation section 4.2.4.

To determine the relationship of soil *ESP* signal with climate, and groundwater depth *Z*, we have fitted a linear model to the soil *ESP* values over the last 50 years of the simulation, as at this point variances and the means seem to have stabilised. Fitting the linear regression indicated generally good fits for all cases with the RMSE being less than 0.3, we believe that fitting is justifiable. It means we can conclude that soil *ESP* signal in heavy clay soil takes 50 years to approach complete dynamic equilibrium. The magnitude and variance of soil ESP decreases with increasing groundwater depth (Figure 4.7).

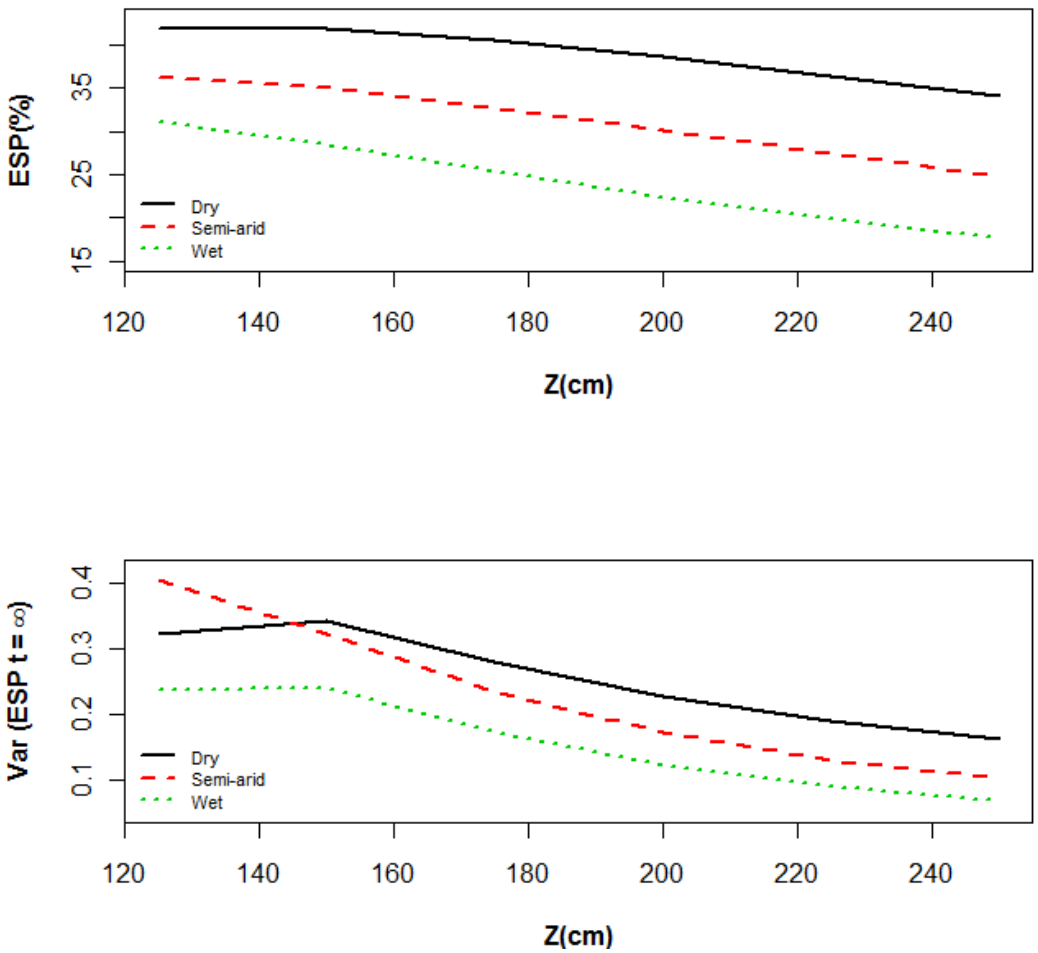

Figure 4.7. Long term (last 50 years) average soil *ESP* and variance of soil $ESP_{t=\infty}$ as a function of groundwater depth under three climates (dry, semi-arid, wet, Table 1). The soil is heavy clay, root zone thickness (Z_r) is 25 cm, and vegetation is grass. Other conditions are the same as mentioned in numerical calculation section 4.2.4.

Based on the linear fits we can demonstrate the relationships between long term average soil *ESP,* and groundwater depth and climate (Figure 4.8). Similar to the sandy clay loam soil, the magnitude of the long term average soil *ESP* decreases with increasing groundwater depth, and increasing wetness (relatively less exchange of cation between soil solution and exchange complex) of climate and vice versa.

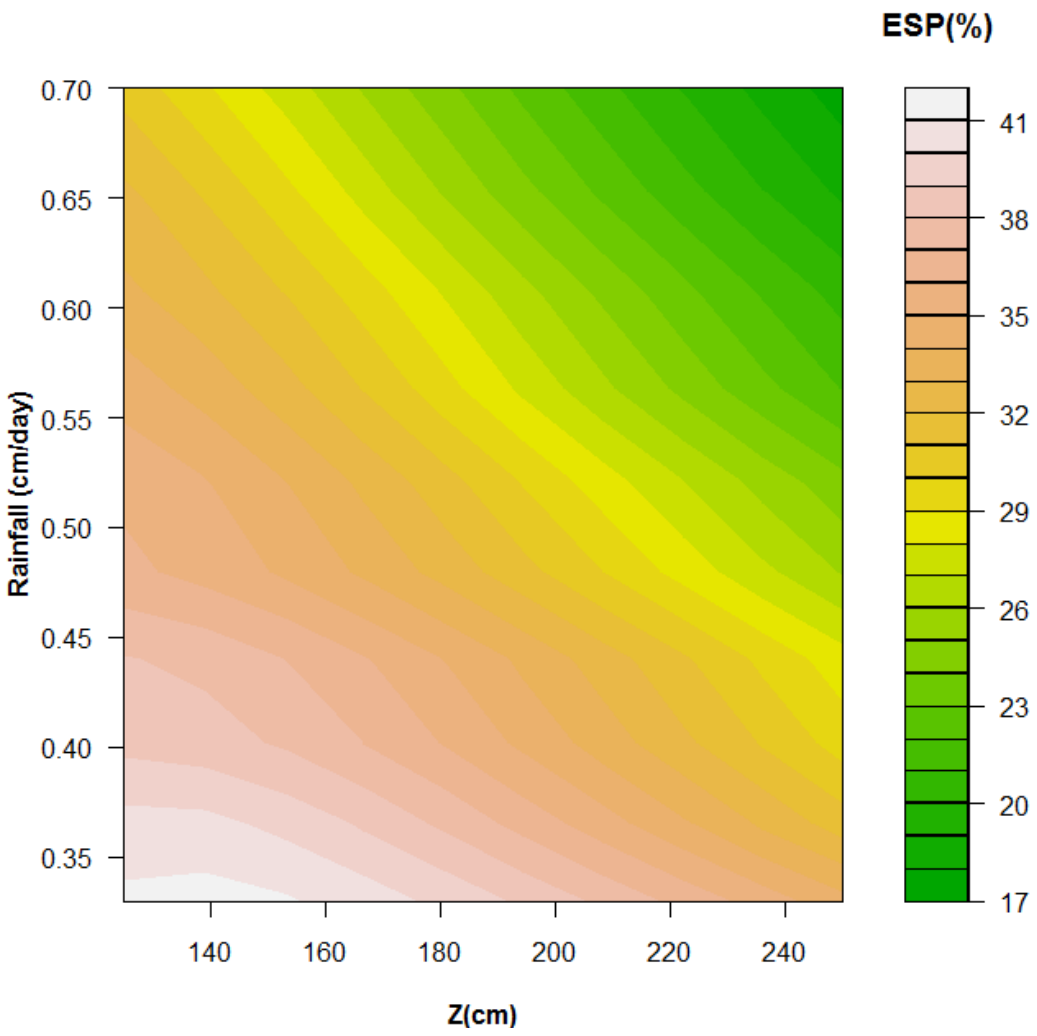

Figure 4.8. 2D representation of long term (last 50 years) average soil *ESP* as a function of groundwater depth (Z in cm) and rainfall (αλ, cm/day). The soil CEC is 0.05 mol_c/kg_{soil}. The soil is heavy clay, root zone thickness (Z_r) is 25 cm, and vegetation is grass. Other conditions are the same as mentioned in numerical calculation section 4.2.4.

4.3.3 Effect of different root zone thickness on salt concentration and soil *ESP*

A different root zone thickness under a constant Z-Z_r distance can have a varying effect on the salt concentration (*Shah et al. 2011*) and therefore also on soil *ESP*. In a dry climate, the salt concentration decreases with increasing Z-Z_r distance for root zone thicknesses of 25 cm and 50 cm (Figure 4.9) and salt concentration for greater root zone (Z_r =100 cm) thicknesses increases until the Z-Z_r distance equals 125 cm and then decreases due to dilution (*Shah et al., 2011*). The trend of salt concentration for root zone thickness of 100 cm under heavy clay soil is similar to the Sandy Clay Loam in Figure 7

of *Shah et al.* (2011), and also different due to use the different vegetation properties. In Figure 7 of *Shah et al.* (2011), the vegetation is trees while the vegetation in this paper is grass. In a dry climate, $<U>$ is dominant over $<L>$ under all root zone thicknesses and the magnitude of $<U>$ and $<L>$ decreases with increasing Z-Z_r distance, therefore, the salt concentration decreases with increasing Z-Z_r distance. Furthermore, the relative and absolute magnitude of $<U>$ is greatest for a 25 cm root zone for the 100 cm Z-Z_r distance, resulting in a greater average salt concentration (Figure 4.9). In contrast for larger Z-Z_r distances, the relative ordering of the salt concentrations between root zone depths reverses. i.e. the salt concentration for 100 cm root zone thickness is greatest and decreases with decreasing root zone thickness due to dilution factor (*Shah et al., 2011*).

In contrast, in a wet climate, the salt concentration decreases with increasing Z-Z_r distance for all root zone thicknesses as $<L>$ is dominant over $<U>$. Furthermore, the magnitude of $<L>$ is greatest for a 100 cm root zone for all Z-Z_r distances resulting in a smaller average salt concentration (Figure 4.9).

In Figure 4.10, the simulation time of the model is 200 years as the soil *ESP* for a greater root zone thickness should take more time to stabilize. However, even at this longer simulation time, soil *ESP* does not reach a stable state (Figure 4.10). Actually for a greater root zone thickness, a greater magnitude of *CEC* (see section 4.2.3), and a dry climate, the relative magnitude of $<U>$ and associated sodium mass coming from groundwater is smaller (*Shah et al., 2011*). As a result the rate of exchange for sodium and calcium between soil solution and the exchange complex decreases and therefore the soil *ESP* does not reach a stable equilibrium (Figure 4.10).

Similarly in a wet climate with a greater root zone thickness, the magnitude of $<L>$ and associated sodium mass leaching from the root zone is greater than for a smaller root zone thickness for a constant Z-Z_r distance. As a result, exchange rate for sodium and calcium between soil solution and the exchange complex decreases and therefore, soil *ESP* also becomes unsteady (and continues to slowly increase, Figure 4.10). Overall this results in a lower magnitude of the soil *ESP*. In contrast, for smaller root zone thicknesses, the magnitude of $<L>$ is smaller relative to a greater root zone thickness.

Consequently, soil ESP approaches a dynamic equilibrium due to the fast exchange rate of cations between soil solution and the exchange complex.

As a result the magnitude and dynamic status of soil *ESP* for a constant Z-Z_r distance depends on the root zone thickness. For greater root zone thickness under constant Z-Z_r distance, the total amount of Ca is too large and cannot be fulfilled by the sodium transport associate with U; therefore the soil *ESP* signal does not stabilize in time.

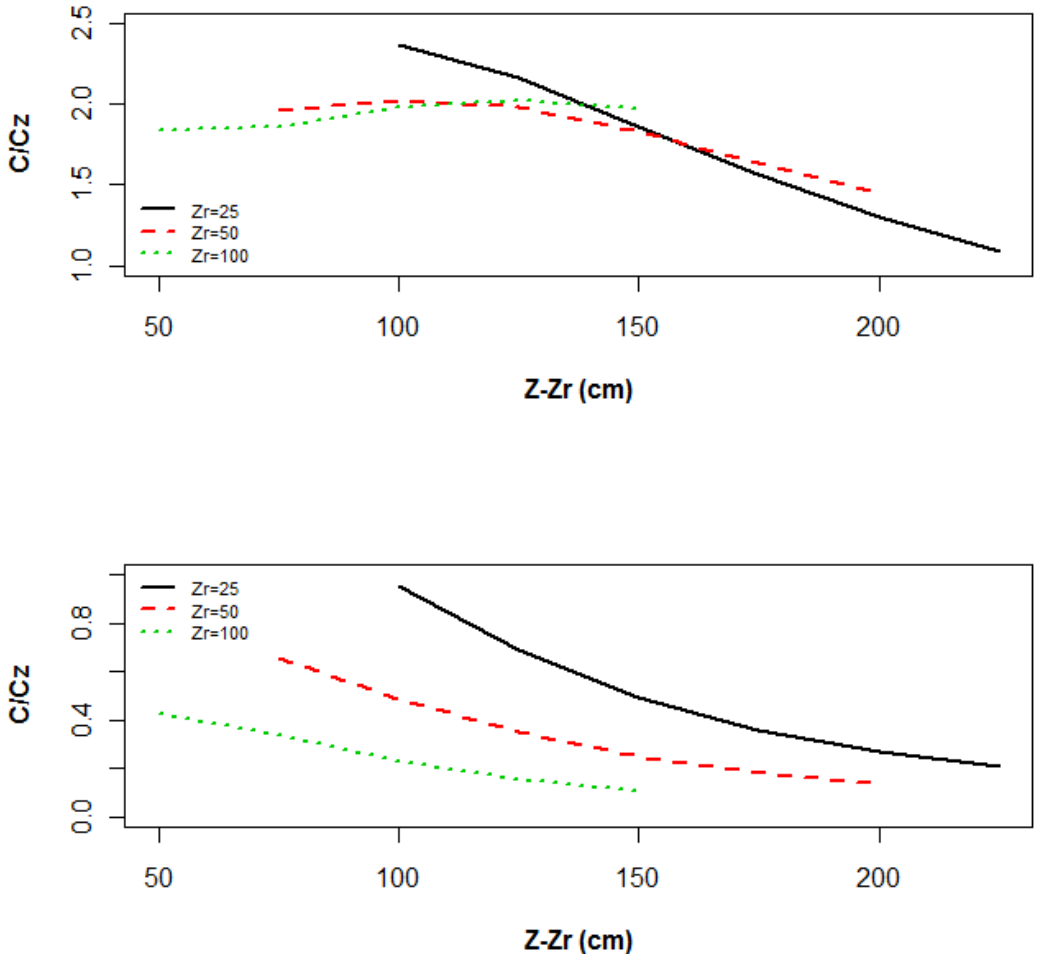

Figure 4.9. Long term average relative salt concentration with respect to groundwater salt concentration as a function of Z-Z_r for different root zone thickness (Z_r = 25 cm; Z_r = 50 cm; Z_r = 100 cm) under two climates (top panel: dry climate, bottom panel: wet climate; Table 1). The soil is heavy clay, root zone thickness (Z_r) is 25 cm, and vegetation is grass. Other conditions are the same as mentioned in numerical calculation section 4.2.4.

For a wet climate, the fitting of the exponential function (equation 4.11) appears quite good compared to a dry climate especially for greater root zone thicknesses (not shown). Generally the magnitude of the root mean square error (RMSE) for the wet climate

ranges between 0.25 and 1.11 and for the dry climate ranges between 0.89 and 1.57. Overall, the magnitude of RMSE in both dry and wet climates is less than 4% of magnitude of the final *ESP*, and therefore, we believe that fitting of the exponential function over the whole range of *ESP* is satisfactory (Figure 4.10).

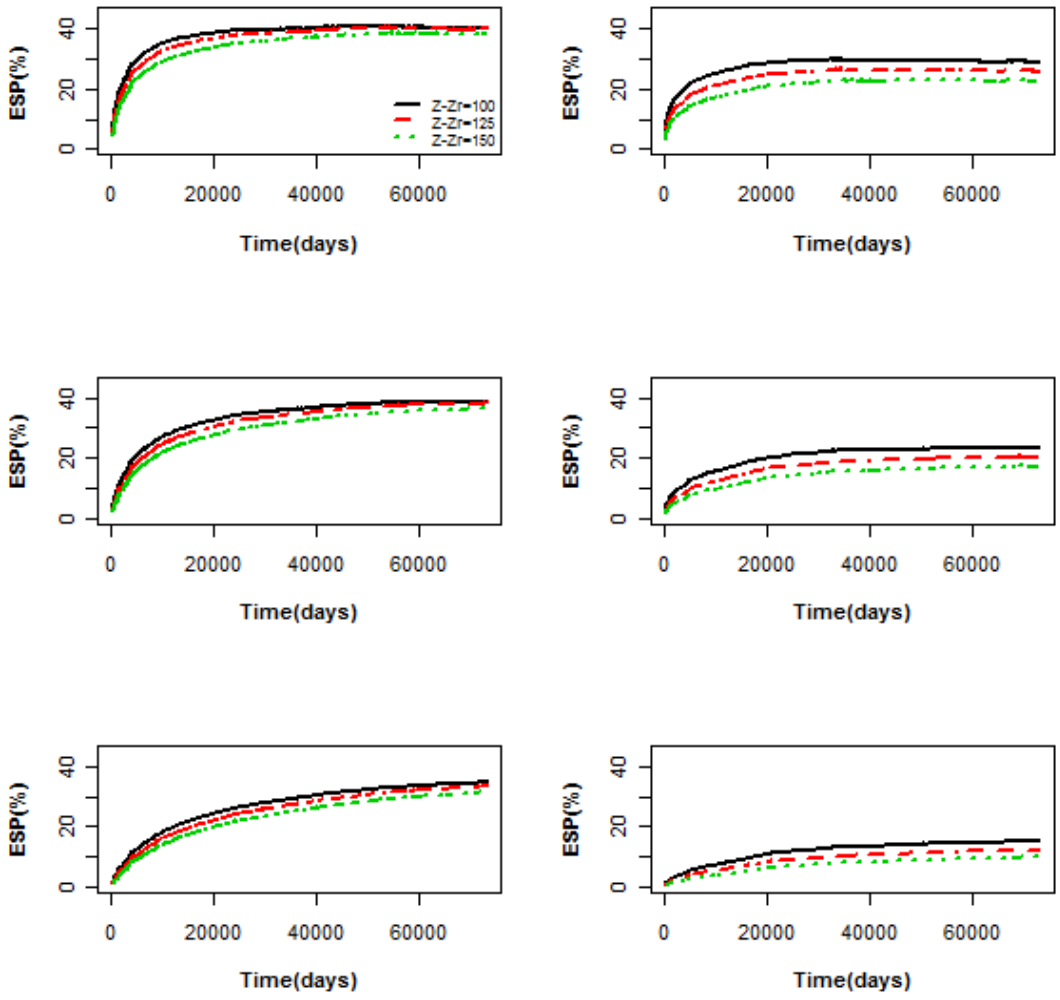

Figure 4.10. Temporal variations of soil *ESP* for three root zone thickness (top: 25 cm, middle: 50 cm, bottom: 100 cm) under three constant Z-Zr distances (100cm, 125 cm, 150cm) and two climates (left side: dry climate, right side: wet climate). The soil cation exchange capacity is equal to 0.20 mol_c/kg_{soil} (see section 2.3). The soil is heavy clay, root zone thickness (Z_r) is 25 cm, and vegetation is grass.

The parameters $ESP_{t=\infty}$, and K_{ESP} decrease with increasing root zone thickness, which confirms that for a greater root zone thickness, dynamic equilibrium is approached slower than for smaller root zone thicknesses (Figure 4.11). The fitting parameter which is inverse characteristics residence time (1/year) of soil *ESP* decreases with increasing root zone thickness. In other words, it means that for greater root zone thickness, the characteristics residence becomes greater than the smaller root zone thickness. Therefore,

K_{ESP} can explain the time where soil *ESP* approaches dynamic equilibrium as a function of the root zone thickness.

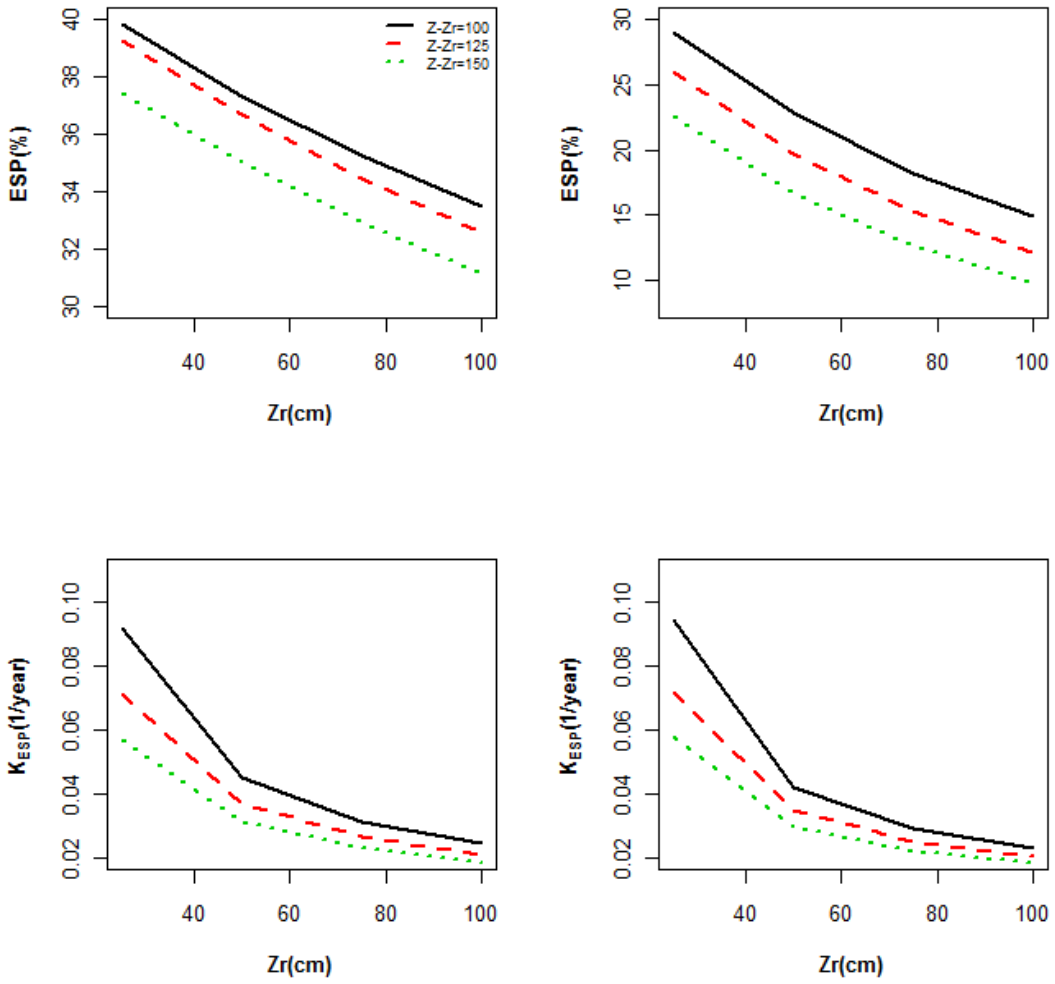

Figure 4.11. The relationship of fitted parameters ($ESP_{t=\infty}$, and K_{ESP} with root zone thickness under three Z-Z_r distances (100 cm, 125 cm, and 150 cm) and two climates (left side: dry, right side: wet). Other conditions are the same as mentioned in Figure 4.9.

We have also fitted a linear regression model to the last 15 years of the soil *ESP* signal to calculate the variance and RMSE of the signal (Figure 4.12). Again the fitting of the linear regression model is relatively good with RMSE in all case ranging from 0.023 to 0.09. In a dry and wet climate, the variance of $ESP_{t=\infty}$ decreases with increasing root zone thickness causing smaller magnitude of soil *ESP* under constant Z-Z_r distance for greater root zone thicknesses (Figure 4.12).

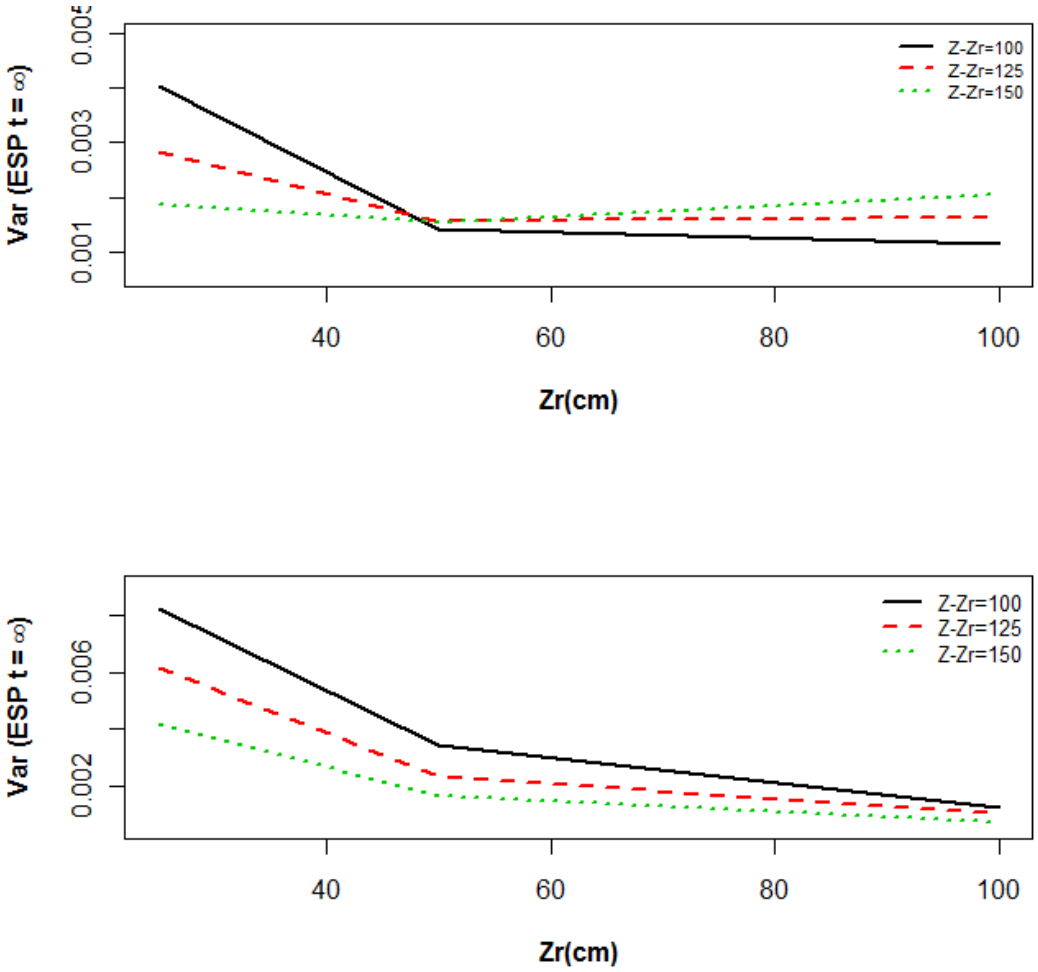

Figure 4.12. The relationship of variance of soil *ESP* based on Figure 11 with root zone thickness under three Z-Z_r distances (100 cm, 125 cm, and 150 cm) and two climates (top panel: dry, bottom panel: wet). Other conditions are the same as mentioned in Figure 4.9.

4.3.4 Effect of different percentage of salt concentration in rainfall on salt concentration and soil *ESP*

To replenish the calcium mass coming from the groundwater, calcium mass is included in rainfall/irrigation. By adding calcium mass in the rainfall, the soil *ESP* approaches into dynamic equilibrium relatively faster than a case where calcium mass in rainfall is ignored. In order to investigate the long term effects of calcium mass coming from rainfall/irrigation and groundwater on the root zone salt concentration and soil *ESP* development, we have considered the following salt and cation balance equations for the cases where salt concentration and soil *ESP* are in complete dynamic equilibrium.

Considering the salt coming from the groundwater and rainfall/irrigation, and salt leaching from the root zone give the following salt balance equation

$$< P > C_P + < U > C_Z =< L >< C > \quad \textbf{(4.12)}$$

Where C_P is the salt concentration in the rainfall/irrigation, $<P>$ is the long term average rainfall entering into the root zone, $<U>$ is the long term average capillary upflow, Cz is groundwater salt concentration, $<L>$ is the long term average leaching flux, and $<C>$ is the long term average root zone salt concentration.

The sum of long term average calcium mass coming from groundwater and rainfall/irrigation gives the calcium mass leaching from the root zone. This mass balance of calcium gives the following calcium mass balance equation.

$$< P > C_P f_P + < U > C_Z f_Z =< L >< C > f_{Zr} \quad \textbf{(4.13)}$$

Where f_P is calcium fraction in rainfall/irrigation, f_Z is the calcium fraction coming from the groundwater; f_{Zr} is calcium fraction in the root zone.

$$f_{Zr} = \frac{\left[< P > C_P f_P + < U > C_Z f_Z\right]}{< L >< C >} \quad \textbf{(4.14)}$$

Inserting equation 4.12 in equation 4.14 gives

$$f_{Zr} = \frac{\left[< P > C_P f_P + < U > C_Z f_Z\right]}{< P > C_P + < U > C_Z} \quad \textbf{(4.15)}$$

From equation 4.14 or 4.15, we can calculate the calcium fraction in the root zone (f_{Zr}), which is function of long term average of rainfall/irrigation and capillary fluxes. Remember that calcium fraction in the rainfall/irrigation (f_P) is equation to 0.5.

In order to quantify the effect of calcium mass coming from rainfall/irrigation water to replenish the calcium mass coming the groundwater, we have considered the following three scenarios: 1. Rainfall contains salt concentration (C_p) equal to 10% of groundwater salt concentration (C_Z). i.e. C_p = 0.002 mol_c/L, C_Z = 0.02 mol_c/L, 2. Rainfall contains salt concentration (C_p) equal to 50% of groundwater salt concentration (C_Z). i.e. C_p = 0.01 mol_c/L, C_Z = 0.02 mol_c/L, 3. Rainfall contains salt concentration (C_p) equal to 100% of groundwater salt concentration (C_Z). i.e. C_p = 0.02 mol_c/L, C_Z = 0.02 mol_c/L. We have simulated the process considering the conditions as mentioned in the scenario 1, scenario 2, and scenario 3 to compare the soil *ESP* (simulation, t =infinity) with ESP (f_{Zr}

from equation above 4.14 or 4.15, C (infinity)), and numerical and analytical salt concentration.

For the heavy clay soil under scenario 1, scenario 2, and scenario 3, the scatter plot for numerical and analytical salt concentration and soil ESP match quite well as shown in Figure 4.13 and Figure 4.14. It means we can approximate the salt concentration and soil *ESP* under different climates and groundwater depths. Furthermore, soil *ESP* among different groundwater depths differs relatively less in magnitude with the increase in percentage of salt concentration in the rainfall under different climates (not shown). The reason is that the calcium mass coming along with rainfall/irrigation become increasingly dominant over the calcium mass coming from groundwater with the increase in percentage of salt concentration in the rainfall/irrigation under different groundwater depths (Figure 4.13).

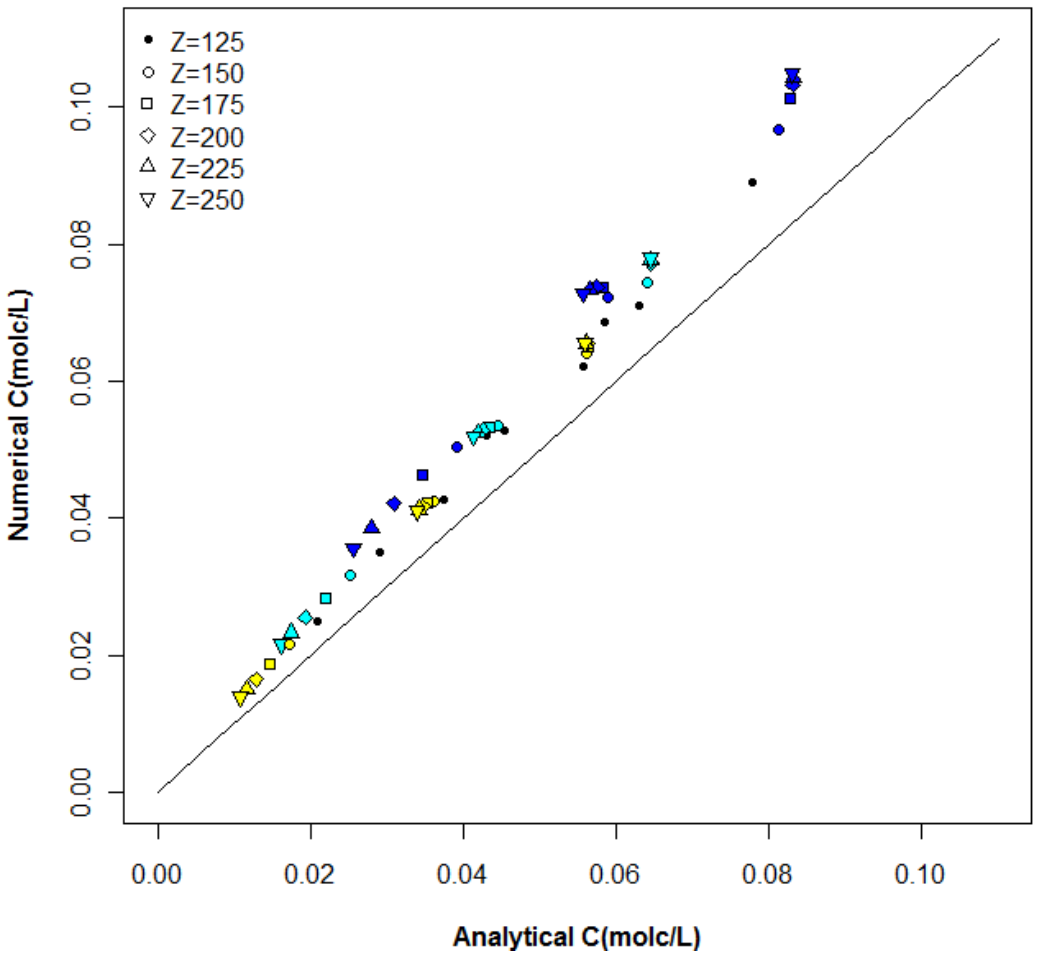

Figure 4.13. Scatter plot of numerical and analytical salt concentration under six groundwater depths and three climates (blue colour: dry climate, turquoise colour: semi-arid, yellow colour: wet). The concentration of salt in rainfall is equal to 100% (0.02 mol_c/L) in case of top blue, turquoise, and yellow, 50% (0.01 mol_c/L) in case of middle blue, turquoise, and yellow, 10% (0.002 mol_c/L) in case of bottom blue, turquoise, and yellow of groundwater salt concentration (0.02 mol_c/L). The calcium fraction in rainfall (f_p) is used 0.5. The soil is heavy clay, root zone thickness (Z_r) is 25 cm, and vegetation is grass. Other conditions are the same as mentioned in numerical calculation section 4.2.4.

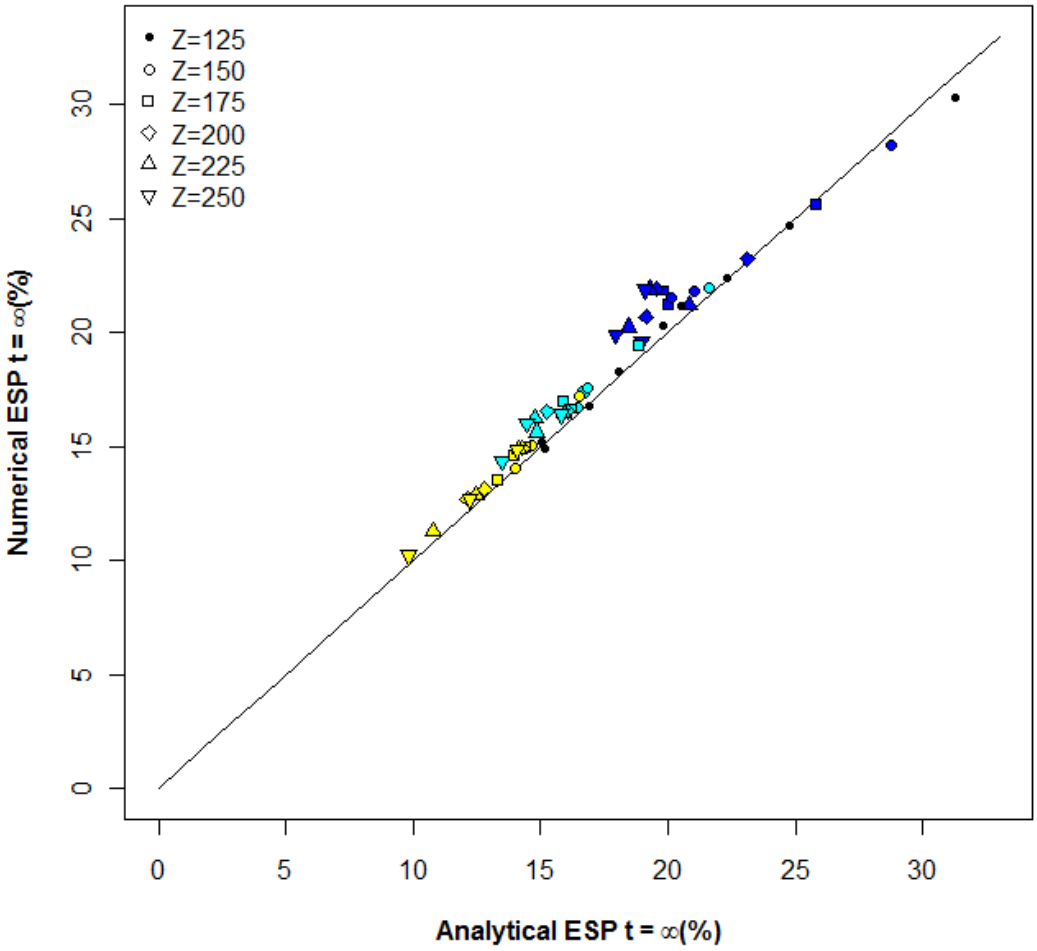

Figure 4.14. Scatter plot of numerical and analytical soil *ESP* under six groundwater depths and three climates (blue colour: dry climate, turquoise colour: semi-arid, pink colour: wet). The concentration of salt in rainfall is equal to 10% (0.002 mol_c/L) of groundwater salt concentration (0.02 mol_c/L). The concentration of salt in rainfall is equal to 100% (0.02 mol_c/L) in case of top blue, turquoise, and yellow, 50% (0.01 mol_c/L) in case of middle blue, turquoise, and yellow, 10% (0.002 mol_c/L) in case of bottom blue, turquoise, and yellow of groundwater salt concentration (0.02 mol_c/L). Other conditions the same as in Figure 4.13.

4.3.5 Analytical solutions of fluxes, salt concentration and soil *ESP*

Salt concentration and soil *ESP* calculated in equation 4.12 and equations 4.14 are semi-analytical solutions, because we have to depend on the long term average of numerical capillary and leaching fluxes. In order to calculate the fully analytical fluxes and consequently salt concentration and soil *ESP*, we have used the analytical solution of probability density function (equation 4.16) developed by *Vervoort and Van der Zee* (2008).

$$p(s)=\begin{cases}\dfrac{C}{(\eta-m_2)}\left[\left(\dfrac{s-s_{cr}}{s^*-s_{cr}}\right)\right]^{\frac{\lambda'(s^*-s_{cr})}{\eta-m_2}-1} e^{-\gamma s} & s_{cr}<s\le s^* \\ C\left[\eta-m_1\left(1-e^{\beta(s-s_{\lim})}\right)\right]^{\frac{-\lambda'}{\beta(\eta-m_1)}-1}\left[\eta-m_2\right]^{\frac{\lambda'}{\beta(\eta-m_1)}}\times & \\ \qquad e^{-\gamma s+\frac{\lambda'}{(\eta-m_1)}(s-s^*)} & s^*<s\le s_{\lim} \\ \dfrac{C}{\eta}\left[1+\dfrac{m}{\eta}\left(e^{\beta(s-s_{\lim})}-1\right)\right]^{\frac{-\lambda'}{\beta(\eta-m)}-1} e^{-\gamma s+\frac{\lambda'}{(\eta-m)}(s-s_{\lim})} e^{\frac{-\lambda'}{(\eta-m_1)}(s^*-s_{\lim})}\times & \\ \qquad \left[1-\dfrac{m_2}{\eta}\right]^{\frac{\lambda'}{\beta(\eta-m_1)}} & s_{\lim}<s\le 1\end{cases} \quad \textbf{(4.16)}$$

Analytical solution of total evapotranspiration (equation 4.19) under stress (E_s) and non-stress (E_{ns}) condition (equation 4.17 and equation 4.18) developed by *Laio et al.* (2001) are:

$$\langle E_s\rangle=\phi Z_r\int_{s_w}^{s^*}E(s)p(s)ds=\alpha\lambda' P(s^*)-\alpha\eta p(s^*) \quad \textbf{(4.17)}$$

$$\langle E_{ns}\rangle=\phi Z_r\int_{s^*}^{1}E(s)p(s)ds=E_{\max}\left[1-P(s^*)\right] \quad \textbf{(4.18)}$$

Where $P(s^*)$ and $p(s^*)$ are cumulative probability density function and probability density function for $s_w<s\le s^*$ and symbol λ' is the rainfall frequency of marked Poisson process called censored process.

The total mean rate of evapotranspiration is equal to the sum of evapotranspiration under stressed and non-stressed conditions.

$$\langle E\rangle=\langle E_S\rangle+\langle E_{ns}\rangle \quad \textbf{(4.19)}$$

Similarly, the mean rate of leaching flux (equation 4.20) developed by *Laio et al.* (2001) is.

$$\langle L\rangle=\phi Z_r\int_{s_{fc}}^{1}L(s)p(s)ds=\alpha\left[\lambda'-\lambda' P(s_{fc})-\left(\eta+\frac{K_s}{\phi Z_r}\right)p(1)+\eta p(s_{fc})\right]-E_{\max}\left[1-P(s_{fc})\right] \quad \textbf{(4.20)}$$

From the analytical solution of evapotranspiration and leaching flux, we have calculated analytically capillary flux (equation 4.21).

$$\langle U\rangle=\langle E\rangle+\langle L\rangle-\langle R_{net}\rangle \quad \textbf{(4.21)}$$

Where <R_{net}> is net rate of rainfall which infiltrates into the root zone.

$$\langle R_{net} \rangle = \alpha\lambda - \langle I \rangle - \langle Q \rangle \quad \textbf{(4.22)}$$

Where αλ is modelled rainfall in cm/day, <I> is the mean interception depth in cm/day and <Q> is the mean runoff in cm/day.

From the analytical solution of fluxes, we can use the following equation 4.23 to calculate the analytical long term average salt concentration.

$$\langle C \rangle = \frac{\langle U \rangle C_z}{\langle L \rangle} \quad \textbf{(4.23)}$$

Where C_z is the groundwater salt concentration and is equal to 0.02 molc/L

By using the analytical solution of salt concentration (equation 4.23), we can approximate the soil *ESP* at t = ∞ by using following equation 4.24.

$$\langle ESP \rangle = 100\left[1 - \frac{1}{1 + K_G\sqrt{2\langle C \rangle}\left(\frac{1}{\sqrt{f_z}} - \sqrt{f_z}\right)}\right] \quad \textbf{(4.24)}$$

Where f_z is the groundwater calcium fraction and is equal to 0.05. For heavy clay soil, the long term root zone calcium fraction becomes equal to the groundwater calcium fraction; therefore, we have used 0.05 as the root zone calcium fraction.

The results of analytical and numerical fluxes (*E*, *L*, and *U*) are shown in Figure 4.15 which match reasonably well. Considering the reasonably well analytical values of fluxes, we have compared the analytical (equation 4.23) and numerical values of salt concentration under different groundwater depths, and climates. For the dry climate especially at shallower groundwater depths, the analytical salt concentration is relatively smaller the numerical salt concentration. The reason is that the analytical solution (equation 4.21) underestimates the capillary flux (due to the underestimation of analytical evapotranspiration), which causes the smaller magnitude of salt concentration compared to numerical salt concentration for the dry climate. As the climates switches from dryer climate to wetter climates, the numerical and analytical salt concentration match reasonable well (Figure 4.16).

Similarly, we have compared the numerical and analytical (equation 4.24) soil ESP under different groundwater depths and climates. Due to the underestimation of capillary flux, again the analytical soil *ESP* for the dry climate especially for shallower groundwater depths is relatively smaller than the numerical soil *ESP* (Figure 4.17). For the semi-arid and wet climate, the analytical and numerical comparison of soil *ESP* is reasonably well. It means that we can use the analytical solution of fluxes, salt concentration and soil *ESP* to approximate the long term values of fluxes, salt concentration and soil *ESP* under different groundwater depths, and climates.

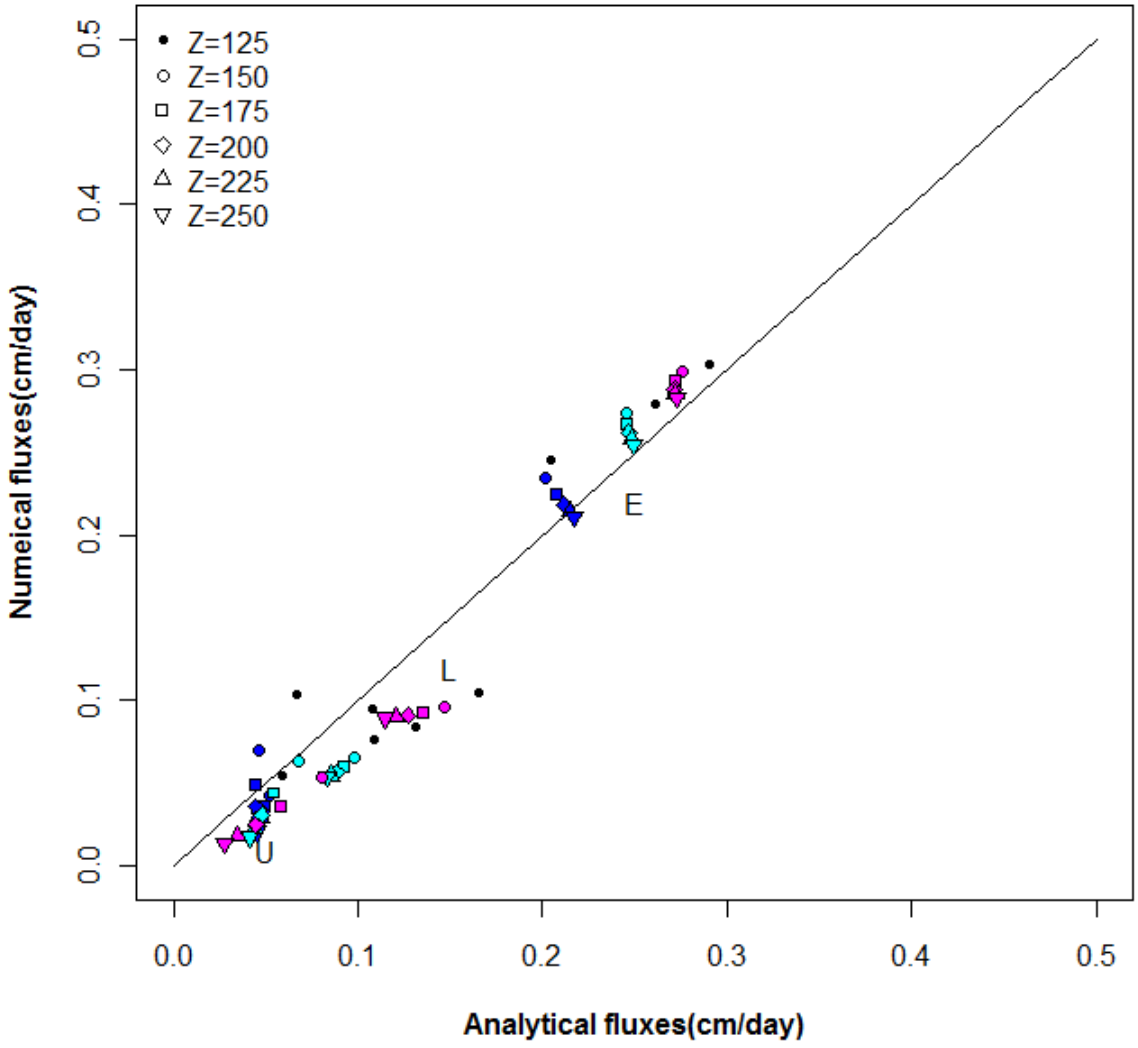

Figure 4.15: Scatter plot of numerical and analytical fluxes (equation 19 for evapotranspiration, equation 20 for leaching flux, and equation 21 for capillary flux) under six groundwater depths and three climates (dry=blue, semi-arid=turquoise, wet = pink). The soil is heavy clay, root zone thickness is 25 cm, and vegetation is grass. Other conditions the same as in calculation section 4.2.4.

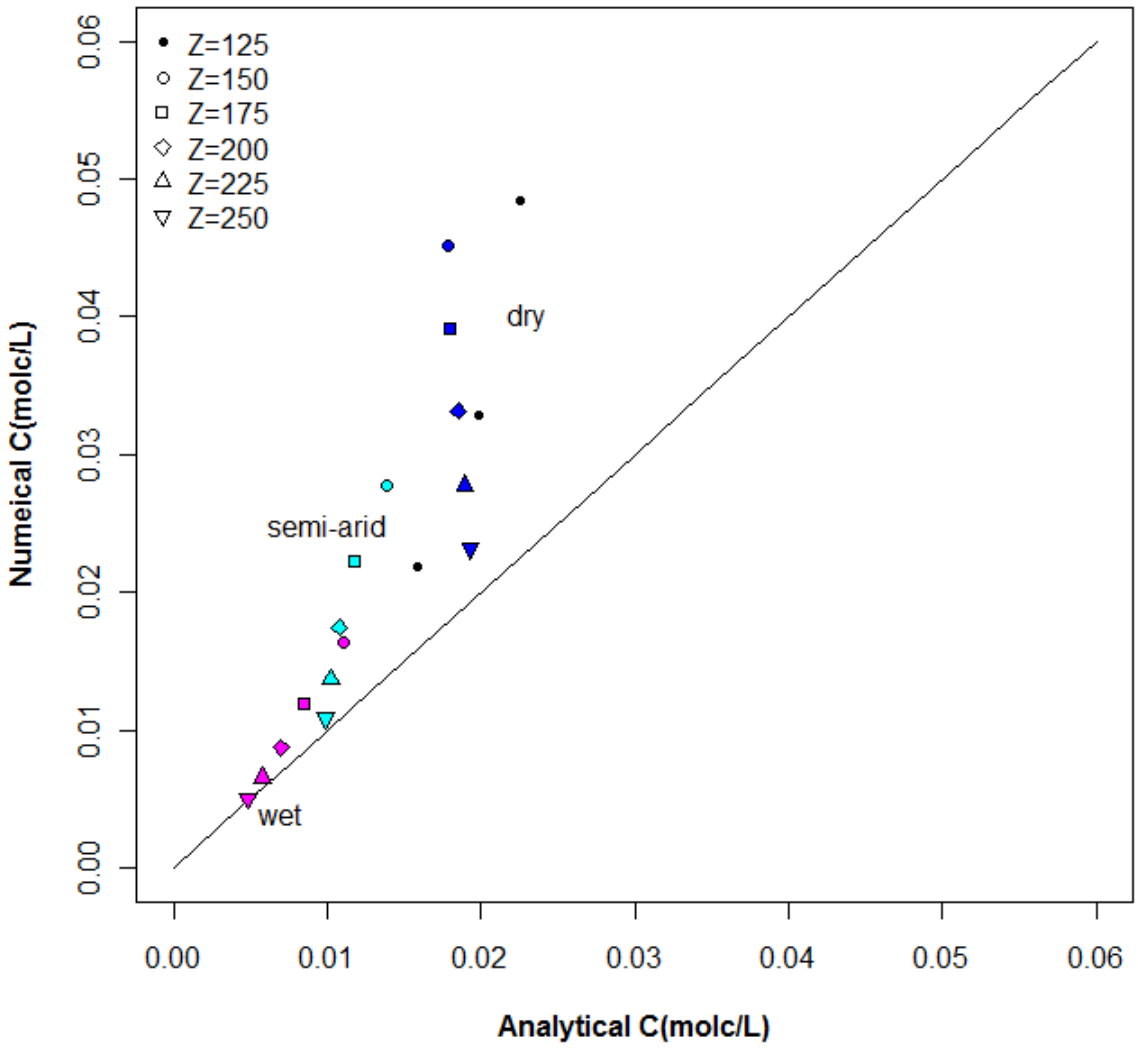

Figure 4.16: Scatter plot of numerical and analytical salt concentration (equation 23) under six groundwater depths and three climates (dry=blue, semi-arid=turquoise, wet = pink). Other conditions the same as in Figure 4.15.

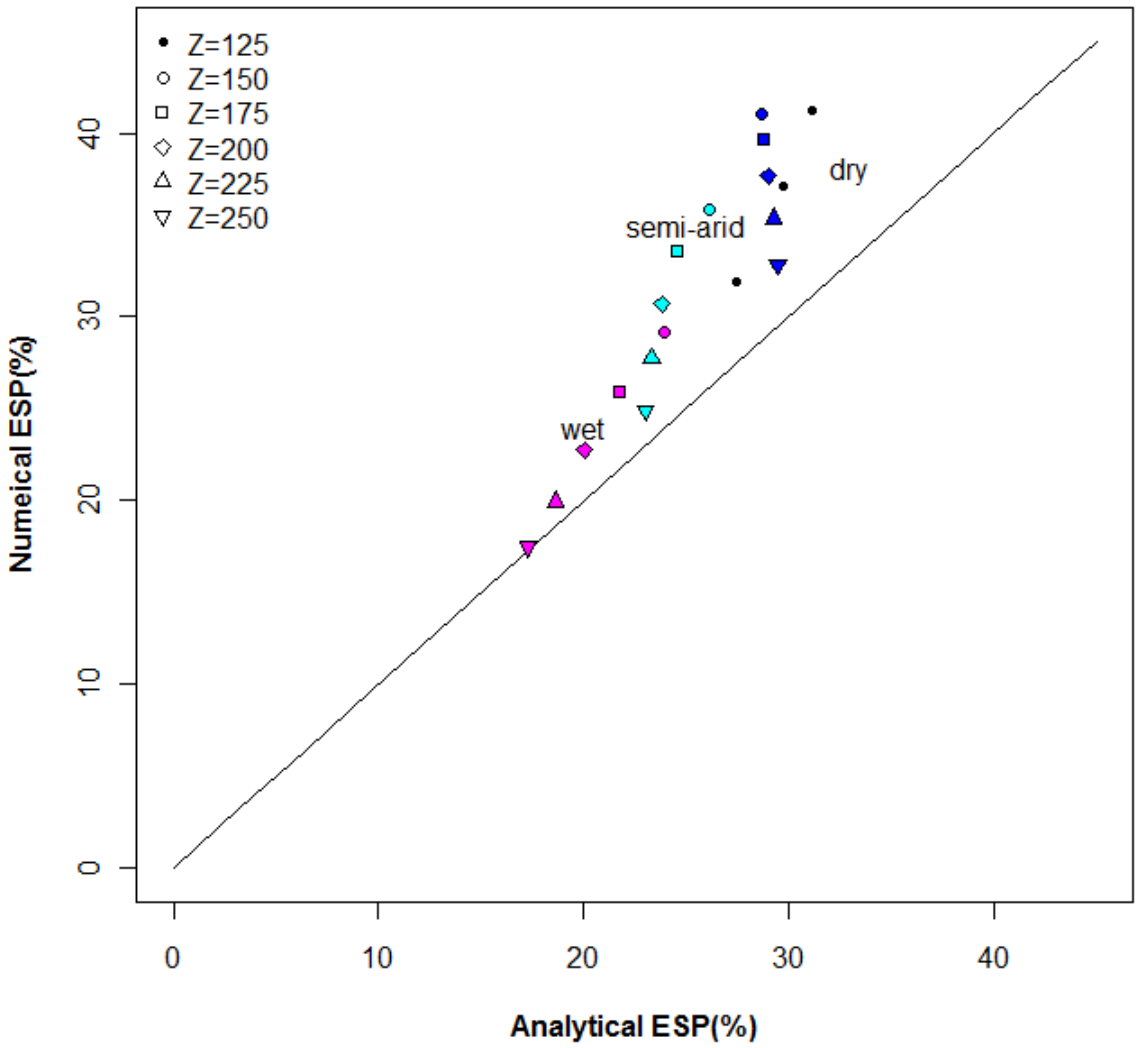

Figure 4.17: Scatter plot of numerical and analytical soil *ESP* (equation 24) under six groundwater depths and three climates (dry=blue, semi-arid=turquoise, wet = pink). Other conditions the same as in Figure 4.15.

4.4 Conclusion

Since model transparency improves our understanding of cause-effect relationships, a root zone salinity model developed by *Shah et al.* (2011) is extended towards cation balance model in this paper. We quantify the long term relationships of salt concentration and soil *ESP* with different climates, soil types, root zone thickness, and groundwater depths. We show that salt concentration approaches dynamic equilibrium faster compared to soil *ESP* due to slow exchange rate of cations between soil solution and exchange complex under all climates (ranging from dry to wet climate) and root zone thickness (ranging from Z_r =25 cm to Z_r =100 cm). Whereas our work is limited to conceptual and

modeling work, our results are supported by strategies for conjuctive use of good quality canal and poor quality groundwater (*Kaledhonkar et al., 2001*) and experimental evidence by *Minhas et al.* (2007). Both our model and the mentioned experiments show that an increase of ESP is possible due to temporal variations in salinity. Confirmation also comes from field experiments of *Tedeschi and Dell'Aquila* (2005) that show an increase of soil salinity and sodicity during seven years with an annual cycle. Experimental evidence was presented by *Miller and Pawluk* (1993) that fluctuation of the salt concentration can be accompanied by an increase of sodium.

Prolonged drought durations and soil having smaller *CEC* (= 0.05 mol_c/kg_{soil}) having smaller soil *CEC* can bring the soil *ESP* to hazardous level (soil *ESP* becomes greater than 15). The smaller magnitude of soil *CEC* increases soil buffering capacity compared to greater magnitude of soil CEC and subsequently causes the soil *ESP* to approach faster into dynamic equilibrium. Furthermore, different values of soil *CEC* reach the same final *ESP*, which is very interesting regarding the rate of development and ultimate value of soil *ESP*. The different magnitude of soil *CEC* reach the same final *ESP* is also verified by *Van der Zee et al.* (2010).

In view of the rapid approach to its asymptotic behavior of saturation, the assumption of a linear reservoir is appropriate for the exponential function of total concentration and soil *ESP*. As the soil *ESP* signal takes more time to approach dynamic equilibrium for greater root zone thickness and under dryer climate, therefore fitting of exponential function give good insight about fitting parameter soil *ESP* at $t = \infty$ and K_{ESP}. As the root zone thickness for heavy clay soil increases, the inverse characteristics time (K_{ESP}) decreases under different climates, which gives us reasonable approximation that how fast soil ESP approaches to dynamic equilibrium.

For the root zone model, it appeared feasible to develop analytical approximations from the analytical solutions developed by *Laio et al.* (2001) for the long term concentration and soil *ESP* levels. To obtain a rapid impression of the salinity levels that may develop, and thus to get a reasonable approximation for sodicity changes under different groundwater depths, climates, and soil types, the analytical approximations can be very useful and assist in practical, soil chemically based water management in groundwater dependent agro-ecosystem.

Acknowledgements

Part of this research was done with funding by the Higher Education Commission of the Government of Pakistan for S.H.H.S., the Knowledge for Climate Research Program, Theme2 Freshwater Supply, Netherlands, the Wageningen Institute for Environment and Climate Research WIMEK and the international training network NUPUS (DFG, Germany & NWO, Netherlands, http://www.nupus.uni-stuttgart.de).

CHAPTER 5

Feedback effects of saturated hydraulic conductivity on root zone fluxes, salinity, and sodicity

S. H. H. Shah[1], R. W. Vervoort[2], S. E. A. T. M. van der Zee[1]

[1]Soil Physics, Ecohydrology and Groundwater Management, Environmental Sciences Group, Wageningen University, P.O.B. 47, 6700 AA, Wageningen, Netherlands

[2]Hydrology and Geo-information Sciences Laboratory, Faculty of Agriculture, Food and Natural Resources, The University of Sydney, Australia

To be submitted

5. Feedback effects of saturated hydraulic conductivity on root zone fluxes, salinity, and sodicity

Abstract

Soil sodicity may lead to soil structure deterioration for certain swelling soils, and if soil water salinity varies. However, this feedback is seldomly taken into account in modelling soil water and salinity dynamics. We have modelled the feedback effects of salt concentration and ESP on saturated hydraulic conductivity *(Ks(C,ESP))* for different groundwater depths and climates. The dependency of *Ks* on salinity (*C*) and *ESP* followed the procedure developed by *McNeal* (1968). Whether or not the *Ks*-value decreases at large *ESP* due to decreasing salinity may have a significant effect on salt concentrations and soil *ESP* that develops. Another important factor is the seasonality of rainfall. Ignoring such seasonality leads to under or over estimation of root zone fluxes (evapotranspiration, runoff, leaching flux and capillary flux), salt concentration and soil ESP. Since the decreasing *Ks*-value leads to smaller water fluxes through the root zone, the feedback implied is a sealing of this zone against further deterioration.

5.1 Introduction

The Soil sodicity problem is more complicated than salinity in groundwater driven agro-ecosystems as it could result in the degradation of soil structure which makes the management options more complex (*Bresler, 1982*). Sodicity describes the relative concentration of sodium (Na^+) compared with the divalent cations mainly calcium (Ca^{2+}) and magnesium (Mg^{2+}) in the soil solution. Sodicity problems manifest at higher relative Na^+ concentration and lead to degradation of soil structure (*Bresler, et al., 1982; Bolt, 1982; Russo and Bresler, 1977a, 1977b*). Sodicity problems are usually inherent with salinity in irrigated clayey soils having significant sodium content. High levels of sodium in groundwater typically result in an increase of soil sodium levels, which affect soil structural stability, infiltration rates, drainage rates, and crop growth potential (*So and Alymore, 1993; Halliwell et al., 2001; McNeal, 1968*).

At relatively high electrolyte concentrations, the swelling process is most likely to be responsible for reducing saturated hydraulic conductivity. At lower electrolyte

concentrations the saturated hydraulic conductivity reduction is attributed mainly to the dispersion process (*McNeal, 1968; Ezlit, 2009*). The dispersion at low electrolyte concentration depends on the osmotic gradient generated between added water and soil solution within the micro-pores (i.e. diffuse double layer) within the clay crystalline structure (*Emerson & Bakker, 1973*).

The effect of sodicity clearly appears in soil hydraulic properties. Hydraulic properties comprising mainly saturated hydraulic conductivity of the soil is the main characteristic that is responsible for the conveyance of water and salt during irrigation, during capillary upflow from groundwater, and plant water uptake (*Ezlit 2009; Shah et al., 2011*). Thus, it is crucial to determine the reduction in saturated hydraulic conductivity (*Ezlit, 2009*).

The feedback of reduction in saturated hydraulic conductivity is seldomly taken into account in modelling soil water, salinity, and sodicity dynamics. The quantification of this feedback on root zone fluxes such capillary flux, leaching flux, runoff, and evapotranspiration leads us in understanding the reasoning of sealing of the soil and guides us for sustainable management of soil, vegetation, and groundwater/irrigation water. The aims of our paper are (i) to quantify the full and partial feedback effects on root zone fluxes, salinity and sodicity (quantified by *ESP*) dynamics under different groundwater depths and climates, (ii) how much feedback effects in distinct seasonality weather differ from Poisson distributed rainfall.

5.2. Methods

5.2.1 Background theory

Modeling is an efficient tool to investigate water and solute movement and salt accumulation in groundwater driven agro-ecosystems. However, in modelling soil water, salinity, and sodicity dynamics, continuing degradation of soil structure as a result of rising Na^+ concentrations is ignored. This aspect is taken into account in some fully numerical models such UNSATCHEM (*Simunek et al., 1996*) and HYDRUS (*Simunek et al., 1998; Somma et al., 1998*). With these tools, it is possible to assess in detail how water flow, solute (salt) transport, and root water uptake affect each other under continued degradation of soil structure.

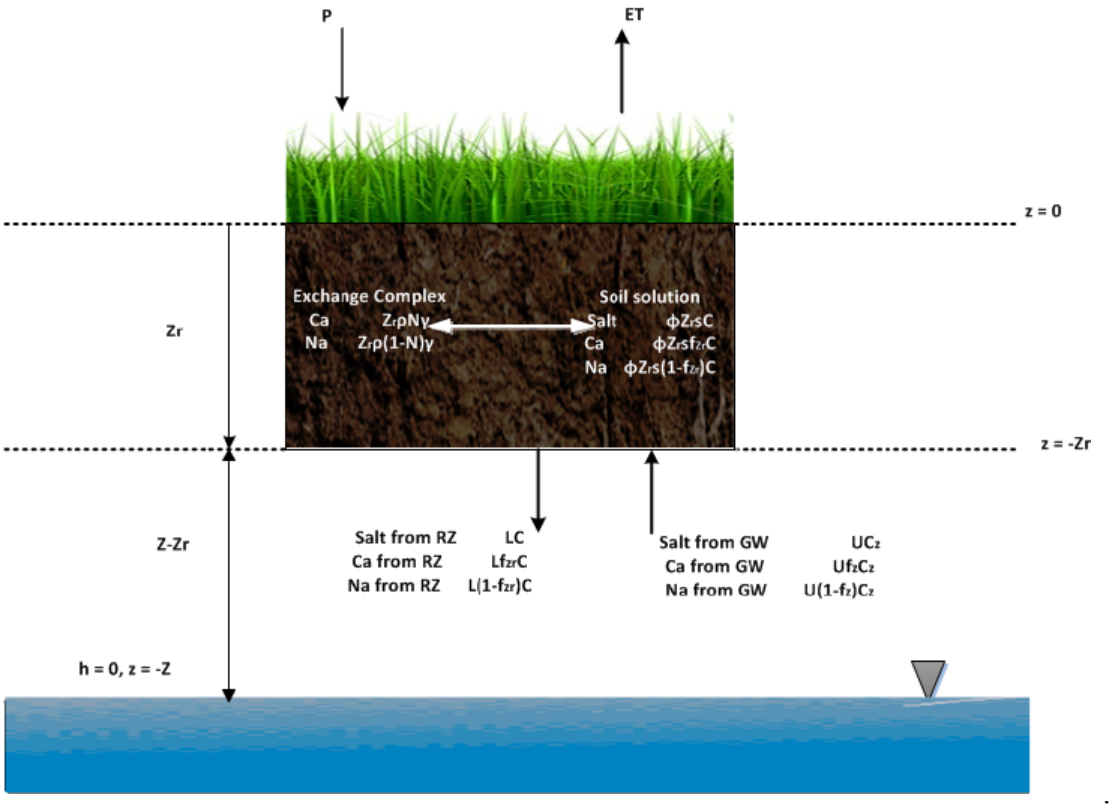

Figure 5.1. The conceptual model for saline groundwater uptake by vegetation in a semi-arid system. The symbols RZ, GW, C_z, and f_z, refer to root zone, groundwater, groundwater salt concentration, and groundwater calcium fraction, respectively.

Although they are computationally more demanding than analytical and analytically inspired numerical models, computational power rapidly increases, and this make this constraint less important.

We have extended the salinity (*Shah et al.* 2011) and sodicity model by incorporating the empirical equations developed by *McNeal* (1968) to determine the reduction in saturated hydraulic conductivity. For the calculation of soil water dynamics, we have used the following water balance equation as used by *Shah et al.* (2011).

The water balance equation (*Shah et al. 2011*) comprises rainfall/irrigation (*P*), leaching (*L*), capillary upflow (*U*), and evapotranspiration (*ET*)

$$\phi Z_r \frac{ds}{dt} = P - ET(s) + U(s) - L(s) \qquad \textbf{(5.1)}$$

Where ϕ is soil porosity, s is soil relative saturation, and Z_r is root zone thickness (Figure 5.1).

Rainfall (P) is modeled as a marked Poisson process as also used by *Shah et al.* (2011). The marked Poisson process means that rainfall is generated independently of soil moisture and it is physically interpreted at a daily time scale, where the pulses of rainfall correspond to daily time scale (*Laio et al., 2001*). The climate depends on two main parameters λ' and γ which arise from the Poisson distributed daily rainfall (*Laio et al. 2001*). The parameter λ' is equal to $\lambda e^{-\Delta/\alpha}$, where λ is mean storm arrival rate in (event/day) and each storm carries a randomly varying amount of rainfall (*Rodriguez-Iturbe et al., 1999*), Δ is the interception depth (cm), and α is the mean storm depth (cm/event). The second important parameter γ is equal to $\frac{\phi Z_r}{\alpha}$ or, equivalently, $1/\gamma$ is the root zone weighted mean storm depth.

The salt mass balance is the same as considered by (*Shah et al., 2011*) and is given by

$$\frac{dM}{dt} = \phi Z_r \frac{dsC}{dt} = U(s)C_Z - L(s)C \qquad \textbf{(5.2)}$$

where C is the salt concentration in the root zone in mol_c/L, C_z is the salt concentration of the groundwater at depth Z in mol_c/L, M is the salt mass in mol_c/m^2.

As we consider two cations (calcium (*Ca*), and sodium (*Na*)), that together make up the total salt concentration, we can eliminate one of these. We have chosen to eliminate *Na*, which implies that we need to consider a mass balance for calcium. The total mass of calcium in the root zone is the sum of calcium mass in the soil solution ($\phi Z_r f_{Zr} Cs$) and calcium mass in the exchange complex ($Z_r \rho \gamma N$) and is used as the basis for mass balance of calcium.

$$T_{Ca} = \phi Z_r f_{Zr} Cs + Z_r \rho \gamma N \qquad \textbf{(5.3)}$$

Where T_{Ca} is the total calcium mass in the root zone in mol_c/m^2, f_{Zr} is the calcium fraction in the soil solution, s is the relative water saturation, ρ is the dry bulk density of soil in kg_{soil}/m^3, γ is the soil cation exchange capacity in $mol_c/kg_{soil.}$ In this equation, N is given by the Gapon equation. We assume a Gapon constant K_G = 0.5 $(mol/L)^{-1/2}$ (*Bolt and Bruggenwert, 1976*), in the Gapon equation given by

$$\frac{1-N}{N} = K_G \sqrt{C}\ \frac{1-f_{Zr}}{\sqrt{f_{Zr}/2}} \qquad \textbf{(5.4)}$$

In agreement with (*Shah et al., 2012*), we have the mass balance equation of cation *Ca* given by

$$\frac{dT_{Ca}}{dt} = \phi ZrCs\frac{df_{Zr}}{dt} + \phi Zrf_{Zr}s\frac{dC}{dt} + \phi Zrf_{Zr}C\frac{ds}{dt} + Z_r\rho\gamma\frac{dN}{dt} = Uf_Z C_Z - Lf_{Zr}C \qquad \textbf{(5.5)}$$

Where f_z refers to calcium fraction in groundwater.

5.2.2 The McNeal approach

Changes as a function of time of salinity and sodicity may lead to a reduction in saturated hydraulic conductivity, and we model this following the procedure developed by *McNeal* (1968). The *McNeal* (1968) clay swelling model was proposed to quantify reduction in saturated hydraulic conductivity (K_s) under sodic soil conditions. *McNeal and Coleman* (1966) found that for a given level of sodicity, the reduction in relative saturated hydraulic conductivity (K_s) was related by a sigmoidal function to the logarithm of the solute concentration (*C*). *McNeal* (1968) subsequently used the concept of a swelling factor to determine the K_s with changes in solution concentration and sodium. The swelling factor is used to predict whether the sodium and solute concentration will induce soil physical degradation or flocculation (*Warrence et al. 2003*). The relationship between K_s and swelling factor (*McNeal, 1968; 1974*) provides a description of the K_s at various combinations of solute concentration and exchangeable sodium percentage (*ESP*):

$$K_S(t) = K_S * f(C, ESP)$$
$$f(C, ESP) = 1 - \frac{cx^n}{1 + cx^n} \qquad \textbf{(5.6)}$$

Where *f(C, ESP)* reflects the effect of the exchangeable sodium percentage and dilution of the solution on saturated hydraulic conductivity defined by *McNeal* (1968). The *f(C, ESP)* is based on a simple clay-swelling model, which treats mixed-ions clays as simple mixture of homoionic sodium and calcium clay. The clay swelling is related to a decrease in soil hydraulic conductivity (*McNeal, 1974*).

The factor *x* is defined in the following way

$$x = 3.6.10^{-4} f_{mont}.ESP^{*}d^{*} \qquad \textbf{(5.7)}$$

Where f_{mont} is a weight fraction of montmorillonite in the soil, d^* is adjusted interlayer spacing [L] and ESP^* is adjusted exchangeable sodium percentage calculated as

$$ESP^* = \max\left[0, ESP - \left(1.24 + 11.63 \log C\right)\right] \quad \textbf{(5.8)}$$

Where C is total salt concentration of the ambient solution in $mmol_c/L$ and ESP is defined as

$$ESP = 100\left[1 - \frac{1}{1 + K_G\sqrt{2C}\left(\frac{1}{\sqrt{f_{Zr}}} - \sqrt{f_{Zr}}\right)}\right] \quad \textbf{(5.9)}$$

The adjusted interlayer spacing, d^*, is given as follows

$d^* = 0$ for C >300 $mmol_c/L$ **(5.10)**

$d^* = 356.4C^{-1/2} + 1.2$ for C <300 $mmol_c/L$ **(5.11)**

Due to irregularity in $K_s(C,ESP)$ curve, the constant n and c values as reported by *McNeal* (1968) have been replaced by functions of ESP according to (*Ezlit, 2009*)

$$n = \left(ESP\right)^a + b \quad \textbf{(5.12)}$$

$$c = ge^{m(ESP)} \quad \textbf{(5.13)}$$

Where a, b, g, and m are empirical fitted parameters. The values of these fitted parameters for the heavy clay soil (same soil type as used by *McNeal*, 1968) are 0.449, 1.005, 0.846, and 10.967 respectively as reported by *Ezlit* (2009) and used in this paper.

We show the standard curves of relative saturated hydraulic conductivity as a function of salt concentration and soil ESP of equations (5.6)-(5.13) in Figure 5.2. The relative saturated hydraulic conductivity decreases with increasing soil ESP. At relatively large salt concentration, the relative saturated hydraulic conductivity does not decrease significantly with increasing soil ESP (*McNeal, 1968*), whereas at small salt concentration, the relative saturated hydraulic conductivity decreases significantly with increasing soil ESP. Due to the fluctuations in salt concentration and soil ESP, the saturated hydraulic conductivity also fluctuates. As the soil saturated hydraulic conductivity can only decrease (cannot increase), we have programmed this constraint in the model. Of course, in reality, other soil hydraulic parameters (b, h_b, α_e) should also change due to soil structure deterioration, but in our simulations, we have ignored those

aspects assuming soil saturated hydraulic conductivity is the most influential parameter (*Ezlit, 2009; Shah et al., 2011*).

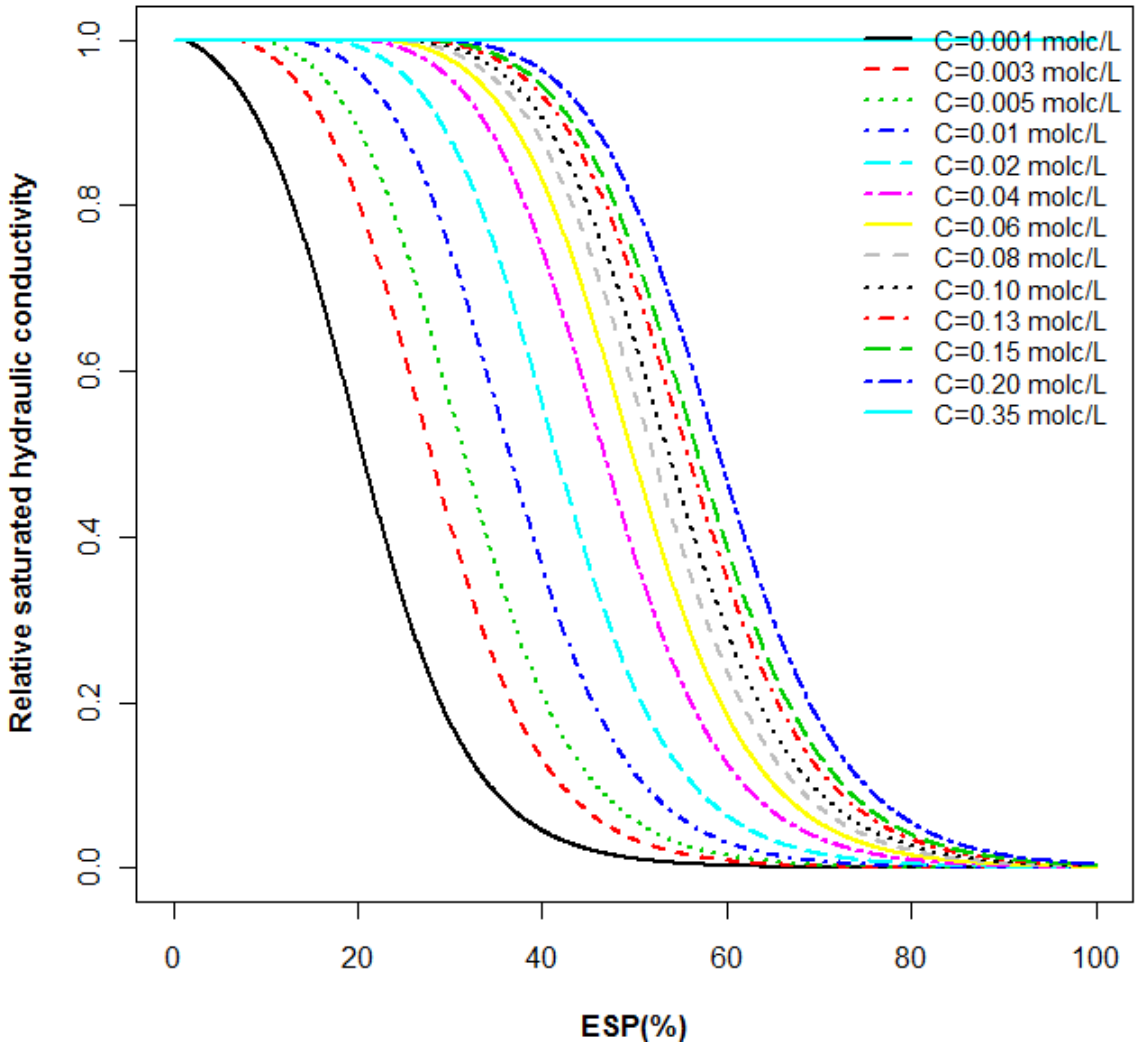

Figure 5.2. Reduction in relative saturated hydraulic conductivity as a function of soil sodicity (*ESP*) for different values of soil salinity (*C*) by using the original expressions (Eq. 5.6-5.11), but replacing the constant values of *c* and *n* by continuous functions of *ESP* ((equation 5.12, 5.13)) as developed by *Ezlit* (2009). Fitting parameters in equation 8, 9 are taken from soil type of Group (c) of McNeal (1968) (having average clay content of 48.5%, see also page 117 of *Ezlit, 2009*).

5.2.3 Numerical calculations

For the numerical simulations, light clay soil with K_s =3.5 cm/day is used. The other soil hydraulic parameters values were ϕ (soil porosity) = 0.42, b (pore size distribution index) = 16, $\overline{\Psi}_s$ (average soil matric potential at saturation)= -1.5E-3 MPa, Ψ_{s,s_h} (soil matric potential at hygroscopic point) = -10 MPa, (based on standard Australian soils in "Neurotheta", *Minansy and McBratney*, 2002). We use s_{lim} (shifting field capacity) in this

paper as used in *Vervoort and van der Zee* (2008) and *Shah et al*. (2011) instead of the field capacity, which is more common. The vegetation parameters values for a grass Zr= 40 cm, Δ = 0.1 cm, E_w (soil evaporation at wilting point) = 0.013 cm/day, ψ_{s,s^*} (matric potential at which stomatal closure begins) = -0.09 MPa, and $\psi_{s,sw}$ (matric potential at which stomatal closure completes) = -4.5 MPa were based on *Fernandez-Illescas et al.* (2001). Maximum evapotranspiration ($E_{\max}$ = 0.43 cm/day) is calculated by using the *Teuling and Troch* (2005) equation 3 and the leaf area index for grass (ξ = 5) is adopted from *Asner et al.* (2003).

In order to compare the effect of seasonality and non-seasonality (Poisson distributed rainfall) on root zone fluxes, salt concentration, and soil *ESP*, we have selected the rainfall data for two locations with distinct seasonality, i.e., Oenpelli, and Tennant Creek Airport located in North Territory of Australia. Figure 5.3 shows the monthly average rainfall of these locations. Total rainfall for the Oenpelli and its equivalent Poisson rainfall is kept same by deriving the Poisson parameters (α and λ) of the Oenpelli climate using the procedure developed by *Rodriguez- Iturbe* (1984). The Poisson parameters for the Oenpelli climate are α = 1.5 cm/event, and λ = 0.4 cm/event. The average rainfall for these Poisson parameters is 0.41 cm/day, which is close to the real (seasonal) average rainfall for the Oenpelli climate of 0.39 cm/day. We disregard this small difference.

Similarly, we have also selected the rainfall data of the location Tennant Creek Airport (Figure 5.3). The climate in Tennant Creek Airport is quite dryer than Oenpelli climate as shown in Figure 5.3. The Poisson parameters for the Tennant Creek Airport climate are α = 0.93 cm/event, and λ = 0.16 cm/event. The average Poisson rainfall for these Poisson parameters is 0.12 cm/day, which is also close to the real (seasonal) average rainfall for the Tennant Creek Airport of 0.13 cm/day.

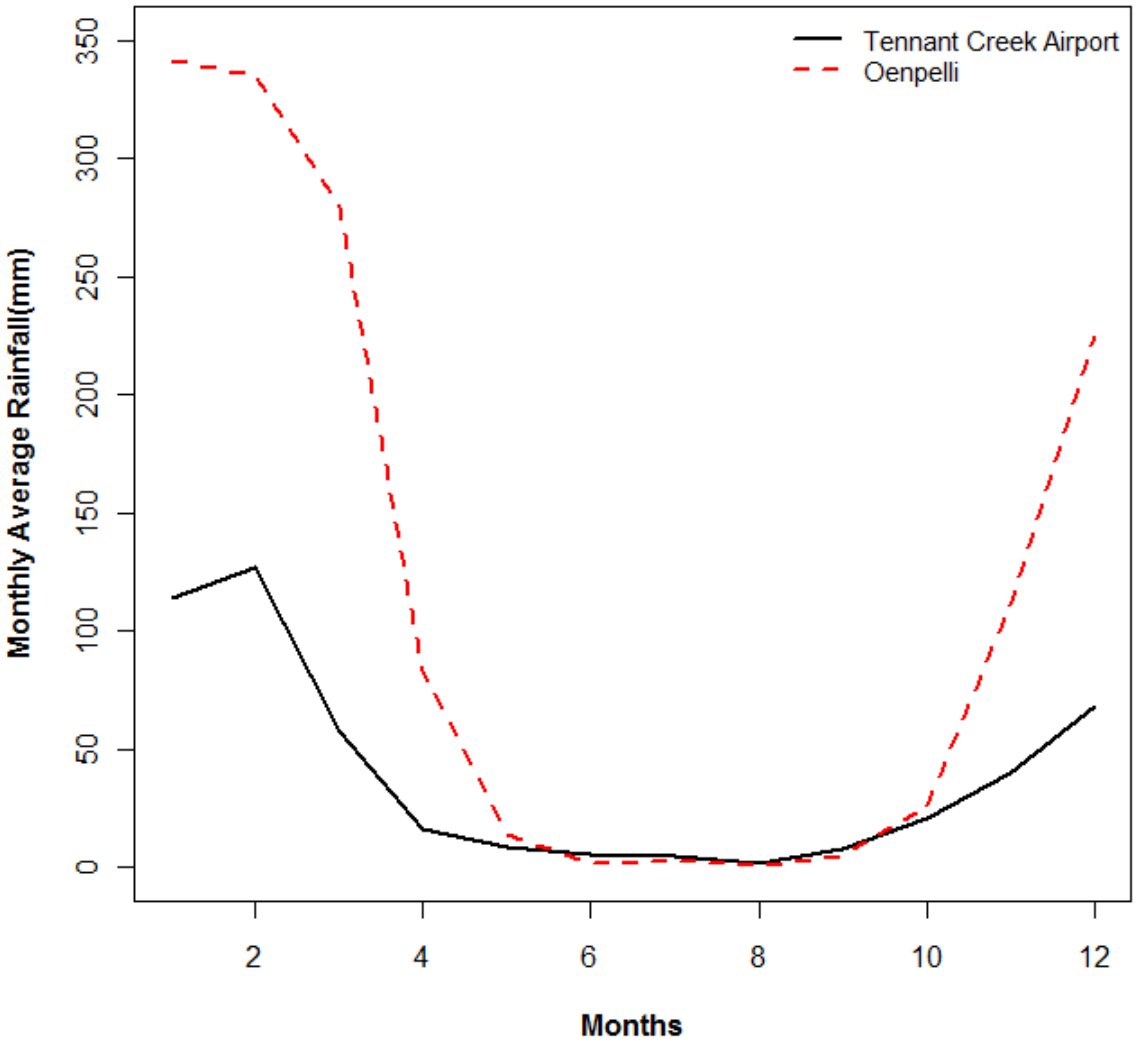

Figure 5.3. Monthly average rainfall for different locations located in North Territory of Australia.

The initial soil and groundwater physical and chemical parameters for the reference case (*Van der Zee et al., 2010*) such as calcium fraction in the soil solution (f_{Zr}=0.98) and groundwater (f_z=0.04), initial root zone salt concentration (C=0.00098 mol_c/L) and groundwater/irrigation water salt concentration (Cz=0.03 mol_c/L) (*Srinivasamoorthy et al., 2008; Sadashivaiah et al., 2008; Shah et al., 2011*), dry bulk density of soil (ρ=1560 kg_{soil}/m^3) (*Richards et al., 1954*), soil cation exchange capacity (γ=0.04 mol_c/kg_{soil}), initial *ESP* of root zone (=0.045) and groundwater/irrigation water (=37.02), and Gapon constant (K_G) were used to simulate the differential equation (equation 5.A7 in Appendix A) of calcium fraction in soil solution (f_{Zr}). From the calcium fraction in soil solution, we have calculated the calcium fraction in the exchange complex

(*N*) (equation 5.A5 in Appendix A) and finally soil sodicity (quantified by *ESP*) by using equation 5.9.

5.3. Results and Discussion

In this chapter, we will consider different scenarios. Besides weather described with Poisson statistics (*Vervoort and van der Zee, 2008, Shah et al., 2011*), we also address weather with a distinct seasonal pattern. For these weather patterns, the rather wet Oenpelli and the much drier Tennant Creek Airport climates are taken into account. We do so, for two cases of feedback between salinity/sodicity and hydraulic conductivity, i.e., where both capillary upflow and leaching (full feedback) or where only leaching is affected by this feedback (partial feedback).

5.3.1 Effect of full feedback for Poisson distributed precipitation for two climates

In order to compare the full feedback effects with no feedback, we have generated the Poisson distributed rainfall equivalent to real climates of Oenpelli and Tennant Creek Airport (TCA). As the real rainfall data for the Tennant Creek Airport is available for 43 years, we have also generated the Poisson rainfall for 43 years for better comparison of seasonal and non-seasonal rainfall. The temporal development of salt concentration and soil *ESP* is shown for groundwater depth of 200 cm from soil surface. The climate of TCA is dryer than Oenpelli climate; therefore, the salt concentration and soil *ESP* for the TCA reach higher levels compared to Oenpelli climate. Due to dryness of the TCA climate, the influence of groundwater becomes more dominant causing the larger salt concentration and soil *ESP* (Figure 5.4).

The probability density functions of salt concentration and soil *ESP* for the Oenpelli climate show a uniform distribution compared to the TCA climate. The reason is that salt concentration and soil *ESP* for the TCA climate are not in dynamic equilibrium due to dryer climate and shorter simulation time (43 years).

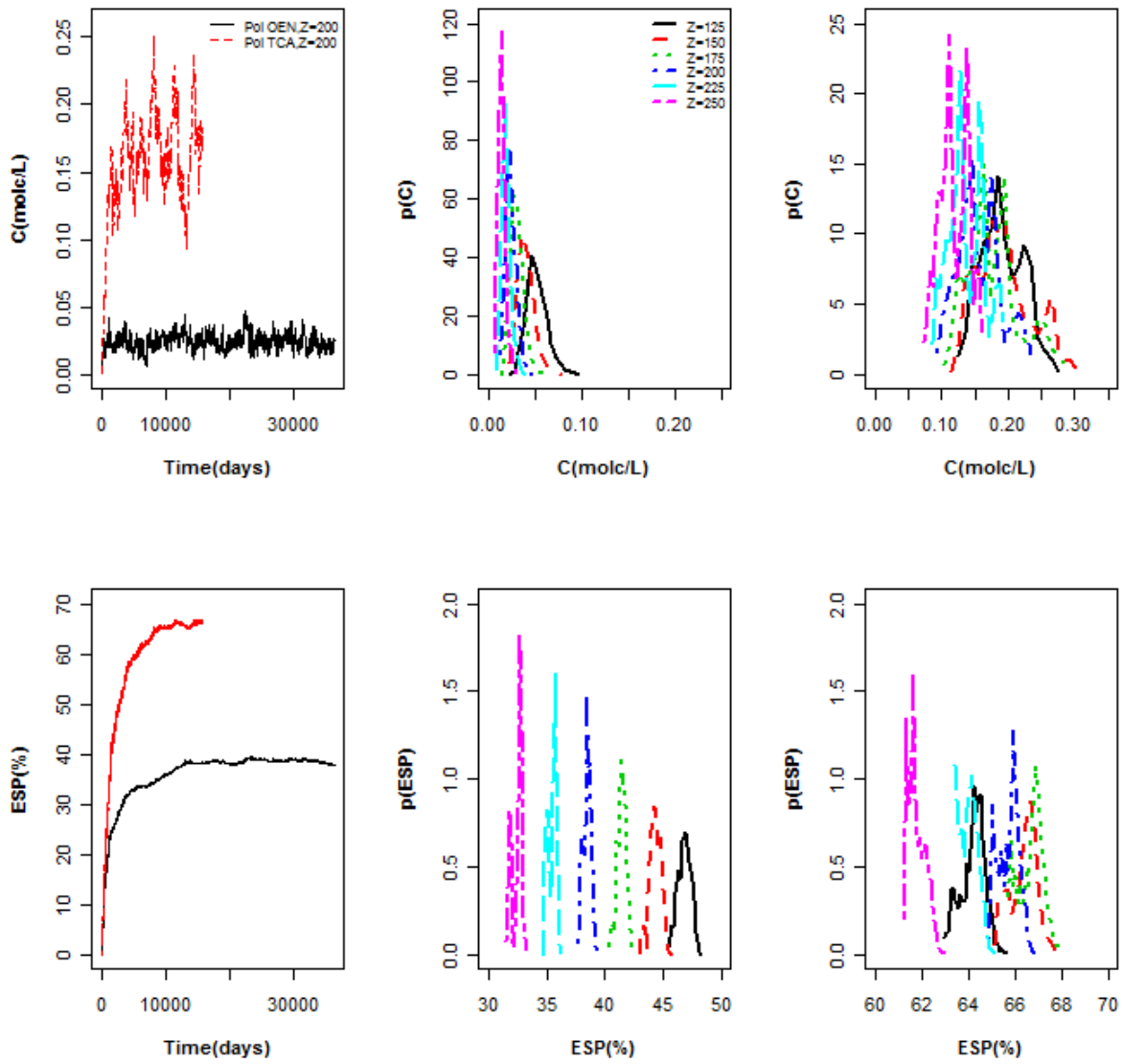

Figure 5.4. Temporal variations of salt concentration (*C*) and soil *ESP* (with no feedback effect) for two Poisson climates (equivalent to Oenpelli, and Tennant Creek Airport) under groundwater depth of 200 cm from soil surface. The corresponding probability density function (last 55 years were selected in case of Oenpelli and last 10 years in case of TCA) of salt concentration (top middle panel: Oenpelli climate, top right panel: Tennant Creek Airport) and soil *ESP* (bottom middle panel: Oenpelli climate, bottom right panel: Tennant Creek Airport) are also plotted. The vegetation is grass (see calculation section) except Zr=25 cm, and the soil is light clay (see numerical calculation section). Other conditions same as mentioned in numerical calculation section.

The full feedback effects of saturated hydraulic conductivity on soil *ESP* are not significantly different from no feedback effects for the Oenpelli and TCA climates (Figure 5.5). Actually, in full feedback case for the Poisson rainfall, the rainfall events are quite frequent and intense (in case of Oenpelli) and relatively less frequent and intense in case of TCA. Due to this reason, saturated hydraulic conductivity does not change

significantly and subsequently feedback effects are not significant. Another reason of this non-significant feedback especially for TCA climate is that the salt concentration and soil *ESP* is greater than Oenpelli climate which subsequently causes less decrease in saturated hydraulic conductivity and non-significant feedback effects. It is clear from the results of *McNeal* [1968] that for greater magnitude of salt concentration and soil *ESP*, the reduction in saturated hydraulic conductivity is not significant. Furthermore, the variability of soil *ESP* more or less decreases with increasing groundwater depth for both climates under both feedback and no feedback cases (Figure 5.5). At deeper groundwater depths for both climates, the variability of soil *ESP* increases. The reason is that we have used single realization of rainfall and more realizations would decrease this bias.

In view of the simplicity of water and salt storage (only in the pore space), the assumption of a linear reservoir is appropriate for the total concentration, hence we may write (identical to equation 4.10 and 4.11):

$$C(t) = C_{t=\infty}[1 - \exp(-K_C t)] \quad \textbf{(5.14)}$$

For the *ESP*, we may also assume such an expression for the changes as a function of time, although the relationship between total concentration and *ESP* is nonlinear (Equation 5.8). Thus,

$$ESP(t) = ESP_{t=\infty}[1 - \exp(-K_{ESP} t)] \quad \textbf{(5.15)}$$

Here $C_{t=\infty}$ and $ESP_{t=\infty}$, represent *C* and *ESP* at infinite times and K_C and K_{ESP}, the inverse characteristic times (1/year), which are the fitting parameters. The two characteristic times depend on the 'buffering' capacity of the root zone reservoir to changes. Hence, these times depend on the root zone thickness, but in the case of *ESP*, also on cation exchange capacity (*CEC)*.

In order to estimate that how fast soil *ESP* approach to dynamic equilibrium, we have fitted the exponential function (equation 5.15) on the numerical soil *ESP*. The fitted parameter K_{ESP} decreases with increasing groundwater depths for both climates and both feedback/no feedback cases (Figure 5.5). For shallow groundwater depths, the inverse characteristic time is greater than for deeper groundwater levels. The reason is that soil *ESP* at shallow groundwater levels approaches dynamic equilibrium faster than for deeper groundwater level due to the dominant effect of groundwater (Figure 5.5).

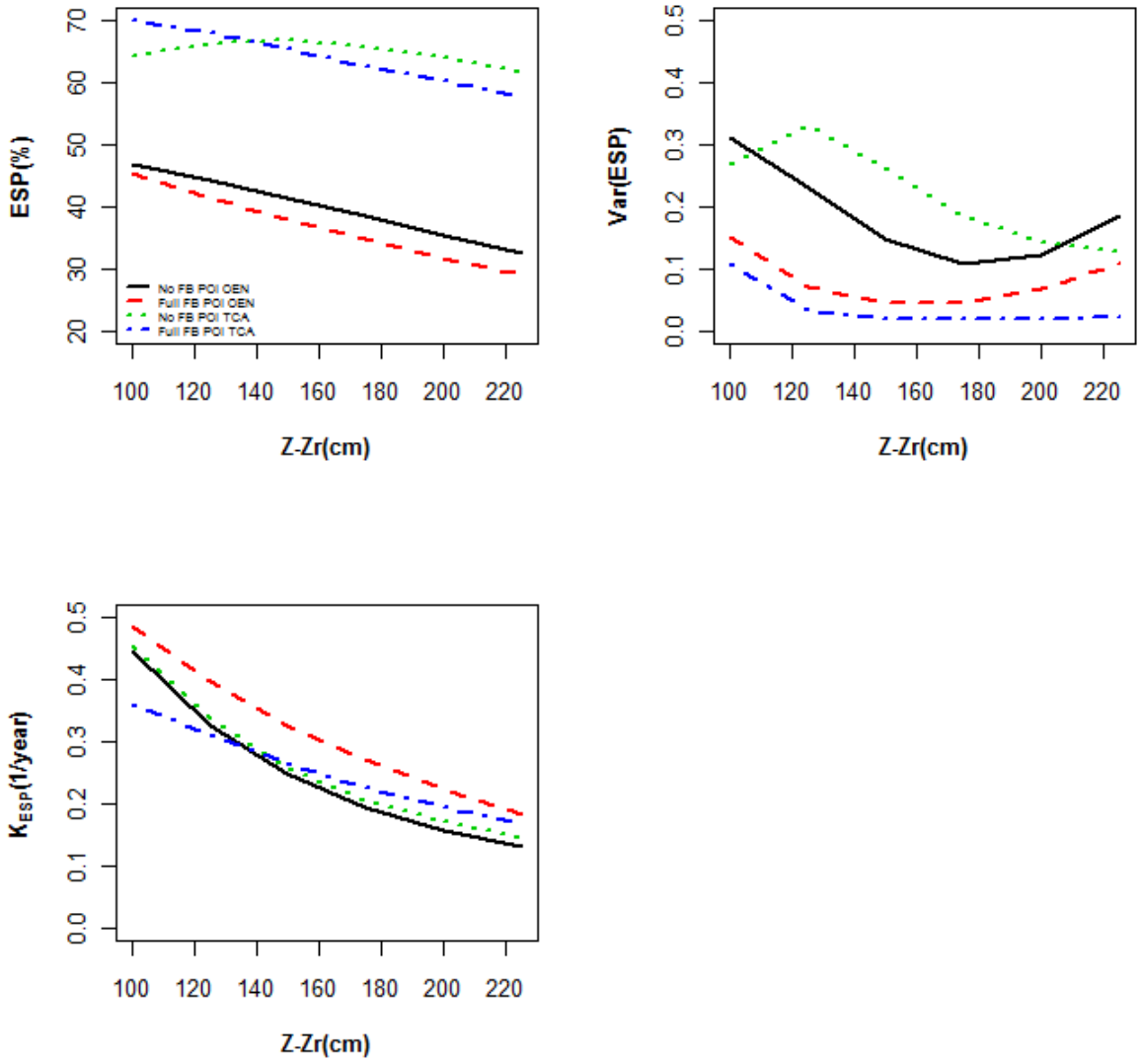

Figure 5.5. Long term average *ESP*, variance of *ESP* and fitted parameter (K_{ESP}, inverse characteristic time) as function of Z-Zr distance for two climates (Poisson distributed rainfall equivalent to Oenpelli and Tennant Creek Airport) under full feedback (feedback affects both capillary and leaching flux) and no feedback effects. Other conditions same as in Figure 5.4.

In order to go further inside of the feedback and no feedback cases (Figure 5.5), we have plotted the corresponding main fluxes such as evapotranspiration (*ET*), runoff (*RO*), leaching flux (*L*), and capillary flux (*U*) as a function of Z-Z_r for the feedback and no feedback cases for both climates with Poisson distributed rainfall (Figure 5.6). The fluxes for both climates in all cases (except leaching flux for Oenpelli) decrease as Z-Zr becomes larger (Figure 5.6). The leaching flux for Oenpelli remains more or less constant. There are differences due to feedback for Oenpelli only for leaching and capillary upflow (i.e. these are directly affected by K_s). For TCA, all fluxes are affected

by feedback, except runoff, but only capillary fluxes are affected modestly and clearly (rest is small effect) (Figure 5.6).

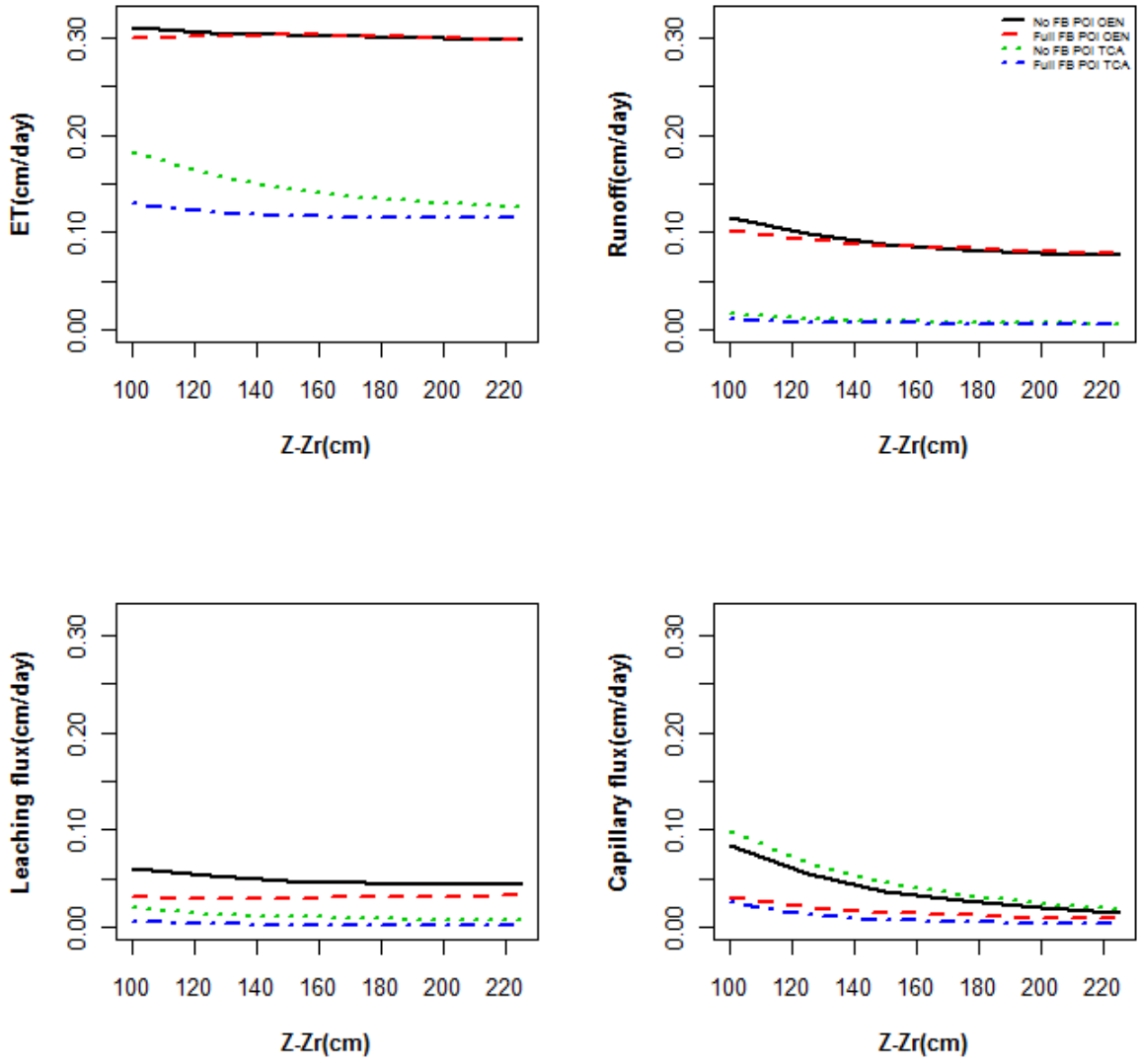

Figure 5.6. Long term average evapotranspiration, runoff, leaching flux, and capillary flux as function of Z-Zr distance for two climates (Poisson distributed rainfall equivalent to Oenpelli and Tennant Creek Airport) under full feedback (feedback affects both capillary and leaching flux) and no feedback effects. Other conditions same as in Figure 5.4.

5.3.2 Effect of full feedback on seasonally distributed precipitation for two climates

The feedback effects for Poisson generated rainfall are generally minor (see 5.3.1), and this is understandable. The Poisson generated rainfall leads to fluctuations of dependent parameters, but is still regular enough to prevent periods of excessive drought and associated high root zone salinity as well as periods dominated by high (good

quality) rainfall. However, for the feedback to become profound, periods of high and of low salinity in a sodic soil should alternate (Figure 5.2) as soil swelling and compression of the larger pore radius fraction occurs only if fresh water enters a sodic soil. Therefore we considered seasonal rainfall with distinct dry and wet seasons of Oenpelli and Tennant Creek Airport, using real weather records. The temporal variations of salt concentration and soil *ESP* for Oenpelli climate are faster in complete dynamic equilibrium than the salt concentration and soil *ESP* of the TCA climate. The reason is that TCA is dryer than Oenpelli climate. Also data available for TCA climate is 43 years; we need more data to obtain the dynamic equilibrium status (Figure 5.7).

Figure 5.7 shows the resulting probability density function of salt concentration for the Oenpelli climate. As the climate of Oenpelli is wet climate, the salt concentration decreases monotonically with increasing *Z-Zr* distance. Although the trend of salt concentration for the current Figure 5.7 is similar as the trend of salt concentration of Figure 7 (wet climate) of *Shah et al.* (2011), the magnitude of salt concentration in the current Figure 5.7 is larger than the magnitude of salt concentration of Figure 7 (wet climate) of *Shah et al.* (2011). The reason is that soil is light clay, the groundwater depths are relatively shallower, and vegetation is grass with E_{max} = 0.43 cm/day compared to the E_{max} = 0.37 cm/day in Figure 7 of *Shah et al.* (2011). It means that due to the greater difference in soil hydraulic parameters, groundwater depths, and vegetation parameters the levels of salt concentration in the current Figure 5.7 is larger than in Figure 7 (wet climate) of *Shah et al.* (2011). On quantitative basis, the magnitude of salt concentration under different groundwater depths in Figure 7 (wet climate) of *Shah et al.* (2011) ranges between 0.004-0.02 molc/L for C_z = 0.04 molc/L. Whereas in current Figure 5.7, the long term average salt concentration varies between 0.02-0.07 molc/L. As we have used in this paper groundwater salt concentration of 0.03 molc/L, even then, the salt concentration in current Figure 5.7 is greater than the salt concentration of Figure 7 (wet climate) of *Shah et al.* (2011) due to the reasons as discussed above.

Due to the availability of relatively short duration of rainfall data of dryer climate of TCA compared to Oenpelli climate, we have selected the last 10 years to plot the probability density functions of salt concentration and soil *ESP*. The average salt concentration and soil ESP decrease with increasing *Z-Zr* distance (Figure 5.7), but the

magnitude of salt concentration and soil *ESP* is greater (due to dryer climate) than the magnitude of salt concentration and soil *ESP* for the Oenpelli climate (Figure 5.7).

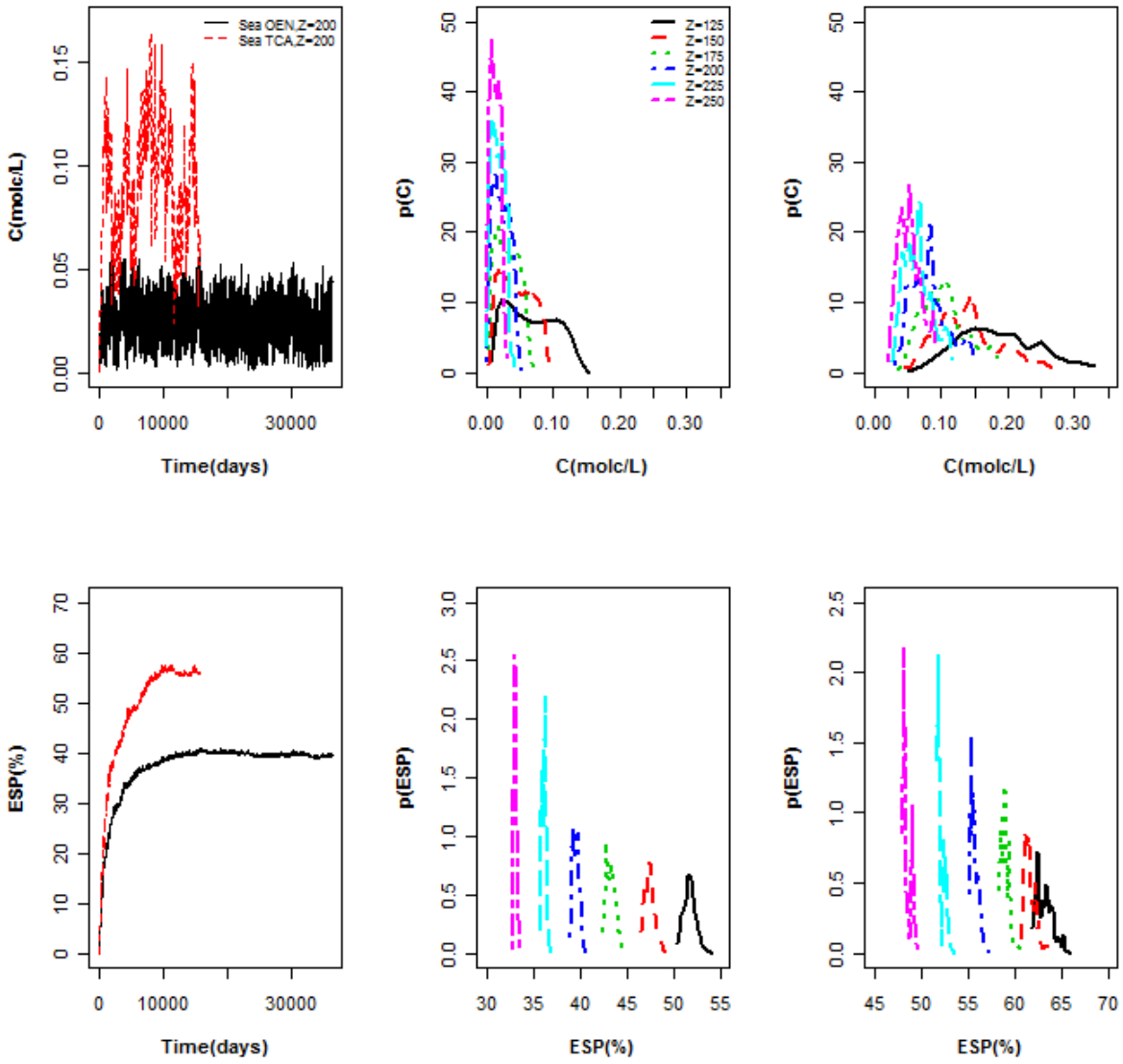

Figure 5.7. Temporal variations of salt concentration (*C*) and soil *ESP* (with no feedback effect) for two real climates (Oenpelli, and Tennant Creek Airport) under groundwater depth of 200 cm from the soil surface. The corresponding probability density function (last 55 years were selected in case of Oenpelli and last 10 years in case of TCA) of salt concentration (top middle panel: Oenpelli climate, top right panel: Tennant Creek Airport) and soil *ESP* (bottom middle panel: Oenpelli climate, bottom right panel: Tennant Creek Airport) are also plotted. The vegetation is grass (see calculation section) except *Zr*=25 cm, and the soil is light clay (see numerical calculation section). Other conditions the same as mentioned in numerical calculation section.

As the rainfall data for Oenpelli climate is seasonal, fluctuations in salt concentration are cyclic. The monthly average rainfall during May to October is below 5 mm and rainfall during November to April is above 150 mm as shown in Figure 5.3. Under full feedback

of saturated hydraulic conductivity, the salt concentration decreases enormously compared to the no feedback effects due to the decrease in saturated hydraulic conductivity (Figure 5.8).

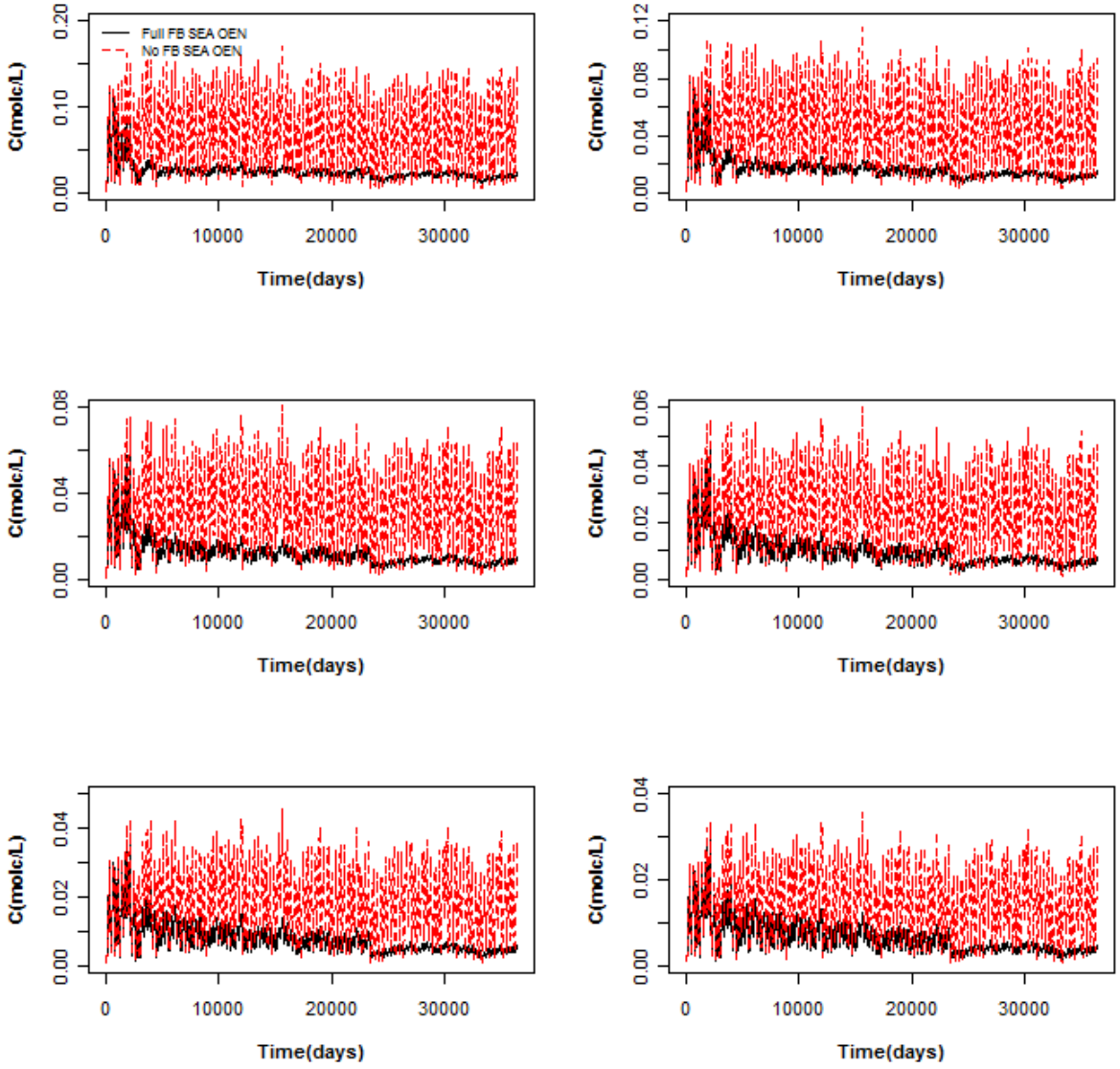

Figure 5.8. Temporal variations of salt concentration (*C*) by considering (solid line: black trajectories) and no considering (dashed line: red trajectories) the feedback of $K_s(C,ESP)$ on both capillary and leaching flux(full feedback) during 99 years for six groundwater depths (top left panel:Z=125 cm, top right panel:Z=150 cm, middle left panel:Z=175 cm, middle right panel:Z=200 cm, bottom left panel:Z=225 cm, bottom right panel: Z=250 cm). The climate is Oenpelli and other conditions the same as in Figure 5.7.

Figure 5.9 shows the no feedback and full feedback effect of reduction in saturated hydraulic conductivity on soil *ESP* for the Oenpelli climate. We have also compared the full feedback/no feedback effects of saturated hydraulic conductivity on

soil *ESP* under different groundwater depths. Figure 5.9 shows that full feedback effects of saturated hydraulic conductivity on soil *ESP* are significantly different from the no feedback effects. The reason is that at smaller salt concentration and greater soil ESP (no feedback), the reduction in saturated hydraulic conductivity is enormous (being less than 0.5 cm/day). Due to the large decrease in saturated hydraulic conductivity, the capillary and leaching fluxes become small and salt concentration and soil *ESP* develop increase much less.

As the climate of the Tennant Creek Airport is dryer than Oenpelli climate, magnitude of salt concentration develops until 0.30 molc/L (Figure 5.7). As we already know that if the magnitude of salt concentration and soil *ESP* is greater than threshold (C=0.06 molc/L, and ESP= 40% are estimated from standard curves in Figure 5.2) magnitude, the reduction is saturated hydraulic conductivity is not significant (*McNeal*, 1968), therefore the full feedback effect is not significant (Figure 5.9) compared to the full feedback case of Oenpelli climate (Figure 5.9). Furthermore, the rainfall data of the Tennant Creek Airport is not completely seasonal data (Figure 5.3). This is also another reason that full feedback effects are not significant.

The variability of soil *ESP* decreases with increasing groundwater depth for both feedback and no feedback case for both climates (Figure 5.9). As the soil *ESP* for the feedback case compared to no feedback case decreases, variability in soil *ESP* also decreases.

In order to estimate that how fast soil *ESP* approach to dynamic equilibrium, we have fitted the exponential function (equation 5.15) appropriate for the perfectly mixed reservoir on the numerical soil *ESP*. The fitted parameter K_{ESP} also known as inverse characteristics residence time in 1/years shows that magnitude of K_{ESP} decrease with increasing groundwater depths for both climates and both feedback/no feedback cases (Figure 5.9). For shallow groundwater depths, the inverse characteristic time is relatively greater than deeper groundwater levels. The reason is that soil *ESP* approaches the dynamics equilibrium relatively faster than the deeper groundwater level due to the dominant effect of groundwater (Figure 5.9).

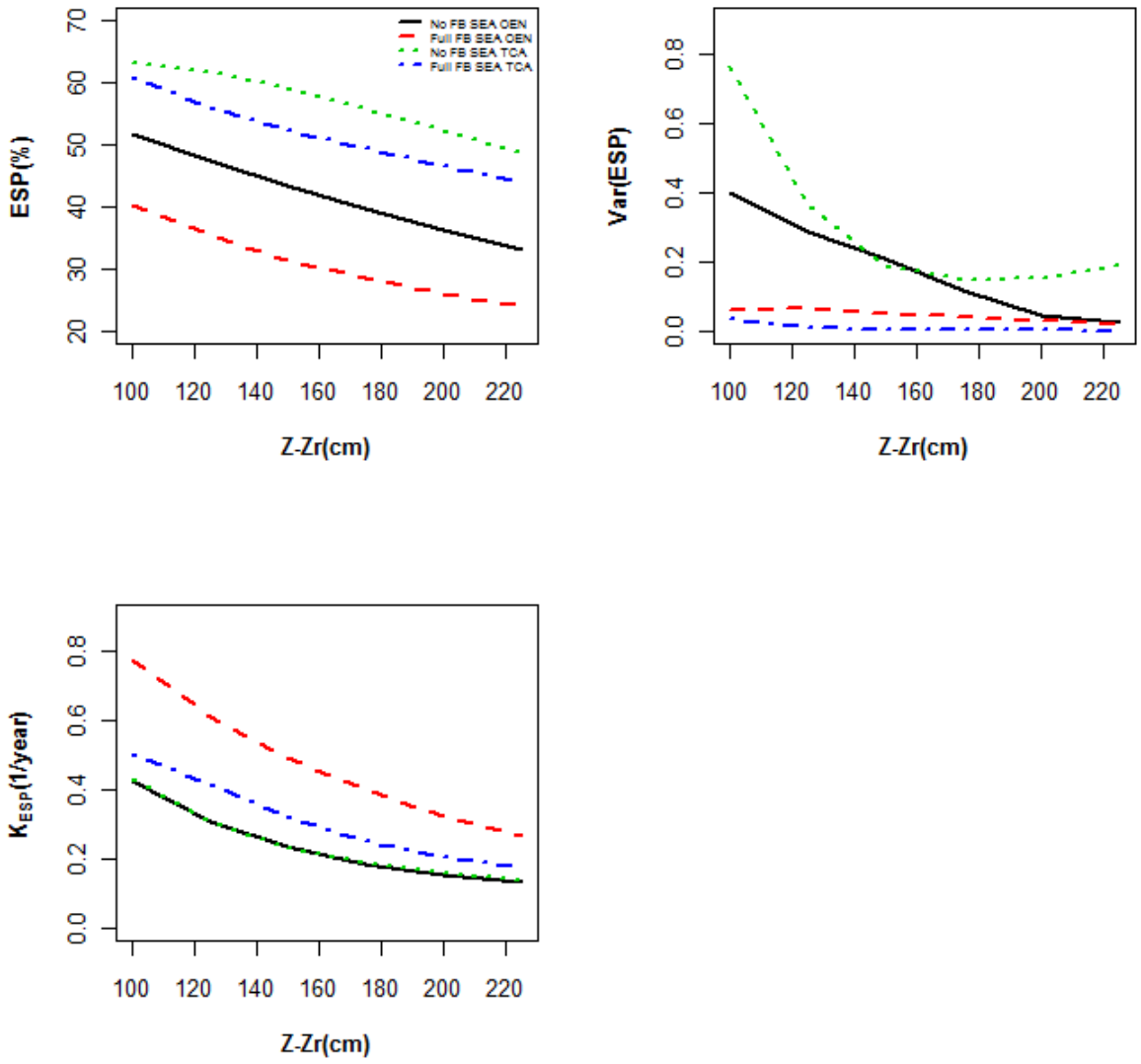

Figure 5.9. Long term average *ESP*, variance of *ESP* and fitted parameter (K_{ESP}, inverse characteristics time) as function of Z-Zr distance for two real climates (Oenpelli and Tennant Creek Airport) under full feedback (feedback affects both capillary and leaching flux) and no feedback effects. Other conditions same as in Figure 5.7.

For a more detailed impression between the feedback and no feedback cases (Figure 5.9), we have plotted the corresponding main fluxes such as evapotranspiration (*ET*), runoff (*RO*), leaching flux (E_{max}, and capillary flux *(U)* as a function of Z-Z_r for the feedback and no feedback cases for both real climates (Figure 5.10). Due to the significant decrease in saturated hydraulic conductivity, although magnitude of evapotranspiration, capillary flux, and leaching flux become smaller than the no feedback case for Oenpelli climate, but the magnitude of runoff in full feedback case becomes greater than the magnitude of runoff in no feedback case (Figure 5.10), which is logical.

Due the decrease in saturated hydraulic conductivity, the rainfall cannot enter the root zone and subsequently becomes the part of the runoff. Another important result from this Figure 5.10 shows that whereas the evapotranspiration, and leaching flux under full feedback case increase with increasing Z-Zr distance (due to the decrease in *Ks(C,ESP)),* the runoff and capillary flux decrease with increasing *Z-Zr* distance. As the leaching flux and capillary flux are inversely related therefore leaching and capillary flux behave oppositely with increasing *Z-Zr* distance. Furthermore, with increasing *Z-Zr* distance, salt concentration and soil *ESP* decrease in relatively less magnitude and subsequently *Ks(C,ESP)* decreases in relatively less magnitude and finally magnitude of runoff decreases (Figure 5.10).

To evaluate fluxes quantitatively under full feedback and no feedback effect of saturated hydraulic conductivity, we have also plotted the evapotranspiration, runoff, capillary flux and leaching flux as a function of *Z-Zr* for the TCA climate (Figure 5.10). Due to the decrease in saturated hydraulic conductivity, although the magnitude of evapotranspiration, capillary flux, and leaching flux become smaller than the no feedback case at all *Z-Zr* distances, the magnitude of runoff in the full feedback case becomes greater than the magnitude of runoff in no feedback case especially at greater *Z-Zr* distances (Figure 5.10). Due the decrease in saturated hydraulic conductivity, the rainfall cannot enter the root zone and subsequently becomes the part of the runoff. Another important result from this Figure 5.10 shows that whereas the evapotranspiration, and leaching flux under full feedback case increase with increasing Z-Zr distance (due to the decrease in *Ks(C,ESP*)), the runoff decreases with increasing *Z-Zr* distance. The reason is that with increasing *Z-Zr* distance, salt concentration and soil *ESP* decrease in relatively less magnitude and subsequently *Ks(C,ESP*) decreases in relatively less magnitude and finally magnitude of runoff decreases with increasing *Z-Zr* distance (Figure 5.10). Furthermore, the feedback effect in case of Poisson rainfall for both climates is affected less than for real rainfall of both climates, therefore capillary flux is relatively larger (Figure 5.6) than in Figure 5.10.

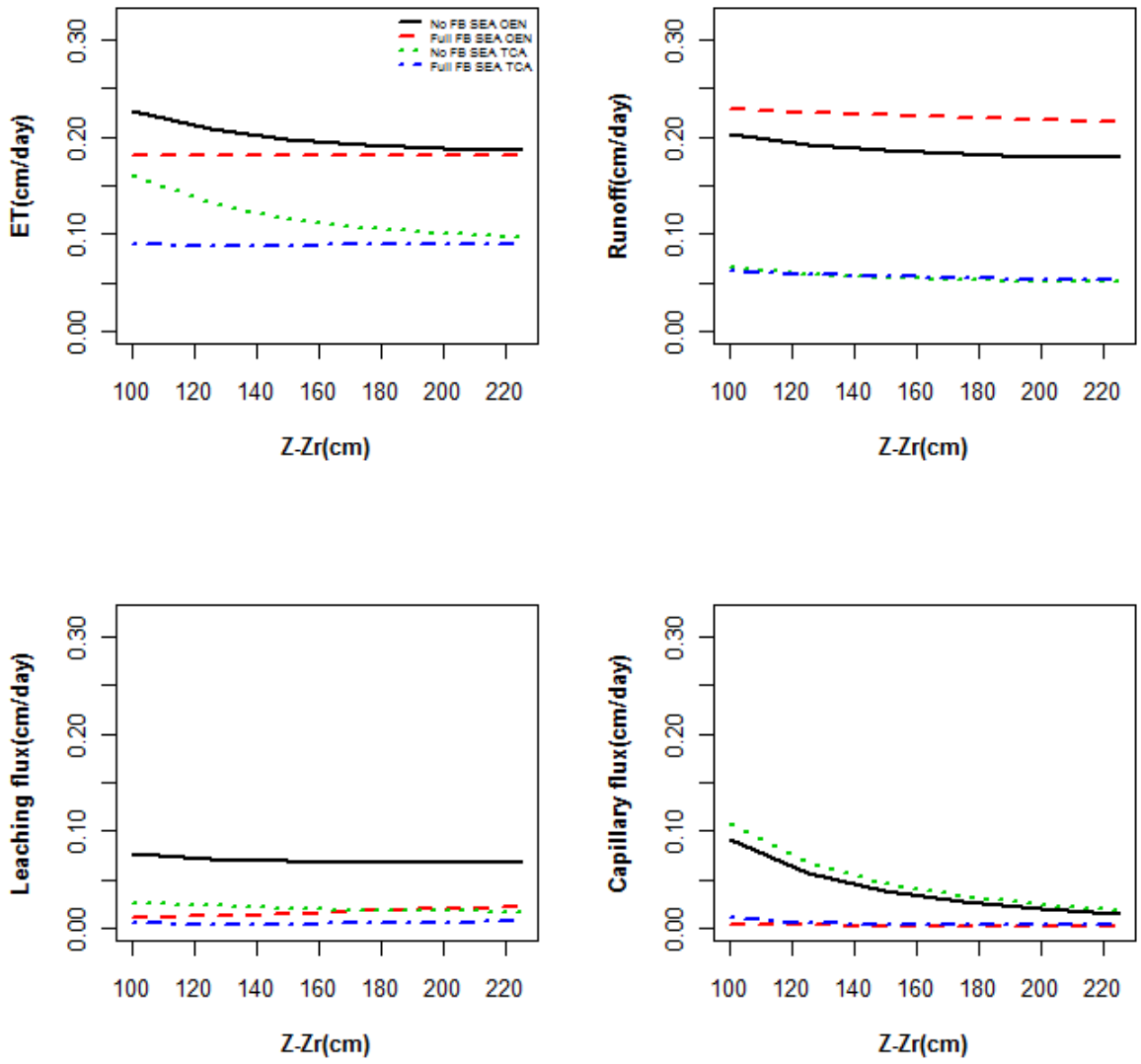

Figure 5.10. Long term average evapotranspiration, runoff, leaching flux, and capillary flux as function of *Z-Zr* distance for two real climates (Oenpelli and Tennant Creek Airport) under full feedback (feedback affects both capillary and leaching flux) and no feedback effects. Other conditions the same as in Figure 5.7.

5.3.3 Effect of partial feedback on seasonally distributed precipitation for two climates

In order to understand whether partial feedback of saturated hydraulic conductivity affects salt concentration and soil *ESP*, we have modeled the feedback effect of saturated hydraulic conductivity on only the leaching flux. For capillary flux, the saturated hydraulic conductivity remains unaffected (remains constant). As the reduction in saturated hydraulic conductivity affects only leaching flux, magnitude of the leaching

flux decreases and subsequently salt concentration increases (not shown). Due to this reason the magnitude of salt concentration under partial feedback case is relatively greater than the magnitude of salt concentration for no feedback case. For shallower groundwater depths, the partial feedback effect of saturated hydraulic conductivity on salt concentration is relatively greater than deeper groundwater depths. The reason is quite clear because at deeper groundwater levels the magnitude of salt concentration and soil *ESP* decrease and subsequently magnitude of *Ks(C,ESP)* decreases relatively less and subsequently difference in salt concentration for partial feedback and no feedback cases decreases (not shown).

Although the effect of the partial feedback on soil *ESP* is significant (Figure 5.11), the effect of full feedback is more significant (Figure 5.9). The reason is automatically explanatory, because in full feedback case, both the capillary and leaching flux are affected by *Ks(C, ESP*), whereas in the partial feedback case only the leaching flux is affected by *Ks(C, ESP*). Another important result can be excluded from the full feedback case and no feedback case. In full back case under all groundwater depths (Figure 5.9), the magnitude of salt concentration and soil *ESP* is smaller than the no feedback case, whereas in partial feedback case for both climates under all groundwater depths (Figure 5.11), the magnitude of salt concentration (not shown) and soil *ESP* is greater than no feedback case, which is quite logical. This type of situation (partial feedback case) occurs in those soils where lower part of the root zone is unaffected (*Ks* is unaffected from salinity and sodicity), whereas the top part of the root zone is affected by the salinity and sodicity. The other situation (full feedback case) also occurs in those soils where complete root zone is affected by salinity and sodicity. Similarly partial feedback effects of saturated hydraulic conductivity on salt concentration (not shown) and soil *ESP* (not shown) for the both non-seasonal (Poisson) climates is not significant compared to Figure 5.9 due the same reason as explained above.

Although the long term (last 55 years in case of Oenpelli and last 10 years in case of TCA) variability of soil *ESP* for the no feedback case of both climates decreases with increasing groundwater depths, in the partial feedback case, this variability increases for deeper groundwater depths, because *Ks(C,ESP)* affects only the leaching flux and salt does leach out of the root zone completely (Figure 5.11). In case of full feedback,

Ks(C,ESP) affects both capillary and leaching flux and therefore variability of salt concentration and soil *ESP* decreases with increasing groundwater depth (Figure 5.9).

Similarly, the fitting parameter inverse characteristic time for the case of partial feedback of both climates decreases with increasing groundwater depths, but the magnitude of K_{ESP} is smaller than the case of full feedback for all groundwater depths (Figure 5.9). The reason is that partial feedback causes the soil *ESP* to approach dynamic equilibrium in relatively longer duration compared to full feedback case (Figure 5.9). This means that partial feedback generates a difference from the no feedback case at the cost of longer duration of equilibrium status.

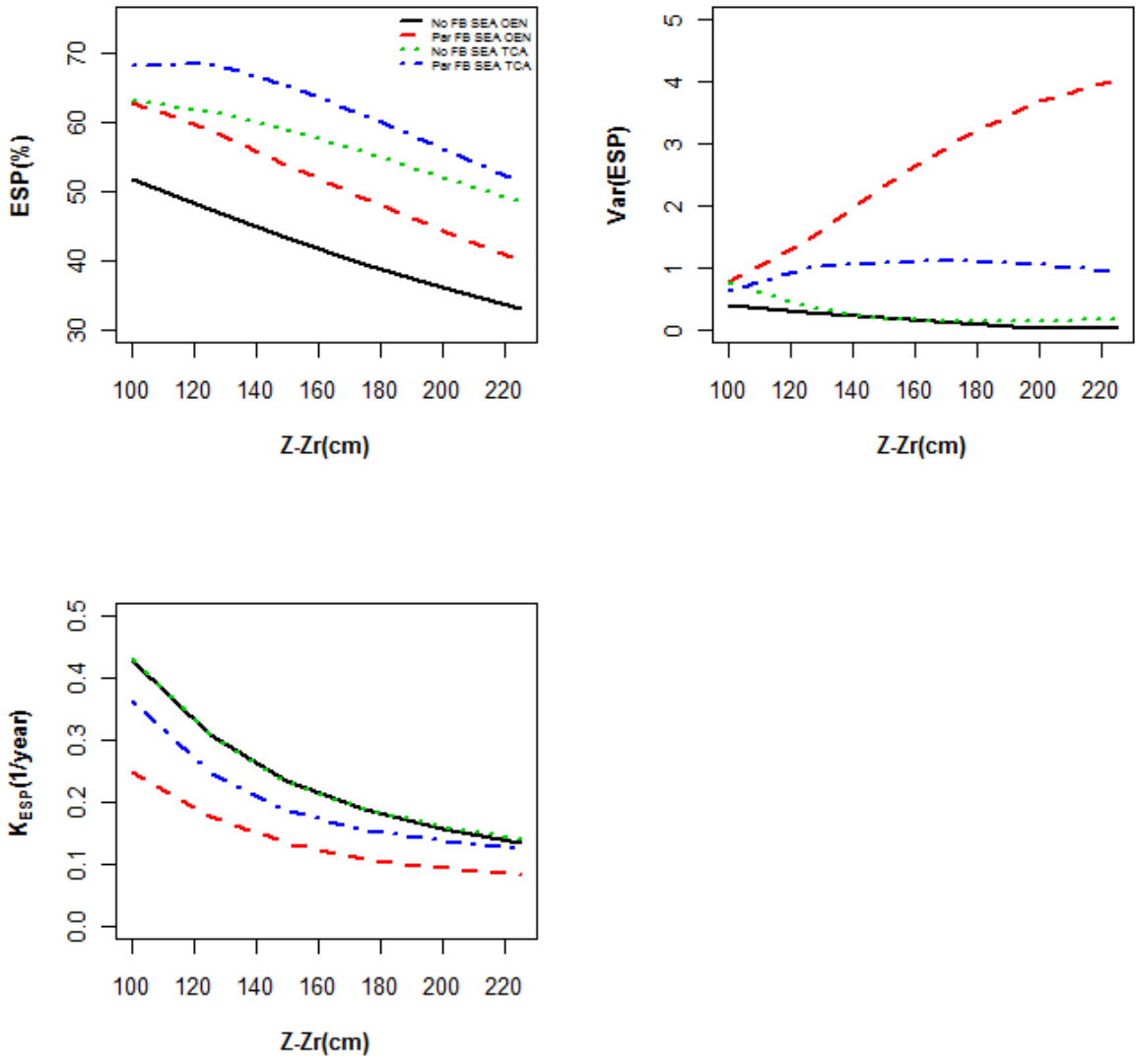

Figure 5.11. Long term average *ESP*, variance of *ESP* and fitted parameter (K_{ESP}, inverse characteristics time) as function of Z-Zr distance for two real climates (Oenpelli and Tennant Creek Airport) under partial feedback (feedback affects only leaching flux) and no feedback effects. Other conditions the same as in Figure 5.7.

As partial feedback affects the leaching flux significantly, therefore, the capillary flux remains almost the same for the both climates under partial feedback and no feedback case (Figure 5.12). Due to this partial feedback, the magnitude of runoff becomes relatively greater than no feedback case and decreases with increasing groundwater depths. On the other hand water balance component evapotranspiration increases with increasing groundwater depth for the partial feedback case and becomes almost the same at deeper groundwater depths for the case of no feedback (Figure 5.12).

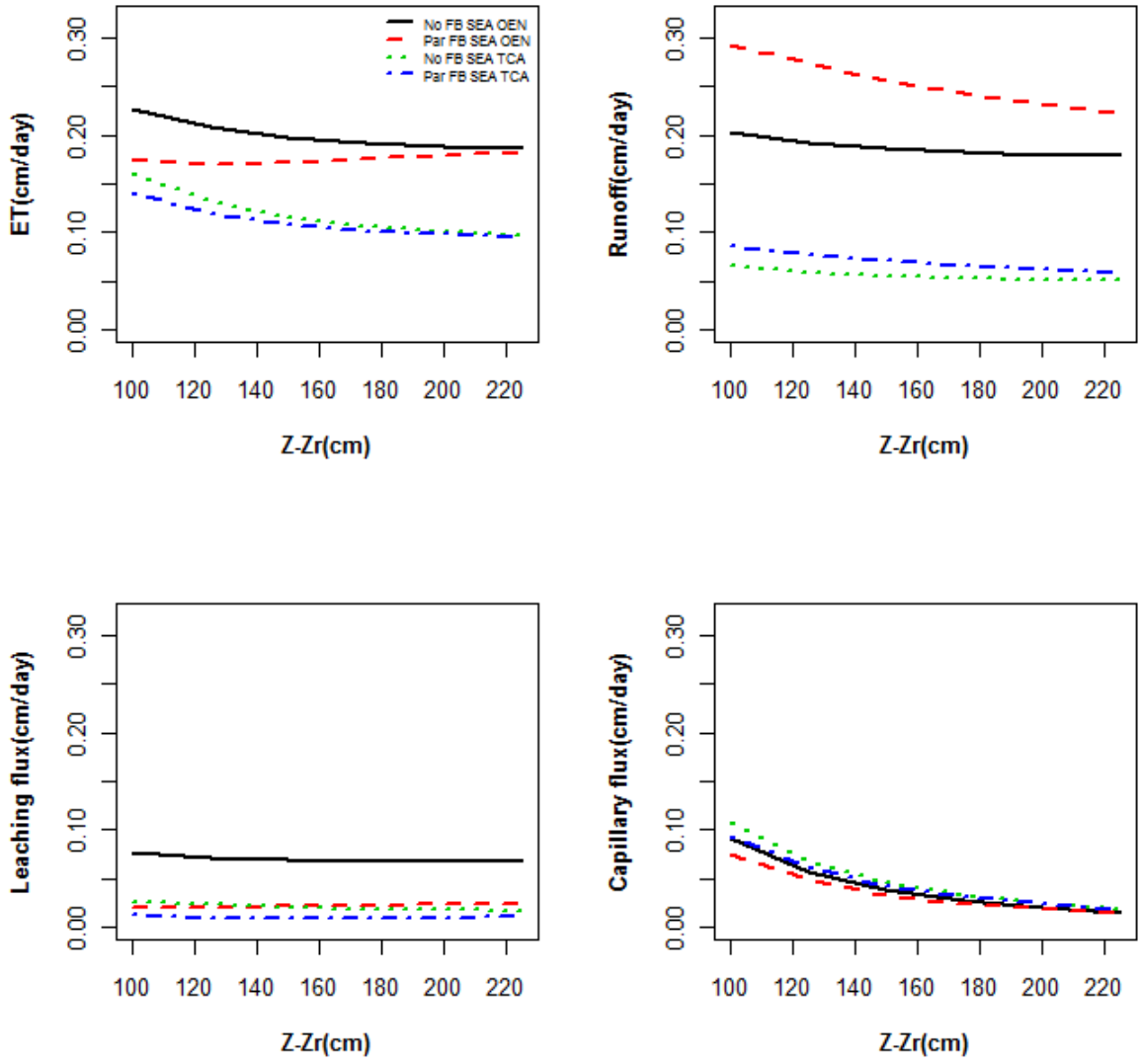

Figure 5.12. Long term average evapotranspiration, runoff, leaching flux, and capillary flux as function of Z-Zr distance for two real climates (Oenpelli and Tennant Creek Airport) under partial feedback (feedback affects only leaching flux) and no feedback effects. Other conditions the same as in Figure 5.7.

5.4. Conclusions

Consideration of the continued decrease in saturated hydraulic conductivity quantifies the under or over-estimated fluxes, salt concentrations and soil *ESP* under different climates (Oenpelli and TCA) and different groundwater depths. We have considered three scenarios to understand the reasoning of these estimations. We show that distinct dry and wet seasons in rainfall can have significant feedback effects on root zone fluxes, salt concentration and soil *ESP*. We have modeled the feedback effects of saturated hydraulic conductivity (*Ks(C, ESP*)) on root zone fluxes, salinity, and sodicity under different groundwater depths and climates of Oenpelli and Tennant Creek Airport located in North Territory of Australia. The feedback effects of saturated hydraulic conductivity have been calculated by using the procedure developed by *McNeal* (1968). The significant feedback effects on salt concentration and soil *ESP* depend on many important parameters like groundwater depth, leaf area index, weather seasonality and non-seasonality (Poisson rainfall), and soil type. Out of these important parameters, weather seasonality is the main driver that can develop significant feedback effects on root zone fluxes, salt concentration and soil *ESP*. The reduction in saturated hydraulic conductivity decreases the capillary flux, leaching flux, and evapotranspiration, but increases the magnitude of runoff compared to no feedback case. Also when *Ks(C, ESP)* affects both capillary and leaching flux under seasonal rainfall, the feedback effects are significant compared to the partial feedback.

Appendix A:

Soil saturation under matric and osmotic effects

As salts in the root zone develop osmotic potential, osmotic potential is important (*Shah et al., 2011; Shani et al., 2007*) in addition to matric potential which is a function of soil saturation (*Vervoort and Van der Zee,* 2008). Therefore, we need to combine the matric and osmotic potentials, and following the concept of chemical potential, determine a 'virtual' saturation, s_v, which then controls only evapotranspiration, but no capillary and leaching fluxes. The reason is that hydraulic conductivity function equivalent to leaching flux function (*Laio et al., 2001*) depends on the matric potential not on osmotic potential, therefore leaching and capillary flux cannot be controlled by virtual saturation. The osmotic potential follows the Van't Hoff's law. Furthermore, We have used a salinity correction based on additive properties of matric and osmotic potentials (*Bras and Seo*, 1987; *De Jong van Lier et al.*, 2008; *Shah et al., 2011*) by assuming the validity of Van't Hoff's law. According to this law, the osmotic potential (π (C)) is a linear function of the salt concentration *C*:

$$\pi(C) = kC \qquad \textbf{(5.A1)}$$

where π is osmotic potential (MPa), *C* is the salt concentration expressed as mol_c/L, and *k* is a coefficient that includes the effect of temperature, electrolyte properties, and unit conversion factor, which is equal to 3.6 $MPa.L/mol_c$. The osmotic potential is combined with the *Brooks and Corey* (1966) matric potential function of soil saturation:

$$h(s) = h(1)\left(\frac{s}{s_s}\right)^{-b} \qquad \textbf{(5.A2)}$$

Where $h(1)$ is the saturated soil matrix potential (MPa), *b* is a parameter related to conductivity and tortuosity (pore size distribution index), and s_s is soil saturation (s_s =1). We combine (5.A1) and (5.A2) and rearrange to obtain the virtual saturation s_v (*Bras and Seo*, 1987; *Shah et al., 2011*),

$$s_v = s_s h(1)^{1/b}\left(h(1)\left(\frac{s}{s_s}\right)^{-b} + kC\right)^{-1/b} \qquad \textbf{(5.A3)}$$

The resulting virtual soil saturation is the soil saturation that reflects the availability that plants sense, and depend on both matric and osmotic effects. Other fluxes were kept

independent of the osmotic potential. Primary reason is that whereas the chemical potential may affect the driving force, the hydraulic conductivity function is determined by the matric potential, but not by the osmotic potential. We believe that accounting for the osmotic potential in the various other fluxes (that evapotranspiration) would bias the analysis, whereas our parsimonious approach does not easily allow separating osmotic impacts on gradient and on constitutive relationships.

Derivation of differential equation of calcium fraction in soil solution (f_{Zr})

We can only rewrite *dN/dt* in terms of *df/dt* and *dC/dt*, after choosing an appropriate exchange equation for the functional dependence $N\ (f_{Zr}, C)$. We choose the Gapon equation, because it is quite common in salinity related research, despite its empirical nature. We assume a Gapon constant $K_G = 0.5\ (\text{mol/L})^{-1/2}$ (*Bolt and Bruggenwert, 1976*), in the Gapon equation given by

$$\frac{1-N}{N} = K_G\sqrt{C}\ \frac{1-f_{Zr}}{\sqrt{f_{Zr}/2}} \qquad \textbf{(5.A4)}$$

Equation (5.A4) implies a larger affinity for divalent cation sorption compared with sorption of monovalent cations, and this affinity decreases as the total concentration of salt *(C)* increases.

Rewriting equation 5.A4 for *N* gives:

$$N = \frac{1}{1+K_G\sqrt{2C}\left(\frac{1}{\sqrt{f_{Zr}}}-\sqrt{f_{Zr}}\right)} \qquad \textbf{(5.A5)}$$

Differentiating equation 5.A5 with respect to time, we obtain

$$\frac{dN}{dt} = N^2\left(\frac{K_G\sqrt{f_{Zr}}}{\sqrt{2C}} - \frac{K_G}{\sqrt{2f_{Zr}C}}\right)\frac{dC}{dt} + N^2\left(\frac{K_G\sqrt{C}}{\sqrt{2f_{Zr}}} + \frac{K_G\sqrt{C}}{\sqrt{2f_{Zr}^{\ 3}}}\right)\frac{df_{Zr}}{dt} \qquad \textbf{(5.A6)}$$

We obtain an explicit form of df_{Zr}/dt by using equation (5.5) and (5.A6)

$$\frac{df_{Zr}}{dt} = \frac{Uf_z C_z - Lf_{Zr} C - \phi Z_r f_{Zr} C \frac{ds}{dt} + \left(\frac{Z_r \rho \gamma N(1-N)}{2C} - \phi Z_r f_{Zr} s \right) \frac{dC}{dt}}{\phi Z_r Cs + Z_r \rho \gamma N^2 K_G \sqrt{C/2} \left(\frac{1}{\sqrt{f_{Zr}}} + \frac{1}{f_{Zr}\sqrt{f_{Zr}}} \right)} \quad \textbf{(5.A7)}$$

The calcium fraction (f_{Zr}) calculated from equation 5.A7 is used in equation 5.A5 to calculate the calcium fraction in exchange complex (N), which gives indirectly the sodium fraction in the exchange complex (1-N) and finally the soil *ESP* ((1-N)*100). The equations (5.1), (5.2) and (5.A7) are solved together numerically to provide root zone saturation, salt mass and salt concentration (C), soil sodicity (quantified by *ESP*), and the contribution of various water fluxes.

Acknowledgements

Part of this research was done with funding by the Higher Education Commission of the Government of Pakistan for S.H.H.S., and the Knowledge for Climate Research Program, Netherlands.

CHAPTER 6

Management of irrigation with saline water: accounting for externalities by considering soil-water-plant feedback mechanisms

S. H. H. Shah[1], A. Ben-Gal[2], H. P. Weikard[3], S .E. A. T. M. van der Zee[1]

[2]Environmental Physics and Irrigation, Agricultural Research Organization, Gilat Research Center, Israel.

[3] Environmental Economics and Natural Resources Group, Wageningen University

[1] Soil Physics, Environmental Sciences Group, Wageningen University, POB 47, 6700 AA Wageningen, The Netherlands

Submitted to Water Resources Research

6. Management of irrigation with saline water: accounting for externalities by considering soil-water-plant feedback mechanisms

Abstract

In arid and semi-arid regions, irrigation water is scarce and often saline. To reduce negative effects on crop yields, the irrigated amounts must include water for leaching and therefore exceed evapotranspiration. The leachate (drainage) water returns to water sources such as rivers or groundwater aquifers and increases their level of salinity and the leaching requirement for irrigation water of any sequential user. We develop a sequential (upstream-downstream) model of irrigation that predicts crop yields and water consumption and tracks the water flow and level of salinity along a river dependent on irrigation management decisions. The model incorporates a agro-physical model of plant response to environmental conditions including feedbacks. For a system with limited water resources, the model examines the impacts of water scarcity, salinity and technically inefficient application on yields for specific crop, soil, and climate conditions. As a general pattern we find that, as salinity level and inefficiency increase, the system benefits when upstream farms use less water and downstream farms are subsequently provided with more and better quality water. We compute the marginal value of water, i.e. the price water would command on a market, for different levels of water scarcity, salinity and levels of water loss.

Keywords: irrigation, water management, salinity management, water pricing for irrigation, stock pollution problems

6.1 Introduction

In semi-arid regions in particular, but also in regions with a temperate climate, irrigation to supplement natural precipitation is inevitable for agricultural primary production. The volume of water that is used for primary production is by far larger than the demand for high quality water for household consumption and industry. As

the world population steadily grows, the demand for good quality water for different purposes also grows. In view of the costs involved in purifying and desalinizing water, the supply of good quality water for agricultural needs is particularly becoming scarce and costly. For this reason, the use of low to marginal quality water for irrigation is increasing (*Hamilton et al., 2007; Qadir et al., 2007*), most notably in water scarce countries (*Noory et al., 2010; Rengasamy, 2006*).

Irrigation water is supplied to enhance transpiration. While transpiration is proportional to primary production, most salts present in water are not taken up by plants and remain in the soil. Hence, by irrigation salts are being concentrated in the root zone of plants. Excess application of water is therefore required at least periodically to remove accumulated salts and maintain agricultural productivity, as has been conceptualized decades ago with the so-called leaching requirement (*Richards et al., 1954*). In situations where irrigation water is high in salts, continuous leaching is required to minimize the negative effects of salts. The amount of leaching depends upon: irrigation water salinity, soil type, climate, crop type, rainfall, and level of soil salinity (level of loss of potential yield) deemed acceptable by the grower (*Dudley et al., 2008*).

In addition to the need for leaching, it is crucial that leached and drained water is removed from the system in order to avoid water logging (*Haq, 2000; Wolter and Bhutta, 1997; Smedema, 2000*). Removal of leached water may be through groundwater or surface water flow. Return flows of water with an elevated salinity lead to a deterioration of the ground or river water quality. Examples of river systems where drainage outflows from upstream users salinize the river for downstream users can be found on each continent, for instance Pakistan's Indus River (*Tanji and Keilen, 2002*), the western United States' Colorado River (*Gardner and Young, 1988*) and Southern Australia's River Murray (*Rengasamy, 2006*). In many arid and semi-arid river basins groundwater systems are affected by agricultural return flows as well (*El-Ashry et al., 1985*), as exemplified in California's San Joaquin Valley (*Schoups et al., 2005*). The inherent importance of downstream river water salinity build-up and the economic devaluation of this resource have long been recognized. From an economic perspective, this has resulted in considerations of allocation and pricing for either

control of salinity, efficiency, or equity among water consumers (*Scherer, 1977; Ancev, 2011*).

The objective of this paper is to determine optimal water management strategies for water use chains using an explicit agro-physical model for yield reductions caused by salt stress. With our model approach we arrive at explicit values for water as a function of salinity and of technical inefficiency of water use.

The physical yield model that we use is an implicitly solved analytical solution of crop response to environmental conditions (ANSWER) formulated from established governing equations (*Shani et al., 2007; Shani et al., 2009*). This model can be solved for each user in a chain along the river, where excess water from "upstream" users, used for leaching salts, becomes part of the irrigation water resource for "downstream" users. ANSWER integrates plant performance under varied environmental, biological and management parameters.

6.2 A chain model of water use for irrigation

Our model considers a chain of water users, (say, countries, districts, farms, or fields) that are ordered from upstream to downstream along a river. For brevity, we refer to either users or farms. In this section, we describe the physical relationships of water, salinity and primary production (or crop yield) along the chain of water users. In practice, in semi-arid regions often three main water supplies are in principle available: surface (river) water, groundwater or waste water for re-use (*Shah et al., 2011; Vervoort and van der Zee 2008; Mobin-ud-Din Ahmad 2002; Bhutta and Velde, 1992*).

We assume that for the most upstream user only river water is available. Similarly, for all farms that follow river water only is the only available water, but this water is considered to be perfectly mixed with the return flows, i.e. the excess water use that is drained upstream.

We thus consider a single physical source of water (the river) that can be used for irrigation or passed on to the next user. The system considered is characterized in Figure 6.1. We consider a set of water users (farms) N that are ordered along a river. The most upstream farm is denoted by 1 and farm i is upstream of j if and only if $i < j$. The most downstream farm is denoted by n.

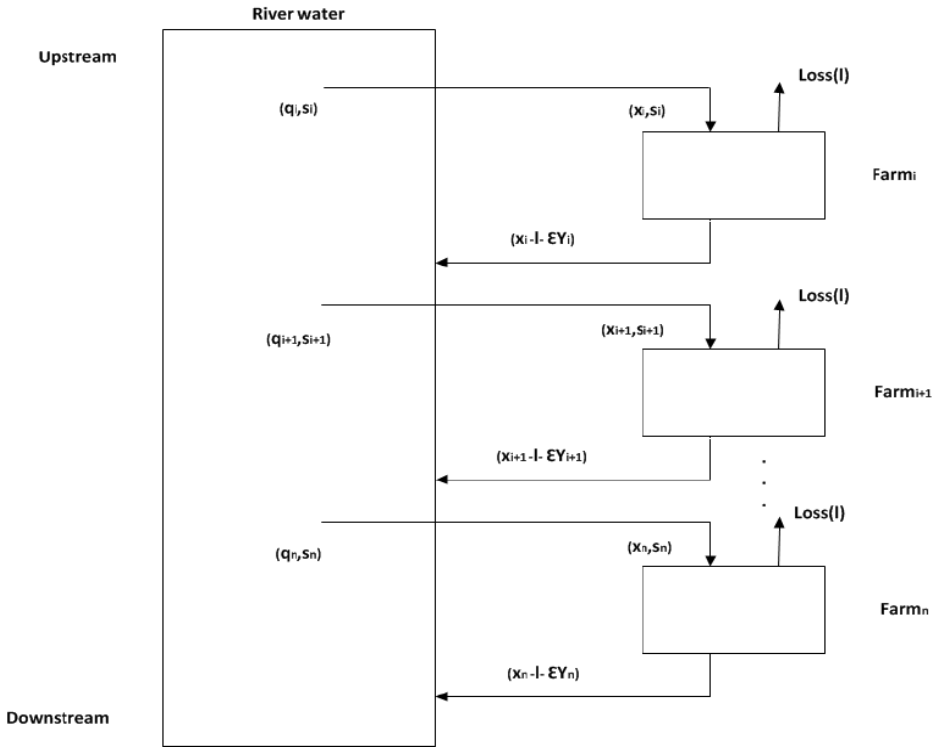

Figure 6.1. Conceptual upstream to downstream farm chain model.

The water available to any farm *i* is characterized by its quantity *q* and its quality or salinity level *s* and is formally written as (q_i, s_i). The actual use of water by farm *i*, denoted by x_i will determine the water quantity and quality available to the next farm (q_{i+1}, s_{i+1}) (Figure 6.1).

As we assume a single water source, and water quantity declines due to transpiration and surface evaporation losses, we can stipulate that $q_i \geq q_{i+1}$ and $s_i \leq s_{i+1}$, such that water availability (*q*) declines and salinity (*s*) increases from upstream to downstream. Water is used for irrigation and we assume that all users (farms/regions) have to deal with equal ambient conditions (climate, soil type, crop in production, etc.) except for water availability and quality. This assumption is necessary to postulate that the yield function dependency of production factors is everywhere the same, and that e.g. the potential yield is determined only by the amount of water used for transpiration (*Ben-Gal and Shani, 2003; Ben-Gal et al., 2003; De Jong van Lier et al., 2008; De Wit, 1958; Shani et al., 2007; Shani-et al., 2009; Shani and Dudley, 2001*), and not by e.g. soil

nutrient status or other management or environmental factors. Hence, irrigation water is productive if it increases transpiration for situations that otherwise would be constrained by water availability. However, we additionally assume that water productivity is reduced if its salinity is higher. This is an obvious assumption, in view of the adverse effects of salts on water availability caused, notably, by osmotic (*Homaee et al., 2002*), but also some salt specific toxic effects (*Marschner, 1995*). Enhanced salinities lead to additional constraints on the transpiration water that is available for primary production, and therefore yields diminish when salt stress increases.

We can express relative yield Y as a function of the applied amount of water x, and its salinity s.

$$Y_i = Y(x_i, s_i)\,. \qquad \textbf{(6.1)}$$

It is a common assumption that production increases as a function of 'effective' water application (for the range of x-values relevant here), but the marginal productivity decreases as a function of x. Hence, $\partial Y / \partial x > 0$. Furthermore production decreases as soil water salinity increases $\partial Y / \partial s < 0$ in a sigmoidal manner (*van Genuchten and Gupta, 1993*).

It is reasonable that the initial river water quantity and salinity are input parameters, dictated by other factors than those of primary concern here. However, we assume that these factors are constant over time. Quantities and salinities for farms downstream of the first farm depend on management and crop response decisions of each previous farm and are dependent on the amount of available water, amount of water applied, and amount water leached at each previous stage. Water use at each farm i affects availability and quality of water downstream as Farm i removes some portion of the river water and applies it as irrigation. Of that water, some, depending on Y_i is consumed (transpires) and the remainder leaches out of the root zone and returns to the river. Water is consumed by crops but salts are not. Therefore, salinity increases downstream as concentrated return flows are added to the original water source.

Water availability and quality can, therefore, be recursively described at the farm level as follows:

$$q_{i+1} = q_i - x_i + \left(x_i - \varepsilon Y_i\right),\ i = (2,...,n),\ q_1\ \textit{given} \qquad \textbf{(6.2)}$$

and

$$s_{i+1} = \frac{q_i - x_i}{q_{i+1}} s_i + \frac{x_i - \varepsilon Y_i}{q_{i+1}} s_i^r,\ i = (2,...,n),\ s_1\ given \quad \textbf{(6.3)}$$

The mass balance is:

$$q_{i+1} \cdot s_{i+1} = \left(q_i - \varepsilon \cdot Y_i\right) \cdot s_i \Rightarrow \varepsilon \cdot Y_i \cdot s_i = x_i \left(s_i - s_i^r\right) + \varepsilon \cdot Y_i \cdot s_i^r, \quad \textbf{(6.4)}$$

where ε is the evapotranspiration per unit of production and s_i^r is the salinity of the return flow $x_i - \varepsilon Y_i$.

6.3 Production function

The (primary) production or yield function, that expresses the magnitude of the yield in its dependency of the two (only) explicitly accounted for production factors, i.e., water *x* and salinity of this water *s*, is given by (6.1). For this function, several approaches are feasible, that differ in generality, physical robustness, and number of parameters. We have opted to approximate eq. 6.1 for each farm *i* using the ANSWER model (*Shani et al., 2007; Shani et al., 2009*). Our motivation is that this model is smooth (i.e., has continuous derivative $\partial Y / \partial x$ and $\partial Y / \partial s$), is analytically tractable, and, has been shown to be compatible in describing these responses as far as salinity is concerned compared to more difficult to employ numerical models (*Shani et al., 2007; Tripler et al., 2012*). For the present analysis, the first reason for adopting this approach is particularly important, as a completely numerical approach may be more versatile at the expense of elegance and generality, whereas the empirical basis of model validation is limited.

In short, using the ANSWER model for the yield function, we obtain from *Shani et al.* (2009) yield as a function of *x* and *s* interactions:

$$Y_i = \frac{\min\left\{T_p, \left[\left[\psi_{root} - \frac{\psi_w}{\left[\frac{(x_i - Y_i)}{K_s}\right]^{\frac{1}{\eta}}}\right](x_i - Y_i)b\right]\right\}}{1 + \left[\frac{s_i x_i \left[\theta_r + (\theta_s - \theta_r)\left[\frac{(x_i - Y_i)}{K_s}\right]^{\frac{1}{\delta}}\right]}{EC_{50}(x_i - Y_i)\theta_s}\right]^p} \quad \textbf{(6.5)}$$

for soil hydraulic properties (ψ_w, θ_r, θ_s, K_s, b, δ, η), plant sensitivity parameters (ECe_{50}, p, ψ_{root}), and climate (T_p) given in Table 6.1. Equation (6.5) thus integrates a number of climate, plant, and soil specific parameters. We assume that the parameters given in Table 6.1 are fixed.

Table 6.1. Soil and plant parameters for ANSWER model input parameters.

Soil	Arava Sandy Loam
K_S (mm/d)	3600
δ (unitless)	4.91
β (unitless)	0.55
θ_s (m^3/m^3)	0.41
θ_r (m^3/m^3)	0.06
ψ_w (mm)	-200
Plant	*Capsicum annum c*v. Celica
ψ_{root} (mm)	-6000
ECe_{50} (dS/m)	2.5
T_p (mm/d)	5

***Source*: *Ben-Gal et al.* (2008) and *Shani et al.* (2007). *Ks*, saturated hydraulic conductivity; δ and β, empirical soil characteristic parameters for the Brooks and Corey (1966) hydraulic model; ψ_w, air entry value; θ_s, soil water content at saturation; θ_r, residual soil water content; ψ_{root}, minimum possible water head at the root soil interface; ECe_{50}, plant characteristic parameter for salinity response function (EC of the soil saturated paste where $Y_r = 0.5$); T_p, potential transpiration.**

6.3.1 Irrigation application efficiency

Irrigation can be practiced various ways (sprinkling, drip, flood), which each have their own positive and negative aspects. As water conservation is a major reason to develop new irrigation methods, the irrigation/evaporation ratio is a major distinguishing factor between irrigation methods. From an elementary water balance, it is clear that the difference is in how much of applied (or rainfall) water is effectively taken up by plants for transpiration and, hence, crop production, and how much is evaporated from the soil surface without benefiting production. Since specific irrigation methods are not of our prime concern here, we consider application system efficiencies that range from fully efficient (no evaporative loss) to highly inefficient (40% loss). The first can be exemplified as subsurface drip irrigation where the other extreme could represent flood irrigation on a crop without full canopy cover. Therefore, we consider efficiency in cases where not all applied irrigation water is available for transpiration, due to evaporative losses by introducing a loss term (l) that is related to this technical inefficiency in the water balance Equation (6.2). This yields:

$$q_{i+1} = q_i - x_i + \left(x_i - l - \varepsilon Y_i\right) . \qquad \textbf{(6.6)}$$

The loss also affects the downstream salinity

$$s_{i+1} = \frac{q_i - x_i}{q_{i+1}} s_i + \frac{x_i - l - \varepsilon Y_i}{q_{i+1}} s_i^{\,r} . \qquad \textbf{(6.7)}$$

6.3.2 Illustration of the crop yield function

With our model we can generate plots of the yield function for different amounts of irrigation water applied. In Figure 6.2A, the production curve of Farm 1, the most upstream farm is given. It gives relative yield as a function of relative irrigation, with both yield and irrigation normalized to potential transpiration (yield). Relative irrigation is defined as the amount of applied irrigation water x divided by the amount needed to attain maximum transpiration (yield) if salinity and water stresses are absent.

Figure 6.2A presents the relative yield, given by Y as a function of relative irrigation x for Farm 1. For zero salinity ($s_1 = 0$) we have two linear sections (the dashed lines). For all s unequal to zero, a smooth curve results.

A similar production curve can be drawn for Farm 2. However, that curve depends on choices made by Farm 1. Hence, we get a family of curves the shape of which is dependent on the salinity of drainage water of Farm 1; also the amount of water available to Farm 2 depends on the quantity used by Farm 1. Schematically, this is shown in Figure 6.2B.

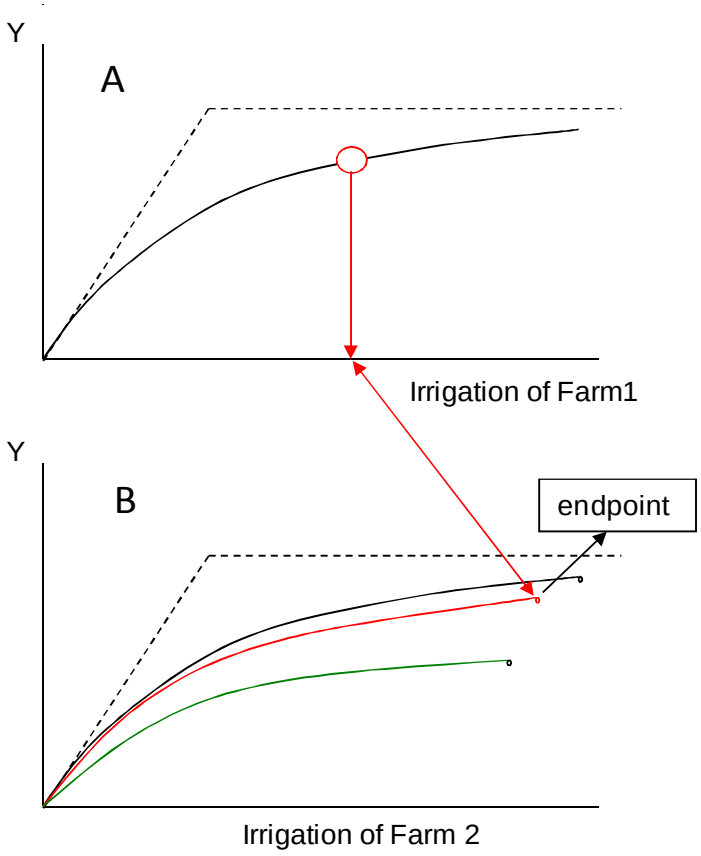

Figure 6.2: Production curves for Farm 1 (A) and Farm 2 (B). Simulation of a sequential system with 2 farms. Decision of Farm 1 (use of irrigation water of given quality) dictates production possibilities for Farm 2. Horizontal axis in each frame is irrigation of the respective farm. Vertical axis is relative yield *Y*. Different lines in (B) are examples of response curves for Farm 2 based on possible decisions made by Farm 1.

The essential insight here is that each point on the production curve of Figure 6.2A leads to a new curve in Figure 6.2B. If we assume a system of two farms, then the implication is that Farm 2 will always benefit from using all remaining available water and therefore, only the end-point (also shown in Figure 6.2B) is of interest.

We have programmed the above, including criteria for choosing optimized water allocation for maximal system yields, using the R environment (R Development Core Team, 2011).

6.4 Management scenarios

Having formally described the physical system, we now turn to its management. We consider the system in a series of steady state solutions, such that flows into and out of each farm are constant and of constant quality. Then, the irrigation regime $(x_1,...,x_n)$ is also constant. Because our focus is on water management, we do not consider other inputs to agriculture explicitly (implicitly we assume that the value of the yields is net of costs, except water costs). We normalize the price of crops to one. Hence yields equal revenue. Generally, profits are

$$\pi_i = Y_i(x_i, s_i) - x_i p(s_i), \qquad \textbf{(6.8)}$$

where the second term captures water costs if we allow for a quality dependent water price $p(s)$.

We consider a series of management scenarios, the first one being an unregulated river where a farm can use whatever is available and there are no water charges. In a second scenario, we allocate river water equally between farms, prior to any consumption. We will then introduce socially optimal water management that maximizes the sum of the yields of all farms along the river. Finally, we determine efficient water prices. As our main interest is the study of water management for irrigation, we do not consider other water uses such as urban water consumption. We present our scenarios for different levels of irrigation system efficiency (water loss l due to evaporation and therefore not available for consumption by crops or return flow), for a range of initial river water salinities, and for different levels of water scarcity.

In the absence of any water regulation there are no water charges, $p = 0$. Every farm maximizes its profits given the quantity and quality of available water. The water use that gives maximum yields is denoted by $\hat{x}_i$. Note that $\hat{x}_i$ varies with the prevailing salinity level s_i. Unregulated water use implies for Farm 1 that $x_1 = \min(q_1, \hat{x}_1)$. Using Eqs. (6.2)-(6.4), the entire path of water use and the corresponding salinity levels can be

determined. Unregulated water use is $\hat{x}_i$ for all unconstrained upstream farms. The first upstream farm, for which the water supply is constrained, will use all of the water in the river for irrigation and pass on only return flows. Admittedly, this simple response indicates that many crucial factors were still left out of consideration.

If, under unregulated use, the last farm, Farm *n*, is unconstrained and can consume $\hat{x}_n$, then we do not have water scarcity. Water scarcity, then, means that at least Farm *n* faces water constraints. We will refer to a situation where Farm *n* does not receive any water as 'severe scarcity'. Obviously, if there is no scarcity, then there is no management problem. If water is scarce, then the unregulated water allocation may be inefficient. This can be seen from the fact that the marginal productivity of water use of the unconstrained upstream farm is zero (as they maximize yields) while the downstream farms have a positive marginal productivity of water. In such a case, reallocation from upstream to downstream would increase overall production and, hence, profits. We may observe two effects of 'overconsumption' of water by upstream farms. First, there could be a direct effect. Higher water consumption (i.e. water application minus return flows) will leave less water downstream. Second, higher water consumption will increase the salinity of the water that is available downstream.

Now consider that there is an agency that controls water allocation. In order to make the most out of the available water, the agency maximizes the sum of yields of all farms along the river under the water constraint while considering the impact of return flows on downstream salinity. The optimal water use path, denoted by $(x_1^*,...,x_n^*)$, can then be determined as the solution to the following optimal control problem:

$$Max \sum_{i \in N} Y_i \qquad \textbf{(6.9)}$$

subject to

$$q_{i+1} - q_i = -\varepsilon Y_i, \qquad \textbf{(6.10)}$$

$$s_{i+1} - s_i = -\frac{q_{i+1} - q_i + x_i}{q_{i+1}} s_i + \frac{x_i - \varepsilon Y_i}{q_{i+1}} s_i^r,$$

$$x_i \le q_i, \quad q_1 \text{ given}, \quad s_1 \text{ given}.$$

6.5 Simulations and Results

We consider a chain of 2 farms with a single water source and evaluate the effect of the upstream user's water application x_1 on yields of both farms (and total system yield). We have simulated this scenario for a range of the amounts of initial water in the river, q_1, for a range of the initial river water salinity, s_1, and for different levels of technical system efficiency (losses due to evaporation l). As explained before we leave crop type, soil type and climate equal for each farm (Table 6.1).

As mentioned before we consider four scenarios. (i) First we consider a situation with unregulated water resources. This means that an upstream farm can take any quantity of water as desired. (ii) We consider an equal allocation of river water between all farms (here: the upstream farm may use up to half of the available water). (iii) We consider an agency that manages irrigation on all sites, with the aim to maximize system yields – a social planner approach. (iv) We consider water markets in which the price of water is determined by its marginal productivity (*Albersen et al. 2003, Houba 2008*). In all scenarios we have absolute water scarcity in the sense that even if all water is used, yields cannot reach their potential on every farm.

Results are given in terms normalized to potential transpiration T_p. This implies that water quantities *q* and *x* are given in units of T_p (i.e. normalized to $T_p = 1$) and $Y = 1$ at T_p. For our analysis, we evaluated *q* values that varied in the range from 1 to 2, for a two-farm system. Irrigation application rates varying from 0 to q_1 were compared. For three levels of initially available river water q_1, two initial levels of salinity s_1, and three levels of loss *l*. Water production functions (yield as function of irrigation water application) were determined for the first farm by simulating $x_1 = 0,...,x_1 = q_1$. For each level of x_1, the subsequent yield for the second farm was calculated assuming that all water, left after Farm 1, was actually applied by Farm 2 (i.e. $x_2 = q_2$).

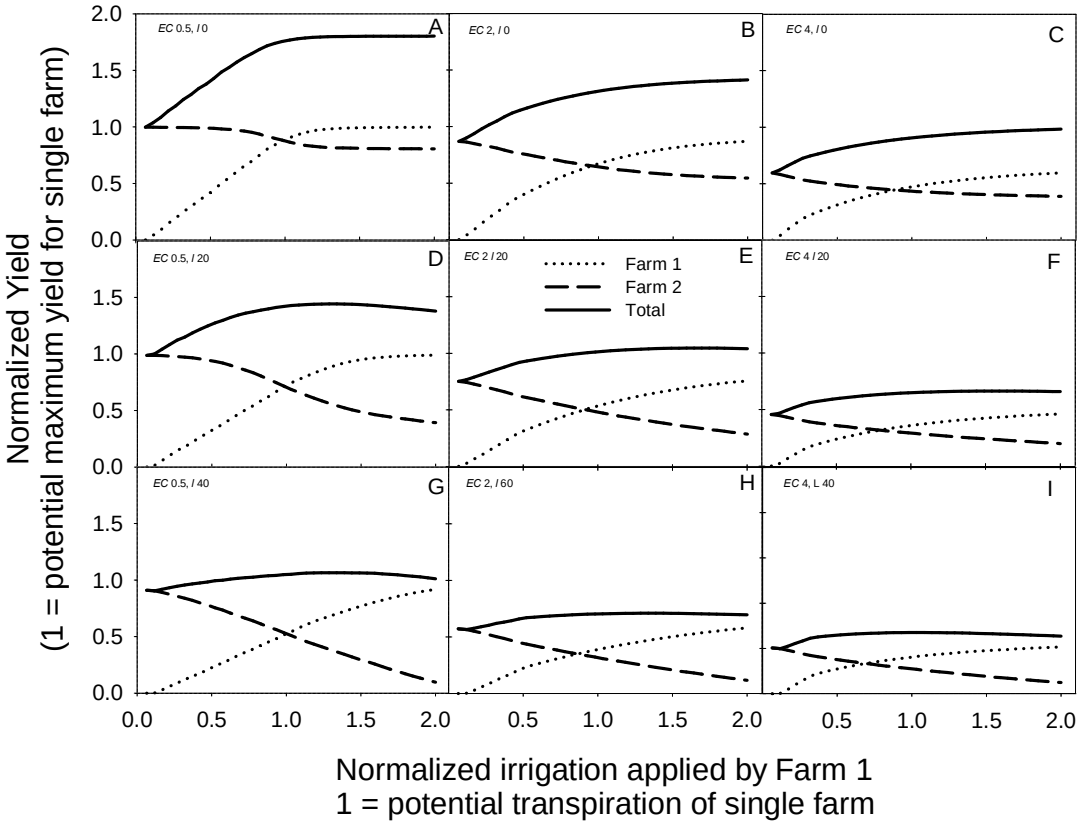

Figure 6.3: Yield of consecutive irrigators (Farm 1 and Farm 2) and total relative yield as a function of water applied by the first farm for different losses and initial irrigation water salinity. Total initial available water q_1 = 2.0. Initial river salinity s_1 = 0.5 dS/m (A, D, G), 2 dS/m (B, E, H) and 4 dS/m (C, F, I). System loss due to efficiency *l* = 0% (A, B, C), 20% (D, E, F) and 40% (G, H, I). The crop is pepper, T_p = 5 mm/day, EC_{50} = 2.5 dS/m, and soil is Arava sandy loam (see Table 6.1).

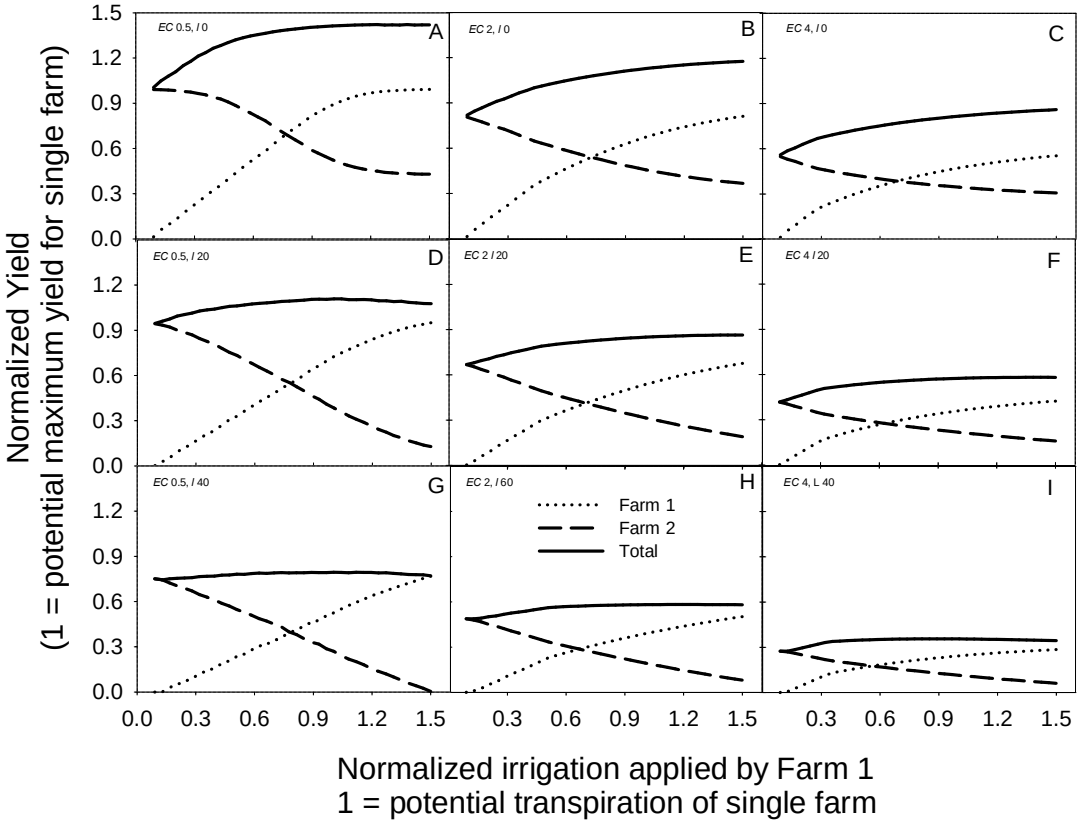

Figure 6.4: Yield of consecutive irrigators (Farm1 and Farm 2) and total relative yield as a function of water applied by the first farm for different losses and initial irrigation water salinity. Total available water q_1 = 1.5. Initial river salinity s_1 = 0.5 dS/m (A, D, G), 2 dS/m (B, E, H) and 4 dS/m (C, F, I). System loss due to efficiency *l* = 0% (A, B, C), 20% (D, E, F) and 40% (G, H, I). Other parameters as in Figure 6.3 and Table 6.1.

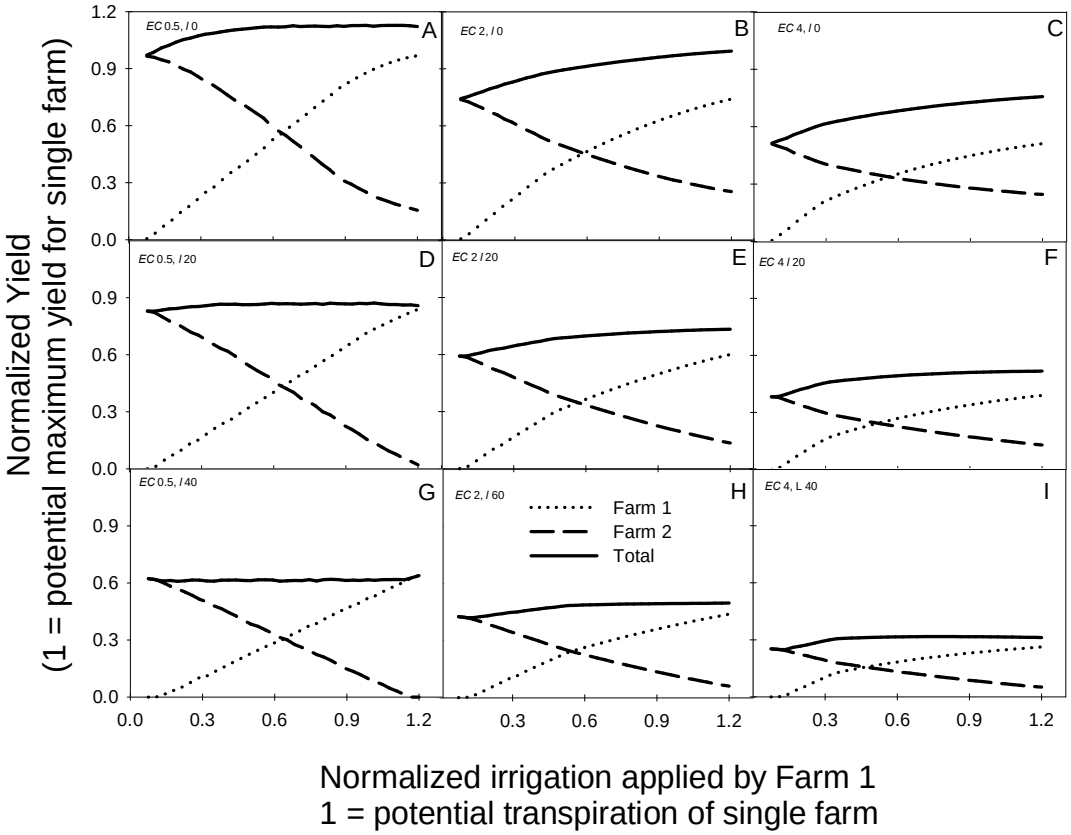

Figure 6.5: Yield of consecutive irrigators (farm1 and farm 2) and total relative yield as a function of water applied by the first farm for different losses and initial irrigation water salinity. Total initial available water q_1 = 1.2. Initial river salinity s_1 = 0.5 dS/m (A, D, G), 2 dS/m (B, E, H) and 4 dS/m (C, F, I). System loss due to efficiency *l* = 0% (A, B, C), 20% (D, E, F) and 40% (G, H, I). Other parameters as in Figure 6.3 and Table 6.1.

Yields of each farm and total system yield (summing Farm 1 and 2) are shown as a function of the irrigation quantity of Farm 1 for the cases of s_1 = 0.5, 2 and 4 dS/m and l = 0%, 20% and 40% in Figures 6.3 (q_1 = 2), 6.4 (q_1 = 1.5) and 6.5 (q_1 = 1.2). The figures range from a normalized irrigation of 0 till 2, 1.5, and 1.2, in Figures 6.3, 6.4 and 6.5 respectively. The water available for Farm 2 is a function of that used by Farm 1 as described in Eq. (6.2). Farm 2 irrigates all available water regardless of 1's irrigation level. Yields decrease with increasing salinity and decreasing technical efficiency. Yield of Farm 1 (as seen theoretically in Figure 6.2) increases with increasing water application and motivates the farmer to use all available water, irrespective of its salinity and of level of loss by evaporation.

Under non-limiting water of low salinity and no losses due to technical inefficiency (Figure 6.3A) Farm 1 achieves near maximum yield when irrigating slightly more than (normalized) potential transpiration T_p. As salinity and/or losses increase (Figure 6.3) Farm 1 must use more water to maximize yields. At the highest salinities and lowest efficiencies, due to water scarcity, Farm 1 must use all the available water. Figures 6.4 and 6.5 show the respective results, when the quantities of river water that is initially available are reduced from 2 to 1.5 and 1.2 times the transpiration demand of each farm. As water scarcity increases (amount of water available for Farm1 decreases), the options decrease and Farm1 must use relatively larger amounts of water to achieve maximum relative yields (Figures 6.6 and 6.7).

Since we are interested in water management, in Figures 6.3-6.5 the maximum total yield is of particular interest. Hence, we considered the entire range of q_1, s_1 and l and determined the maximum summed yield of the two farms for each simulation case. We show this maximum total system yield (relative to T_p) as a function of loss rate and initial river salinity in Figure 6.6. Assuming that Farm 1 constrains water application, in order to obtain maximum system yield (i.e. total yield for the two farms together), the quantity of river water, normalized to T_p, applied as irrigation by each of the farms depends on both initial salinity and on the loss rate.

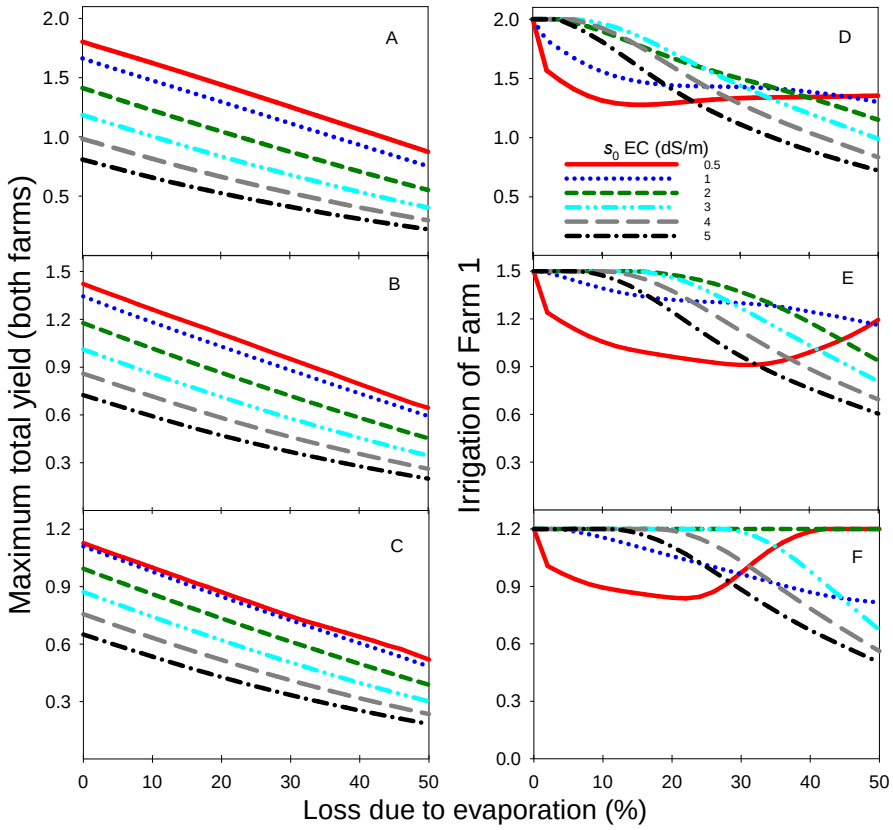

Figure 6.6. Maximum possible total relative yield of two consecutive irrigators as a function of system efficiency (loss due to evaporation) for different initial river salinity s_1, with EC (0.5, 1, 2, 3, 4, 5 dS/m) (A, B,C) and relative irrigation of Farm 1 as a function of system efficiency for different initial river salinity s_1 with EC (0.5-5 dS/m) (D, E, F). Initial river water quantity q_1 = 2 (A, D), 1.5 (B, E) and 1.2 (C, F). Other parameters as in Table 6.1 and Figure 6.3.

While the maximum system yields reached (Figure 6.6, A, B, C) are inherently straightforward and predictable in that they are reduced by both initial salinity and water losses, the irrigation rates of Farm 1 applied to reach these yields (Figure 6.6, D, E, F) are complex in their dependency of water losses. First notice that for salinity levels of EC = 2 dS/m or greater, and low to moderate levels of water loss, maximum yields are reached when Farm 1 irrigates with all available water (Figure 6.6 D, E, F). The range of loss levels where Farm 1 uses all the water increases with water scarcity. This range corresponds to corner solutions when maximizing total system yields, see Figures 6.3-6.5. At low salinities, however, Farm 1 does not use all available water. Farm 1's water application first declines and then increases with water losses. At low salinity levels downstream water quality is not much affected; but it is increasingly affected as losses

increase. This implies that Farm 1 leaves more water to Farm 2. As losses increase further, however, Farm 1, requiring more water to leach salts, increases its application.

A comparison of our first three scenarios; no regulation, equal split of river water and regulation for optimal use (maximum yields), is shown in Figure 6.7 for the case with initial river water equal to $q_1 = 1.5$ (Figure 6.4). Here it can be seen that as the loss due to system inefficiency becomes larger, system maximization diverges from the obvious supplying of the upstream farm with all available water.

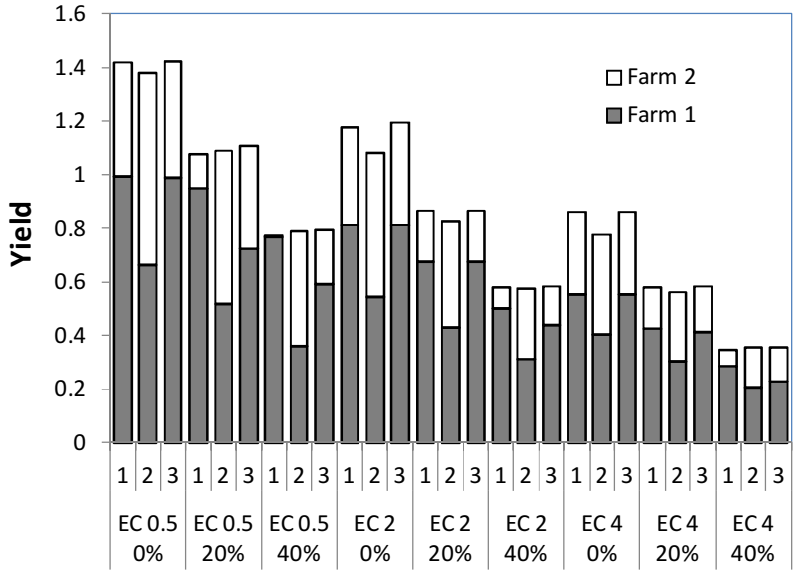

Figure 6.7 Comparison of scenarios. 1- Farm 1 irrigates with all available water. 2- Farm 1 irrigates with ½ of available water. 3- Allocation for maximal yield. Normalized yields of each user for each scenario. For initial river water quantity $q_1 = 1.5$. Parameters as in Table 6.1 and Figure 6.4.

6.6 Water prices at system maximum relative yield

With unregulated water use the most upstream user can use all the available water. This leaves downstream users with return flows of higher salinity and would usually be inefficient and therefore reallocation of water from the upstream to the downstream user would increase total yields, at least when salinity levels and water scarcity are moderate. In such case the upstream user, if he holds the rights to water, can offer water to downstream users and claim its price. In our case of two farms, Farm 1 sells an amount of water to Farm 2 such that marginal yields are equal for both farms. The marginal yield equals the price of water (as the price of the crop is normalized to 1 in

our model). More technically, in order to calculate the water prices, we determine marginal yields (the slopes of the production functions, see Figures 6.3-6.5) at the maximum of the total yield. Clearly, when water is shared efficiently between both farms the marginal yields at maximum system yield are equal and that slope reflects the water price. Figure 6.8 shows the marginal values of water for both farms. At low levels of loss with river water $q_1 = 2, 1.5, 1.2$ marginal values of water are generally higher for Farm 1. Hence, there is no option for water trade (left panels of Figure 6.8). The reason is that Farm 1 uses all the water to get maximum system relative yield at zero loss. Farm 2 uses only return flows from Farm 1.

In all cases where the valuations of water coincide, water trade takes place and we have an interior solution of the maximisation of system yields. The general pattern is that water prices decline with salinity (lower water quality) and they increase with scarcity of river water and loss levels. The exception is the situation when there are no losses (Figure 6.8, A, B, C), moderate salinity and moderate or no water scarcity. In Figure 6.8A we observe that the water price is zero when salinity is sufficiently close to zero. In this case there is sufficient water to reach maximum production. Hence there is no water scarcity and water does not have a positive price.

When water is severely scarce but losses are moderate, then Farm 1 places a higher value on water than Farm 2 and water would not be traded whenever initial salinity exceeds $s_1 = 0.5$ dS/m. This can also be seen from the corner solutions in Figure 6.4, panels B and C where farm 1 uses all the water to maximise system yield.

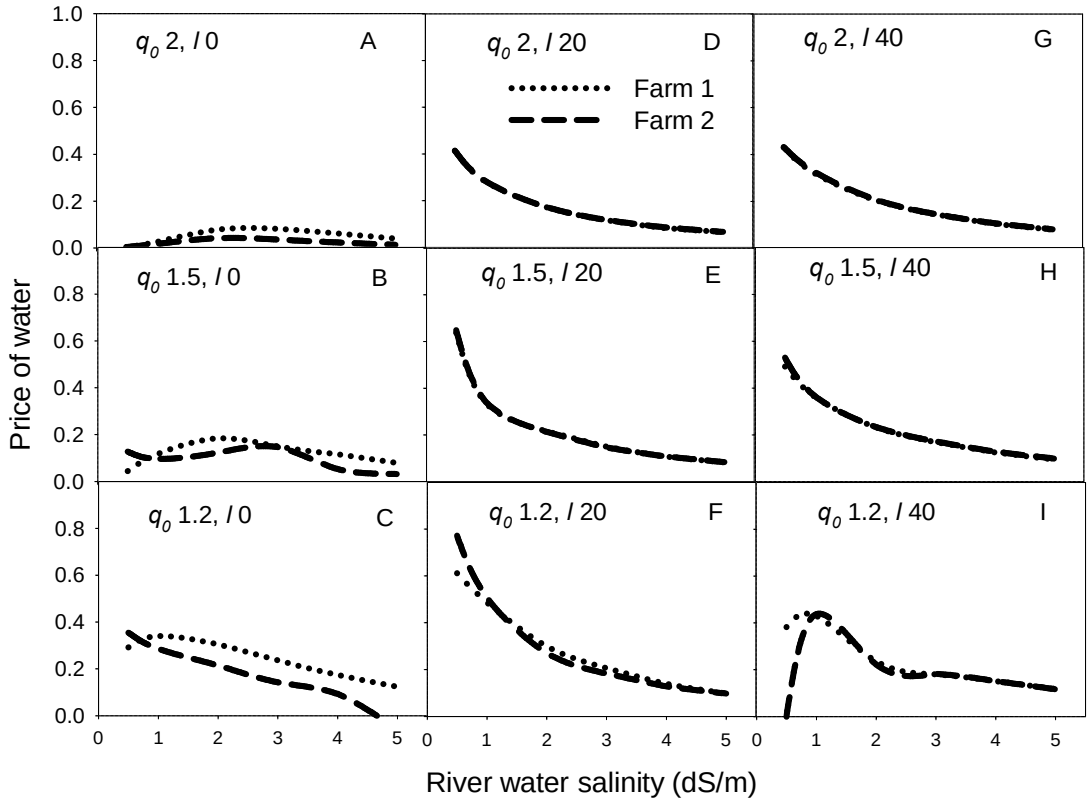

Figure 6.8. Water prices (where the system yield is maximum) as a function of initial river salinity under three levels of river quantity: 1.2 (A, D, G) , 1.5 (B, E, H), 2.0 (C, F, I), and three levels of losses: 0% (A, B, C), 20% (D, E, F), 40% (G, H, I) for Farm 1 (dotted line) and Farm 2 (dashed line). Other parameters as in Figure 6.2.

6.7 Discussion and conclusions

Our paper develops a conceptual model for the optimal management of scarce and saline irrigation water. But we move beyond the formulation of a conceptual frame and apply the model to the irrigation of *Capsicum annum* on Arava Sandy Loam. We show for this case how water application should be distributed between upstream and downstream plots or farms. We identify those situations where water is traded from upstream to downstream farms (assuming that the upstream farm holds the water rights). We find that water trade will improve efficiency except when loss levels are low. In that case marginal productivity of water of the upstream farm is large and the return flows available to the downstream farm are less saline and, hence, more productive compared to higher loss levels.

The case presented in this study has been simplified (e.g., only two farms, same crops and soil types). Nevertheless, considerations of externalities of irrigation due to leaching of salts are not trivial, when the plant response processes are captured in a physically and agronomically rigorous way. Whereas it is obvious, that total yields decline as initial river water quality gets worse as well as if losses increase, the optimal use of irrigation water by an upstream farm can be a complicated function of initial river water quality and losses due to irrigation inefficiencies. For most presented scenarios, we find some gain from trade of water from upstream to downstream.

It is a novelty of this paper to combine a coupled agro-physical model, that has been validated (*Shani et al., 2007*), with an economic model for water resource and irrigation management in a parsimonious way. Despite the already apparent complexity of the results, even more complexity is needed for real world applications. With respect to the physical environment, one may think of different soil types, and water resources (e.g. waste water, groundwater, river water). From an agronomic perspective, crop choice and rotation schemes may be considered that take into account different salt tolerances and product prices. Although this would significantly complicate the computations, our approach is sufficiently general to allow such applications. By adding complexity stepwise, we keep our investigations transparent.

Obviously, our model can also be extended to account for more farms, by introducing farms at appropriate locations with their corresponding benefits from water use and the resulting return flows. The model allows determining efficient water prices such that profit maximizing behavior under these prices will result in an overall optimal water allocation. The model also allows consideration of river water quantity and quality after the last (*n*th) user to provide for evaluation of potential additional water consumers or comparison of scenarios as to their environmental consequences. Furthermore our analysis is relevant to determine fair compensations to settle international conflicts over scarce freshwater resources.

Acknowledgements

This research was carried out while Alon Ben-Gal was spending a sabbatical at Wageningen University and we gratefully acknowledge funding by WIMEK, Wageningen Institute for Environment and Climate Research. Part of this research was funded by the Dutch Knowledge for Climate Programme, Theme 2.

CHAPTER 7

General Discussion

7.1 Introduction

Global food production will need to increase with 38% by 2025 and 57% by 2050 (*Wild, 2003*) if food supply to the growing world population is to be maintained at current levels. Most of the suitable land has been cultivated and expansion into new areas to increase food production is rarely possible or desirable. The aim, therefore, should be to increase yield per unit of land rather than the area cultivated. More efforts are needed to improve productivity as more lands are becoming degraded. It is estimated that about 15% of the total land area of the world has been degraded by soil erosion and physical and chemical degradation, including soil salinization (*Wild, 2003*).

The main sources of soil salinity and sodicity development are groundwater and irrigation water. In discharge areas of the landscape, water exits from groundwater to the soil surface bringing the salts dissolved in it. The driving force for upward movement of water and salts is evaporation from the soil plus plant transpiration. Salt accumulation is high when the water table is less than a threshold depth. However, this threshold depth may vary depending on soil hydraulic properties and climatic conditions. Furthermore groundwater associated salinity and sodicity affect around 350 X 10^4 km^2 area in the world.

In order to quantify and understand the salinity, sodicity, and effect of salinity and sodicity on saturated hydraulic conductivity in groundwater dependent agro-ecosystems, we have developed a root zone model of the mass balances of water, salt, and cation. For sodicity calculations, we have used the Gapon equation which is favoured in salinity research. The combined effect of salinity and sodicity is translated into reduction in saturated hydraulic conductivity by using the *McNeal* approach under different climates and groundwater depths. In the second theme of this thesis, we have optimized irrigation water between two farms depending on the water quantity, quality and irrigation water inefficiency. Furthermore, we have calculated the water prices at system (farm 1 and farm 2) maximum relative yield depending on the water scarcity, salinity and irrigation water inefficiency. This final chapter reflects on the most important conclusions derived from each chapter of this thesis and integrates these aspects. Finally some ideas for future research are put forward.

7.2 Soil sodicity due to periodical drought

In Chapter 2, we considered the change in sodicity for a soil, that is subject to temporal variations of soil salinity, e.g. due to periodic drought. Since model transparency improves our understanding of cause-effect relationships, we favored a model with small or modest complexity. We have shown that fluctuations in salt concentration in the soil solution can lead to an increase in sodicity to hazardous levels even in the absence of a gradual increase of salt concentration at time scales larger than one year. The motor of such increasing sodicity can be the variation of salinity and sodium concentration in incoming water as a function of time, even when at the end of the year, the salt concentration C has returned to its initial value. Even if soil and water salinity are controlled by wise water management, for sodicity this may not be the case: soil chemical aspects of soil water management may be more demanding than salinity management in a more strict sense, i.e., aimed at controlling salt concentrations. The extent to which irrigation managers allow soil to dry out between water applications becomes a factor to take into consideration in water management.

Whereas our work focused on conceptual and modeling work, our results are supported by current strategies for conjuctive use of good quality canal and poor quality ground water (*Kaledhonkar et al., 2001*) and experimental evidence (*Minhas et al., 2007*). Both our model and the mentioned experiments show that an increase of *ESP* is possible due to cyclical variations in salinity. Confirmation also comes from field experiments of *Tedeschi and Dell'Aquila* (2005) that show an increase of soil salinity and sodicity during seven years with an annual cycle. Experimental evidence was presented by *Miller and Pawluk* (1993) that fluctuations of the salt concentration can be accompanied by an increase of sodium.

For the root zone model, it appeared feasible to develop very simple analytical approximations for the concentration levels that correspond with the periodic variations. To obtain a rapid impression of the salinity levels that may develop, and thus, to get an approximation for sodicity changes, the analytical approximations can be very useful and assist in practical, soil chemically based water management. Furthermore, the regular pattern of salt accumulation and leaching is quite constraining. In reality, weather is much

more complex, erratic and diverse and this aspect as a first step towards feedback calculations for reduction in saturated hydraulic conductivity is considered in Chapter 3.

7.3 Stochastic modeling of salt accumulation in the root zone

In Chapter 3, we have considered the impact of salt coming from groundwater with capillary fluxes, into the root zone water and the resulting root zone salt balance. Capillary groundwater fluxes influence the soil moisture balance in a limited range of groundwater levels, as was discussed by *Vervoort and Van der Zee* (2008). If groundwater is brackish or saline, the upward capillary fluxes carry along salt that may accumulate in the root zone. These salts may lead to a reduced transpiration due to the moisture stress caused by osmotic effects. In Chapter 3, we considered the salt dynamics in the root zone, and take osmotic effects on the water fluxes into account, for erratic atmospheric forcing. Thus, compared with Chapter 2, not only were the water flow dynamics taken explicitly into account, but also the rainfall was represented by a Poisson distributed process. The latter causes the root zone water saturation as well as all water fluxes depending on this saturation, to be stochastic processes also.

The upward transport of salts from groundwater into the root zone is larger if the upward water flow rate is larger, but since it may also induce the root zone to become wetter on average and more prone to solute leaching events, the salt concentration that develops depends in a complex way on capillary upward flow. The long term salt concentration is not a monotonically increasing or decreasing function of the various system parameters such as hydraulic conductivity, groundwater depth, or climate parameters. This is due to different counteracting processes. Dependencies can also be different, compared with those found by *Suweis et al.* (2010), where salt inputs derived only from atmospheric deposition.

Salt accumulation in the root zone is characterized by very erratic patterns of concentration and salt mass as a function of time, as caused by the Poisson distributed daily rainfall. If we allow these patterns to stabilize, it is possible to determine the pdfs (probability density functions) of important variables. If the stochasticity of weather is replaced by the average root zone water fluxes, a simple analytical approximation for the

root zone salt concentration is feasible. This approximation of salt concentration depends on the numerically averaged fluxes, and is largely in analogy to the expression derived in Chapter 2. The very simple approximation of long term averaged root zone concentration appears to correspond well with the numerical results.

Whereas Chapter 3 indicates how soil type, climate, and groundwater level affect the salinity building up in the root zone, if salts derive originally from the groundwater, an associated problem of sodicity is not addressed. For soils that are vulnerable for soil structure deterioration, due to the presence of sufficient swelling/shrinking clay minerals, sodicity may be an important hazard to soil functioning. Hence, also the composition of salts, notably the presence of sodium (Na^+) compared to aggregating higher valency cations is worthwhile to investigate, which is discussed in Chapter 4.

7.4 Modelling of soil sodicity

For an accurate assessment, some of the assumptions made in Chapter 2 may need further consideration. For instance, the assumption of a constant Gapon constant has been mentioned to limit the actual validity range of *f*-values. Ignored was also the effect of salt concentration, *C*, and the composition of the exchange complex, *N*, on the soil hydraulic functions. As reviewed by *Bresler et al.* (1982, pp 38-52), in particular the alternation of large and small concentrations can have profound effects on the hydraulic functions as soon as Na occupies more than a few per cents of the cation exchange complex. This feedback renders systems as considered in Chapter 2 even more complicated and worthwhile of investigation. The application of conceptual model with deterministic input of irrigation/groundwater quantity and quality developed in Chapter 2 is extended by considering stochastic input of rainfall in the root zone model as done in Chapter 3 and composition of exchange complex, *N* as a second step towards feedback calculations for reduction in saturated hydraulic conductivity in this Chapter 4.

Soil sodicity (quantified by *ESP* and/or by the fraction of calcium in solution *f*) model based on the soil salinity model (*Shah et al., 2011*) is developed in this Chapter 4. To do so, additional to a water and salt balance, also a cation balance (expressed here for calcium, with sodium (Na) as complementary cation), needs to be solved. We quantify the long term relationships of salt concentration and soil *ESP* with different climates, soil types, root zone thickness, and groundwater depths. We show that salt concentration

approaches the dynamic equilibrium faster than soil *ESP* due to the chemical buffering of Na/Ca exchange, under all climates (ranging from dry to wet climate), groundwater depths, and root zone thickness (ranging from Z_r =25 cm to Z_r =100 cm). Our modeling results are in agreement with strategies for conjuctive use of good quality canal and poor quality groundwater (*Kaledhonkar et al., 2001*) and experimental evidence by *Minhas et al.* (2007). Both our model and the mentioned experiments show that an increase of *ESP* is possible due to temporal variations in salinity. Confirmation also comes from field experiments of *Tedeschi and Dell'Aquila* (2005) that show an increase of soil salinity and sodicity during seven years with an annual cycle. Experimental evidence was presented by *Miller and Pawluk* (1993) that fluctuation of the salt concentration can be accompanied by an increase of sodium. Prolonged drought durations and smaller soil *CEC* can bring the soil *ESP* to hazardous level (international conventions are that this is the case if soil *ESP* becomes greater than 15). In agreement with the Gapon equation, different values of soil *CEC* lead to the same final *ESP*, as was shown in Chapter 2 also.

In view of the made assumptions, the approximation of a linear reservoir is appropriate for the root zone, leading to an exponential function of total concentration and soil *ESP*. Therefore, fitting of exponential function on the salt concentration and soil ESP trajectories under different root zone thicknesses give good insight about the fitting parameters $C_{t=\infty,}$ $ESP_{t=\infty}$ and K_C, $K_{ESP.}$ The K_C and K_{ESP} are inverse characteristic times for salt concentration and soil *ESP*, which give a reasonable approximation to how fast salt concentration and soil *ESP* approach the dynamic equilibrium under different root zone thicknesses, and climates. The inverse characteristic time for soil ESP (K_{ESP}) is relatively smaller than $K_{C.}$ The reason is that salt concentration deals only with the soil solution phase, whereas soil ESP deals with both the soil solution and exchange phase, which slow down the chemical buffering of Na/Ca exchange and consequently causes the decrease in inverse characteristic times. Furthermore, the inverse characteristic time for salt concentration and soil *ESP* decreases with increasing root zone thickness, which is understandable.

For the developed root zone sodicity model, we show that the resulting concentration and *ESP* levels can be predicted well on the basis of long term average water fluxes, and groundwater quality (C and f). Moreover, if also precipitation water is of poor quality

(which is more relevant if we consider irrigation water than if we consider rain water), such a prediction can be made equally well. This extends the relevance of our approach and results considerably.

Since the impact of different water fluxes on the root zone water saturation has been solved analytically by *Vervoort and Van der Zee* (2008), the long term water fluxes can be excellently predicted, similar as outlined by *Laio et al.* (2001). This enables us to fully analytically predict the long term concentration and soil *ESP* levels. These predictions were made for a subset of conditions, and revealed a moderate to good agreement with the numerical results. In view of the complexity of the modelled system (with erratic rainfall/irrigation forcing and nonlinear soil chemical relationships), such analytical results can still be quite useful. A limitation, though, of the work of Chapter 4 is that it disregards the impact of soil sodicity on soil structure, which after all is the main reason to consider sodicity in practice in the first place. Therefore, this aspect was considered in the next chapter.

7.5 Feedback related with saturated hydraulic conductivity

Consideration of continued decrease in saturated hydraulic conductivity quantify the under or over-estimate fluxes, salt concentration and soil *ESP* under different climates (Oenpelli and TCA) and different groundwater depths. We have considered three scenarios to understand the reasoning of these estimations. We show that distinct dry and wet seasons in rainfall can have significant feedback effects on root zone fluxes, salt concentration and soil *ESP*. We have modelled the feedback effects of saturated hydraulic conductivity (*Ks(C, ESP)*) on root zone fluxes, salinity, and sodicity under different groundwater depths and climates of Oenpelli and Tennant Creek Airport located in the North Territory of Australia. The feedback effects of saturated hydraulic conductivity have been calculated by using the procedure developed by *McNeal* (1968). The significant feedback effects on salt concentration and soil *ESP* depend on many important parameters like groundwater depth, leaf area index, weather seasonality and non-seasonality (Poisson rainfall), and soil type. Out of these important parameters, weather seasonality is the main driver that can develop significant feedback effects on root zone fluxes, salt concentration and soil *ESP*. The reduction in saturated hydraulic conductivity decreases the capillary flux, leaching flux, and evapotranspiration, but increases the

magnitude of runoff compared to no feedback case. Also when *Ks(C, ESP)* affects both capillary and leaching flux under seasonal rainfall, the feedback effects are significant compared to the partial feedback.

The second aspect of this thesis discusses the optimization of irrigation with saline water by considering soil-water-plant feedback mechanisms.

7.6 Management of irrigation with saline water: accounting for externalities by considering soil-water-plant feedback mechanisms

In Chapter 6, we have developed a conceptual model for the optimal management of scarce and saline irrigation water. But we move beyond the formulation of a conceptual frame and apply the model to the irrigation of *Capsicum annum* on Arava Sandy Loam. We show for this case how water application should be distributed between upstream and downstream plots or farms. We identify those situations where water is traded from upstream to downstream farms (assuming that the upstream farm holds the water rights). We find that water trade will improve efficiency except when loss levels are low. In that case marginal productivity of water of the upstream farm is large and the return flows available to the downstream farm are less saline and, hence, more productive compared to higher loss levels.

The case presented in this study has been simplified (e.g., only two farms, same crops and soil types). Nevertheless, considerations of externalities of irrigation due to leaching of salts are not trivial, when the plant response processes are captured in a physically and agronomically rigorous way. Whereas it is obvious that total yields decline as initial river water quality gets worse as well as if losses increase, the optimal use of irrigation water by an upstream farm can be a complicated function of initial river water quality and losses due to irrigation inefficiencies. For most presented scenarios, we find some gain from trade of water from upstream to downstream.

7.7 Suggestions?! Ideas for future research

The considered simplicity of the mass balance approaches for water, salt and cations used in this thesis compared to other detailed models (such as SWAP, UNSATCHEM, and HYDRUS) guide us to predict the long term salinity and sodicity trends and their effects of soil saturated hydraulic conductivity under different groundwater depths, and climates on regional scales for sustainable management of

agriculture and natural vegetation. For this purpose, we should gather data of soil type, climatic parameters ($\alpha\lambda$), vegetation properties (leaf area index, rooting depth), groundwater depth, and groundwater SAR of the area of interest. The developed salinity and sodicity model can be applied based on the soil, climate, vegetation and groundwater data to predict the long term salinity, sodicity tends and their relationship with climate, soil type, and groundwater depths. This applied research would sustain on the longer terms crop production, and soil and groundwater productivity from field to regional scale.

Furthermore, the rainfall generated through Poisson process is independent of soil moisture. We should generate soil moisture dependent rainfall to accommodate more real effects of rainfall (such as seasonality and non-seasonality in rainfall) in the stochastic root zone salinity sodicity model. Furthermore the feedback effects of reduction in saturated hydraulic conductivity on root zone fluxes, salinity and sodicity in soil moisture dependent rainfall would be more realistic.

Regarding the second aspect of this thesis, we have coupled the agro-physical model, that has been validated (*Ben-Gal et al., 2008; Shani et al., 2007*) with an economic model for water resource and irrigation management in a parsimonious way. Despite the already apparent complexity of the results, even more complexity is needed for real world applications. With respect to the physical environment, one may think of different soil types, and water resources (e.g. waste water, groundwater, river water). From an agronomic perspective, crop choice and rotation schemes may be considered that take into account different salt tolerances and product prices. Although this would significantly complicate the computations, our approach is sufficiently general to allow such applications. By adding complexity stepwise, we keep our investigations transparent. The model also allows consideration of river water quantity and quality after the last (*n*th) user to provide for evaluation of potential additional water consumers or comparison of scenarios as to their environmental consequences. Furthermore the analysis is relevant to determine fair compensations to settle international conflicts over scarce freshwater resources.

Summary

Recent trends and future projections suggest that the need to produce more food and fibre for the world' s expanding population will lead to an increase in the use of marginal-quality water and land resources (*Bouwer, 2000; Gupta and Abrol, 2000; Wild, 2003*). This is particularly relevant to less-developed, arid and semi-arid countries, in which problems of soil and water quality degradation are common (*Qadir and Oster, 2004*). The aim, therefore, should be to increase yield per unit of land rather than the area cultivated. More efforts are needed to improve productivity as more lands are becoming degraded. It is estimated that about 15% of the total land area of the world has been degraded by soil erosion and physical and chemical degradation, including soil salinization (*Wild, 2003*).

The main sources of soil salinity and sodicity development are groundwater and irrigation water. In discharge areas of the landscape, water exits from groundwater to the soil surface bringing the salts dissolved in it. The driving force for upward movement of water and salts is evaporation from the soil plus plant transpiration. Salt accumulation is high when the water table depth is less than a threshold. However, this threshold depth may vary depending on soil hydraulic properties and climatic conditions. Groundwater associated salinity and sodicity affects around 350 X 10^4 km^2 in the world (*Szabolcs, 1989*).

In this thesis, the focus is to quantify and understand the salinity and sodicity dynamics, and the feedback on dynamics in groundwater dependent agro-ecosystems and the feedback on dynamics. First we have considered the impact of salt coming from groundwater on capillary fluxes and on the root zone water and salt dynamics. Groundwater can be a source of both water and salts in semi-arid areas, and therefore capillary pressure induced upward water flow may cause root zone salinization. To identify which conditions result in hazardous salt concentrations in the root zone, we combined the mass balance equations for salt and water, further assuming a Poisson-distributed daily rainfall and brackish groundwater quality. For the water fluxes (leaching, capillary upflow, and evapotranspiration), we account for osmotic effects of

the dissolved salt mass using Van't Hoff's law. Root zone salinity depends on salt transport via capillary flux and on evapotranspiration, which concentrates salt in the root zone. Both a wet climate and shallow groundwater lead to wetter root zone conditions, which in combination with periodic rainfall enhances salt removal by leaching. For wet climates, root zone salinity (concentrations) increases as groundwater is more shallow (larger groundwater influence). For dry climates, salinity increases as groundwater is deeper due to a drier root zone and less leaching. For intermediate climates, opposing effects can push the salt balance in either way. Root zone salinity increases almost linearly with groundwater salinity. With a simple analytical approximation, maximum concentrations can be related with the mean capillary flow rate, leaching rate, water saturation and groundwater salinity, for different soils, climates and groundwater depths.

A Soil sodicity (quantified by *ESP*) model based on the soil salinity model (as discussed above) has been developed. For sodicity calculations, we have used the Gapon equation favored in salinity research. The simulation results show that soil salinity and sodicity development in groundwater driven agro-ecosystems play a major role in soil structure degradation. To identify which conditions can make soil sodic, we have modeled the coupled water, salt, and cation balances. The root zone salinity C and sodicity *ESP* gradually change to their long term average values. These long term average values are independent of the cation exchange capacity *CEC*. The rate of change depends inversely on the size of the root zone reservoir, i.e., on root zone thickness for C, and additionally on *CEC*, for *ESP*. Soil type can have a large effect on both the rate of approach of the long term steady state salinity and sodicity, and on the long term levels, as it affects the incoming and out-going water and chemical fluxes. Considering two possible sources of salts, i.e., groundwater and irrigation water (here represented by rainfall), the long term salt concentration C of the root zone corresponds well with a flux weighted average of infiltrating and upflowing salt mass divided by the average water drainage. In full analogy, the long term *ESP* can be approximated very well for different groundwater depths and climates. A more refined analytical approximation, based on the analytical solution of the water balance of *Vervoort and Van der Zee* (2008), leads to a quite good approximation of long term salinity and sodicity, for different soils, groundwater depths, and climates.

Modeling is an efficient tool to investigate water and solute movement in groundwater driven agro-ecosystems. However, in most available models (*SWAP, MODFLOW/MT3D*) continuing degradation of soil hydraulic properties as a result of rising Na^+ concentrations is ignored. Disregarding the soil hydraulic degradation due to sodicity level in some cases makes modeling water and solute movement within the soil profile questionable. We have translated the effects of soil salinity and sodicity into reduction in saturated hydraulic conductivity to quantify the feedback effects of reduction in saturated hydraulic conductivity on root zone fluxes, salinity, and sodicity under different groundwater depths and climates of Oenpelli and Tennant Creek Airport located in the North Territory of Australia. The reduction in saturated hydraulic conductivity due to salinity and sodicity *(Ks(C,ESP))* has been calculated by using the procedure developed by *McNeal* (1968). The significant feedback effects of *Ks(C,ESP)* on salt concentration and soil *ESP* depend on many important parameters like groundwater depth, leaf area index, weather seasonality and non-seasonality, and soil type. Out of these important parameters, weather seasonality is the main driver that can develop significant feedback effects of *Ks(C,ESP)* on salt concentration and soil *ESP*. Furthermore, *Ks(C,ESP)* although decreasing the capillary flux, leaching flux, and evapotranspiration, it increases the magnitude of runoff. Also when *Ks(C,ESP)* affects both capillary and leaching flux under seasonal rainfall, the feedback effects are significant compared to the partial feedback (*Ks(C,ESP)* affects only leaching flux, but not capillary flux).

In the second theme of this thesis, we have focused on optimizing irrigation water between two farms under water scarcity and salinity regimes. In arid and semi-arid regions, irrigation water is scarce and often saline. To reduce negative effects on crop yields, the irrigated amounts must include water for leaching and therefore exceed evapotranspiration. The leachate (drainage) water returns to water sources such as rivers or groundwater aquifers and increases their level of salinity and the leaching requirement for irrigation water of any sequential user. We develop a sequential (upstream-downstream) model of irrigation that predicts crop yields and water consumption and tracks the water flow and level of salinity along a river dependent on irrigation management decisions. The model incorporates an agro-physical model of plant response

to environmental conditions including feedbacks. For a system with limited water resources, the model examines the impacts of water scarcity, salinity and inefficient application on yields for specific crop, soil, and climate conditions. As a general pattern we find that, as salinity level and technical inefficiency increase, the system benefits when upstream farms use less water than is available to them, to provide downstream farms with more and better quality water. We compute the marginal value of water, i.e. the price water that would command on a market, for different levels of water scarcity, salinity and levels of water loss.

In summary this thesis aims to understand theoretically how soil salinity and sodicity develop under different climates, groundwater depths, soil types, root zone thicknesses, and different groundwater salinities. The developed salinity sodicity model can be applied in potential salt affected areas to predict the long term salinity, sodicity trends. Furthermore, quantification of feedback effects of reduction in saturated hydraulic conductivity (*Ks(C,ESP))* on root zone fluxes, salinity, and sodicity guide us towards better management of soil, vegetation, and irrigation/groundwater.

Samenvatting

Recente trends en prognoses wijzen erop dat de noodzaak om meer voedsel en vezels te produceren voor de groeiende wereldbevolking zal leiden tot een toename in het gebruik van water en land van marginale kwaliteit (*Bouwer, 2000; Gupta en Abrol, 2000; Wild , 2003*). Dit is met name relevant voor minder ontwikkelde, aride en semi-aride landen, waarin problemen van bodem- en waterkwaliteitsdegradatie vaak voorkomen (*Qadir en Oster, 2004*). Het gaat er dus om de opbrengst per eenheid land te verhogen in plaats van de bebouwde oppervlakte. Meer inspanningen zijn nodig om de productiviteit te verbeteren als meer landoppervlak wordt aangetast. Er wordt geschat dat ongeveer 15% van de totale landoppervlakte van de wereld is aangetast door erosie en andere vormen van fysische en chemische bodemdegradatie, inclusief de bodemverzilting (*Wild, 2003*).

De belangrijkste bronnen van zouten die leiden tot bodemverzilting en-alkaliteit (hier aangeduid met de Engelse term sodicity) zijn grond- en irrigatiewater. In kwelgebieden verdampt het grondwater aan het bodemoppervlak waardoor de opgeloste zouten, die niet verdampen, daar accumuleren. De drijvende kracht voor opwaartse beweging van water en zouten is immers de verdamping uit de grond en transpiratie door planten. Zoutaccumulatie is hoog wanneer de grondwaterstand ondieper is dan een drempeldiepte. Deze drempeldiepte kan variëren, afhankelijk van bodemhydraulische eigenschappen en klimatologische omstandigheden. Door grondwater veroorzaakte verzilting en sodicity betreft mondiaal ongeveer 350 X 10^4 km^2 (*Szabolcs,1989*).

In dit proefschrift ligt de nadruk op het kwantificeren en begrijpen van de dynamiek van verzilting en sodicity, en de effecten daarvan op de verzadigde hydraulische geleidbaarheid van grondwater afhankelijke agro-ecosystemen en de feedback daarvan op de dynamiek. Eerst werd beschouwd wat de impact van het zout afkomstig van het grondwater is op capillaire fluxen naar de wortelzone en water- en zoutdynamiek. Grondwater kan een bron van water en zouten in semi-aride gebieden, en daarom kan de door capillaire krachten veroorzaakte stijgende waterstroom wortelzone-

verzilting veroorzaken. Om vast te stellen welke voorwaarden leiden tot gevaarlijke zoutconcentraties in de wortelzone, combineerden we de massabalansvergelijkingen voor zout en water, uitgaande van een Poisson-verdeelde dagelijkse neerslag en een brakke grondwaterkwaliteit. Voor het water fluxen (uitspoeling, capillaire opwaartse stroming, en evapotranspiratie), hebben we osmotische effecten van de opgeloste zout in rekening gebracht met behulp van Van 't Hoff's wet. Wortelzonezoutgehalte is afhankelijk van zoutaanvoer via capillaire flux en verdamping, wat zout concentreert in de wortelzone. Zowel een nat klimaat en ondiep grondwater leiden tot nattere wortelzone-omstandigheden, wat leidt tot zoutverwijdering door uitspoeling tijdens periodieke neerslag. Voor natte klimaten neemt het zoutgehalte (concentratie) in de wortelzone toe naarmate het grondwater ondieper is (grotere grondwater invloed). Voor de droge klimaten, neemt het zoutgehalte toe naarmate het grondwater dieper is, hetgeen te wijten is aan een drogere wortelzone en minder uitspoeling. Voor tussenliggende klimaten, kunnen tegengestelde effecten de zoutbalans in beide richtingen duwen. Het zoutgehalte van de wortelzone neemt bijna lineair toe met het zoutgehalte van het grondwater. Met een eenvoudige analytische benadering, kan de maximale concentraties worden gerelateerd aan de gemiddelde capillaire debiet, uitspoeling, waterverzadiging en zoutgehalte van het grondwater, voor verschillende bodems, klimaten en grondwater diepte.

Sodicity van de bodem (gekwantificeerd door ESP, Exchangeable Sodium Percentage of Uitwisselbaar Natriumpercentage) is gemodelleerd op basis van het zoutmodel (dat hierboven is beschreven). Voor sodicity berekeningen hebben we gebruik gemaakt van de Gapon vergelijking, waaraan veelal de voorkeur wordt gegeven in bodemzoutonderzoek. De simulatie resultaten tonen aan dat de ontwikkeling van bodemverzilting en sodicity in door het grondwater bepaalde agro-ecosystemen een belangrijke rol speelt in de bodemstructuurdegradatie. Om vast te stellen onder welke voorwaarden de bodem sodic kan worden, hebben we de gekoppelde water-, zout- en kationbalanzen gemodelleerd. De zoutconcentratie C en de sodiciteit ESP veranderen geleidelijk tot aan hun lange termijn gemiddelde waarden. Deze lange termijn gemiddelde waarden zijn onafhankelijk van de kationuitwisselingscapaciteit CEC. De veranderingssnelheid is omgekeerd evenredig aan de grootte van de wortelzone reservoir,

dat wil zeggen de wortelzonedikte v.w.b. C, en bovendien van de CEC voorzover het de ESP betreft. Bodemtype kan een groot effect hebben op zowel de snelheid van benadering van de lange termijn steady state zoutgehalte en sodicity als op het lange termijn niveau, door de invloed op de inkomende en uitgaande water- en stofstromen. Rekening houdend met twee mogelijke bronnen van zouten, te weten het grondwater en irrigatiewater (hier vertegenwoordigd door neerslag), blijkt de lange termijn zoutconcentratie C van de wortelzone goed overeen te komen met een fluxgewogen gemiddelde van infiltratie en omhoogstromende zout massa gedeeld door de gemiddelde waterafvoer. Volledig analoog kan de lange termijn ESP goed benaderd worden voor verschillende diepten van het grondwater en verschillend klimaat. Een meer verfijnde analytische benadering, op basis van de analytische oplossing van de waterbalans van *Vervoort en Van der Zee* (2008), leidt tot een zeer goede benadering van de lange termijn zoutgehalte en sodicity, voor verschillende bodems, grondwater diepten, en klimaten.

Modeling is een efficiënt hulpmiddel om water en stoftransport te onderzoeken in door het grondwater gedreven agro-ecosystemen. Echter, in de meeste beschikbare modellen (SWAP, MODFLOW/MT3D) wordt de steeds verdere aantasting van de bodemhydraulische eigenschappen als gevolg van de stijgende Na^+ concentratie genegeerd. Het negeren van de bodemhydraulische degradatie als gevolg van sodicity maakt in sommige gevallen het modelleren water- en opgeloste stoftransport binnen het bodemprofiel twijfelachtig. We hebben de effect van het zoutgehalte en sodicity de verzadigde hydraulische geleidbaarheid in rekening gebracht voor de wortelzone fluxen, zoutgehalte, en sodicity, voor verschillende grondwaterdieptes en de klimaten van Oenpelli en Tennant Creek Airport, beide gelegen in Noord Territory van Australië. De vermindering van verzadigde doorlatendheid door zoutgehalte en sodicity (Ks (C, ESP)) werd berekend door de procedure ontwikkeld door *McNeal* (1968). De belangrijke feedback-effecten van Ks (C, ESP) op zoutconcentratie en de bodem-ESP zijn afhankelijk van een groot aantal belangrijke parameters zoals grondwaterdiepte, bladoppervlakte-index, seizoensgebondenheid en niet-seizoensgebonden neerslag, en bodemtype. Van deze belangrijke parameters, zijn de seizoensinvloeden van neerslag de belangrijkste drijfveer voor significante feedback-effecten tussen Ks (C, ESP) en zoutconcentratie en bodem ESP. De doorlatendheid, als deze afneemt, vermindert

weliswaar de capillaire flux, uitloging flux, en evapotranspiratie, maar het verhoogt de oppervlakkige afstroming. Wanneer Ks (C, ESP) zowel de capillaire als de uitspoelingsflux beïnvloedt onder seizoengebonden regenval, zijn de feedback effecten significant in vergelijking met de gedeeltelijke feedback (waarbij Ks (C, ESP) alleen invloed heeft op de uitspoelingsflux, maar niet op de capillaire flux).

In het tweede thema van dit proefschrift hebben we ons gericht op het optimaliseren van irrigatiewater tussen twee bedrijven onder waterschaarste en verziltingsregimes. In aride en semi-aride gebieden, is irrigatiewater schaars en vaak zout. Om negatieve effecten op oogsten te verminderen, moeten de irrigatiegiften groot genoeg van omvang zijn om zouten uit te spoelen en dus hoger zijn dan evapotranspiratie. Het percolaat (drainage) water keert terug naar waterbronnen zoals rivieren of grondwaterlagen en verhoogt het zoutgehalte en de uitspoeling behoefte aan irrigatiewater van een sequentiële gebruiker. We ontwikkelden een sequentiële (upstream-downstream) model van irrigatie die gewasopbrengsten en waterverbruik voorspelt en de waterstroom en het niveau van het zoutgehalte langs een rivier volgt, afhankelijk van irrigatiebeslissingen van het management. Het model is uitgerust met een agro-fysisch model van plantaardige reactie op omgevingsfactoren inclusief feedbacks. Voor een systeem met beperkte watervoorraden, kan met het model onderzocht worden wat de effecten van waterschaarste, zoutgehalte en inefficiënte toepassing zullen zijn op de opbrengsten voor specifieke gewas-, bodem- en klimatologische omstandigheden. Als algemene patroon vinden we dat als zoutgehalte en technische inefficiëntie toenemen, het geheel van (hier) twee boerderijen voordeel heeft indien stroomopwaarts gelegen boerderijen minder water gebruiken dan beschikbaar is voor hen, waardoor stroomafwaartsgelegen bedrijven gebruik kunnen maken van meer en betere kwaliteit water. We berekenen de marginale waarde van het water, dat wil zeggen de prijs van water op de watermarkt, voor verschillende niveaus van waterschaarste, zoutgehalte en het niveau van water verlies door inefficiëntie.

Samengevat is dit proefschrift er op gericht om theoretisch te begrijpen hoe zoutgehalte van de bodem en sodicity ontwikkelen onder verschillende klimaten, het grondwaterpeil, bodemtypen, dikte van de wortelzone en verschillende zoutgehaltes van het grondwater. Het ontwikkelde zout- en sodicity model kan worden toegepast op

plaatsen waar deze processen tot negatieve effecten kunnen leiden, om de op de lange termijn ontwikkelende zoutgehaltes en sodicity te voorspellen. Beter inzicht ten aanzien van de kwantitatieve effecten van de feedbacks van vermindering van de verzadigde hydraulische geleidbaarheidfunctie Ks (C, ESP) op root zone fluxen, zoutgehalte, en sodicity leiden ons naar een beter beheer van bodem, vegetatie, en irrigatie / grondwater.

References

Abersen, P. J., H. E. D. Houba, M. A., Keyser (2003), Pricing a raindrop in a process-based model: General methodology and a case study of the Upper-Zambezi, *Physics and Chemistry of the Earth,* 28, 182-193.

Ancev, T., (2011), Salinity Offsets in Australia. EU-EPI WATER Deliverable D6.1 – IBE Review reports. http://www.feem-project.net/epiwater/docs/d32-d6-1/CS22_Australia.pdf.

Angelaskis, A. N., M. H. F. M. Domonte, L. Bontoux, and T. Asano (1999), Status of wastewater reuse practice in the Mediterranean basin: Need for guidelines, *Water Resources* 33, 2201-2217.

Appelo, C. A. J., D. Postma (2nd Edition), (2005), Geochemistry, Groundwater and Pollution, Balkema Publishers, Leiden, pp. 649.

Appels, W. M., P. W. Bogaart, and S. E. A. T. M. Van der Zee (2011), Influence of spatial variations of microtopography and infiltration on surface runoff and field scale hydrological connectivity, *Advances in Water Resources*, *34*, 303-313.

Armstrong, A. S. B., D. W. Rycroft, T. W. Tanton (1996), Seasonal movement of salts in naturally structured saline-sodic clay soils, *Agricultural Water Management*, 32, 15-27.

Asano, T., A. Levine, D. Audrey (1996), Waste water reclamation, recycling, and reuse: Past, present, and Future, *J. Wat. Sci. Technol.*, 33, 1-14.

Asner, G. P., Scurlock, J. O., Hicke, J. A. (2003), Global synthesis of leaf area index observations: implications for ecological and remote sensing studies. *Global Ecology & Biogeography,* 12, 191–205.

Beltman, W. H. J., Boesten, J. J. T. I., Van der Zee, S. E. A. T. M., Quist, J. J. (1996), Analytical modeling of application frequency on pesticide concentrations in wells, *Ground Water*, 34, No. 3.

Ben-Gal, A., E. Ityel, L. Dudley, S. Cohen, U. Yermiyahu, E. Presnov, L. Zigmond, and U. Shani (2008), Effect of irrigation water salinity on transpiration and on leaching

requirements: A case study for bell peppers, *Agricultural Water Management,* 95, 587-597.

Ben-Gal, A., U. Shani (2003), Effect of excess boron on tomatoes under water stress, *Plant Soil*, 256, 179-186.

Ben-Gal, A., U. Shani (2002b). Yield, transpiration and growth of tomatoes under combined excess boron salinity stress, *Plant Soil*, 247, 211-221.

Ben-Gal, A., L. Karlberg, P. E. Jansson, U. Shani (2003), Temporal robustness of linear relationships between production and transpiration, *Plant Soil*, 251, 211-218.

Berret-Lennard, E. G. (2003), The interaction between waterlogging and salinity in higher plants: causes, consequences and implications, *Plant and Soil*, *253*, 35-54.

Bernstein, L. (1964), Salt tolerance of Plants, Agric. Info. Bull, U.S. Dept. of Agric. Washington, D.C., 283, 23pp.

Bernstein, L. (1961), Osmotic adjustment of plants to saline media I, Steady state, *American Journal botany*, vol. 48, pp. 909-918.

Bernstein, L. Francois, L. E. (1973), Leaching requirements studies: Sensitivity of alfalfa to salinity of irrigation and drainage waters, *Soil Science Society of America Journal*, vol. 37, no. 2, pp. 931-943.

Bhutta, M. A., E. J. Vender Velde (1992), Equity of water distribution along secondary canals in Punjab, Pakistan, *Irrigation and drainage systems,* 6, 161-177.

Bolt, G. H. (2nd Ed.) (1982), *Soil chemistry*, Elsevier Scientific Publishing Company, Amsterdam.

Bolt, G. H. (1982), Cation-exchange equations used in soil science: A review, *Neth. J. Agric. Sci.* 15, 81-103.

Bolt, G. H. and M. G. M. Bruggenwert (1976), *Soil Chemistry: A. Basic Elements*, 281 pp., Elsevier Scientific Publishing Company, Amsterdam-Oxford-New York.

Bouwer, H. (2000), Integrated water management emerging issues and challenges, *Agricultureal Water Management*, 45, 217-228.

Bras, R. L., D. Seo (1987), Irrigation control in the presence of salinity: Extended linear quadratic approach, *Water Resources Research*, *23*(7), 1153-1161.

Bresler, E. (1981), Transport of salts in soils and subsoils *Agric. Water Management*, *4*, 35-62.

Bresler, E., B. L. MacNeal, D. L. Carter (1982), Saline and sodic soils: Principles-Dynamics-Modeling, Springer-Verlag, Berlin/Heidelberg/New York, 236 pp.

Brooks, R. N., A. T. Corey (1966), Properties of porous media affecting fluid flow, *ASCE: Journal of Irrigation and Draining Division*, *92*(IR2), 61-68.

Caldwell, M. M., T. E. Dawson, and J. H. Richards (1998), Hydraulic lift: consequences of water efflux from the roots of plants, *Oecologia*, *113*(2), 151-161.

Corwin, D.L., J. D. Rhoades, J. Simunek (2007), Leaching requirement for soil salinity control: steady-state versus transient models, *Agricultural Water Management*, 90, 165-180**.**

Datta, K. K., C. D. Jong (2002), Adverse effect of waterlogging and soil salinity on crop and land productivity in northwest region of Haryana India, *Agricultural Water Management*, *57,* 223-238.

Dawson, T. E. (1993), Hydraulic lift and water use by plants: implications for water balance, performance and plant-plant interactions, *Oecologia*, *95*, 565-574.

Dehayr, R., I. Gordon (2005), Irrigation water quality: salinity and soil structure stability, Natural Resource Sciences, Queensland Government, Viewed 3 April, 2006.

De Jong van Lier, Q., J. C. van Dam, K. Metselaar, R. de Jong, W. H. M. Duijnisveld (2008), Macroscopic root water uptake distribution using a matric flux potential approach, *Vadose Zone Journal*, *7*, 1065-1078. doi: 10.2136/vzj2007.0083.

De Wit, C. T. (1958), Transpiration and and crop yield, Versl Landbowckd Onderz, 64(6), 1-88.

Dudley, L. M., Ben-Gal, A., Shani, U. (2008), Influence of plant, soil, and water on the leaching fraction, *Vadose Zone Journal,* 7, 420-425.

Dudley, L., U. Shani (2003), Modeling plant response to drought and salt stress: Reformulation of root sink term, *Vadose Zone Journal*, 2, 751-758.

Eagleson, P. S. (Ed.) (2002), Ecohydrology: Darwinian Expression of Vegetation Form and Function 496 pp., Cambridge University Press Cambridge.

El-Ashry, M. T., J. van Schilfgaarde, S. Schiffman (1985), Salinity pollution from irrigated agriculture, *Journal of Soil and Water Conservation,* 40, 48-52.

Emerson, W. W., A. C. Bakker (1973), The comparative effects of exchangeable calcium, magnesium, and sodium on some physical properties of red-brown earth subsoils: II.

The spontaneous dispersion of aggregates in water, *Australian Journal of Soil Research*, vol. 11, no. 2, pp. 151-157.

Entekhabi, D., I. Rodriguez-Iturbe, and R. L. Bras (1992), Variability in large-scale water balance with land surface-atmosphere interaction, *Journal of Climate*, *5*, 798-813.

Evangelov, V.P., J. R. McDodonald (1999), Influence of sodium on soils of humid regions in M Pessaraki (ed), Handbook of Plant and Crop Stress, 2.edn, Marcel Dekkar, New York, PP. 17-50.

Ezlit, Y. D. (2009), Modelling the Change in Conductivity of Soil Associated with the Application of Saline–Sodic Water. PhD Thesis, Faculty of Engineering and Surveying, University Of Southern Queensland, Australia.

Felhender, R., I. Shinberg, H. Frenkel (1974), Dispersion and hydraulic conductivity of soils in mixed solutions., In International Congress in Soil Science Transaction 10, Moscow, 1 (1), PP. 103-112.

Fernandez-Illescas, C.P., A. Porporato, F. Laio, I. Rodriguez-Iturbe (2001), The ecohydrological role of soil texture in a water-limited ecosystem, *Water Resources Research*, 37(12), 2863-2872.

Flowers, T. J., and T. D. Colmer (2008), Salinity tolerance in halophytes, *The New Phytologist*, *179*(4), 945-963.

Fortmeier, R., S. Schubert (1995), Salt tolerance of maize (Zea mays L.): the role of sodium exclusion, *Plant, Cell and Environment,* 18, 1041– 1047.

Fox, J. (2002), Nonlinear regression and nonlinear least squares. Appendix to an R and S-PLUS Companion to Applied Regression.

Gardner, R. L., R. A. Young (1988), Assessing Strategies for Control of Irrigation-Induced Salinity in the Upper Colorado River Basin. *American Journal of Agricultural Economics,* 70, 37-49.

Goldberg, S., H. S. Forster, E. L. Heiek (1991), Flocculation of illite/Kaolinite/Montmorillonite mixtures as effected by sodium adsorption ratio and pH, clay and clay minerals, Vol. 39, 4, pp. 375-380.

Grattan, S. R., C. M. Grieve (1999), Salinity-mineral nutrient relations in horticulture crops, *Scientia Horticulturae,* 78, 127-157.

Grattan S. R, C. M. Grieve (1994), Mineral nutrient acquisition and response by plants grown in saline environments. In Handbook of Plant and Crop Stress, Pessarakli M (ed.). Marcel Dekker: NY; 203–229.

Green, S. R., B. E. Clothier, and D. J. McLeod (1997), The response of sap flow in apple roots to localised irrigation, *Agric. Water Management*, *33*, 63-78.

Gupta, R.K., I. P. Abrol (2000), Salinity build-up and changes in the rice-wheat system of the Indo-Gagnetic Plains, *Experimental Agriculture*, 36, 273-284.

Guswa, A. J., M. A. Celia, and I. Rodriguez-Iturbe (2002), Models of soil moisture dynamics in ecohydrology: A comparative study, *Water Resour. Res.*, *38*(9), 1166, doi:1110.1029/2001WR000826.

Guswa, A. J., M. A. Celia, and I. Rodriguez-Iturbe, 2004, Effect of vertical resolution on predictions of transpiration in water-limited ecosystems, *Advances in Water Resources*, *27*, 467-480 doi:410.1016/j.advwatres.2004.1003.1001.

Halliwell, D. J., Barlow, K. M., Nash, D. M. (2001), A review of the effects of wastewater sodium on soil physical properties and their implications for irrigation systems, *Australian Journal of Soil Research*, CSIRO publishing, 39, 1259-1267.

Hamilton, A. J., F. Stagnitti, F. Xiong, X., Kreidi, S., Benke K. K. P. Maher (2007), Wastewater Irrigation: The State of Play, *Vadose Zone J*, 6:823-840.

Hanks, R.J. (1974), Model for predicting plant yield as influenced by water use, *Agronomy Journal*, 66, 660-665.

Haq, A.U. (20000, Self regulation, total control or a gradual and holistic approach? Institutional framework for groundwater management in Punjab, Pakistan.

Homaee, M., Feddes, R.A., Dirksen, C. (2002), Simulation of root water uptake: III. Non-uniform transient combined salinity and water stress, *Agricultural Water Management,* 57, 127-144.

Houba, H. (2008), Computing alternating offers and water prices in bilateral river basin management, *International Game Theory Review,* 10(3), 257-278.

Howell, T.A. (1988), Irrigation Efficiencies: Handbook of engineering in agriculture, CRC Press: 13. Boca Raton, Florida. pp. 173-184.

Isidoro, D., and S. R. Grattan (2011), Predicting soil salinity in response to different irrigation practices, soil types and rainfall scenarios, *Irrigation Science*, *29*, 197-211, DOI 110.1007/s00271-00010-00223-00277.

Jalali, M., H. Merikhpour, M. J. Kaledhonkar, S. E. A. T. M. Van der Zee (2008), Effects of wastewater irrigation on soil sodicity and nutrient leaching in calcareous soils, *Agric. Water Management*, *95*, 143-153.

Kaledhonkar, M. J., N. K. Tyagi, S. E. A. T. M. Van der Zee, (2001), Solute transport modelling in soil for irrigation field experiments with alkali water, *Agric. Water Management*, *51*, 153-171.

Katul, G. G., and M. B. Siqueira (2010), Biotic and abiotic factors act in coordination to amplify hydraulic redistribution and lift, *New Phytologist*, *187*, 3-6.

Kim, J. (2005), A projection of the effects of the climate change induced by increased CO2 on extreme hydrologic events in the western U.S., *Climatic change*, *68*, 153-168.

Kroes, J. G., J. C. van Dam, P. Groenendijk, R. F. A. Hendriks, C. M. J. Jacobs (2008), SWAP version 3.2, Theory description and user manual, 262 pp, Wageningen University and Research Centre, Wageningen.

Laio, F., A. Porporato, L. Ridolfi, I. Rodriguez-Iturbe (2001), Plants in water-controlled ecosystems: active role in hydrologic processes and response to water stress: II. Probabilistic soil moisture dynamics, *Advances in Water Resources*, *24*(7), 707-723.

Laio, F., S. Tamea, L. Ridolfi, P. D'Odorico, I. Rodriguez-Iturbe (2009a), Ecohydrology of groundwater-dependent ecosystems: 1. Stochastic water table dynamics, *Water Resour. Res.*, *45,* W05419, doi: 10.1029/2008WR007292.

Lamontagne, S., P. G. Cook, A. O'Grady, and D. Eamus (2005), Groundwater use by vegetation in a tropical savanna riparian zone (Daly River, Australia), *Journal of Hydrology*, *310*, 280-293, doi:210.1016/j.jhydrol.2005.1001.1009.

Martinez-Beltran, J., C. L. Manzur (2005), Overview of salinity problems in the world and FAO strategies to address the problem. Proceedings of the international salinity forum, Riverside, California, 311–313.

McNeal, B.L. & N. T. Coleman (1966), Effect of solution composition on soil hydraulic conductivity, *Soil Science Society of America Journal*, vol. 30, no. 3, pp. 308-312.

McNeal, B. L., W. A. Norvell, N. T. Coleman (1966), Effect of solution composition on the swelling of extracted soil clays, *Soil Science Society of America Journal*, vol. 30, no.3, pp. 313-317.

McNeal, B.L., D. A. Layfield, W. A. Norvell, J. D. Rhoades (1968), Factors influencing hydraulic conductivity of soils in the presence of mixed-salt solutions, *Soil Science Society of America Journal*, vol. 32, no. 2, pp. 187-190.

McNeal, B. L. (1968), Prediction of the effect of mixed-salt solutions on soil hydraulic conductivity, *Soil Science Society of America Journal*, vol. 32, no. 2, pp. 190-193.

McNeal, B. L. (1974), Soil salts and their effects on water movement, in J Van Schilfgaarde(ed.), *Drainage for Agriculture*, American Society of Agronomy, Madison, Wis.

McNulty (2010), Hydraulic redistribution of soil water by roots affects whole-stand evapotranspiration and net ecosystem carbon exchange, *New Phytologist*, *187*, 171–183, doi: 110.1111/j.1469-8137.2010.03245.x

Mensforth, L. J., P. J. Thorburn, S. D. Tyerman, G. R. Walker (1994), Sources of water used by riparian *Eucalyptus camaldulensis* overlying highly saline groundwater, *Oecologia*, *100*(1 - 2), 21-28.

Mengel. K., E. A. Kirkby (2001), Principles of Plant Nutrition. Kluwer Academic Publishers: Dordrecht.

Miller, J. J., S. Pawluk (1993), Genesis of solonetzic soils as a function of topography and seasonal dynamics, *Canadian Journal of Soil Science*, 74, 207-217.

Milly, P. C. D. (2001), A minimalist probabilistic description of root zone soil water, *Water Resour. Res.*, *37*(3), 457-463, 2000WR900337.

Minasny, B., A. B. McBratney (2002), The efficiency of various approaches to obtaining estimates of soil hydraulic properties. *Geoderma*, *107*, 55-70.

Minhas, P.S., S. K. Dubey, D. R. Sharma (2007), Comparative effects of blending, intera/inter-seasonal cyclic uses of alkali and good quality waters on soil properties and yields of paddy and wheat, *Agricultural Water Management*, 87, 83-90.

Mobin-ud-din, A. (2002), Estimation of net groundwater use in irrigated river basin using geo-information techniques: A case study in Rechna Doab, Pakistan. PhD thesis, Wageningen University, The Netherlands.

Munns, R. (2002), Comparative physiology of salts and water stress, *Plant cell Environ*., 25, 239-250.

Nadezhdina, N., T. S. David, J. S. David, M. I. Ferreira, M. Dohnal, M. Tesar, K. Gartner, E. Leitgeb, V. Nadezhdin, J. Cermak, M. S. Jimenez, and D. Morales (2010), Trees never rest: the multiple facets of hydraulic redistribution, *Ecohydrology*, *3*, 431-444, DOI: 410.1002/eco.1148.

Naidu, R., P. Rengasamy (1993), Ion interactions and constraints to plant nutrition in Australian sodic soils, *Australian Journal of Soil Research,* 31, 801–819.

Oliveira, R. S., T. E. Dawson, B. S. S. O., and D. C. Nepstad (2005), Hydraulic redistribution in three Amazonian trees, *Oecologia*, *145*, 354-363.

Oster, J. D., N. S. Jayawardane (1998), Agricultural management of sodic soils: Distribution, Management and Environmental Consequences, Oxford University Press: NY; 126–147.

Pichu, R. (2006), World salinization with emphasis on Australia, *Journal of Experimental Botany*, *57*(5), 1017-1023.

Porporato, A., F. Laio, L. Ridolfi, and I. Rodriguez-Iturbe (2001), Plants in water-controlled ecosystems: active role in hydrologic processes and response to water stress: III. Vegetation water stress, *Advances in Water Resources*, *24*(7), 725-744.

Press, W. H., S. A. Teukolsky, S. A., Vetterling, W. T., Flannery, B. P. (2nd Edition) (1992), Numerical recipes in C-the art of scientific computing. Cambridge University Press, Cambridge.

Qadir, M., A. D. Noble, S. Schubert, R. J. Thomas, A. Arslan (2006), Sodicity-induced land degradation and its sustainable management: problems and prospects, *Land Degradation & Development* (in press), doi: 10.1002/ldr.751.

Qadir, M., S. Schubert (2002), Degradation processes and nutrient constraints in sodic soils, *Land Degradation & Development*, 13, 275–294.

Qadir, M., B. R. Sharma, A. Bruggeman, R. Choukr-Allah, F. Karajeh (2007), Non-conventional water resources and opportunities for water augmentation to achieve food security in water scarce countries, *Agricultural Water Management,* 87, 2-22.

Quirk, J. P., R. K. Schofield (1955), The effect of electrolyte concentration on soil permeability, *Journal of Soil Science*, vol. 6, no. 2, pp. 163-178.

Raats, P. A. C. (1975), Distribution of salts in the root zone, *Journal of Hydrology*, *27*, 237-248.

Rengasamy, P. (2006), World salinization with emphasis on Australia, *J. Exp. Bot,* 57,1017-1023.

Rhoades, J. D., J. D. Oster, R. D. Ingvalson, J. M. Tucker, and M. Clark, (1973), Minimizing the salt burdens of irrigation drainage waters, *J. Environ. Qual.*, *3*, 311-316.

Rhoades, J. D. (1974), Drainage for salinity control. In: Van Schilfgaarde J. (ed), Drainage for Agriculture *Rep.*, 433–461 pp, SSSA, Madison, WI.

Richards, L. A., L. E. Allison, L. Bernstein, C. A. Bower, J. W. Brown, M. Fireman, J. T. Hatcher, H. E. Hayward, G. A. Pearson, R. C. Reeve, L. V. Wilcox (1954), Diagnosis and Improvement of Saline and Alkali Soils. U.S. Dept. Agr. Handbook No. 60, U.S. Govt. Printing Office, Washington D.C., 160 pp.

Ridolfi, L., P. D'Odorico, F. Laio, S. Tamea, I. Rodriguez-Iturbe (2008), Coupled stochastic dynamics of water table and soil moisture in bare soil condition, *Water Resources Research*, *44*. W01435.

Rodriquez-Iturbe, I., and A. Porporato (2004), Ecohydrology of water-controlled ecosystems: soil moisture and plant dynamics, Cambridge University Press, Cambridge, UK.

Rodriguez-Iturbe, I., V. K. Gupta, and E. Waymire (1984), Scale considerations in the modelling of temporal rainfall, *Water Resour. Res.*, *20*(11), 1611-1619.

Rodriguez-Iturbe, I., A. Porporato, L. Ridolfi, V. Isham, D. R. Cox (1999), Probabilistic modelling of water balance at a point: the role of climate soil and vegetation, *Proceedings of the Royal Society of London Series A*, *455*, 3789-3805.

Rozema, J., and T. Flowers (2008), Crops for a salinized world, *Science*, *322*, 1578-1582.

Runyan, C. W., and P. D. Odorico (2010), Ecohydrological feedbacks between salt accumulation and vegetation dynamics: Role of vegetation-groundwater interactions, *Water Resour. Res.*, *46, in press.*

Russo, D. & E. Bresler (1977a), Effect of mixed Na-Ca solutions on the hydraulic properties of unsaturated soils, *Soil Science Society of America Journal*, vol. 41, no. 4, pp. 713-717.

Russo, D. & E. Bresler (1977b), Analysis of the saturated-unsaturated hydraulic conductivity in a mixed sodium-calcium soil system, *Soil Science Society of America Journal*, vol. 41, no. 4, pp. 706-710.

R Development Core Team, 2011, R: A language and environment for statistical computing. R Foundation for Statistical Computing, Vienna, Austria. ISBN 3-900051-07-0, URL http://www.R-project.org/.

Sadashivaiah, C., C. R. Ramakrishnaiah, G. Ranganna (2008), Hydrochemical Analysis and Evaluation of Groundwater Quality in Tumkur Taluk, Karnataka State, India. *Int. J. Environ. Res. Public Health*, *5(3),* 158-164.

Scherer, C. R. (1977), Water allocation and pricing for control of irrigation-related salinity in a river basin, *Water Resour Res.* 13, 225-238.

Schoups, G., and J. W. Hopmans (2002), Analytical Model for Vadose Zone Solute Transport with Root Water and Solute Uptake, *Vadose Zone Journal*, *1*, 158–171.

Schoups, G., J. W. Hopmans, C. A. Young, J. A. Vrugt, W. W. Wallender, K. K. Tanji, and S. Panday (2005), Sustainability of irrigated agriculture in the San Joaquin Valley, California. Proceedings of the National Academy of Sciences of the United States of America 102:15352-15356.

Scott, R., T. E. Huxman, D. G. Williams, and D. C. Goodrich (2006), Ecohydrological impacts of woody-plant encroachment: seasonal patterns of water and carbon dioxide exchange within a semiarid riparian environment, *Global Change Biology*, *12*, 311-324, doi: 310.1111/j.1365-2486.2005.01093.x.

Shah, S. H. H., R. W. Vervoort, S. Suweis, A. J. Guswa, A. Rinaldo, S. E. A. T. M. Van der Zee (2011), Stochastic modeling of salt accumulation in the root zone due to capillary flux from brackish groundwater, *Water Resources Research*, 47, W09506, doi: 10.1029/2010WR009790.

Shainberg, I., J. Letey (1984), Response of soils to sodic and saline conditions. Hilgardia 52: 1–57.

Shalhevet, J., T. C. Hsiao (1986), Salinity and drought: A comparison of the their effects on osmotic adjustments, assimilation, transpiration, and growth, *Irri. Sci.,* 7, 249-264.

Shani, U., A. Ben-Gal, E. Tripler, L. M. Dudley (2007), Plant response to the soil environment: An analytical model integrating yield, water, soil type, and salinity *Water Resour. Res.*, *43,* W08418, doi: 10.1029/2006WR005313.

Shani, U., A. Ben-Gal, E. Tripler, and L. M.. Dudley (2009), Correction to Plant response to the soil environment: An analytical model integrating yield, water, soil type, and salinity, *Water Res. Res*., 45, W05701, doi:10.1029/2009WR008094.

Shani, U., L. M. Dudley (2001), Field studies of crop response to drought and salt stress, *Soil Sci. Soc. Am. J*., 65, 1522-1528.

Simunek, J., M. Sejna, and M. Th. van. Genuchten (1998), The HYDRUS-ID software package for simulating the one-dimensional movement of water, heat and multiple solutes in variably saturated media. Version 2.0. IGWMC-TPS-70., edited by I. G. M. Center, Golden, CO.

Simunek, J., M. Sejna, and M. Th. van. Genuchten, 1999, The HYDRUS-2D software package for simulating the two-dimensional movement of water, heat, and multiple solutes in variably saturated media. Version 2.0. *Rep.*, USDA, ARS, Riverside, California, CA.

Simunek, J., D. L. Suarez, M. Sejna (1996), The UNSATCHEM software package for simulating one-dimensional variably saturated water flow, heat transport, carbon dioxide production and transport, and solute transport with major ion equilibrium and kinetic chemistry, version 2, Res. Report No. 141, pp. 186, USDA-ARS, U.S. Salinity Laboratory, Riverside, CA.

Smedema, L. (2000), Irrigation-induced River Salinization: Five major Irrigated basins in the Arid Zone, *International Water Management Institute*, Colombo, 87pp.

So, H. B., L. A. G. Aylmore (1993), How do Sodic Soils Behave? The Effects of Sodicity on Soil Behavior, *Australian Journal of Soil Research*, 31, 761-778.

Somma, F., J. W. Hopmans, and V. Clausnitzer (1998), Transient three-dimensional modeling of soil water and solute transport with simultaneous root growth, root water and nutrient uptake, *Plant Soil, 202*, 281-293.

Srinivasamoorthy, K., S. Chidambaram, M. V. Prasanna, M. Vasanthavihar, J. Peter, P. Anandhan (2008), Identification of major sources controlling groundwater chemistry

from a hard rock terrain – A case study from Mettur taluk, Salem district, Tamil Nadu, India, *Journal of Earth System Science*, 117(1), 49-58.

Sumner, M. E. (1993), Sodic soils: new perspectives, *Australian Journal of Soil Research,* 31, 683–750.

Surez, D. L., J. D. Rhoades, R. Lavado, C. M. Grieve (1984), Effect of pH on saturated hydraulic conductivity and soil dispersion, *Soil Science Society of America Journal*, 48 (1), 50-55.

Sustainable Soils & Management (2005), Assessment of soil on 'Windibri' for sprinkler irrigation with berwyndale South Coalbed Methane Production Water, ACN, 105 201 581, Warren, NSW.

Suweis, S., A. Rinaldo, S. E. A. T. M. Van der Zee, A. Maritan, A. Porporato (2010), Stochastic modeling of soil salinity, *Geophysical Research Letters*, 37, L07404, doi:10.1029/2010GL042495.

Szabolcs, I. (1989), Salt affected soils, pp. 274., CRC Press Inc, Boca Raton, Florida.

Tamea, S., F. Laio, L. Ridolfi, P. D'Odorico, I. Rodriguez-Iturbe (2009b), Ecohydrology of groundwater-dependent ecosystems: 2. stochastic soil moisture dynamics, *Water Resour. Res.*, *45*. W05420, doi: 10.1029/2008WR007293.

Tanji, K. K. (1990), Nature and extent of agricultural salinity. In Agricultural Salinity Assessment and Management, Tanji KK (ed.). Manuals and Reports on Engineering Practices No. 71. American Society of Civil Engineers: NY; 1–17.

Tanji, K. and N. Kielen (2002), Agricultural drainage water management in arid and semi-arid areas. FAO Irrigation and Drainage Paper 61. FAO, Rome, Italy.

Tedeschi, A., R. Dell'Aquila (2005), Effects of irrigation with saline waters, at different concentrations, on soil physical and chemical characteristics, *Agricultural Water Management*, 77, 308-322.

Tedeschi, A., M. Menenti (2002), Simulation studies of long-term saline water use: model validation and evaluation of schedules, *Agricultural Water Management*, 54, 123-157.

Teuling, A. J., and P. A. Troch (2005), Improved understanding of soil moisture variability dynamics, *Water Resour. Res.*, *32*, L05404. course

Thorburn, P. J., and G. R. Walker (1994), Variations in stream water uptake by *Eucalyptus camaldulensis* with differing access to stream water, *Oecologia*, *100*(3), 293-301.

Toth, T., and G. Szendrei (2006), Types and distribution of salt affected soils in Hungary, and the characterisation of the processes of salt accumulation (in Hungarian), *Topographia Mineralogica Hungariae*, *IX*, 7-20.

Toth, T. (2008), Salt-affected soils in Hungary, needs and priorities for research and education in biotechnology applied to emerging environmental challenges in SEE countries, Novi Sad, Serbia.77-81.

Tripler E., U. Shani, A. Ben-Gal, and Y. Mualem (2012), Apparent steady state conditions in high resolution weighing-drainage lysimeters containing date palms grown under different salinities, *Agric. Water Management,* 107, 66-73.

UNESCO (2003), World Water Development Report, Water for People, Water for Life, UNESCO Publishing, Barghahn Books.

United Nations World Water Programme (2003), UN World Water Development Report: Water for People, Water for Life, UN.edu.Sci.Cult.Org. Paris.

Van Beek, C. L., T. Toth, A. Hagyo, G. Toth, L. Recatala Boix, C. Ano Vidal, J. P. Malet, O. Maquaire, J. J. H. van den Akker, S. E. A. T. M. van der Zee, S. Verzandvoort, C. Simota (2010), The need for harmonizing methodologies for assessing soil threats in Europe, *Soil Use and Management*, *26*, 299-309.

Van der Zee, S. E. A. T. M., S. H. H. Shah, C. G. R. Van Uffelen, P. A. C. Raats, N. dal Ferro (2009), Soil Sodicity as a result of periodical drought, *Agric. Water Management*, *97*(1), 41-49, doi: 10.1016/j.agwat.2009.08.009.

Van Genuchten, M. T., S. K. Gupta (1993), A reassessment of the crop response function, *H. Indian Soc. Soil Sci,* 41, 730-737.

Varrallyay, G. (1989), Soil mapping in Hungary, *Agrokemiaes Talajtan*, *38,* 696-714.

Vervoort, R. W., S. E. A. T. M. van der Zee (2008), Simulating the effect of capillary flux on the soil water balance in a stochastic ecohydrological framework, *Water Resources Research,* 44, W08425.

Vervoort, R. W., S. E. A. T. M. van der Zee (2009), Stochastic soil water dynamics of phreatophyte vegetation with dimorphic root systems, *Water Resources Research,* 45, W10439, doi: 10.1029/2008WR007245.

Walker, J., F. Bullen, B. G. Williams (1993), Ecohydrological changes in the Murray-Darling Basin. I- the number of trees cleared over two centuries, *J. Appl. Ecology*, *30*, 265-273.

Whitehead, D., C. L. Beadle (2004), Physiological regulation of productivity and water use in *Eucalyptus*: a review, *Forest Ecology and Management*, *193*, 113-140.

Wild, A. (2003), Soils, land and food: managing the land during the twenty-first century. Cambridge, UK: Cambridge University Press.

Wolters, W., M. N. Bhutta (1997), Need for integrated irrigation and drainage management, example of Pakistan, Proceedings of the ILRI symposium, Towards Integrated Irrigation and Drainage Management, Wageningen, The Netherlands.

Acknowledgements

I would like to express my profound gratitude to the Almighty Allah for all good graces and mercies he granted me in my life. I am also grateful to the Higher Education Commission of Pakistan for granting me a fulltime scholarship to follow my PhD study abroad. The work presented in this thesis was made possible with the support and contribution of many individuals whom I like to acknowledge sincerely.

With deep gratitude, I wish to express my sincere thanks to my Promotor, Prof. S. E. A. T. M. van der Zee. Dear Sjoerd, I thank you for your valuable comments, suggestions, support and encouragement throughout my PhD research. I learned a lot from you and I am honoured to have had the opportunity to do my PhD under your supervision. I will never forget the five years of my life that I was involved in the learning and working environment that you managed and provided. Your comprehensive guidelines and support in all steps of my research enabled me to follow and finally get the job done.

I would like to extend my sincere appreciation to the person mostly involved with this dissertation, my Co-promotor Dr. R. W. Vervoort. Dear Vervoort, from your kind comments and guidelines, I learned a lot about programming in R environment and solving differential equations numerically.

I would like to take the opportunity to express my gratitude to all the Pakistani community here in Wageningen. Our occasional gatherings and your emotional support prevented me and my family to get homesick. Thanks all.

I enjoyed the friendly atmosphere of the chair group of Soil Physics, Ecohydrology, and Groundwater Management. I experienced very pleasant times during parties, drinks and dinner organized by people in the group. My special thanks go to Annelies and Tress who were always ready to help me. I also would like to thank all my friends and colleagues in the chair group of SEG: Jos, George, Klaas, Toon, Feddes, Dieuwke, Bram, Harm, Tineke, Henny, Sija, Esther, Willemijn, and Merieke, Anton, and Ype. My dear colleagues and friends, I enjoyed very much working with you. I benefitted from your thoughts and ideas during our formal and informal meetings and parties. You

showed me how rich the culture of Netherlands is. I take this opportunity to express my sincere thanks to all of you.

I wish to express my deepest appreciations to my late parents, my brothers, my sisters, father-in-law, and my mother-in-law. Although I was living far from them, their continuous emotional support and encouraging words helped me to accomplish my academic study successfully.

Most important of all, I am extremely grateful of my wife Saba. I am sure that it would not have been possible to accomplish my PhD without benefiting their patience, tolerance, good willing, and emotional support. Dear Saba, you have done a good job. My dear you always accompanied me and provided a source of happiness throughout the period of our common life. THANK YOU for everything.

Syed Hamid Hussain Shah
Wageningen
March 19 2013

Short biography

Syed Hamid Hussain Shah was born on 5th August 1981 in Faisalabad, Pakistan. In 1997 he qualified secondary school certificate from M. C. High school, Faisalabad, and in 1999 he qualified higher secondary school certificate from Government College of science, Faisalabad. He graduated with B.Sc. degree Agricultural Engineering (2001-2005) and a M.Sc. degree in Agricultural Engineering (2005-2007) from University of Agriculture, Faisalabad, Pakistan. During M.Sc. he defended his thesis on the Groundwater quality management in Bari doab using MODFLOW model. During M.Sc. he was also appointed as a lecturer from January 2007 to September 2007 in Bahauddin Zakariya University Multan, Pakistan. In February 2007, he was awarded with an overseas scholarship by the Higher Education Commission (HEC) Pakistan to pursue the doctorate studies in the Netherlands. In September 2007, he started his PhD at Soil Physics, Ecohydrology, and Groundwater Management group in Department of Environmental Sciences of Wageningen University. During his PhD (2007-2012), he worked on the modeling the effects of saline groundwater and irrigation water on root zone salinity and sodicity dynamics in agro-ecosystems.

Contact e-mail address:

Shahgee1347@hotmail.com
Hamidshah_syed@yahoo.com

Publications

Shah, S. H. H., R. W. Vervoort, S. Suweis, A. J. Guswa, A. Rinaldo, S. E. A. T. M. van der Zee (2011), Stochastic modelling of salt accumulation in the root zone due to capillary flux from brackish groundwater, *Water Resources Research*, doi:10.1029/2010WR009790.

Shah, S. H. H., A. Ben-Gal, H. P. Weikard, S. E. A. T. M. van der Zee (2011), Management of irrigation with saline water: accounting for externalities by considering soil-water-plant feedback mechanisms, under review in *Water Resources Research Journal*.

Zee, S. E. A. T. M. van der; S. H. H. Shah; C. G. R. van Uffelen; P. A. C. Raats; N. dal Ferro (2010), Soil sodicity as a result of periodical drought, *Agricultural Water Management 97 (1), 41 - 49.*

Shah, S. H. H., R. W. Vervoort, N. dal Ferro, and S. E. A. T. M. van der Zee (2009), Water and salinity interactions between groundwater, root zone, vegetation and climate, in Proceedings of HydroEco'2009, 2nd International Multidisciplinary Conference on Hydrology and Ecology—Ecosystems Interfacing With Groundwater and Surface Water, edited by J. Bruthans, K. Kovar, and P. Nachtnebel, Univ. fuer Bodenkult.,Vienna, Austria.

SENSE Certificate

The research described in this thesis was financially supported by the Higher Education Commission, Government of Pakistan and NUFFIC, The Netherlands.

Financial support from Wageningen University for printing this thesis is gratefully acknowledged.

Netherlands Research School for the
Socio-Economic and Natural Sciences of the Environment

C E R T I F I C A T E

The Netherlands Research School for the
Socio-Economic and Natural Sciences of the Environment
(SENSE), declares that

Syed Hamid Hussain Shah

born on 5 August 1981 in Faisalabad, Pakistan

has successfully fulfilled all requirements of the
Educational Programme of SENSE.

Wageningen, 19 March 2013

the Chairman of the SENSE board	the SENSE Director of Education
Prof. dr. Rik Leemans	Dr. Ad van Dommelen

The SENSE Research School has been accredited by the Royal Netherlands Academy of Arts and Sciences (KNAW)

KONINKLIJKE NEDERLANDSE
AKADEMIE VAN WETENSCHAPPEN

The SENSE Research School declares that **Mr. Syed Hamid Hussain Shah** has successfully fulfilled all requirements of the Educational PhD Programme of SENSE with a work load of 52 ECTS, including the following activities:

SENSE PhD Courses

- Environmental Research in Context
- Research Context Activity: Co-organizing WIMEK/SENSE Symposium on Water & Energy Cycles at Multiple Scales, Wageningen, 1 March 2012
- Spatio-Temporal Models in Ecology
- Basic Statistics
- Introduction to R for Statistical Analysis
- Uncertainty Propagation in Spatial and Environmental Modelling
- Advanced Soil Physics
- Physical Modelling

Other PhD and Advanced MSc Courses

- Calibration and Uncertainty of Groundwater Models
- Multivariate Mathematics Applied
- Information Literacy PhD and EndNote Introduction
- Techniques for Writing and Presenting Scientific Papers

Didactic Skills Training

- Supervising an MSc Thesis
- Teaching Practicals for the course *Ecohydrology*

Oral Presentations

- *Salt accumulation in the rootzone in contact with groundwater in a stochastic ecohydrological framework.* Symposium on Land-Water and Atmosphere Interactions, 9 March 2010, Wageningen, the Netherlands

SENSE Coordinator PhD Education

Drs. Serge Stalpers